

1. Introduction and motivation for the study

1.1 Background

1.1.1 Fuel cells- the future of electricity generation?

A fuel cell is a highly efficient energy conversion device that produces direct current electricity from the electrochemical combination of fuel with an oxidant^[1]. It is a device that will operate continuously so long as reactants are supplied to its electrodes, distinguishing its operation from that of a battery which becomes discharged after a finite period of operation. The concept of a fuel cell was first proposed by Sir William Grove in 1839^[1]. Development of the technology in the intervening years has been relatively slow and despite providing power on board the Apollo space craft^[2], fuel cells have yet to make a serious impact as commercial products. However, increasing awareness of the need to move to more sustainable and secure methods of electricity generation have provoked more intense interest and investment in the technology, to the extent that in a recent UK government white paper, fuel cells were cited as one of the key technologies to the nations future energy policy^[3]. The US Solid State Conversion Alliance (SECA) project alone will involve 800 million dollars of investment in fuel cell technology by 2010^[4].

1.1.2 Motivation for development of fuel cell systems

Over the past two decades there has been heightened concern over the problems posed by diminishing fossil fuel reserves^[5,6] and global warming^[7-13] caused by emissions of greenhouses gases such as Carbon dioxide. This has led to the pursuit of alternatives to the combustion of hydrocarbons for electricity generation and transport, leading some to propose a move towards a ‘Hydrogen economy’. The notion of a Hydrogen economy involves a society where Hydrogen, generated from renewable sources, is the main energy carrier^[14-22]. Due to their high efficiencies fuel cells have been proposed as the devices to convert the Hydrogen to electricity at the point of use for stationary^[22,23]

applications and to provide power for transportation^[24-30]. The major advantage of such a system is that the only emissions from the conversion of Hydrogen to electricity would be water. Other advantages of moving from centralised electricity generation to distributed generation include increased security of supply and utilisation of the waste heat for space or water heating^[31]. The efficiency of fuel cells emanates from the fact that the conversion of the chemical energy to electrical energy happens in a single step, unlike in conventional fossil fuel power stations where there are many intermediate energy conversion steps. Avoiding these intermediate steps reduces the irreversible losses of energy to the atmosphere and enables fuel cells to achieve efficiencies in the region of 40-60%. The efficiency of high temperature fuel cells can be further increased by utilising the high grade heat produced in the fuel cell in a downstream device such as a gas turbine. This high efficiency means that even before Hydrogen becomes readily available, fuel cells fuelled by hydrocarbons should be able to reduce emissions of Carbon dioxide compared to conventional power stations. Fuel cells produce negligible or undetectable amounts of nitrous oxides^[1] and should also produce less noise pollution than conventional generators.

1.1.3 Types of fuel cell

A number of different types of fuel cells have been developed but all of them include three main components: an electrolyte; a positive electrode (Cathode); and a negative electrode (Anode). The electrolyte material is generally used to classify different types of fuel cells and largely determines the characteristics of their operation. Table 1.1 shows the main types of fuel cell, the ion transferred across the electrolyte and their operating temperature.

Fuel Cell Type		Mobile ion	Operating
Alkaline	(AFC)	OH^-	323 – 473 K
Proton exchange membrane	(PEMFC)	H^+	313 – 373 K
Direct methanol	(DMFC)	H^+	293 – 363 K
Phosphoric acid	(PAFC)	H^+	≈ 493 K
Molten carbonate	(MCFC)	CO_3^{2-}	≈ 923 K
Solid Oxide	(SOFC)	O^{2-}	773 - 1273 K

Table 1.1 Table showing the different type of fuel cell^[2]

Each of these different types of cell has advantages and limitations. Whilst there are some common principles there are also aspects unique to the operation of each type of cell. Therefore, the work in the thesis has solely been concerned with the operation of the Solid Oxide Fuel Cell, SOFC.

1.2 Solid oxide fuel cells

1.2.1 Principles of operation

The Solid Oxide Fuel Cell, SOFC, is made up of a solid ceramic electrolyte which separates two electrodes. This electrolyte is most commonly made from yttria stabilised Zirconia, YSZ, first used as fuel cell electrolyte by Baur and Preis in 1937^[32], whilst a Nickel/YSZ cermet, and Lanthanum Strontium Manganate, LSM, are the materials commonly used for the anode and cathode respectively. To generate electricity an oxidant, usually Oxygen, is fed to the cathode where it accepts electrons from the external circuit, to form Oxygen ions. These ions are then transferred through the electrolyte to the interface with the anode where they react with a fuel. This reaction at the anode releases electrons that travel through the external circuit to the cathode resulting in the production of direct-current electricity. In order to produce a significant amount of power, individual

cells are connected together to form a stack. Hydrogen is normally used as a fuel, with Oxygen supplied in air as the oxidant. The reaction scheme for this system is shown in

Fig. 1.1

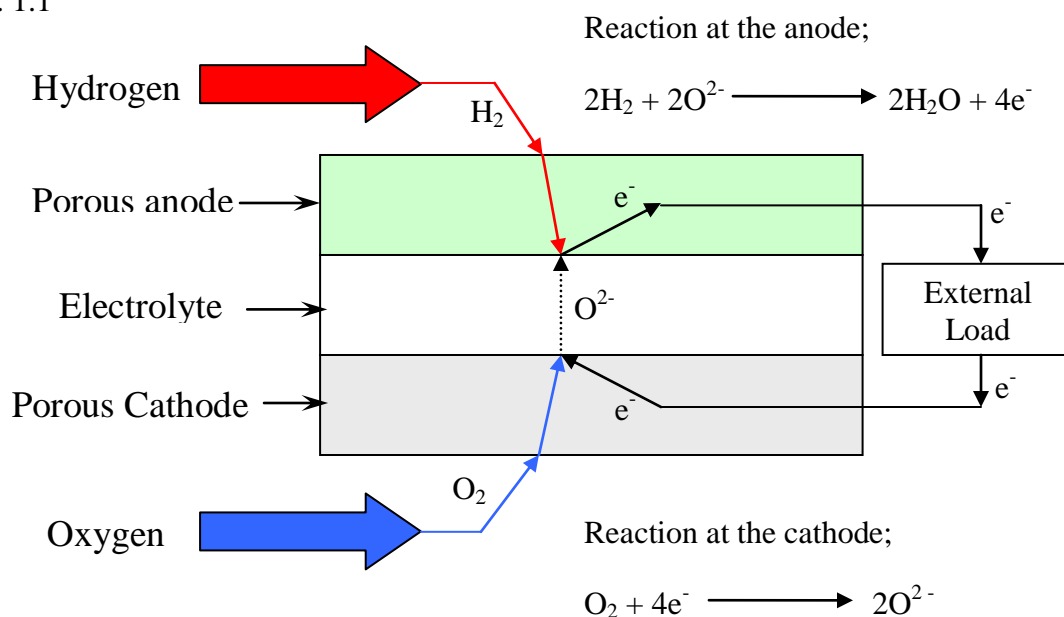


Fig. 1.1 Schematic showing reactions and charge transfer in a typical solid oxide fuel cell fuelled with Hydrogen

The conductivity of the fuel cell materials typically increases with temperature^[33,34] and, as ohmic resistance losses tend to be the dominant losses in SOFCs, so the efficiency is normally enhanced by increasing the temperature. Whilst attempts have been made to develop electrolytes that can operate at lower temperatures to reduce the cost of system components and improve cell longevity^[35], SOFCs, generally operate between 1073 K and 1273 K.

1.2.2 Advantages of SOFC over other types of fuel cell

By definition SOFCs have a solid electrolyte which eliminates the electrolyte management problems associated with PAFCs, and MCFCs^[33]. The high operating temperature enables relatively inexpensive electrode materials to be used in contrast to PEM cells which require expensive Platinum. Whilst the need to use pure Hydrogen,

which is not readily available, is a major challenge to the implementation of low temperature fuel cells^[2], the SOFC is capable of using other fuels. Carbon monoxide can be oxidised by SOFCs which enables them to be fuelled with reformed hydrocarbons or to use the catalytic properties of the Nickel anode to reform hydrocarbons within the cell^[36-40]. A further advantage of the high operating temperature of the SOFC is that the hot exhaust gases can be utilised in a downstream process such as a gas turbine to increase the overall system efficiency to in excess of 70%^[41,42].

1.3 Micro-tubular SOFC

There are several different designs of SOFC based on different cell geometries, fabrication techniques and methods of stack assembly. The three main designs to have been developed are the planar, tubular and monolith designs but variations on these have also emerged^[43]. This thesis is concerned with SOFC stacks using a variation of the conventional tubular design, referred to as micro-tubular SOFC. With a 2 mm diameter and length of 55mm they are considerably smaller than the more established design of large tubular SOFCs developed by Siemens Westinghouse, with a 22 mm diameter and 1500 mm length^[45]. The development and advantages of the micro-tubular design are discussed at length in Chapter 2.

1.4 Thermal Management in SOFC stacks

The high operating temperature of SOFCs means that the control of temperature and efficient thermal management is a crucial part of stack development. The thermal management system in a SOFC is responsible for raising the temperature of the stack to its operating temperature before system start-up, and for maintaining the operating

temperature and temperature uniformity across the stack during its operation. For the SOFC stack to be viable, the functions of the thermal management system must be achieved without compromising the overall efficiency of the system.

1.5 Motivation and objectives for the study

The tolerance of micro-tubular cells to sharp changes in temperature makes them suitable for rapid-starting applications for which other types of SOFC are unsuitable. In order to produce a significant amount of power and take advantage of these properties, the micro-tubular SOFCs must be arranged in a stack, which throws up a number of questions particularly in regard to the thermal management of the system:

- How should the tubes be arranged?
- How can a suitable operating temperature be maintained?
- What sort of temperature gradients are to be expected for a given stack configuration?
- How much of this could be recovered and how much would be lost to the atmosphere?
- How many cells are required before the heat generated in a stack is sufficient to maintain the operating temperature without any additional heating?
- How much energy would it require to achieve the desired stack temperature, and how quickly could this be achieved?

The overall objective of this study was to start to address these questions and contribute to the further development of efficient micro-tubular SOFC stacks.

With little existing experimental data or a clear theoretical approach on which to base stack designs, it became apparent that computer simulations could be a useful tool with

which to conduct these investigations. Therefore, the development of a computer model for micro-tubular SOFC stacks became one of the primary goals of this study.

As discussed in Chapter 2, many previous works on the simulation of SOFC stacks have lacked experimental validation, but this aspect was seen as crucial to producing a model that could act as a functional design tool. Therefore, another key objective of the work was to produce an experimental SOFC stack, which could be used to generate data for the validation of computer models.

In particular, the main objective was to demonstrate and model the thermal behaviour of the micro-tubular stack, especially its rapid heating capability.

1.6 The layout of the thesis

Chapter 2 begins with a review of the previous research on micro-tubular SOFC and on the modelling of SOFCs. This is followed, in Chapter 3, by a description of the experimental system used in this study. Chapter 4 then describes the modelling approach used in the subsequent Chapters of the thesis. The key step of evaluating the model against experimental results is described in Chapter 5. From there, in Chapter 6 the model is used to study the effect of operating parameters on the temperature profile through a 20 cell stack and in Chapter 7 the influence of leaks on this system is considered. In Chapter 8 the scale-up to 100 cells is investigated before the thesis is completed by Chapters reporting the conclusions and scope for further work.

2. Literature review

2.1 Introduction

To explain the origins of this work and the direction taken in this study, a review of the work published previously in experimental and computational research of SOFCs has been presented in this Chapter.

The Chapter begins in section 2.2, with a review of the work published on micro-tubular SOFC. Little of this work has been concerned with stack design and most of the literature has focused on the development of the cells and their behaviour with various hydrocarbon fuels; these two issues have a significant impact on the requirements for stack and system designs. It also provides useful background to the properties of the cells used in this study, the potential benefits of the design, and the status of micro-tubular SOFC stack development.

In section 2.3 the previous work on modelling of SOFCs is reviewed. Since little work has been published on the modelling of micro-tubular stacks specifically, the literature review has been broadened to include aspects of the modelling of larger planar and tubular SOFC cells and stacks that may be relevant to modelling of micro-tubular SOFC. Due to the common materials, chemistry and physical processes there are obviously some elements of the methods used to model larger systems that could be applied to simulation of micro-tubular SOFC. However, due to some of the specific demands of the micro-tubular geometry, the applicability of these methods for the modelling of micro-tubular stacks have to be considered.

2.2 Studies of micro-tubular SOFC

Initial concept

In 1994 a patent^[44] was filed for a novel design of SOFC based on small diameter tubular cells. It was proposed that this new design could overcome three of the limitations inhibiting the realisation of the existing designs as commercial products, particularly in smaller units. These issues were those of:

- 1) Sealing
- 2) Cost of manufacture
- 3) Slow start-up time.

At the time there were two basic designs of SOFC, planar and tubular. The major advantage of the tubular design was that it addressed the problem of sealing cells in a stack to prevent cross over of reactants. Using a tubular cell limits the regions to be sealed to either end of the tube, thus vastly reducing the area that requires sealing compared to the planar cell, as shown in Fig.2.1. The most established tubular design, developed by Westinghouse reduced the sealing problem further by closing one end of the tube thus forming a fuel cell shaped like a test tube. Air was introduced to the cathode, on the inside of the cell, through a smaller diameter tube, which released the air close to the closed end of the cell. Whilst at the open end of the cell there was also no need for sealing, as the fuel and air were designed to meet in a post combustion zone, as shown in part B of Fig. 2.1.

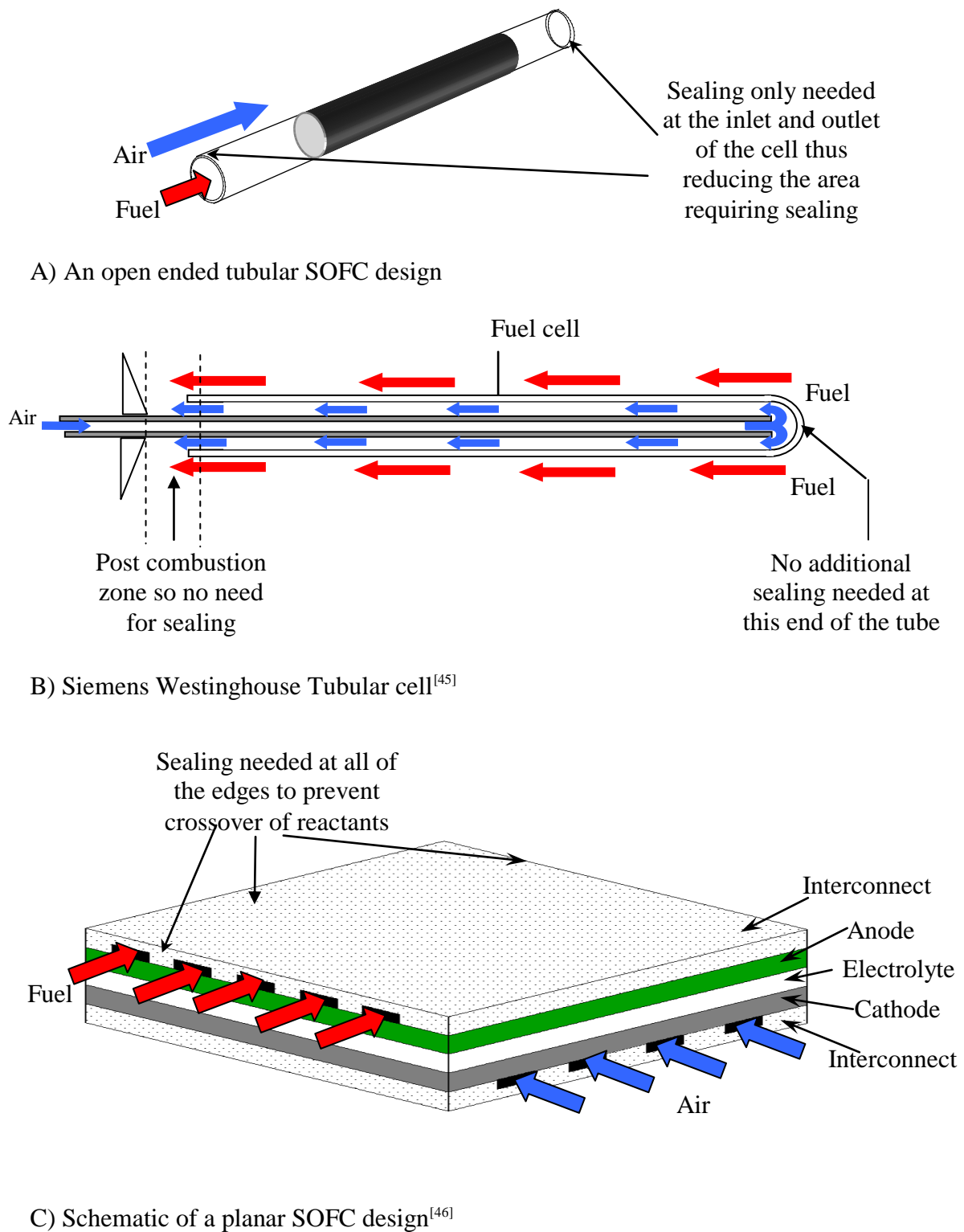


Fig. 2.1 Schematics to show sealing in planar and tubular cells

Unfortunately for Siemens Westinghouse, the fabrication of the tubular cells through electrostatic vapour decomposition, EVD, is expensive. Indeed, it has been predicted that SOFC systems manufactured using this technique may not be viable as commercial products^[47]. Costs reductions have been achieved by reducing the number of cell components manufactured using EVD^[48], and other manufacturers have pursued wet-sintering rather than EVD^[33], but the costs associated with exotic fabrication techniques remain an major inhibitory factor to the commercialisation of large tubular SOFC.

The planar design of SOFC facilitates lower fabrication costs by utilisation of methods such as tape casting, slurry coating, screen printing, or other deposition techniques^[46] and has been regarded as the configuration most likely to deliver the cheapest SOFC system. However, with planar cells there is the problem of sealing between neighbouring cells at their extremities to prevent crossover of reactants, as shown in Fig 2.1 part C. This presents an additional engineering challenge to be overcome to enable the cheaper planar cells to form a viable stack design, not a trivial issue in the high temperature and aggressive oxidising and reducing environments associated with SOFC operation. Compressive sealing was difficult to achieve and glass based seals have been the most common solution. However, migration of silica to the fuel cell components can still cause problems^[33].

The third problem, of start-up time, could not be addressed by either of these existing designs. The relatively high thermal expansion and low strength of these designs meant they had to be heated up slowly to avoid large temperature gradients that would cause cracking due to stress caused by differential rates of expansion. For example: the Siemens Westinghouse tubular cells require several hours to be heated up safely^[49].

Chapter 2- Literature review

The new micro-tubular design inherited the potential to reduced sealing issues from large tubular SOFC but, by reducing the diameter of the tubes from 22 mm to around 2 mm^[50], the cheaper process of extrusion could be employed to fabricate a tubular cell. The cells were also a tenth of the length and wall thickness of the 150 mm of the cells developed by Westinghouse. The combination of these changes to the geometry meant that the new design was also much more robust when it came to withstanding rapid changes in temperature. This enhanced thermal shock resistance was demonstrated by placing tubes of Zirconia in a furnace heated to 1273 K and passing cold air over or through the tubes. The tubes could not be cracked even with high air flow rates in contrast to flat sheets of Zirconia subjected to the same treatment that cracked readily at low air flows^[50]. Their ability to withstand thermal shock means that micro-tubular cells can be heated rapidly enabling power to be produced within minutes of start-up. This enables micro-tubular SOFC stacks to be considered for use in applications demanding a short start-up time, for which conventional planar and large tubular SOFC would be unsuitable.

The ability to withstand temperature gradients meant a novel method of sealing could be proposed for the micro-tubular cells. As with the Westinghouse design, post combustion was used at the outlet end of the cells, which avoided the need for a seal at one end of the tube. Unlike the Westinghouse arrangement, the anode was on the inside of the tubes, and rather than closing one end, the supporting electrolyte layer of the tube was extended such that it would pass out of the thermal insulation housing the SOFC stack. A low temperature rubber based seal could therefore be used to seal the electrolyte tube to the fuel inlet manifold as shown in Fig. 2.2

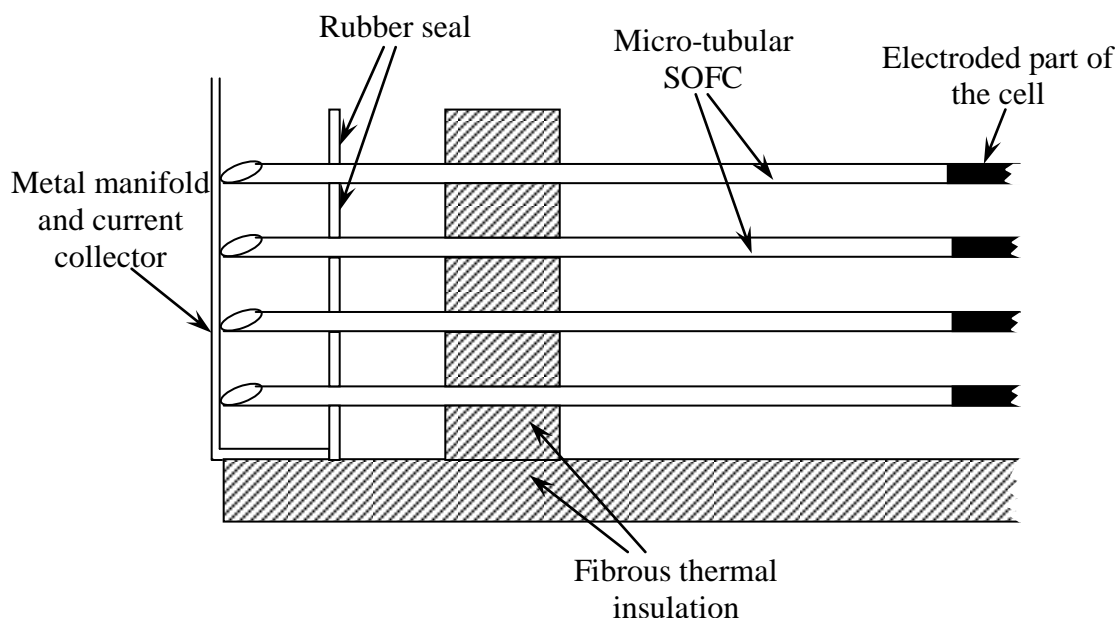


Fig. 2.2 Schematic showing cold sealing concept for micro-tubular SOFC^[50]

It was reported that a stack of 16 micro-tubular cells employing this cold seal system could be heated to 1123 K within 1 minute, thus demonstrating the potential for SOFC cells to form a power generator that would be suitable for small domestic applications.

Cell development

The work published by Kilbride^[51] in 1996 reveals how some of the cell dimensions and materials for the SOFCs used in this study came to be selected. The study outlines the fabrication process and materials used to make SOFC similar to the ones described in Chapter 3 of this thesis and a number of key design issues were investigated.

In the course of demonstrating the ability of the micro-tubular SOFC to endure operation under repeated thermal cycling, it was demonstrated that silver wire performed much better than two different Nickel based wires as the interconnect attached to the cathode. The resistance of the silver wire remained low whilst that of the Nickel alloys increased with thermal cycling, with the increased resistance attributed to oxidation of the Nickel

alloys. The failure to find a cost effective replacement for the silver interconnect has meant that it is still used in the cells in this study and its melting point has limited the maximum temperature for stack operation.

The importance of contact resistance, between the LSM cathode and interconnect, to the Ohmic polarisation losses was also discussed in the same paper. Silver ink was applied between the cathode and silver wire to reduce this resistance^[52].

In Kilbride's study^[51], Nickel wire was used as the interconnect attached to the anode but the author reports difficulties in achieving consistency in the connection between the two components leading to differences in contact resistance at the anode. Despite improvement of this system by Adelan Ltd, by replacing the wire with a Nickel mesh, this inconsistency of anode current collection is partly responsible for the variations in electrical performance from the cells used for the 20 cell stack described in Chapter 3.

There is further result from the work presented by Kilbride^[51] that impacted on the design of the cells used in this thesis. It was shown that whilst the current drawn from cells at a fixed cell voltage increased if the length of the cathode was increased, the current per unit area (specific current) decreased. The specific current for cells with a cathode of length 40 mm was 5 times that of a 100 mm cell. The result was attributed to increased current transfer along the length of the cell resulting in higher Ohmic losses. The result implies that power density of a micro-tubular SOFC stack is enhanced by using lots of short cells rather than a small number of longer cells. The case for shorter cells was supported by modelling of the resistance losses in the electrodes^[53]. Following on from these findings

the length of the cathode was further reduced to 25 mm for additional optimisation of power density. The details of the cell designs are described in Chapter 3.

Stack and system developments and potential applications

The micro-tubular design was first utilised as a stack capable of producing significant electrical power, in a 200 cell unit built at Keele University^[54]. This system utilised SOFCs with the Zirconia tube extending out of the furnace through thermal insulation, with a 40 mm section coated with anode and cathode layers. The fuel exited the tubes into a combustion zone above the cells where it mixed with the air that had passed over the cells and was ignited. Heat from this combustion reaction preheated the incoming air to raise the SOFC temperature to 1073 K. This 200 cell device produced 0.1 W.cm^{-2} at 0.7 V which would correspond to around 0.4 W per cell and 80 W for the whole stack. The performance of the cells in the stack was lower than those tested individually prior to their insertion to the stack. This reduced performance was attributed to an 80 K temperature gradient across the active part of the cells, which highlights the importance of management of the temperature profile within micro-tubular stacks and the emphasis given to this issue in this thesis. A cross section of the 200-cell device is shown in Fig. 2.3

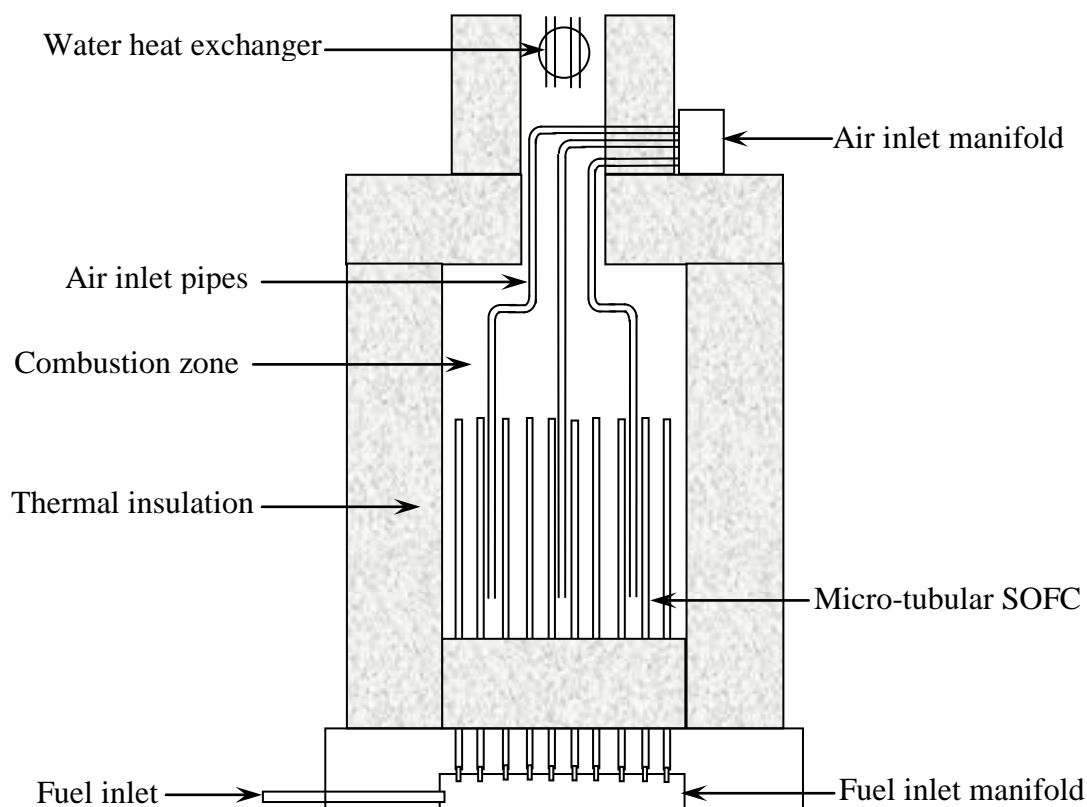


Fig. 2.3 Schematic representation of a 200 cell cold seal micro-tubular SOFC reactor

The 200-cell system was later scaled up to a 1000 cell system with an improved heat exchanger and the electroded section of the tubes reduced to 30 mm. This system was run on both Hydrogen and Methane premixed with air and was used to demonstrate the ability of micro-tubular cells to survive thermal cycling, by subjecting them to 50 cycles from 673 to 1073 K over 3 hours^[55].

Since the 1000 cell stack was built, commercialisation of the micro-tubular concept has been pursued by a number of companies, most notably Adelan Ltd, Nanodynamics and Acumentrics Corp. There has been a little further work published on stack and system designs but some stack concepts have been presented as patent applications ^[56-58].

Acumentrics Corp. have reportedly been working towards the production of a 3-10 kW_e SOFC unit as part of the US Department of Energy's Solid State Energy Conversion Alliance (SECA) program^[59]. The company has reported the shipment of 2 and 5 kW_e SOFC units designed as computer or telecommunication back-up power supplies ^[60-62]. Whilst the technical details of the stack designs used in these systems have not been published, Fig 2.4 shows one proposed design for an integrated SOFC stack and reformer, taken from the 2004 patent application by Acumentrics Corp.

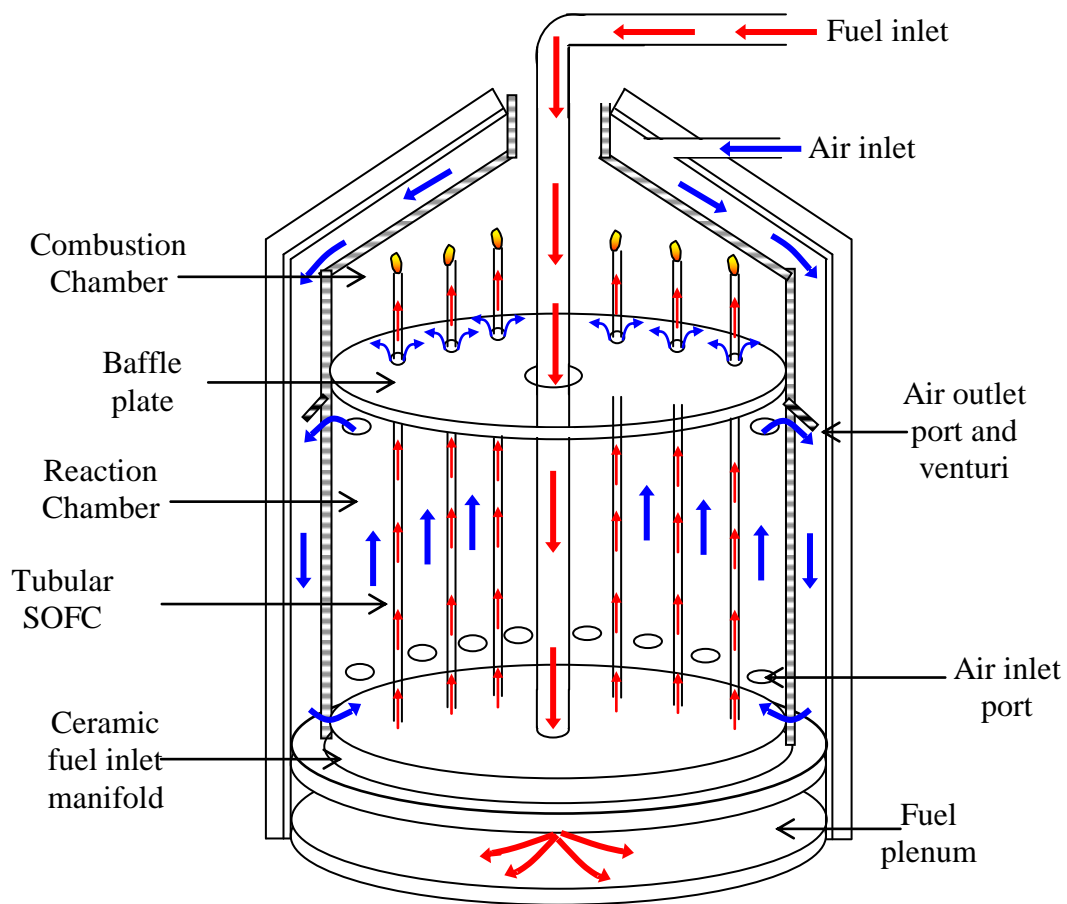


Fig. 2.4 Schematic of a design for a 1.5 kW Micro-tubular SOFC stack^[56]

The stack design shown in Fig. 2.4 is for an 800 cell stack designed to provide 1.2 kW_e when running on Hydrogen. The design is loosely described but it is proposed that the SOFCs to be used in the systems are said to have a length of 500 mm and a 1-5 mm

diameter. As such, they are longer than cells supplied by Adelan Ltd but much smaller than the Westinghouse design. The micro-tubular SOFCs are mounted vertically in a ceramic manifold at the base of the stack. Fuel flows up through the cells from a plenum underneath the manifold. Whilst the cells are sealed to the fuel inlet manifold the outlet end of the cells is open allowing the fuel to mix with air in a combustion chamber at the top of the system. A baffle plate separates the combustion chamber from the reaction chamber, where the electrochemical activity takes place. Whilst allowing some air to pass into the combustion chamber, the baffle plate encourages part of the air flow to be drawn through an orifice in the walls of the chamber for recycling. The recycled air mixes with fresh air flowing in an annulus around the reaction chamber, before being re-introduced at the bottom of the system.

It is reported that the system is heated to its operating temperature within 1 minute of ignition of the fuel in the combustion chamber. This is achieved using a flow of fuel 5 to 10 times higher than the nominal gas flow required for electricity generation during start-up such that a 1 kW_e system would use an additional 10-20 kW of heat during start-up.

The system described in the patent application appears similar to the design of the 1000 cell stack discussed previously^[55]. The drawback of these systems, using longer cells to allow sealing in cold or cooler regions of the stack, is that extending the section of the electrolyte not coated with electrodes means that the volume of the stack is increased, reducing the power density of the system. In contrast, the cells supplied by Adelan Ltd. for this thesis were 55 mm long with only 30mm of uncoated electrolyte. This means that the same amount of electrical power could be produced in a smaller volume than for the Acumentrics stack. Shortening the length of the ceramic cells, which are inherently

fragile, should also reduce the chance of cell breakage, which is particularly important if the stack is to be robust enough for portable applications. The drawback of using the shorter cells was the need to seal the cells to the fuel manifolds in high temperature regions of the systems. This problem is discussed in the subsequent Chapters of this thesis. No work on stacks using the shorter design of small diameter stacks has yet been published, other than that produced in the course of this study^[63].

Reaction with hydrocarbon fuels

The ability of SOFCs to use readily available fuels such as natural gas without extensive treatment makes them one of the most attractive types of fuel cells for the present day fuel economy. There are 3 potential system designs for the reforming of natural gas in a SOFC system.

- a. External reforming- carried out in a separate reforming reactor outside of the SOFC stack
- b. Indirect internal reforming- performed in a reforming reactor incorporated into the SOFC to make use of the heat generated by the SOFC reactions
- c. Direct internal reforming- performed within the stack on the SOFC anodes.

Method c. is possible in SOFCs due to the high operating temperatures and because the Nickel catalyst that is typically used as an anode can act as a reforming catalyst. If steam reforming is used, this reaction is endothermic so heat can be supplied from the heat released as a by-product of the electrochemical reactions. Thus use of internal reforming can increase the simplicity and efficiency of a SOFC system. The drawback to direct internal reforming is that, under certain conditions, Carbon is deposited. A number of studies have looked at reaction of hydrocarbons and Carbon deposition in micro-tubular

SOFCs^[64-66]. As a result of developments in this area it has been demonstrated that micro-tubular SOFC can run on a range of fuels from gaseous fuel such as methane^[67], biogas^[68,69], propane and butane^[70-72], to liquid fuels^[66]. During investigations into the effect of reactant mixtures on Carbon deposition, Kendall et al.^[66] found that diluting Methane with Carbon dioxide reduced Carbon deposition on Nickel anodes compared to pure Methane. The implication of this work is that recycling of the anode stream with a high recycle ratio may improve the operation of SOFCs running on Methane. With a view to producing a system in which the anode stream could be recycled, the stack designs discussed in this thesis involve the collection of the depleted fuel stream leaving the cells rather than combustion of this mixture as used in previous micro-tubular stacks.

2.3 Modelling of SOFCs

2.3.1 Overview

Over the past decade extensive effort has gone into development of comprehensive fuel cell models. Models have been sought as a tool to predict performance and improve understanding of the factors affecting fuel cell performance^[73]. With the time and cost required to build and test SOFC stacks, the use of computer simulations allow design considerations and operating conditions to be evaluated more efficiently, to speed up the progression of SOFC designs.

The existing literature covering modelling of SOFC studies can be classified in a number of ways based on either:

Chapter 2- Literature review

- The specific type of SOFC modelled
- The processes included in the model
- The scale of the model
- The methods used

Models have been developed for most of the various designs of SOFC including large tubular cells^[74-80], planar^[81-98] monolith^[99,100], and also for variations on these such as the integrated planar design^[99,100]. So far there has been little work on the modelling of micro-tubular SOFC and the work that has been done is reviewed in section 2.3.2

In the remainder of this Chapter, the literature covering the modelling of other SOFC designs has been reviewed based on the processes included in the model. In a recent review of modelling of SOFC the author concluded that there is an absence of a comprehensive approach capable of fully coupling fluid flows, species transport, heat transfer and electrochemical kinetics^[105]. With no clearly defined approach, it was therefore useful to look at how previous models have dealt with each of the processes occurring in a SOFC stack, then to discuss the modelling of micro-tubular stacks.

Many of the processes occurring within a SOFC happen at different length scales, ranging from the atomic-molecular level, via the cell component level, the cell to stack level, and finally to the system-level^[73]. It is difficult to include detailed modelling of the processes happening at a molecular level or cell component level in a model of the operation of the whole SOFC stack or system as the computational requirements can become enormous. Therefore models tend to be aimed at a particular level. This study was concerned with processes at the stack level but there was discussion of how work carried out at smaller and larger scales could be incorporated into a stack model and the limitations to this.

The methods used in existing models vary from 3-D finite volume modelling with energy and mass balances coupled to the electrochemical reactions^[85], to treatment of the SOFC as a plug flow reactor with uniform properties^[106]. Many of the models are for steady state conditions but others have included modelling of transient behaviour during changes in electrical load^[87,97], or for start-up^[92] and cool down^[83].

2.3.2 Modelling of micro-tubular and small SOFCs

There has previously been no work reported on the modelling of SOFC stacks with cells of a similar design to those used in this study. However, Ota *et al.*^[107] carried out modelling of a SOFC cell based on the Westinghouse design but scaled down to the dimensions of the micro-tubular cells used in this study. The model incorporated modelling of the current and temperature distributions and used the 'slice technique' to split the tubular SOFC into sub units along its length. Each 'slice' was then meshed concentrically. The cells were modelled with Hydrogen as the fuel and with the gas concentration assumed to be uniform in each slice. The temperature was assumed to be uniform through each slice and heat transfer through neighbouring solid slices was neglected, as this was assumed to be small compared to heat transfer between solids and fluids. The current distributions were calculated as a first step; from these results the temperature distribution and the heat generated within the cell were calculated. The model was used to show that the temperature gradient, over a given length, in micro-tubular cells would be higher than in large tubular cells. This showed that the resistance of micro-tubular cells to thermal shock, demonstrated by Kendall *et al.*^[50], was likely to be due to the resistance of the design to stress, rather than a reduced temperature gradient. The limitation of this study was that the heat transfer between adjacent cells and between the SOFCs and the surroundings via the thermal insulation was neglected. This approach

is probably valid for modelling of a cell at the centre of a stack of several hundred SOFCs, but as the number of the cells is reduced, or the position of the cell modelled moves closer to the edge of the stack, it is likely that the heat losses to the surroundings will have a significant influence on the temperature distribution along the length of the cell.

The other reported simulation of a micro SOFC system considers a SOFC stack with two burners fabricated in a silicon stack^[106]. The proposed model and optimisation methodology assumes that heat transfer within the stack is fast enough that the stack can be assumed to be at uniform temperature. Practical investigation has already shown that significant temperature gradients exist in stacks using the micro-tubular design of YSZ electrolyte^[54]. The only other modelling of the micro-tubular SOFC was that referred to previously in section 2.2 in which the losses due to the passage of current along the length of the cell are modelled^[53].

2.3.3 Fluid Flow and Mass transfer

The level of detail used to model the heat transfer through SOFC varies significantly from assumption of plug flow behaviour to detailed analysis of the diffusion of species through the porous electrodes.

The assumption of plug flow has enabled authors to simplify the model of gas flow to a one dimensional problem making it possible to include fairly detailed modelling of the electrochemistry. This approach was used by Costamagna *et al.*^[101] to simulate the behaviour of an arrangement of 3 integrated planar SOFCs and was used to estimate the

contribution of different forms of polarisation losses under different conditions. Planar or monolith SOFCs lend themselves to this form of simplification much more readily than tubular cells because both the air and fuel flows are confined to a regular channel. In a micro-tubular stack the flow of air is relatively unrestricted, with the air flow likely to flow across neighbouring cells rather than just along the length of a particular cell. It is quite difficult to achieve true co-current flow or counter current flow in a micro-tubular stack without a complicated manifolding system, or baffles, to distribute the air evenly at the inlet end of the cell and collect it at the outlet end. The flow in the micro-tubular stack investigated in this thesis could not be simplified in this way.

Other authors, such as Pei Wen Li *et al.*^[77], have reduced the modelling of tubular cells in a stack to a 2-D axial-symmetric problem. The boundary of the model was drawn around the cell as shown in Fig 2.5

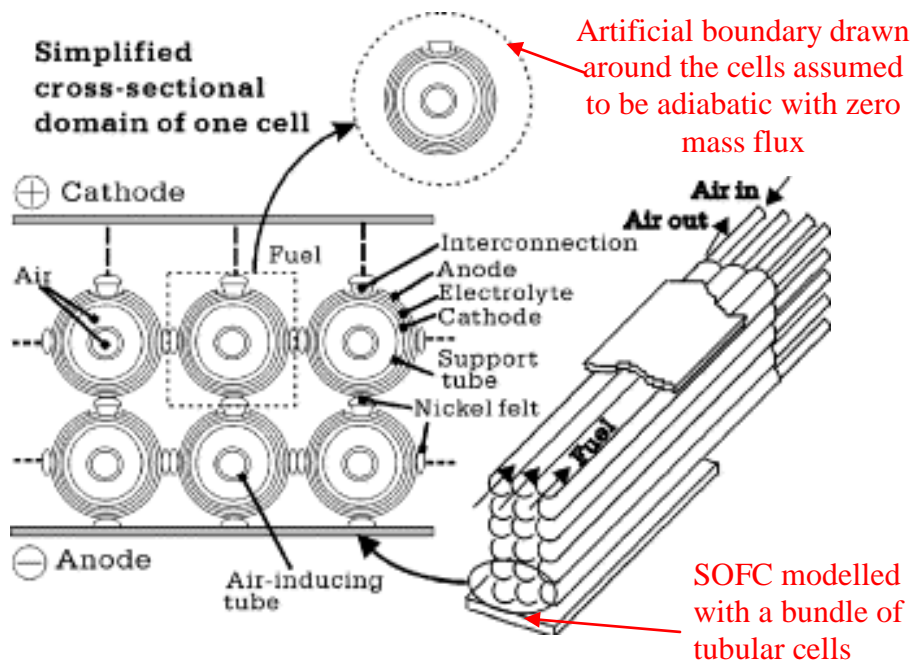


Fig. 2.5 Diagram showing simplification of tubular SOFC model by Pei Wen Li *et*

al.^[77]

It was assumed that no mass or energy was transferred across this boundary marked with the dotted line in Fig. 2.5 and then symmetry was used to reduce the model to a 2-D problem. Equations were derived and solved for the conservation of mass, species, charge and energy using finite volume methods. As with the assumption of plug flow, the limitation of this approach for a micro-tubular system is that the assumption of zero flux across the artificial boundary drawn up around the cell is not likely to be valid as it is difficult to direct the flow so that it only moves in the direction parallel to the walls of the cells.

With no obvious method of simplifying the modelling of flow for a micro-tubular stack, it was decided to model a micro-tubular stack using a 3D commercial computational fluid dynamics (CFD) package. This approach had been used previously in the modelling of planar and monolith SOFC stacks^[85,98,108,109] and is discussed in more detail in Chapter 4.

2.3.4 Electrochemical reactions

Modelling of the electrochemical reaction inside the fuel cell can be based on the potential balance for the fuel cell which can be written as follows:

$$V_0 = E_{eq} - iR_i - \eta_C - \eta_A \quad \text{Eq.2.1}$$

Where V_0 represent the operating voltage, E_{eq} is the equilibrium, or open circuit voltage, i is the current, R_i is the Ohmic resistance and η_A and η_C are the anode and cathode polarisation losses respectively^[110].

The most general expression for the reversible voltage in a SOFC is given by the Nernst equation in the form:

$$E_{eq} = \frac{RT}{4F} \ln \frac{P_{O_2,C}}{P_{O_2,A}} \quad \text{Eq.2.2}$$

For a certain partial pressure at the cathode the concentration of Oxygen at the cathode can be related to the composition of the fuel supplied to the anode^[73]. For example for Hydrogen fuelled SOFC Eq.2.2 would become:

$$E_{eq} = E^0 + \frac{RT}{4F} \ln P_{O_2,C} + \frac{RT}{2F} \ln \frac{P_{H_2,A}}{P_{H_2O,A}} \quad \text{Eq.2.3}$$

Where E^0 is defined as the standard cell potential. Eq.2.1 can be re-arranged to provide the expression for the operating current under a given set of operating conditions:

$$i = \frac{E_{eq} - \eta_C - \eta_A - V_O}{R_i} \quad \text{Eq.2.4}$$

If the composition of the fuel and the operating conditions are known the open circuit voltage can be calculated using Eq.2.3 but there remains the problem of the calculation of the polarisation losses at the anode and cathode. Estimation of these polarisation losses is less straightforward and generic, as they vary non-linearly with the current density and they depend on the exact formulation and fabrication of the fuel cell components. The voltage losses due to polarisation can be split into those due to activation polarisation at the anode, η_{Aa} , and cathode, η_{Ca} , and those related to concentration polarisation at the anode, η_{Ac} , and cathode, η_{Cc} .

Activation polarisation is most influential when the current density is low^[73], and relates to the voltage loss incurred due to the activation of charge transfer. The losses due to activation polarisation have often been modelled using the Butler-Volmer equation^[73]:

$$i = i_0 \left\{ \exp \left[\frac{-\alpha z F \eta_a}{RT} \right] - \exp \left[\frac{(1-\alpha) z F \eta_a}{RT} \right] \right\} \quad \text{Eq.2.5}$$

Where z is the number of electrons participating in the reaction and α is the anodic transfer rate, lying between 0 and 1. i_0 is the exchange current density, which corresponds to the dynamic electron transfer rate at equilibrium, and can in turn be expressed by:

$$i_0 = P_x \exp\left(\frac{-E_{act}}{RT}\right) \quad \text{Eq.2.6}$$

E_{act} is the activation energy and along with the pre-factor P_x is specific to the electrode/electrolyte phase being modelled. Since the factors P_x , α , E_{act} , and z are all specific to the materials used to form electrodes and electrolyte and the micro-structure, use of Butler-Volmer equation requires extensive calibration and validation experiments for which very small cells, known as button cells, are often used. The Butler-Volmer equation, or the simplified form of the equation for operation at high current densities known as the Tafel equation, has been used in numerous previous works to calculate the effect of concentration polarisation^[100,101,111-119], although it is less common for this level of detail to be included in modelling at the stack level^[114,117,118].

Concentration polarisation relates to losses due to the mass transport of the reactant from the bulk anode and cathode gas flows to, or close to, the interface of the electrodes and the electrolyte^[120]. Concentration polarisation is most influential at high current densities, when the fuel utilisation is high or when the concentration of fuel species in the anode streams is low. Various models for concentration polarisation have been formulated, based on relationships for the mass transport of reactant and product species to and from the active sites at the electrolyte/electrode interfaces. The mass transport is influenced by the operating pressure, temperature, concentration but like activation polarisation it is also strongly dependent upon the micro-structure and properties of the electrodes. Many previously reported simulations of SOFCs at the cell level or cell component level have

included modelling of effects of concentration polarisation^[88,90,91,100,101,113,121,122] but this level of detail is rarely practical for modelling of a complete stack.

2.3.5 Heat transfer

The challenge for designers of SOFC systems is to meet the high temperature requirements of the SOFC operation whilst minimising temperature gradients and avoiding the formation of 'hot spots' where the stack temperature rises above a maximum temperature determined by the material properties of the cell components. Measuring temperature within the SOFC stack can be difficult and expensive, particular when testing new operating conditions which may lead to damage to the stack. Therefore, modelling has a key role to play in improved understanding of how heat transfer affects the operation of SOFCs and to provide guidance for optimisation of stack designs.

2.3.5.1 Heat losses to the surroundings

The heat lost from the stack can be difficult to estimate as the wall temperature may vary considerably across its area. As such, heat losses by conduction to the surroundings have frequently been ignored, even in some of the most comprehensive previous models^[85,98]. In large SOFCs, a large amount of heat is generated within the stack and excess air is required to remove heat and prevent overheating. The effect of this heat generation and the convective heat transfer with the air flow may be the dominant heat transfer process within a large SOFC system, such that the assumption of adiabatic conditions at the periphery may have little effect on the cell temperature. In contrast to this cooling problem, SOFC units producing in the region of 100 W_e require efficient thermal insulation to prevent heat loss from the stack^[105]. From initial investigations, carried out using finite element modelling, it was estimated that the heat loss from a stack with enough volume to house 36 cells capable of producing 0.5 W each would be around 20 W

even if 50 mm of high quality thermal insulation surrounded the stack (see appendix 1). Therefore, unlike most previous models of SOFCs, it was thought that for a micro-tubular stack accurate modelling of the heat losses to the surroundings should be an important part of the model. The detailed modelling to the surroundings through the thermal insulation is one of the significant new aspects of this thesis.

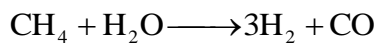
2.3.5.2 Heat generation

The principle source of heat generation in SOFC stacks is that caused by Ohmic heating due to the resistances of the fuel cell components. Thus the rate of heat generation varies with the current density. In order to estimate the local rate of heat generation, the localised current distribution, potential difference and resistance of the fuel cell components are required. The localised current distribution will in turn be determined by the pressure and the concentration of fuel and Oxygen in the anode and cathode bulk flows and the losses due to various polarisation processes. An example of a study where the local rate of heat generation has been calculated is the 2-D axis-symmetric model by Pei Wen Li *et al.*^[77], where the finite volume approach was used to calculate the local heat generation rate. The limitations of this model have been discussed in section 2.3.5.1, but the model facilitated investigation of the effect of current density on temperature profile, and from this it was predicted that the hot spot in the cell would shift along the length of the cell depending upon the operating conditions.

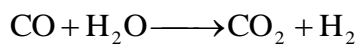
Commercial CFD codes have also been adapted to predict temperature distributions influenced by heat generation from Ohmic losses. This approach has been used to produce data suitable for use with other models designed to look at the critical issue of the effects of thermal stresses on the mechanical integrity of the fuel cell components^[123].

The heat balance within an SOFC becomes more complicated if the fuel cell is fuelled by a reformed hydrocarbon or if reforming takes place inside the SOFC. Both the steam reforming reaction and the shift reaction, which converts Carbon monoxide to Hydrogen, are endothermic.

Steam reforming reaction:



Shift reaction:



This can lead to the creation of cold spots in regions of the cells where these reactions are most prevalent. In these cold spots the reduced temperature will suppress the rate of electrochemical reaction, and subsequently the rate of heat generation by Joule heating which would exacerbate the problem of localised cooling.

The effect of the shift reaction and steam reforming has been included in the energy balance within a number of previous SOFC models. Achenbach^[87] compared cross current, co-current and counter-current flow configurations for cells in a planar stack. It was found that the rapid reforming reaction caused cooling and the largest temperature gradients in the cross current mode, whilst co-current flow produced the most even temperature distribution. However, the most efficient operation was obtained with counter current flow. This finding was supported by the work of Ferguson *et al.*^[124] who showed the temperature distribution obtained for counter current flow is better for the efficiency of the reforming reaction. The focus of the simulation of Yakabe *et al.*^[98] was to minimise the stress developed in planar cells due to temperature gradients and it was found that this was best achieved using the co-flow orientation, which was also in agreement with

reference 87. It was found that the endothermic internal reforming produced cooling in the section of the cell adjacent to the fuel inlet. The more even temperature distribution created by the co-flow configuration can be attributed to the fact that this cooling can be offset by rapid heat generation due to Joule heating when the air and fuel streams meet without having been depleted by electrochemical reaction. In the simulations performed by Recknagle *et al.*^[85] the anode was fed with pre-reformed gasoline and no reforming reactions took place inside the fuel cell, however, the co-flow configuration was still found to give the most even temperature distribution. This was attributed to the fact that rapid rate of reaction next to the fuel inlet where the fuel concentration was highest, was aligned with where the cold air entered the stack.

2.3.5.3 Radiation

With the high operating temperature of SOFCs, radiation would be expected to play a significant part in the heat transfer process within a stack. Murthy and Federov^[108] showed that inclusion of radiation in the modelling of heat transfer in monolith SOFC significantly affected the predicted temperature profile. Yakabe *et al.*^[98] also compared the profile along a SOFC with and without radiation modelling and found a more even temperature distribution and lower maximum temperature when radiative effects were considered. However, in this work radiation was only included in single cell models as its inclusion was found to increase the computation time for the solution to reach convergence by a factor of ten compared to one when the CFD model only accounted for convection and conduction.

The difficulties in calculating radiation transfer has led authors to omit heat transfer by radiation from their simulations^[84,99,124]. In addition some of the other models have only

included radiation by incorporating it into an effective thermal conductivity^[81,87,97]. The problem with this approach, as reported by Petruzzi *et al.*^[81], is that the value of the effective thermal conductivity will vary greatly as a function of temperature and the operating conditions, so unless extensive experimental data is available for calibration, then this may introduce significant inaccuracies into the model. Other models to include radiation have restricted its influence to that between a limited number of the stack surfaces, such as between the outer surfaces of the bottom and top cells and the internal wall of the furnace^[82,86], while some models of tubular cell have only considered the radiative transfer between the internal wall of the tubular cells and the air preheat tube inside them^[77,107].

In other reported models^[81] the exclusion of the effects of radiation have been justified on the basis that its effect on the temperature profile may be considered small if channel length for gas flow in the fuel cells is small compared to the cross section of the channel. This assumption may be valid inside the interior of the micro-tubular cells and between the external surface of cells if they are closely packed. From the literature there is no clear solution for the treatment of radiation in a stack model particularly in a tubular stack where there are many adjacent surfaces between which radiation could be exchanged.

2.3.6 Modelling of transients

Most of the previous work that has been reported on the modelling of SOFC has been based on steady-state conditions but transient situations are of critical importance to the operation of SOFCs.

The start-up of SOFCs is a crucial part of its operation. As this may involve heating the stack from room temperature to over 1000 K, start-up needs to be carefully orchestrated for most SOFCs to avoid sharp temperature gradients which could result in damage to the ceramic components due to thermal shock. There is little previous work on the modelling of this part of the SOFC operation. Petruzzi *et al.*^[81] modelled the start-up of a planar SOFC stack, designed to act as an auxiliary power unit (APU) for an automobile, using a global heat transfer co-efficient to model the heating of the SOFC to its operating temperature. The simulations predicted problems with temperature gradients and a slow heat-up time of over 20 minutes. With micro-tubular cells the issue of thermal shock is less of a problem but the question of how the stack can be raised to its operating temperature most efficiently is an important one if the potential for rapid start-up is to be realised.

Once the operating temperatures have been established, the next transient event a SOFC may be likely to be subjected to, is a change in electrical load. Increasing the electrical load applied in the external circuit reduces the electrical efficiency of the stack and increases the magnitude of the heat generated in the stack. Simulation of the effect of changes to the current density in planar cells was reported by Achenbach^[97]. From the simulation results it was predicted that it would take 400 to 600 seconds for a steady-state voltage to be re-established, in response to a step change in current density from 500mA to 400mA depending upon the properties of the bimetallic plate. Whilst the relaxation time was sensitive to the cell characteristics, such as the material properties, it was relatively independent of the size of the step change in current density. The maximum temperature in the stack took a similar duration to reach a new steady state value as the cell voltage. A strong dependence between the relaxation time and the cell design

parameters was also found by Ota *et al.*^[107] in the simulation of changes to the operating voltage in tubular cells. The predicted time for a steady-state power output to be restored, after an decrease in operating voltage from 0.7 to 0.5V, was 120 seconds for a standard Siemens Westinghouse cell. When the dimensions of the cell were scaled down to those similar to micro-tubular cells, the simulation predicted that the steady-state power output would be reached within 15 seconds. From these results it appears that the transient response to changes in load is probably less of a significant issue for micro-tubular SOFCs than for larger SOFCs.

The third transient process in SOFC operation to be simulated is the cool-down of the stack. In applications such as vehicle APUs, the long heat-up times associated with most SOFC designs could not be tolerated. Therefore, Chen *et al.*^[83] investigated how long from when a stack is switched to open circuit, it will take to cool from its operating temperature, to below the temperature required for it to be capable of producing power. It is highly desirable for this duration to be longer than the expected interval between power being drawn from the SOFCs as this will eliminate the slow heat-up phase. This cool-down phase was simulated for planar SOFCs with a normal operating temperature of 1273 K, but capable of producing power above 1073 K^[83]. The cool-down was simulated with three different insulation configurations: 5 cm of insulation with a thermal conductivity of 0.17 W.m⁻¹.K⁻¹; 5 cm of insulation with a thermal conductivity of 0.03 W.m⁻¹.K⁻¹; and 1 cm of insulation with a thermal conductivity of 0.001 W.m⁻¹.K⁻¹. It was found that the predicted time taken to cool from 1273 K to 1073 K was 2 hours, 6 hours and 31 hours for these configurations respectively. The second insulation configuration was similar to that used in the experimental and modelling work in this thesis. With a micro-tubular SOFC stack, which is capable of being heated-up at a rapid rate from room

temperature, a slow cool-down may be disadvantageous as fuel or inert gas is required to be circulated across the anodes until the stack temperature is below 700 K to prevent re-oxidation of the anodes.

2.4 Conclusion

There is a growing collection of literature on solid oxide fuel cells, some of which has been reviewed in this Chapter. There is a more limited collection of work specific to the micro-tubular design of SOFC and the work that has been published tends to focus on cell development, demonstration of advantages and properties of the design, and electrochemical reactions with a variety of fuels. There is a shortage of work on stack design and the operating parameters for a stack, particularly for short cells designed to be manifold inside the hot part of the stack.

Numerous works on the computer modelling of SOFC behaviour have been published and many of them were reviewed briefly in this Chapter. Most of these previous works had a particular focus in terms of the type of SOFCs modelled, the scale of the model, or the processes considered. Little of the previous work includes modelling of temperature gradients through a SOFC stack, a critical issue in stack operation. In the simulations that have included modelling of temperature gradients, factors such as the heat loss to the environment, more important to the operation of small stacks, have been neglected by the assumption of adiabatic boundary conditions. Also little work has been presented on the study of the transient behaviour during start-up. Moreover, many of the models in the literature have not been verified experimentally^[83-86,99,100,107,124].

Chapter 2- Literature review

The work that follows in the rest of the thesis was aimed at helping to satisfy the shortage of literature on micro-tubular SOFC stack design. These included the complex flow of air around the tubular SOFC, accurate simulation of heat loss to the environment, and leakage. To validate the model, an experimental system was developed and is described in Chapter 3.

3. Experimental system

3.1 Introduction

This Chapter discusses the development and operation of a 20 cell experimental system used to investigate heat transfer in a micro-tubular SOFC stack. The Chapter begins with a discussion of the single cell test used to characterise the electrical performance of the cells used in this study. This is followed by a description of a 4 cell system developed to demonstrate the potential of micro-tubular SOFC to form a rapid starting portable power generator. This unit was the basis for scale-up to the 20 cell system discussed in the remainder of this Chapter. The 20 cell system was tested and shown to take about 1 hour to warm up, which is too slow for rapid start-up applications.

The operation of larger stacks of 200 and 1000^[67] cells and smaller systems from single cells^[64-69,71,125] to 3^[71] or 5^[126] cells has been reported previously in the literature but no work on a 20 cell micro-tubular stack of this size has been reported. The main purpose of this experimental system was to identify the parameters that have the greatest influence on the temperature in the micro-tubular SOFC stacks. The apparatus was also used to provide temperature profile data that could be used to validate the computer model described in Chapter 4.

3.2 The cells

The electrolyte supported micro-tubular cells were supplied by Adelan Ltd. The cells had an internal diameter of approximately 2 mm and were 55 mm long. The electrolyte was 8 mol% yttria stabilised Zirconia (8YSZ) formed into a tube by an extrusion process resulting in a wall thickness of approximately 0.2 mm after firing.

Chapter 3-Experimental System

The anode was created by injecting a Nickel and Zirconia cermet ink onto the inside of the electrolyte tubes. This was achieved by attaching an automated volumetric pipette to one end of the tube via a silicon tube and sucking the ink up from a reservoir through the other end of the tube. The volume of ink sucked up was such that the inside of the tube was fully coated apart from then 20 mm at the end of the tube. The pipette was then used to blow excess ink out of the tube. The anode cermet was applied in two layers. The first layer comprised of 50% Zirconia and 50% Nickel to help form the interface between the electrolyte and anode. This first layer was allowed to dry before a second layer was applied containing 10% Zirconia and 90% Nickel, to ensure good electrical conductivity.

The cathodes were formed from a Lanthanum Strontium Manganate, LSM, coating that was applied by painting. Fig. 3.1 shows that only a 25 mm section of the tube was coated with the cathode. This section will be referred to as the 'active length'. The cathode was also applied in two layers with the layer closest to the electrolyte tube containing 20% Zirconia mixed with the LSM.

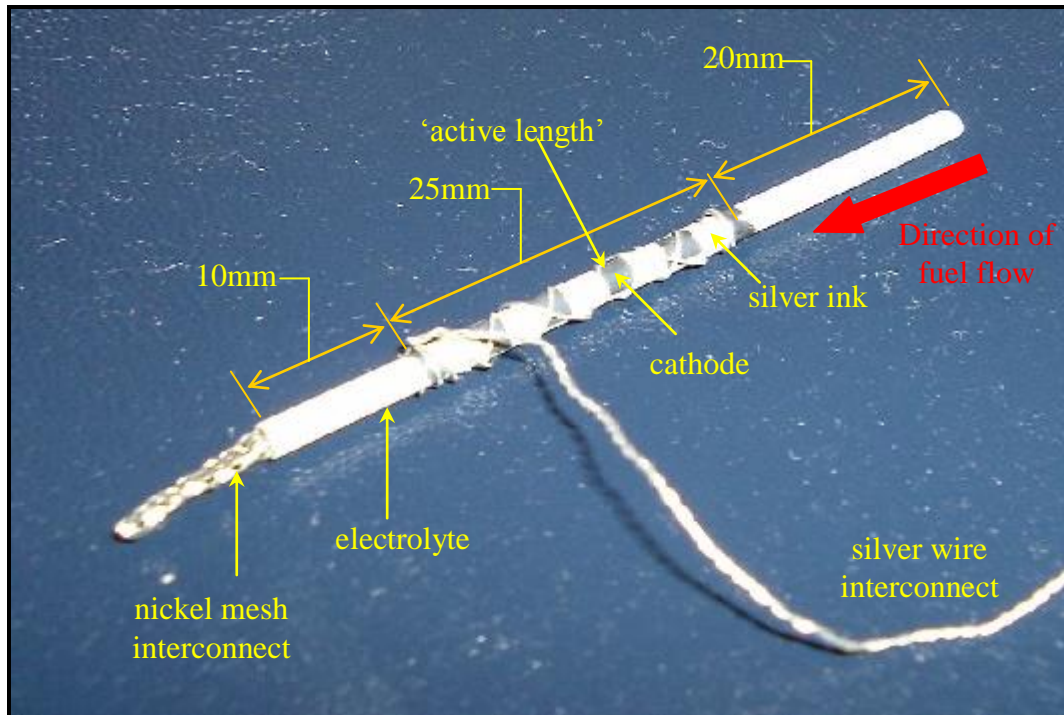


Fig. 3.1 Photograph of a micro-tubular cell

A Nickel mesh rolled into a tube and inserted inside the cell acted as the interconnect from the anode. At the cathode, an interconnect was formed from 0.2 mm diameter silver wire wrapped around the cell and braided to increase its mechanical strength.

3.3 Testing of individual cells

3.3.1. Objectives

The first objective of the testing was to develop a standard test for each cell used in the stack. One of the advantages of micro-tubular cells is that their relatively small size and cost means that it is comparatively inexpensive to carry out single cell tests compared with some of the other SOFC designs. Thus the ease with which feedback on the effect of developments made to cell components can be obtained should speed the advancement of micro-tubular cells. For this purpose a basic single test was developed. This testing procedure was used to check the performance of each of the cells deployed in the 20 cell

stack described in the section 3.5. A similar set-up was also used to test the response of the SOFCs to changes in temperature.

3.3.2. Equipment

In order to control the temperature of a SOFC during single cell testing a furnace was constructed. This comprised of two refractory bricks that were hollowed out to house electrical heating elements and a small manifold to hold a micro-tubular SOFC, as shown in Fig. 3.2.

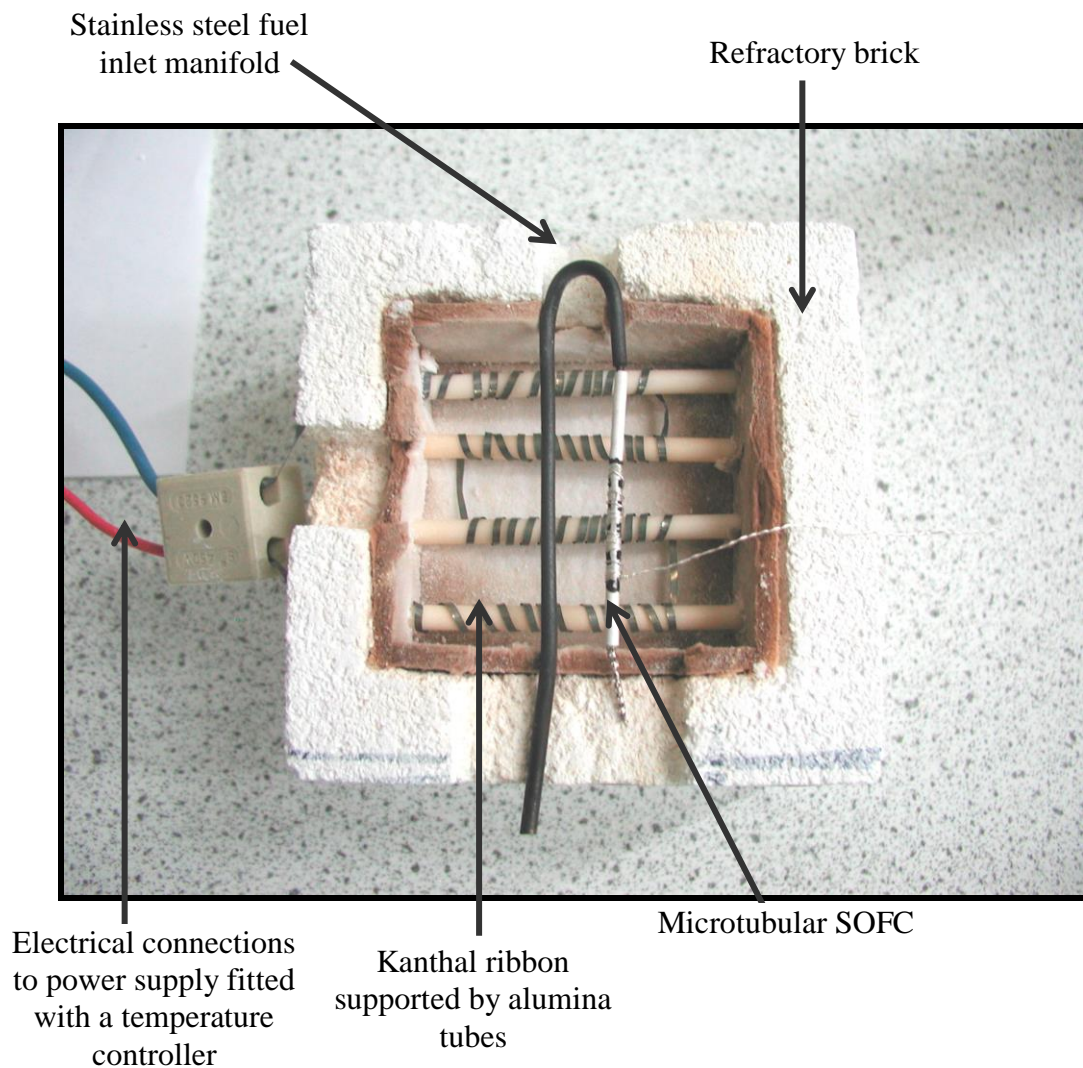


Fig. 3.2 Photograph showing the furnace used for single cell testing

Chapter 3-Experimental System

The heating elements were constructed from Kanthal ribbon, with resistivity 5.476 Ohm m⁻¹ wound around supporting alumina tubing. These heating elements were connected to a power supply fitted with a temperature control device. A thermocouple positioned alongside the SOFC was also connected to the temperature controller so that power supply to the heating elements could be adjusted such that the temperature in the furnace was maintained to a programmed set point temperature.

The fuel inlet manifold was constructed from 1/8" stainless steel tubing and was bent into a 'U' shape so that incoming fuel would be heated on its way through the furnace before entering the cell. A smaller tube welded into the end of the stainless steel tube was designed to fit snugly inside the SOFC being tested. There was no permanent seal between the cell and the inlet tube, allowing the cell to be fitted easily on the gas supply tube. The outlet end of the cell was free allowing unconverted fuel to combust at the exit of the tube.

Silver wire was connected from the Nickel mesh at the anode of the cell to a potentiostat. The wire from the cathode was connected to the other terminal of the potentiostat which completed the external circuit between the anode and cathode. The potentiostat allowed an electrical load to be introduced to the circuit in order to test the electrical output from the cell.

The fuel was supplied to the inlet manifold through a system of mass flow controllers which allowed the cell to be supplied with Hydrogen, Helium, Methane or a mixture of

these or other gases. As only Hydrogen and Helium were required in basic tests a simplified diagram of the system is shown in Fig. 3.3.

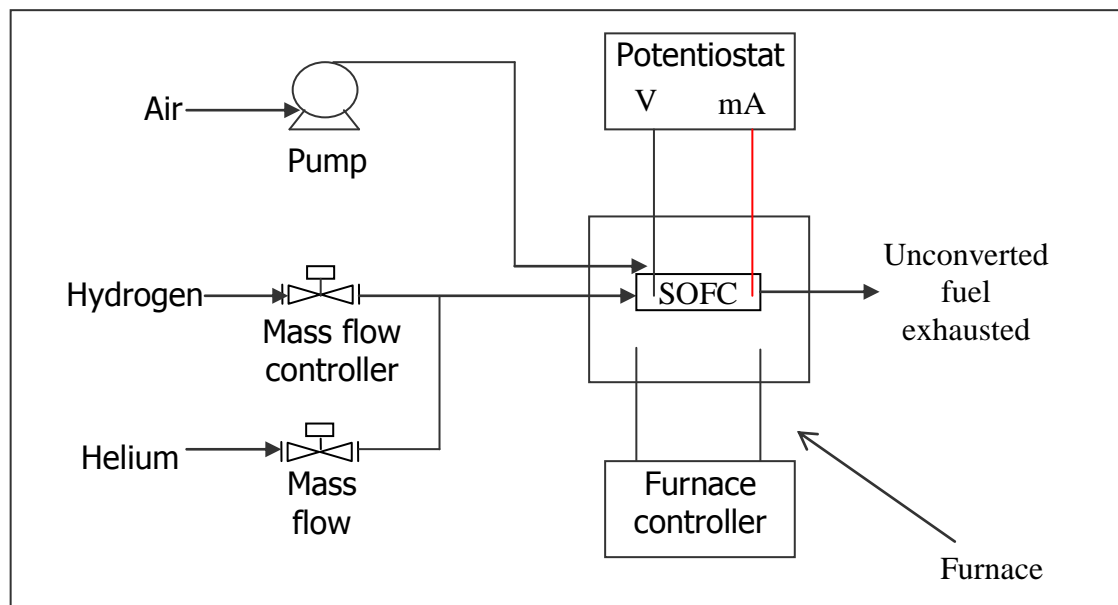


Fig. 3.3 Flow diagram showing the apparatus for single cell testing

3.3.3. Testing procedure

During the standard test to evaluate the electrochemical performance of cells they were supplied with $0.025 \text{ std. l min}^{-1}$ ($3.4 \times 10^{-8} \text{ kg s}^{-1}$) of Hydrogen. The temperature in the furnace was set to 1123 K and the cells were left under these conditions for 30 minutes whilst no current was drawn. The open circuit voltage was then recorded before the potentiostat was used to load the cells. The current produced at 1 V was recorded then the electrical load was increased to lower the cell voltage at 0.05 V intervals down to 0.45 V. The current was recorded at each interval with the load adjusted such that the current stabilised at each voltage before moving on to the next reading. A typical I-V curve is shown in Fig.3.4.

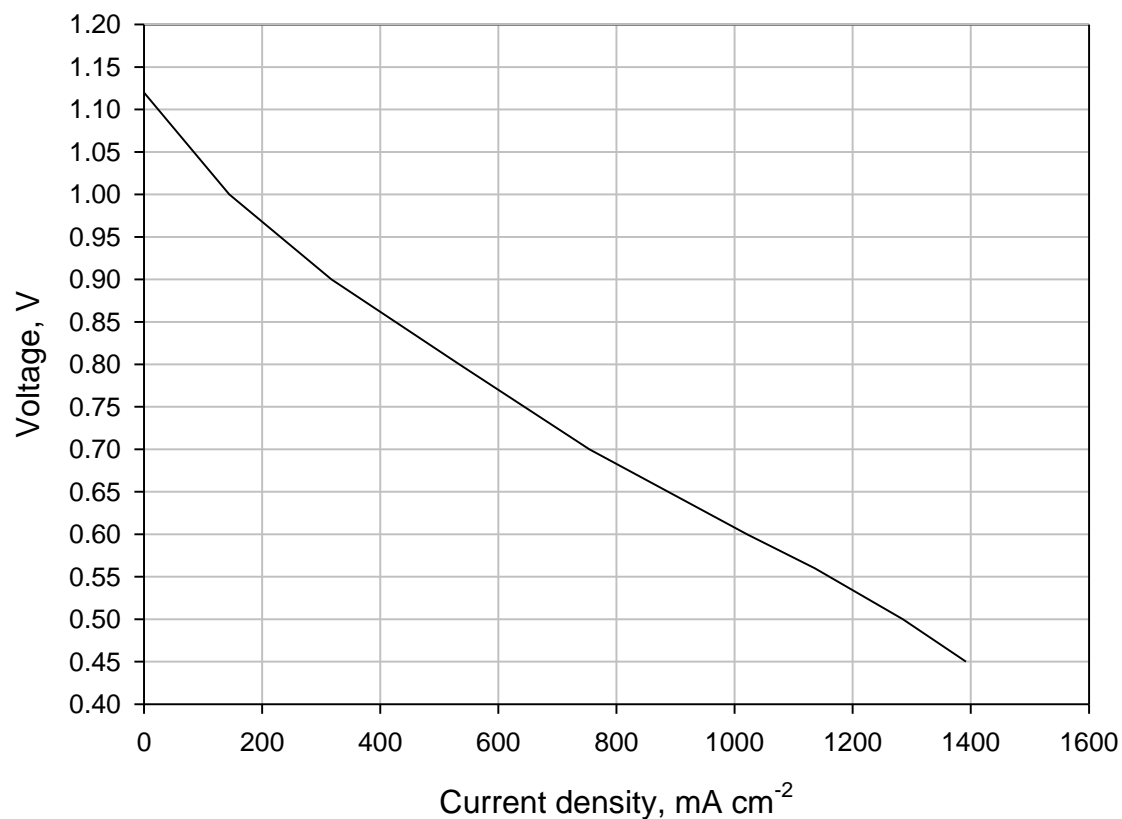


Fig. 3.4 Typical I-V curve for a micro-tubular SOFC at 1123 K with 0.025 std.

1 min⁻¹ of Hydrogen

The plot shown in Fig. 3.4 is for one of the cells used later in this study as part of a 20 cell stack. The area of the electrodes used to calculate the current density was calculated based on the mean area of the anode and cathode, as the tubular design means the area covered by the (external) cathode is slightly greater than that of the anode. The performance compares favourably to that reported for other designs of SOFC cells but the power density of a micro-tubular stack will depend on how closely the cells can be packed^[49].

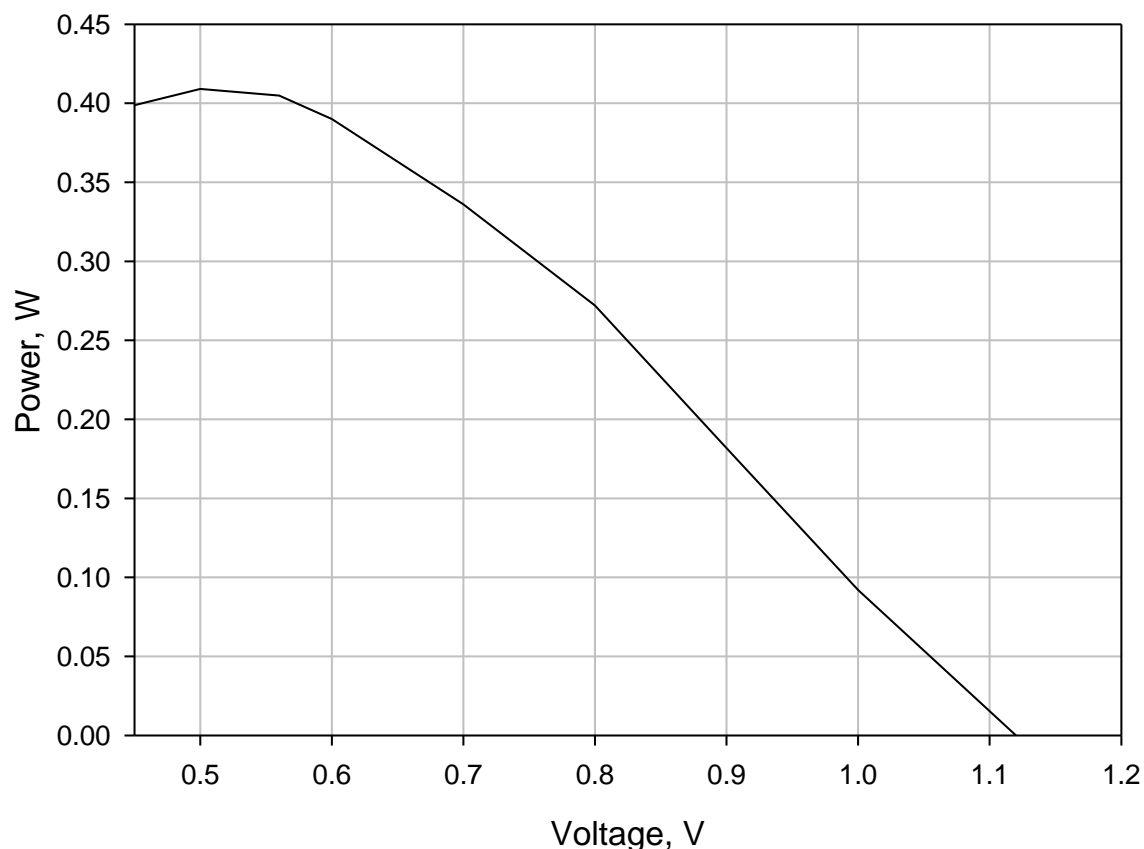


Fig. 3.5 Plot of power versus voltage for a micro-tubular SOFC at 1123 K with 0.025 std. l min⁻¹ of Hydrogen

Fig 3.5 shows the power output increases as the cell voltage across the cell is lowered. The maximum power output, of 410 mW, was recorded at 0.5 V and further reductions to the voltage across the cell yielded a decrease in the power output. After the performance had been recorded the cells were cooled to below 673 K before the Hydrogen supply was switched off to prevent re-oxidation of the anode.

This method was used to check the performance of 30 cells from which 20 cells were selected for the system discussed in section 3.5. The current drawn from these cell at 0.5 V ranged from 0.560 A to 1.022 A, corresponding to 0.280-0.511 W. Whilst it would

have been preferable if all of the cells had more comparable electrochemical performance, the range of outputs reflected the variability amongst each batch of cells prepared at the time of construction.

3.4 Effect of temperature on performance

In addition to assessing the performance differences between individual cells and batches, the single cell test equipment was used to study the effect of the temperature on electrical performance. This was done in order to determine the optimum operating temperature for a micro-tubular SOFC stack and to show how deviation from this temperature would affect the cell performance.

A micro-tubular SOFC was placed in the single cell test furnace and supplied with 0.025 std. $l\ min^{-1}$ of Hydrogen. The cell was heated to 1133 K and was left under these conditions with no current drawn for 30 minutes. After this time the cell was loaded to 0.5 V. Previous longevity testing, to monitor the degradation of cell performance with time, had shown a considerable fall in performance in the first 15 minutes of producing power, before the decline slowed to a much less significant rate. To reduce the effect of the degradation of the cell performance with time, the SOFC was left under electrical load at 1133 K for 30 minutes. Once this time had elapsed the current was recorded. The temperature was then reduced by 10 K and the SOFC was held at this temperature for 5 minutes. The response of the furnace temperature to the change in set point was rapid. The load was adjusted so that the voltage across the cell was 0.5 V and the current was recorded. The procedure was repeated until the temperature had been reduced to 500 K at which point the current drawn from the cell was minimal. The temperature was then

increased at 10 K intervals to check that decrease in performance was due to the temperature and not the inherent decrease in performance with time. Whilst the current recorded at each temperature was slightly lower than the original reading, the curve followed the same trend. This procedure was repeated with 5 cells to check that the trend was consistent for each of the cells.

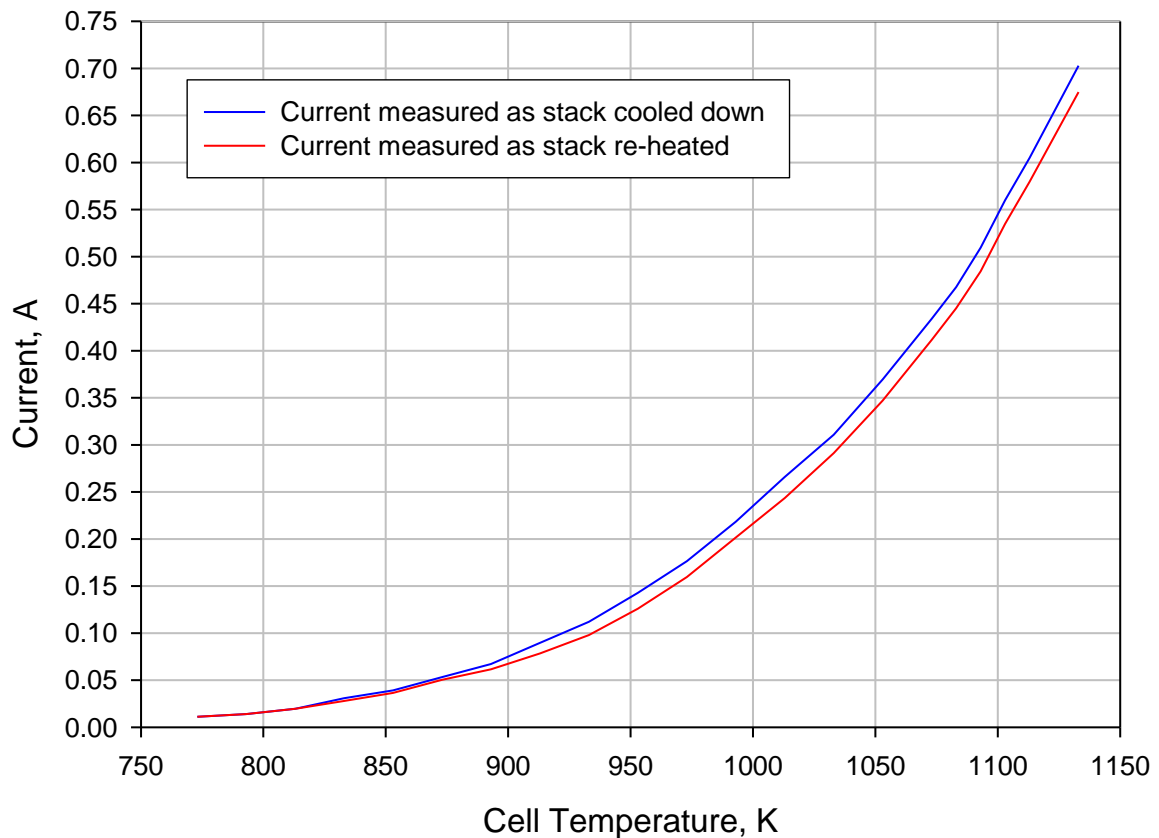


Fig. 3.6 Plot showing effect of the temperature on the current drawn from a SOFC at 0.5 V

The performance of the cell is shown to have fallen by 50% when the temperature was reduced from 1133 K to 1043 K and by a further 50% when the temperature was reduced to 973 K. These results were used to guide the work done in Chapter 6.

3.5 The 4 cell demonstration stack

The 20 cell test unit developed in this study was based upon a 4 cell system developed by Adelan Ltd to demonstrate the potential of micro-tubular SOFCs to form portable power generators. The system provided between 1 and 2 W of electrical power from the four cells which was used to power a range of appliances from multiple personal fans to a radio controlled clock. Whilst the power output was modest, the system was used to demonstrate that a micro-tubular stack could produce power within 2 minutes of start-up and that such a stack could run on a variety of different hydrocarbon fuels. As the 20 cell stack used in the bulk of this investigation was essentially scaled up from the 4-cell system, the details of this system have been presented here to reveal the status of development when this work started.

3.5.1 Overview of the system

The demonstration system was assembled in three sections. The largest section contained the SOFC stack surrounded by thermal insulation and was housed in a plastic box 150 × 150 × 100 mm. This was stacked on top of a second box containing the Balance of Plant, BOP. The system was completed by the control system which was housed in another 150 × 150 × 50 mm unit at the base of the system.

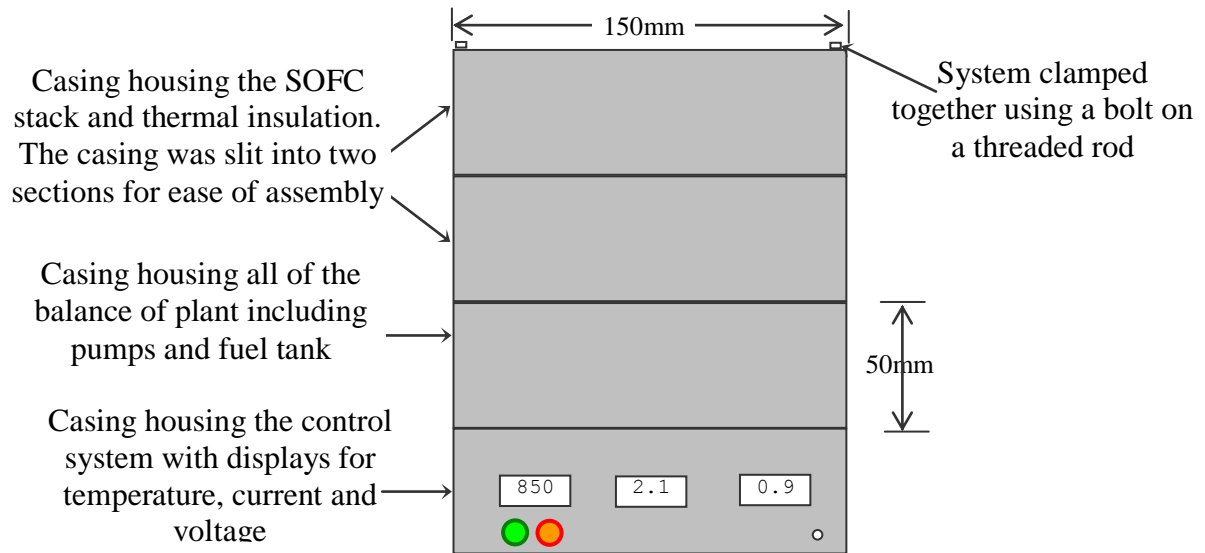


Fig. 3.7 Diagram of the 4-cell micro-tubular SOFC demonstration unit

A flow diagram of the overall system for the 4 cell demonstration unit is shown in Fig.

3.7. Each part of the system has been discussed in the subsequent text.

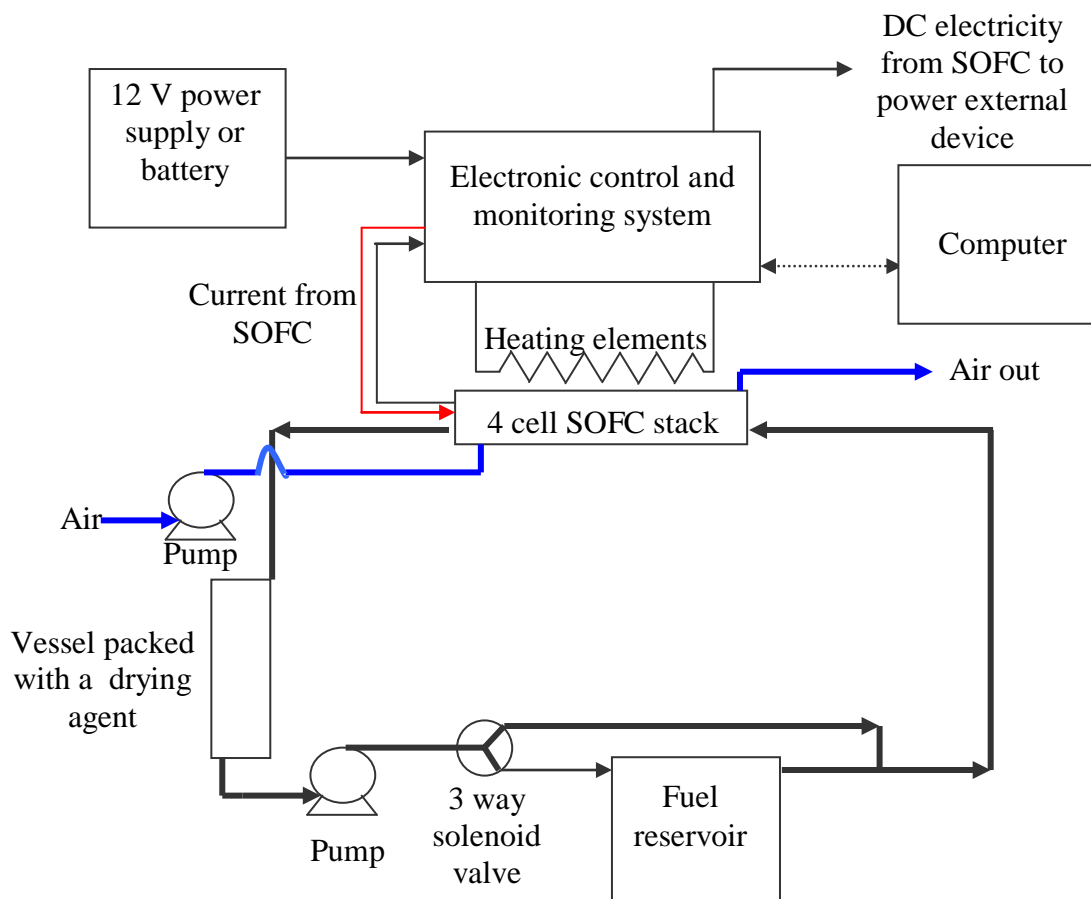


Fig. 3.8 Schematic of the 4 cell demonstration system

3.5.2 The SOFC stack

The cells used were 55 mm long with 25mm coated in electrodes as described in section 3.2. These were supplied with fuel via a stainless steel inlet manifold and the mixture of reaction products and unconverted fuel was collected in a ceramic outlet manifold. A photograph of the complete stack assembly is shown in Fig.3.4.

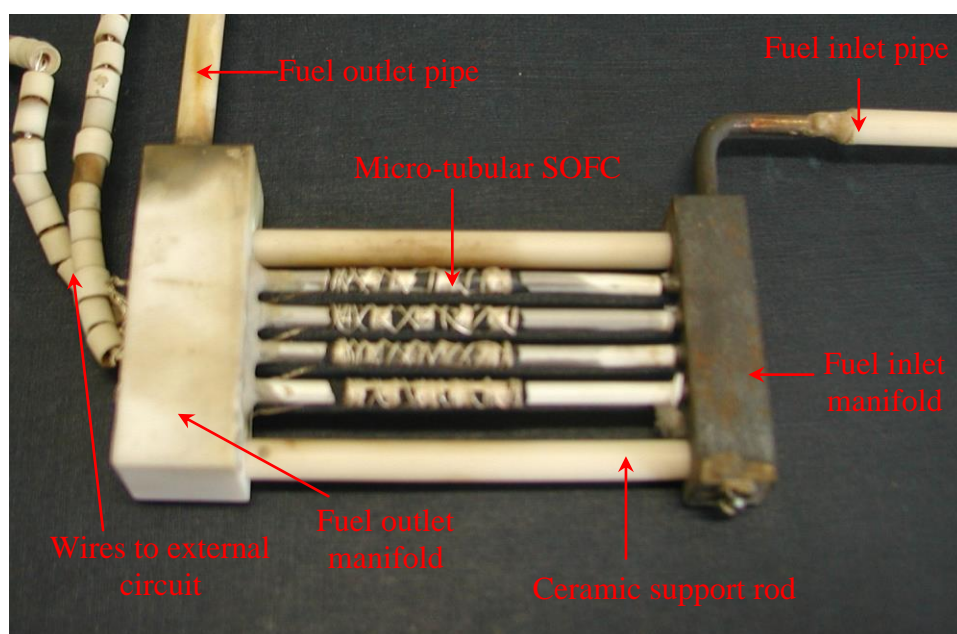


Fig. 3.9 Photograph of 4 cell stack

The fuel inlet manifold was fabricated from a 316 stainless steel block with a 4 mm hole milled through to create a plenum to carry the fuel from the inlet pipe to the cells. Stainless steel tubes with an external diameter of 1.85 mm were inserted into holes drilled through the wall into the plenum. These steel tubes were designed to fit closely inside each micro-tubular SOFC to deliver fuel from the manifold to the interior anode side of the cells, as shown in Fig. 3.9.

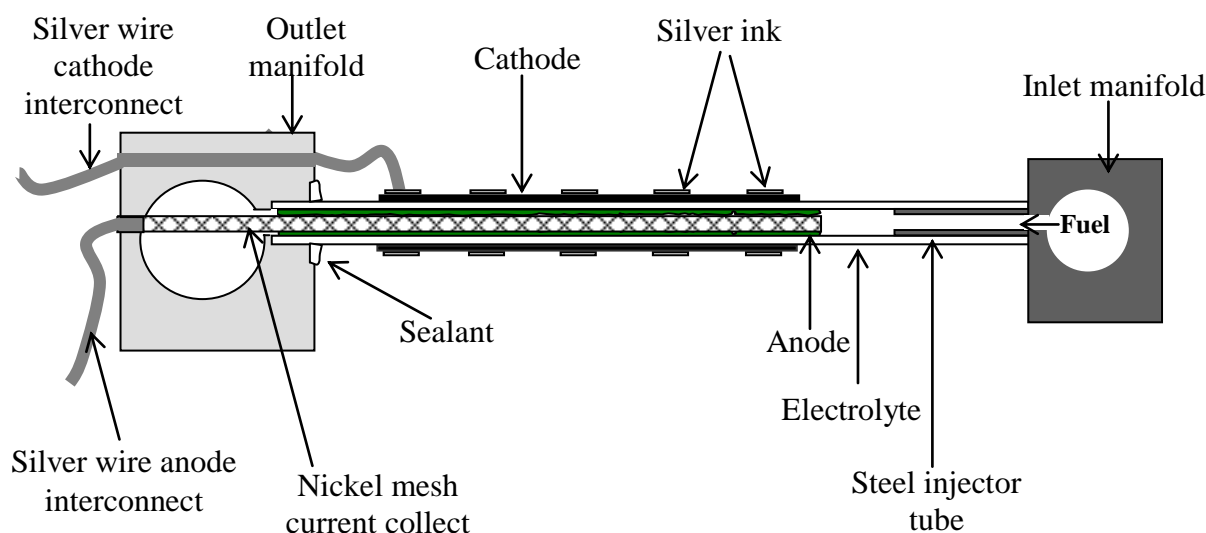


Fig. 3.10 Schematic showing a cross section through a fuel cell and fuel manifolds

No seal was formed between the steel fuel injection tube and the fuel cells but the tube extended 10 mm into the cell and was tight fitting such that the leakage was small and any fuel escaping was combusted around the inlet. This design permitted the cell some freedom of movement with thermal expansion and shrinkage.

The fuel outlet manifold was fabricated from Macor. This ceramic material was chosen because it is an electrical insulator with a similar thermal expansion to Zirconia, and can be machined. To fabricate the manifold, a 4 mm hole was bored through a $45 \times 14 \times 14$ mm block of Macor. The hole formed a plenum to collect fuel from the outlet of all of the cells. Holes were then drilled 5 mm into the front face of the manifold to receive the outlet end of the fuel cells. The assembly of the stack began with the positioning of the cells into the holes in the outlet manifold, once all of the cells were in position the inlet manifold was slid towards the outlet manifold using the support rods so that the cells received the steel fuel injectors. The cells were sealed into the outlet

manifold using a Zirconia based sealant supplied by Cotronics Ltd. Holes with 1 mm diameters drilled through the back of the manifold allowed the Nickel mesh interconnect from each of the cells to protrude through to the back face of the manifold. A plug made of silver was inserted inside the mesh to seal the holes on the back face of the manifold and provide a connection between the Nickel interconnect and a silver wire. This seal was enhanced by painting silver ink around the plug and Nickel mesh.

The stack was positioned in between 2 blocks of granular thermal insulation with dimensions $150 \times 150 \times 50$ mm. A recess was cut in each of the blocks to house the SOFCs and allow air to circulate around the cells.

The performance of the cells was monitored by an electronic control system and the voltage and current were displayed on LCD displays. This information could also be relayed to a computer running Labview 6.0 software for monitoring and logging.

The current drawn from cells could either be supplied directly to an external device, such as a personal fan, or the voltage could be 'stepped up' to power a device requiring low current but a higher voltage such as a radio controlled clock.

3.5.3 Fuel supply loop

The 4-cell demonstration unit was developed to have the capacity to run on a variety of liquid hydrocarbon fuels and included a fuel recycle loop. A small pump drew the exit gases from the fuel cell stack through a unit packed with solid pellets designed to remove some of the water from the loop by adsorption. The remaining gas was then bubbled

through fresh fuel in the fuel reservoir before being delivered to the SOFCs. After a single pass some of the fuel was fully oxidised to water and Carbon dioxide, but more was reformed to Hydrogen and Carbon dioxide using the remaining steam in the mixture. Thus the mixture leaving the fuel cell would be mixture that could more readily be oxidised by the SOFCs than the original hydrocarbon fuel. A recycle loop made use of this mixture and increased the overall fuel utilisation of the system. It was found that better performance and longevity could be achieved when fresh fuel was only introduced to the loop intermittently. This was achieved using a 3 way solenoid valve enabled the fuel loop to by-pass the fuel reservoir for a period. This system enabled the SOFCs to run on a variety of liquid fuels from methanol through to vodka. The system could also be run on gaseous fuels by plumbing a line into a connection at the fuel reservoir.

3.5.4 Air supply

Atmospheric air was supplied to the stack via a small pump. The pump was capable of supplying up to 3 std. l min⁻¹ (5.83×10^{-5} kg s⁻¹) of air which entered the system beneath the heating elements below the cells. Both the air pump and fuel pump were powered by electricity from the 12 V power supply connected to the electronic control system.

3.5.5 Control and monitoring system

In the most basic mode of operation the electronic control system relayed power from the external power supply to the pumps and solenoid valve and controlled the temperature of the stack. The temperature was controlled by pulsing the power supplied to heating elements positioned above and below the SOFCs 'on' and 'off'. The duration that the power was 'on' would change in response to the difference between the temperature measured inside the stack, by a K-type thermocouple, and a set point temperature. The

heating elements were able to raise the stack temperature to 1123 K within 2 minutes to enable power to be drawn from the stack after this time. The fuel cell current and voltage were displayed on LCD displays on the front of the electronic section of the stack.

The control system included manual controls for the speed of the air and fuel pumps and the position of the 3 way solenoid valve but, for more sophisticated control and monitoring, the control system could be connected to a computer running a program written for Labview 6.0. From the computer, the position of the 3 way solenoid valve could be changed automatically to introduce fresh fuel to the cells whenever the fuel cell output dropped below a set voltage. The computer package could also be set to change the temperature of the cells periodically to test the ability of a stack to withstand thermal cycling.

3.5.6 Assessment of 4 cell demonstration units

This 4-cell demonstration SOFC unit was largely successful with the unit providing 1-2 W of electrical power. The units accomplished the goal of demonstration of the capability of micro-tubular cells to produce power within minutes of start-up. They also illustrated the capacity of the system to run on a variety of hydrocarbon fuels using the catalytic properties of the Nickel anode for reforming. In keeping with the aim of producing a portable power supply, they survived air travel and were demonstrated at variety of locations including conferences such as ET2002, Birmingham.

The major limitation of the system as a demonstration unit was the need for an external power supply to provide energy for the balance or plant, BOP, items. Whilst the output from the fuel cells was close to meeting the power required by the pumps and valves,

many more cells would be needed to generate enough power to warm the heating elements to keep the stack at the operating temperature. It is clearly not practical for a commercially viable SOFC device to be a net consumer of electrical power. Even ignoring the power requirements of the balance of plant (BOP) the 1-2 W output of the SOFCs could only drive very modest applications. The next step was to scale up this design to incorporate a larger number of fuel cells. Analysis of the issues involved in this scale up became the primary objective of this thesis.

3.6 The 20 cell stack

A flow sheet for a larger SOFC system is shown in Fig 3.11.

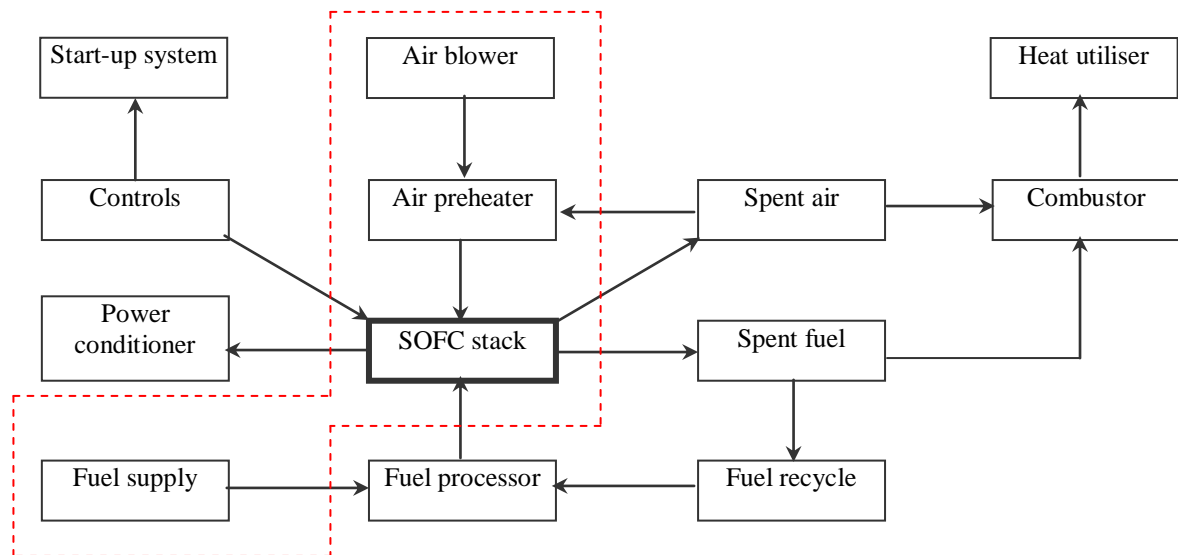


Fig. 3.11 Flow sheet for a small SOFC system^[49]

The dashed red line in Fig 3.11 shows the scope of the 20 cell system developed in this investigation. The study has primarily been aimed at investigating parameters affecting the design of the SOFC stack itself rather than the other auxiliary items that form the balance of plant. This was to enable more detailed analysis of the stack operation without the complication of the interaction with the balance of plant (BOP) items. The design of

these BOP items should be relatively straight forward, as similar items have been used in more established power generation systems or elsewhere in the chemical industry, but these can only be dealt with once the details of the fuel cell stack operation are known. For example, the air pre-heater cannot be sized or specified until the temperature and flow rate of air required to achieve a stable operating temperature across the SOFC stack is known. This in turn makes it difficult to size the combustor and develop a suitable control scheme.

In keeping with the focus on understanding the issues involved with the design of the fuel cell stack the hot air and spent fuel were exhausted without recycling or downstream utilisation. Hydrogen was used as a fuel so a fuel processor was eliminated from the experimental set-up. This avoided the complexity involved with using a hydrocarbon fuel and the many competing fuel processing reactions that would occur. In fact during calibration experiments Helium was used as an anode gas so that the temperature profile through the stack could be studied without the influence of electrochemical and combustion reactions.

3.7 Equipment

An outline of the experimental apparatus is given in Fig 3.12 which is followed by a discussion of the key items of equipment.

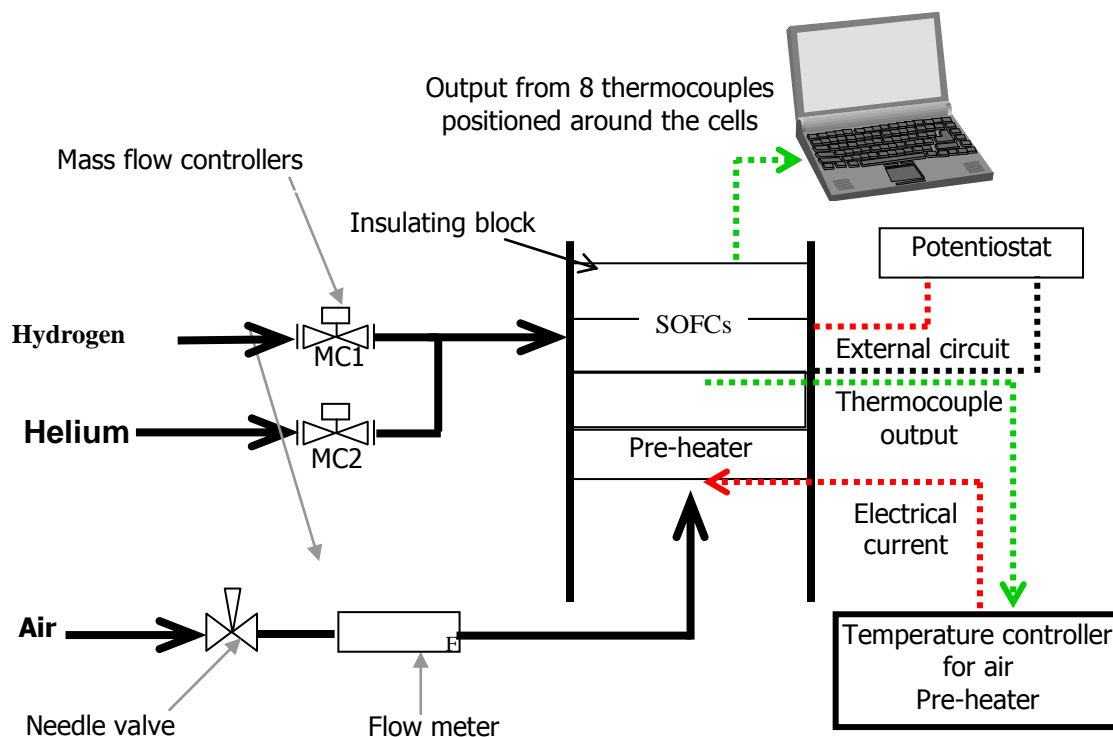


Fig. 3.12 Schematic of the experimental system

3.7.1 The SOFC stack

The design of the micro-tubular SOFCs was the same as those discussed previously in this Chapter and the manifolds, used to supply and collect fuel from the 20 cells, were based on those described formerly for 4-cell demonstration units. A diagram of the complete stack assembly is shown in Fig.3.13.

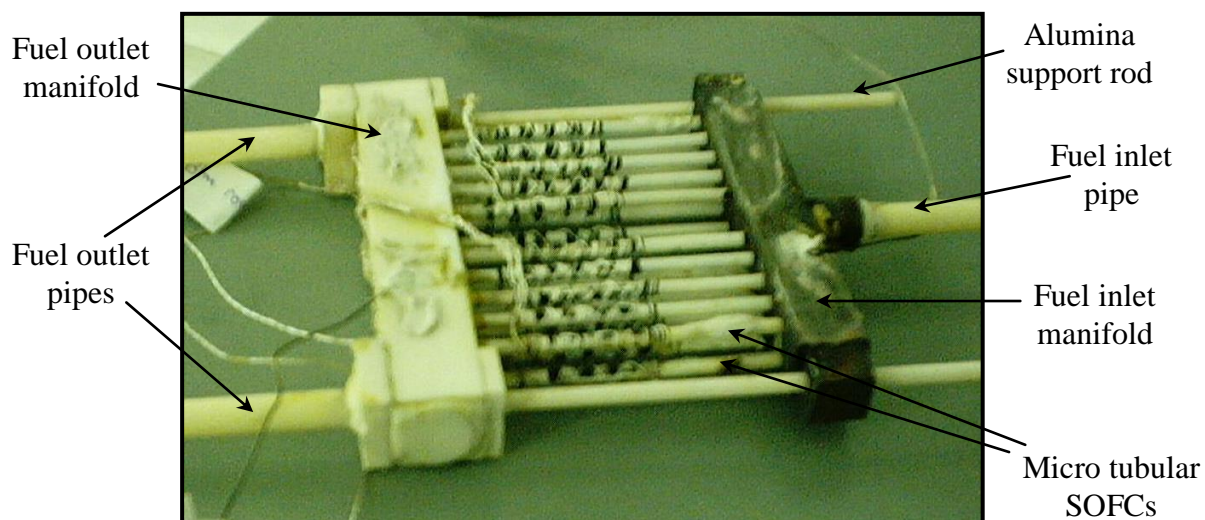


Fig. 3.13 Photograph of stack used for the experimental study

The fuel inlet manifold was fabricated from a 316 stainless steel square section tube with internal dimensions of 10×10 mm and wall thickness of 1.25 mm. A 6 mm diameter hole was drilled in the centre of one face of the tube around which a steel connection tube was welded. The steel connection tube received a ceramic fuel inlet pipe, which was sealed to the manifold using a ceramic sealant. The inlet pipe was fabricated from Macor ceramic rather than a steel tube to reduce the heat loss from the stack by conduction along the fuel inlet pipe.

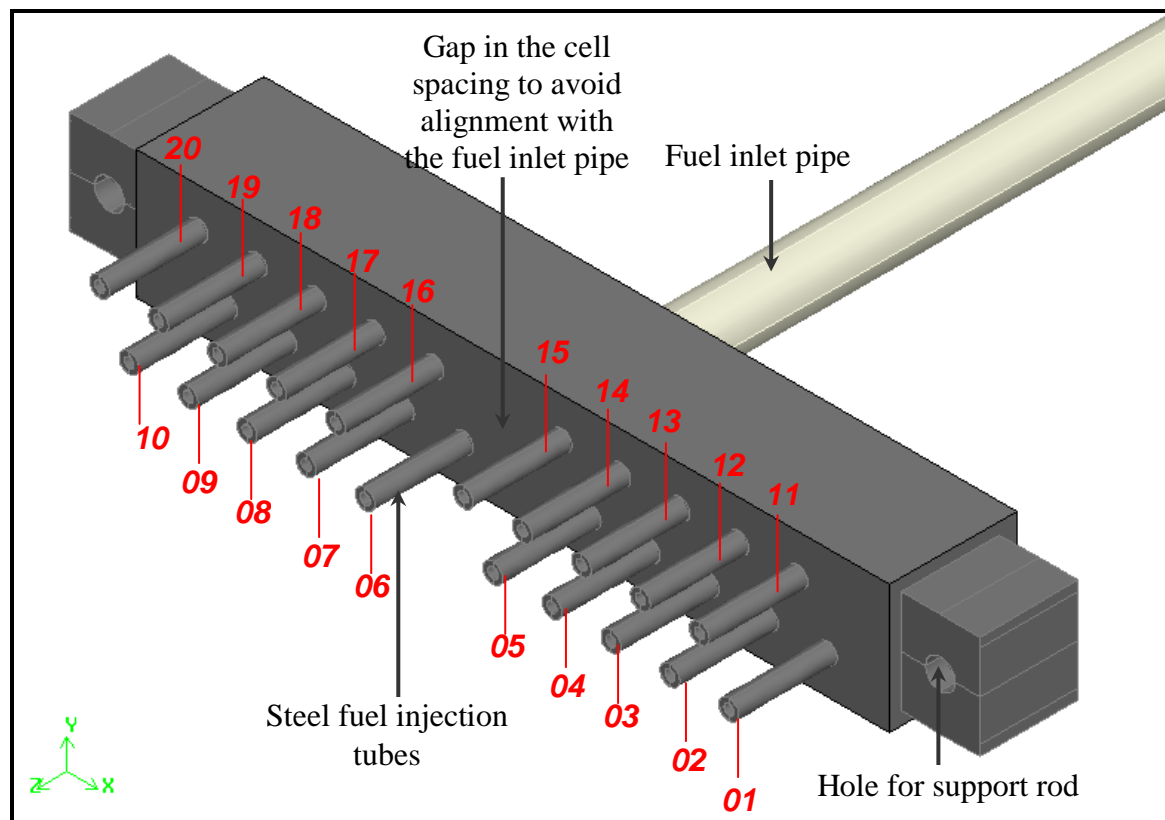


Fig. 3.14 Schematic of fuel inlet manifold

On the opposite face, 20 stainless tubes with an external diameter of 1.85 mm were inserted into holes drilled through the wall. As with the 4-cell design these steel tubes fitted inside the fuel cells and were used to deliver fuel to the anodes. They were spaced

in two lines of 10 split in the middle to avoid direct alignment with the inlet pipe as shown in Fig. 3.14. The spacing between each cell was 6 mm as this was deemed the closest practical spacing for a stack with the current technology. A more compact interconnect than the existing silver wires might facilitate a closer packing in future. The inlet tubes have been labelled 01 to 20 in Fig. 3.14. This numbering system will be used to refer to the fuel cell associated with each of the steel injector tubes. For example, the cell connected to the fuel inlet tube labelled as 01 in Fig.3.5 will be referred to as FC01.

The fuel outlet manifold was fabricated from a $15 \times 15 \times 90$ mm block of Macor. An 8 mm hole was bored through the block of Macor to collect the fuel. Following the 4-cell design sealant was only used between the cells and the outlet manifold. The sealing at the inlet end of the cells relied on the tight fit between the inside wall of the cells and fuel injection tube.

3.7.2 Insulation

In order to optimise the overall efficiency of the system it was important to maximise the use of thermal energy created by the electrochemical reactions in addition to the electrical output. Energy produced in the stack can be recovered to heat up the incoming fluid streams or put to some other useful purpose such as in a combined heat and power system [72,127-129]. To do this it is desirable to minimise the uncontrolled loss of thermal energy to the atmosphere and so high quality thermal insulation was deployed to surround the stack.

Micropore granular insulation product, produced by Microtherm Ltd, was selected to insulate the system because of its excellent overall thermal conductivity of 0.02 to 0.03

$W m^{-1} K^{-1}$ [130] and relatively low density of $400 kg m^{-3}$. Weight is an important consideration with stack designs for deployment as portable power supplies.

The stack insulation was in fact made up of four blocks of Micropore with dimensions of $245 \times 275 \times 50 mm$. The dimensions were determined by the material readily available and the manufacturer's guidelines^[130], which recommended an 80 mm wall thickness to achieve a cool face temperature of 323 K when the hot face temperature is 1123 K. The blocks of insulation were stacked on top of each other as shown in Fig.3.15 and Fig.3.16 with the SOFC stack sitting between blocks 3 and 4 in a recess cut out from the insulation. Blocks 1 and 2 housed the air inlet channel and heating elements.

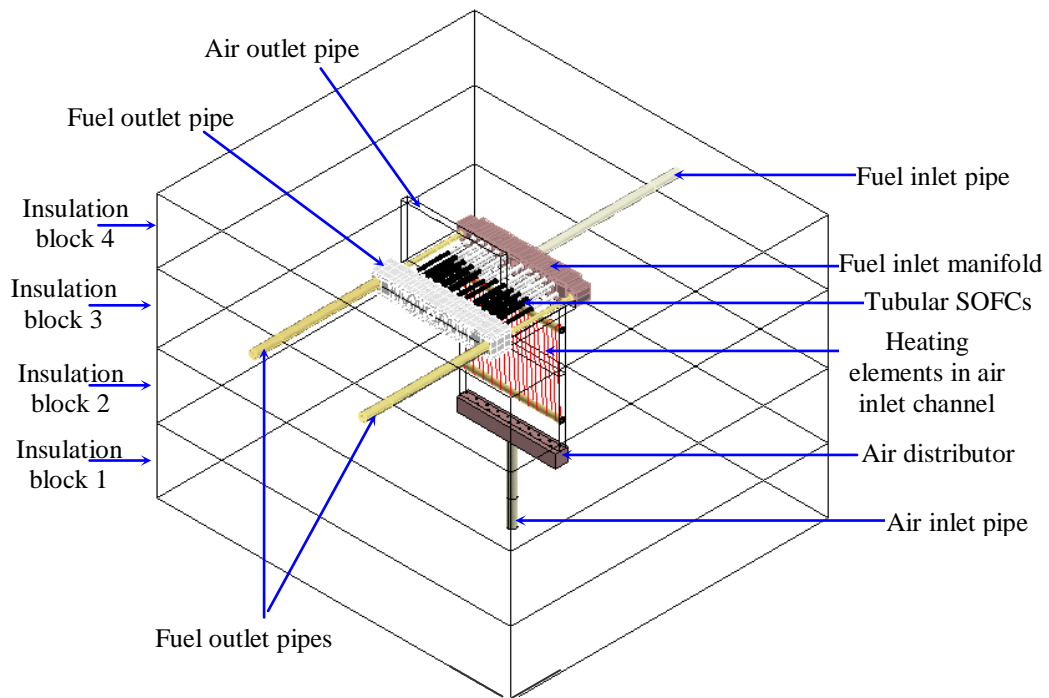


Fig. 3.15 Diagram showing isometric view of stack

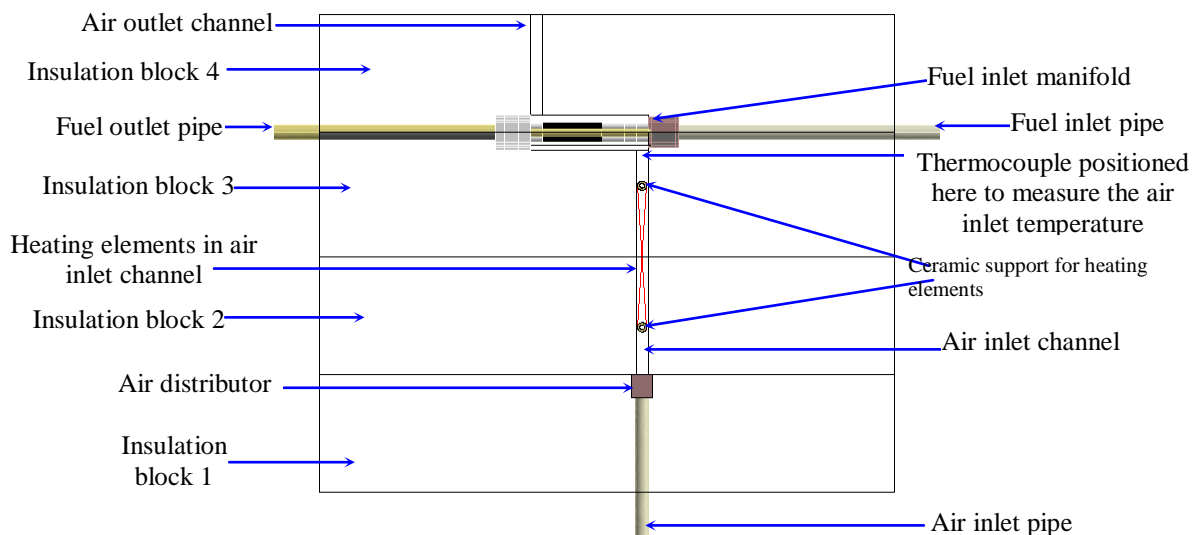


Fig. 3.16 Diagram showing cross section through the stack assembly

3.7.3 Air and fuel supply

Previously calibrated flow meters were plumbed into the fuel inlet pipe such that Hydrogen or Helium could be supplied to the anode over a range of 0 - 0.350 std. l .min⁻¹ of Helium and 0 - 0.6 std. l min⁻¹ of Hydrogen. Helium was used during start-up and shutdown to prevent oxidation of the anodes and also during calibration experiments. The airflow was controlled and measured by a needle valve and a Solartron Mobrey series1100 rotameter-style flow meter. The incoming air was preheated in a channel cut through the insulation below the SOFC stack using heating elements made from nichrome wire supported by ceramic tubes. A stainless steel distributor was constructed to disperse the air width of the channel.

3.7.4 Temperature monitoring and control

As revealed in section 3.7.3, the air entering the stack was preheated before it reached the chamber housing the SOFCs. It was decided to try to use pre-heated air to achieve, and maintain, the stack operating temperature rather than the electrical heating elements

above and below the SOFCs used for the 4 cell demonstration units. Whilst this was a move away from a system that had been successful in the 4-cell units, electrical heating was not seen as a viable solution in the long term because the electricity required would detract too much from the power generated by a small SOFC stack. Although the heating elements used to preheat the air still required a lot of electrical power, it was thought that these could be removed once the demands of the system had been characterised. The air would instead be pre-heated by combustion of a hydrocarbon fuel in place of the electrical elements. It is proposed that the fuel would come from a mixture of spent fuel from the SOFCs and fresh fuel from the same source as used to supply the anodes.

Control of the temperature of the air entering the chamber around the cells was achieved using a Eurotherm furnace controller. The temperature where the pre-heat channel joined the chamber surrounding the fuel cells was measured by a K-type thermocouple connected to the controller. The output from the controller was used to regulate the voltage supplied to the electrical heating elements in the air preheat channel in order that the temperature of the air entering the cell chamber complied with the set-point temperature. The system was capable of heating the incoming air to 1073K within 2 minutes, and maintained a constant air inlet temperature to the stack to within ± 1 K. The inlet temperature of the fuel was not regulated.

A further 8 K-type thermocouples were placed 2 mm above cells FC04 and FC01 at intervals along the length of the cells. These thermocouples were connected through a data acquisition card to a computer running a LABview program to record the

temperatures against operating time. The data was written to a Microsoft Excel file for later analysis.

3.7.5 Monitoring electrochemical performance

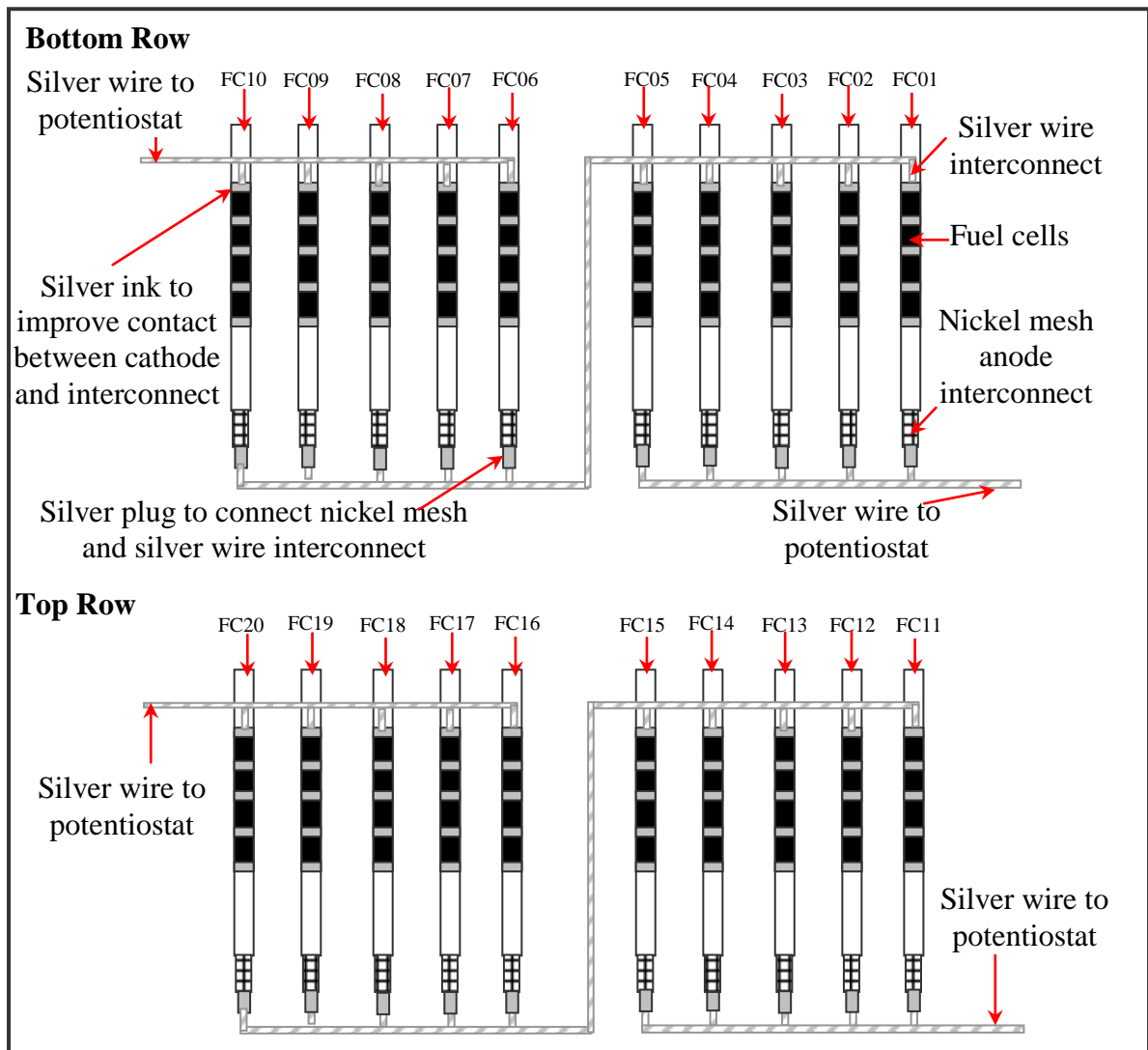


Fig. 3.17 Diagram to show electrical connections in the SOFC stack

A potentiostat supplied and calibrated by Adelan Ltd was used to load the cells and measure the electrical output. The electrical connection between the cells in the stack is shown in Fig.3.17. Cells 1-5, 6-10, 11-15 and 16-20 were connected in bundles of five

cells in parallel. The two bundles on the bottom row were connected in series with each other and then to one channel of the potentiostat with the same arrangement on the upper row connected to a second channel of the potentiostat.

3.8 Testing

The tests carried out on the 20 cell stack are described in more detail in Chapters 5 and 6 but results of the initial testing with Helium are shown in Fig. 3.18. Helium was fed to the anode at a flow of 0.3 std. l min⁻¹ and the air was supplied at a rate of 10 std. l min⁻¹ pre-heated to 1073 K.

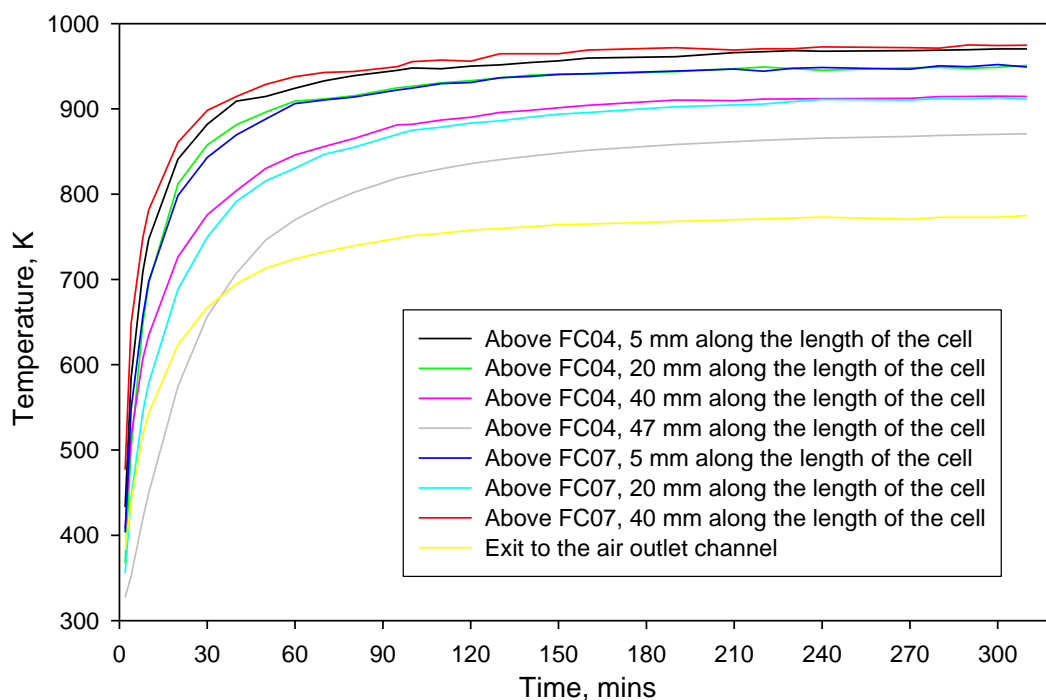


Fig. 3.18 Plot of stack temperature against time for the 20 cell stack fed with Helium

Although these results did not include the effect of any electrochemical activity they highlighted a key issue in the design and operation of micro-tubular stacks especially the thermal requirements for rapid start-up.

3.8.1 Requirement for specific system start-up system to for rapid start-up

The air flow rate of 10 std l min⁻¹, heated to 1073 K, was found to be sufficient to maintain a stack temperature across the stack of close to 1000 K without any contribution from electrochemical or combustion reactions. However, even with this large excess of air the stack took over an hour for the majority of it to reach a temperature above 900 K. This is too slow if the ability of micro-tubular cells to tolerate rapid temperature changes^[51] is to be deployed in a rapid starting device that could produce electrical power within minutes.

The possibilities for improving the start up time are limited with the current system. Increasing the temperature of the incoming air significantly above 1073 K is restricted by the possibility of damaging the cells closest to where the hot air enters the cell chamber. Increasing the air flow rate would provide additional heat inside the cell chamber but would waste large amounts of excess energy required to heat the air during steady state operation. It would also require a large amount of surplus capacity in the air supply and heater. It may be that an additional system is required to reach the operating temperature quickly, beyond that required to maintain temperature during steady operation. Either way the experiments have shown that the transient response of the temperature through the stack during the initial period of operation requires careful consideration if rapid start-up is to be achieved.

3.8.2 Slow response in temperature rise due to gradual accumulation of energy in the thermal insulation

As discussed previously, the rise in temperature through the stack was very gradual. As the amount of mass to be heated up in the fuel cell stack itself is relatively small, this slow response is attributed to the accumulation of heat and gradual rise in temperature through the insulation. Whilst other authors have assumed adiabatic conditions at the boundaries of the stack, rather than modelling the heat transfer, it is clear that the insulation is important in influencing the temperature profile through the stack and therefore should be considered when looking at the design of a micro-tubular stack.

3.9 Conclusion

In this Chapter the construction of the micro-tubular SOFCs used in the remainder of this study have been described. These cells were subjected to individual testing in a purpose built furnace, which was used to characterise the response of the electrical output of the cell to changes in operating voltage and temperature.

The construction of a 4-cell demonstration stack was also described. This unit was used to demonstrate the potential of micro-tubular SOFC to form a portable power generation device. The 4-cell unit was scaled up to form a stack accommodating 20 cells. This system was built and tested and is the subject of further investigations described in Chapters 5, 6 and 7.

The initial testing of the 20 cell stack highlighted the problem of slow heating due to the gradual accumulation of heat in the thermal insulation. Therefore, it was considered

important that computer simulations developed for the micro-tubular stack included accurate modelling of the heat loss through the insulation. It was also considered important that the model for the SOFC stack would have the capacity to facilitate time dependent modelling so that the start-up phase could be simulated. The computer model developed to model the SOFC stack is described in Chapter 4.

4. CFD model

4.1 Introduction

This Chapter outlines the approach used to develop a stack model for a 20-cell micro-tubular SOFC system using the commercial CFD code, FLUENT. The Chapter begins with an overview of the modelling approach and the desired functionality of the model. This is followed by a more rigorous discussion of the geometry, mesh generation and the specification of boundary conditions and parameters used in the model. The Chapter also provides an analysis of the procedure used to solve the model and reports on the sensitivity of the model solutions to the number of the iterations performed and to the mesh density.

4.2 The modelling approach

4.2.1 Modelling level

Various modelling approaches for SOFCs exist, as discussed in Chapter 2, focussing on the specific length scales ranging from the atomic and molecular scale to the overall system performance^[110]. Fig 4.1 shows the scales involved from the nanometre dimension to the metre scale, required for complete description of the systems.

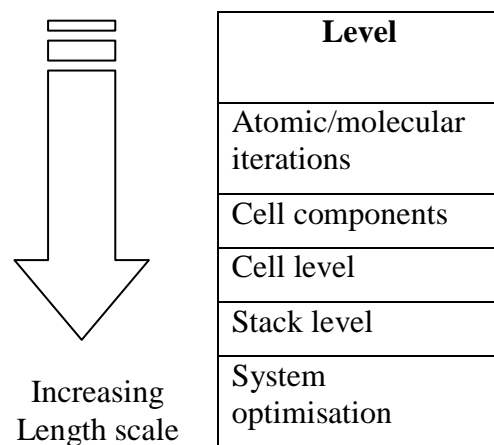


Fig. 4.1 Different levels of modelling used for SOFC systems

Since it would be impossible for this project to cover all these levels, it is necessary to focus on the desired function for the model to determine where the boundaries will be drawn. The focus of this work was at the stack level with the aim of taking the work done on single cell development forward into a system with a useful power output. The main aim was to predict the temperature profile through the stack for a certain stack configuration and operating conditions. As this model was the first to be developed for micro-tubular stacks it was desirable to simplify the model wherever possible. A number of priorities were determined and these are outlined below.

4.2.2 Modelling of the air flow

As already stated, the main aim of this model was to be able to predict temperature profiles through the stack under certain operating conditions. This was to help to design the system for operating conditions that would lead to suitable operating temperatures and acceptable temperature gradients across the stack. It was anticipated that the location, flow rate and temperature of the air entering the stack are the most important variables in controlling the stack temperature in micro-tubular SOFC stacks. It was therefore decided to model the air flow into and through the stack as rigorously as possible.

4.2.3 Detailed modelling of heat transfer to the atmosphere

In large SOFC systems, excess air is normally required to remove heat produced by polarisation losses from the electrochemical reactions^[131]. Previous models of these systems often include such assumptions as adiabatic boundary conditions^[85,86,98] at the edges of the stack, since the heat loss by conduction to the atmosphere can be small

relative to the heat generated inside the stack. Some recent authors have recognised the importance of accurate estimates of the heat flux through the walls for small planar systems and have included in their models the heat lost through the insulation^[94]. With a comparatively low electrical output per cell (0.5 W), micro-tubular cells are initially likely to be used in small systems producing 1 W_e to 1 kW_e^[71,72]. In these smaller systems the heat losses through the insulation will be of more comparable magnitude to the heat produced by the electrochemical reactions and thus will have a more significant influence on the temperature distribution in the stack than in larger systems. For this reason it was decided to build in accurate modelling of the heat losses to the atmosphere into the model.

In the operation of previous small micro-tubular stacks it has been observed that the presence of the fuel inlet and outlet manifolds and pipes significantly affect the temperature distribution through the thermal insulation surrounding the stack and thus the rate of heat loss. Detailed modelling of the flow and heat transfer in these manifolds was also considered an important aspect to include in the model.

4.2.4 Simplified electrochemistry

Having decided to focus on rigorous modelling of the air flow and heat transfer through the manifolds and insulation surrounding the stack, it was decided to simplify the electrochemistry as much as possible. In practice the electrochemical heat generation term is coupled to the resistance to mass and charge transport in the electrodes and electrolyte, which are in turn coupled to the local temperature distribution. The electrochemical heat generation is also a function of the concentration of reactant species at the electrodes surfaces and the external load. It was decided, for the purposes of modelling to simplify

the cell geometry and assume a lumped electrochemical heat generation term which is uniform across the electroded section of the cells.

4.3 Conservation equations

Having identified a number of important criteria for the model the next stage was to derive the equations necessary to calculate the temperature and flow profile through the stack. These equations are derived from the conservation laws in fluid mechanics^[110] and are described below.

Conservation of Mass

A species' mass in a reacting mixture of gases can be determined by solving the species continuity equations:

$$\frac{\partial \rho_i}{\partial t} + \nabla \cdot [\rho_i (\mathbf{v} + \mathbf{U}_i)] = \omega_i \quad \text{Eq. 4.1}$$

Rate of accumulation of the species density of a species, i , in the controlled volume + Net mass flux into the controlled volume = Rate of generation of species i by chemical reaction

where ρ_i is the species density, \mathbf{v} is the fluid velocity, \mathbf{U}_i is the species diffusion velocity, t is time and ω_i is the rate of production of species i due to chemical reactions. In this study, the system was simplified by assuming that only air is present on the cathode side and only pure Hydrogen or Helium on the anode side of the cell. Furthermore, the transport of gases through the porous electrodes has been neglected. As a result of these simplifications, the diffusion term can be omitted from Eq. 4.1. Although the thermal energy source from the electrochemical reactions has been considered the consumption and generation of reacting species at the electrodes has been neglected, hence the source

term due to reaction can also be eliminated and initially steady state conditions were considered so with no accumulation of mass Eq. 4.1 can be simplified to:

$$\nabla \cdot (\rho_i \mathbf{v}) = 0 \quad \text{Eq. 4.2}$$

Conservation of Momentum

In this model the flow field of the gas is initially unknown so the mass balance must be used in conjunction with the conservation of momentum equation to establish the velocity and concentration profiles. The conservation of momentum for a fluid can be expressed in the form of Eq. 4.3 often referred to as the Navier-Stokes equations, in which k represents one of the three orthogonal directions in the co-ordinate system (x, y and z).

$$\frac{\partial(\rho v_k)}{\partial t} + \nabla \cdot (\rho v_k \mathbf{v}) = \rho g_k - \frac{\partial P}{\partial x_k} + \nabla \cdot (\mu_e \nabla v_k) + \Omega_k + \tau_k \quad \text{Eq. 4.3}$$

Hence, P is the pressure, g is the acceleration due to gravity, and μ_e is the effective viscosity. τ_k represents non-Newtonian viscous forces and can be neglected for the fuel cell system^[110]. Ω_k represents source terms but again this is omitted as the consumption and generation of reacting species at the electrodes is neglected. For the steady state model there is no accumulation of momentum with time and the time dependent term on the left hand side of Eq. 4.4 is neglected also.

$$\nabla \cdot (\rho v_k \mathbf{v}) = \rho g_k - \frac{\partial P}{\partial x_k} + \nabla \cdot (\mu_e \nabla v_k) \quad \text{Eq. 4.4}$$

Conservation of Energy

In order to obtain the temperature profile through the system, it is necessary to solve the momentum and mass balance equations alongside equations derived from the

conservation of energy. In the gas phase, the conservation of energy can be written in the form:

$$\frac{\partial(\rho c_p T)}{\partial t} + \nabla \cdot (\rho c_p T \mathbf{v}) = \nabla \cdot (\lambda \nabla T) + Q + \frac{\partial P}{\partial t} + Q_{\text{vis}} + W^V + E^k, \quad \text{Eq. 4.5}$$

where c_p is the specific heat, λ is the thermal conductivity, Q is the non-viscous volumetric heat term, Q_{vis} is the viscous heat generation term. W^V is viscous work and E^k is the turbulent kinetic energy^[110]. In this model, gas phase reactions have been neglected. Energy source terms arising from the electrochemical losses will occur in the solid representing the fuel cell so that Q can be neglected for the gas phase. The gas flows are in the laminar region so turbulent energy losses can be neglected and at the steady state the time dependent terms are eliminated from the model.

$$\nabla \cdot (\rho c_p T \mathbf{v}) = \nabla \cdot (\lambda \nabla T) + \frac{\partial P}{\partial t} + Q_{\text{vis}} + W^V \quad \text{Eq. 4.6}$$

In addition to solving the conservation equations for the fluid in the stack, the solid parts of the stack have been meshed and the energy balance applied to yield the temperature profile through the solids and the heat flux across the outer walls of the stack. For the solid regions equation Eq.4.6 can be simplified since there are no convection or viscous terms and the density is constant.

$$\rho \frac{\partial(c_p T)}{\partial t} = \nabla \cdot (\lambda \nabla T) + Q \quad \text{Eq. 4.7}$$

Again in the steady state model the time dependent terms are eliminated and hence

$$0 = \nabla \cdot (\lambda \nabla T) + Q \quad \text{Eq. 4.8}$$

At this stage the equations Eq.4.6 and Eq.4.8 do not include terms for radiative heat transfer although its influence has been considered later in this thesis.

4.4 Numerical methods and choice of software

By splitting the fuel cell stack into small discrete volumes, the mesh or grid is developed. By successfully solving equations Eq.4.2, Eq.4.4, Eq.4.6 and Eq.4.8 for each of the volumes, an estimate of the flow and temperature profiles through the stack could be obtained. Some authors have reported the development of ‘in house’ codes to do this for other types of SOFC or single cells ^[75,77,82,84,87,101,124,132] but unlike the modelling of individual tubular cells or between flat planar cells, which may comprise of regular cylindrical or rectangular geometries, the air channel around the micro-tubular cells demands the meshing and resolution of the temperature and flow distribution in a complex geometry. As commercial CFD packages have been proven to model complex flow in channels and incorporate powerful mesh generation software, this type of package was chosen as the tool with which to model the stack. The actual specific software chosen was FLUENT 6.1 along with its associated pre-processor, GAMBIT.

The term CFD refers to the analysis of systems involving fluid flow, heat transfer and associated phenomena such as chemical reactions by means of a computer based simulation. The CFD solver uses finite volume methods to solve the Navier-Stokes and the energy and mass conservation equations to give the local conditions in the fluid. CFD was first deployed extensively in the aerospace industry in the 1960’s but has since been applied in the automotive industry and increasingly for the design of industrial products and processes ^[133]. It has already been implemented in different geometries of SOFC ^[85,108,109,117] and other types of fuel cell^[134-139].

Several other commercial codes using the finite volume method could have been chosen such as, CFX, Star-CD and Phoenics. FLUENT was chosen as its origins stem from

combustion modelling which includes modelling of the flows of many of the hydrocarbon gases used in fuel cells. However, the decision was somewhat arbitrary since most of the commercial codes now offer the same features and use similar algorithms.

4.5 Computational Requirements

The model was developed and run using computer facilities at the University of Birmingham. The simulations were run on the Central Applications Service, CAPPs, server that comprised of a cluster of 6 dual processor HP J6700 workstations running at 750Mhz utilising the Hewlett Packard HP-UX operating system. The server was accessed remotely using Exceed version 8.0. Initially the geometry and mesh generation was done using the CAPPs server remotely, but as the complexity of the geometry evolved, extruding faces to form volumes and meshing operations became very slow. It became apparent that the limiting factor was the speed of transfer of information across the network between the server and the local workstation. To overcome this problem the geometry and mesh building was switched to a windows based PC with a 2 GHz Pentium 4 processor and with 524 MB of RAM. Some meshing operations became 60 times faster when the process was switched to the local workstation. To maximise speed and reliability, files were sent to the server to be solved as batch operations.

4.6 The geometry

The first task of implementing the model was to construct the geometry to represent the 20-cell experiment system so that results of experiment and simulation could be compared. It is claimed that it is typical for 50% of the time spent in industry on a CFD project to be devoted to the geometry and grid definition^[133]. The complex nature of the

geometry of air chamber surrounding the cells meant that this was certainly one of the more demanding and time consuming aspects of the study.

The geometry was created using GAMBIT. Attempts were made to ensure the CFD geometry represented the experimental stack as closely as possible. The geometry included the 20 micro-tubular cells, the steel fuel inlet manifold and injectors, the ceramic fuel outlet manifold and the inlet and outlet pipes to the manifolds. The stack was surrounded by thermal insulation with dimensions matching the experimental system. Fig. 4.2 shows a rendering of the final geometry with the top of the insulation block cut away to reveal the fuel cells, manifolds and the stack components. Each of these items is discussed in turn below.

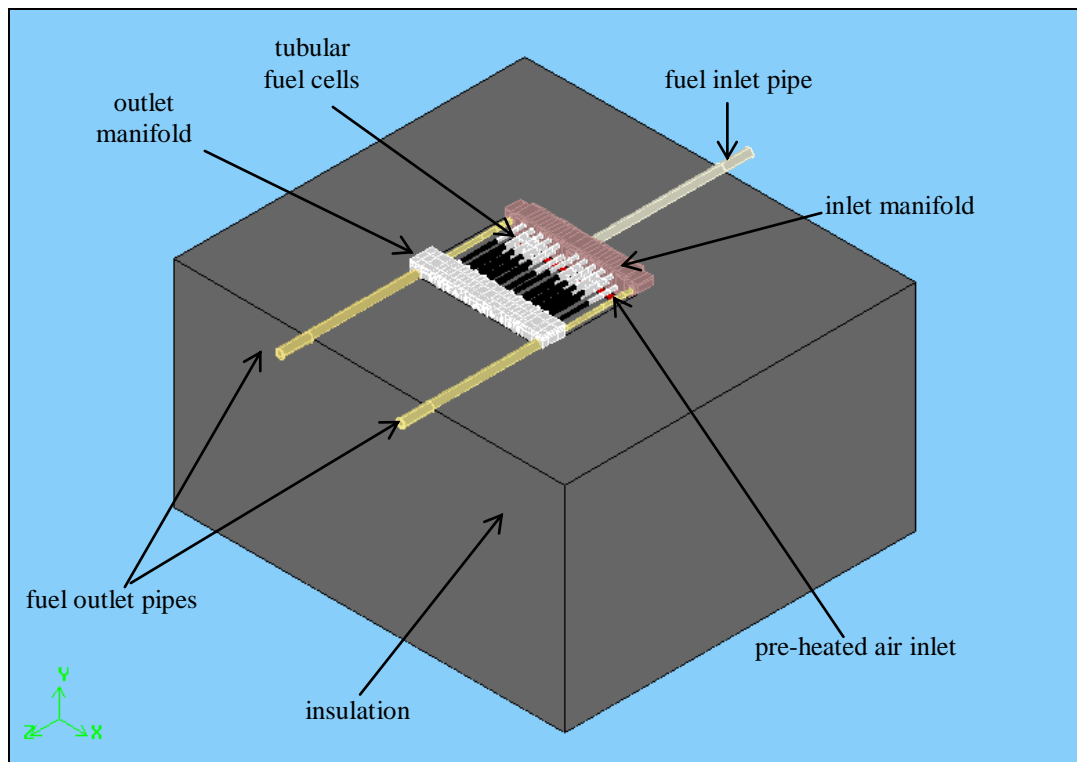


Fig. 4.2 Rendering of the CFD model with the top part of the insulation removed to show the fuel cell arrangement

4.6.1 The fuel cells

The starting point for the creation of geometry was the volume representing the cells. The model of the fuel cell volumes was developed by first constructing single cell 2D models using axis symmetry, then 3D single cell models. The purpose of these models was to check that proposed representation of the fuel cells and surrounding air could be meshed satisfactorily and solved successfully before creating the 20-cell geometry. Fig. 4.3 shows simplified fuel cell geometry.

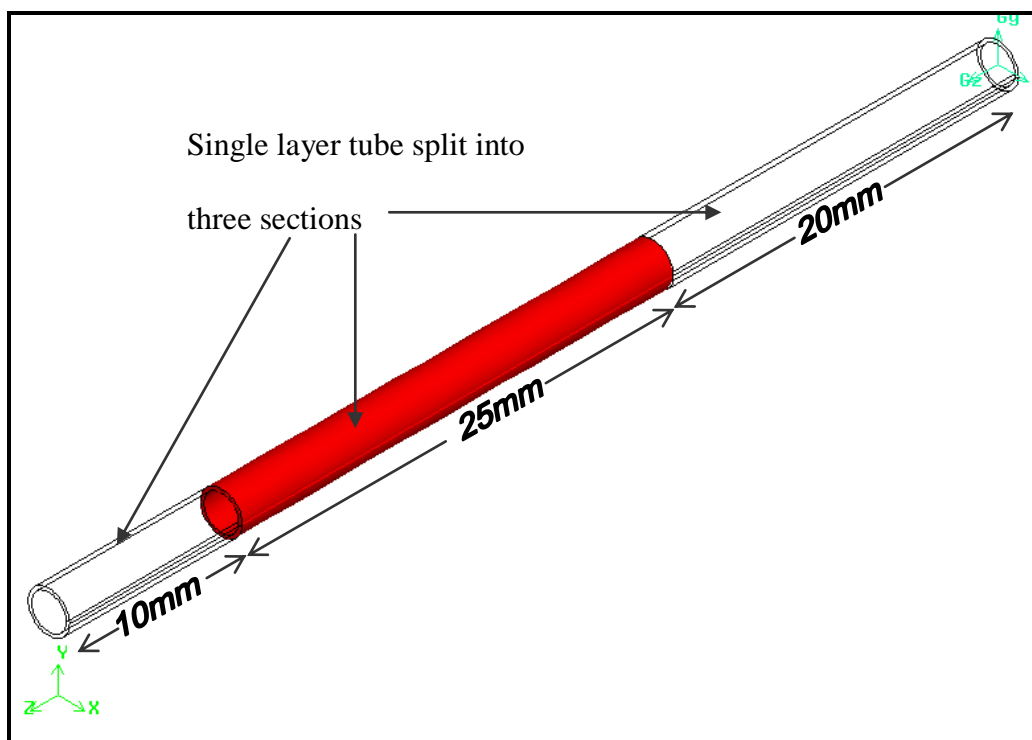


Fig. 4.3 Diagram of simplified cell geometry used in the CFD model

The cell was simplified to a single tube of ceramic Zirconia with the relevant physical properties. This simplification was made since the electrolyte tube, which acts as the mechanical support for the anode and cathode layers, is thick relative to the electrodes and has a low thermal conductivity.

The Adelan Ltd design of micro-tubular cell leaves the ends of the cell uncoated with electrolytes. Since most of the energy produced by electrochemical polarisation losses would be produced in the anodes and cathodes, and the section of electrolyte between them, the cell was split into three sections so that energy source terms arising from electrochemical reactions could be limited to the central section, which is coated with electrodes.

The diffusion of gases through the external layers of the anode and cathode to the three-phase boundary with the Zirconia has also been neglected. Whilst this may affect the temperature in the radial direction through the fuel cell electrolyte, the impact on the temperature profile should be minimal at the stack level.

Another major simplification is the exclusion of the silver wire and Nickel mesh current collectors. Of these omitted structures, the Nickel mesh is more significant as it likely to affect the velocity profile of the fuel on the inside of the tube due to the disruption of the gas boundary layer. The simplification is justified on the basis that the precise fuel flow pattern is likely to be less influential on the temperature distribution than the much larger air flow. It is anticipated nevertheless that conduction through the Nickel mesh leads to a more even temperature distribution through the inside of the cell than predicted through the model.

Amid these simplifications to the fuel cell geometry some details were retained. The steel tubes that fit inside the inlet end of the cells to deliver fuel from the manifold were included in the model. These were incorporated because the wall is relatively thick and

the thermal conductivity of steel is much higher than that of the surrounding materials. This meant that transfer of heat along the steel tubes was likely to affect the stack temperature profile, particularly the temperature of fuel entering the cells.

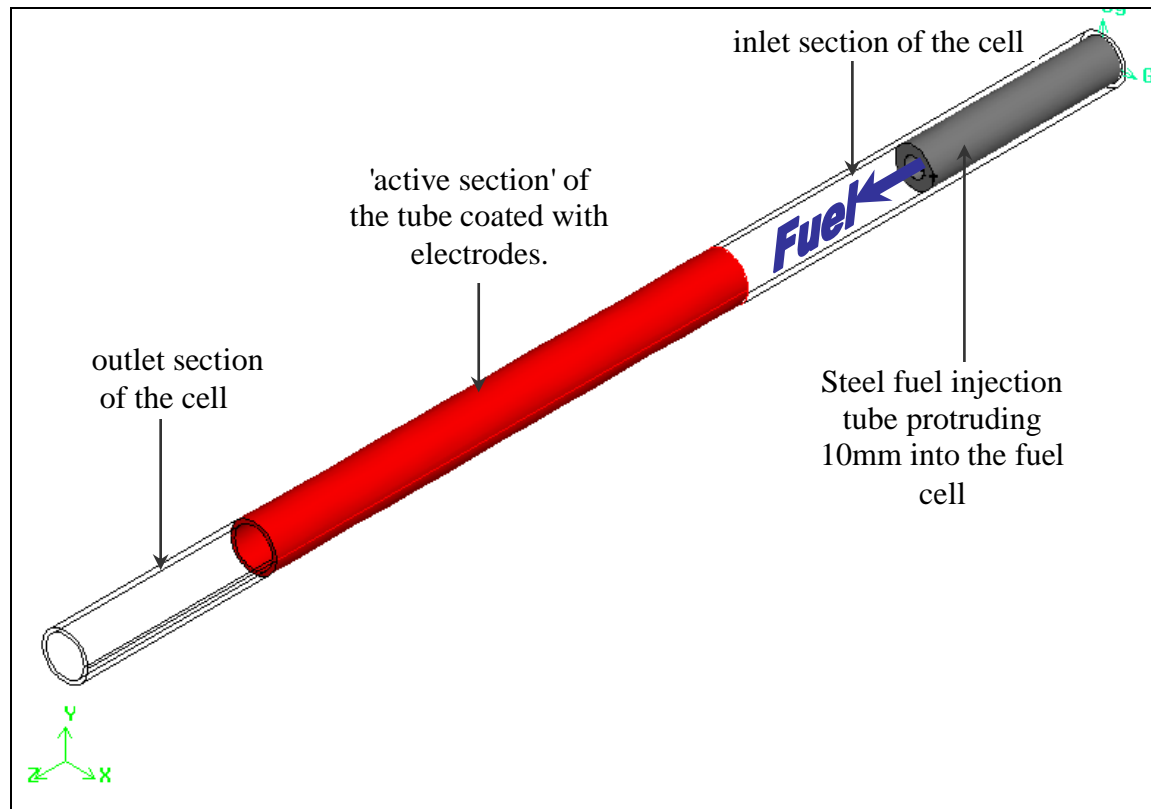


Fig. 4.4 Diagram of the single fuel cell with the fuel injection tube

In Fig. 4.4, each cell and interior has been split into five domains, the inlet and outlet sections of the cell, the active section in the middle of the cell, the fuel on the inside of the cell and the steel fuel injection tube. In order to facilitate use of the structured meshing tools incorporated into Gambit, it was necessary to decompose each cell into a larger number of smaller volumes^[140]. These smaller volumes were then grouped together to form the 5 different domains. The decomposition of the cell was optimised for a single cell before being carried out for the stack. Fig. 4.5 shows how the cell geometry was split along the length to facilitate meshing.

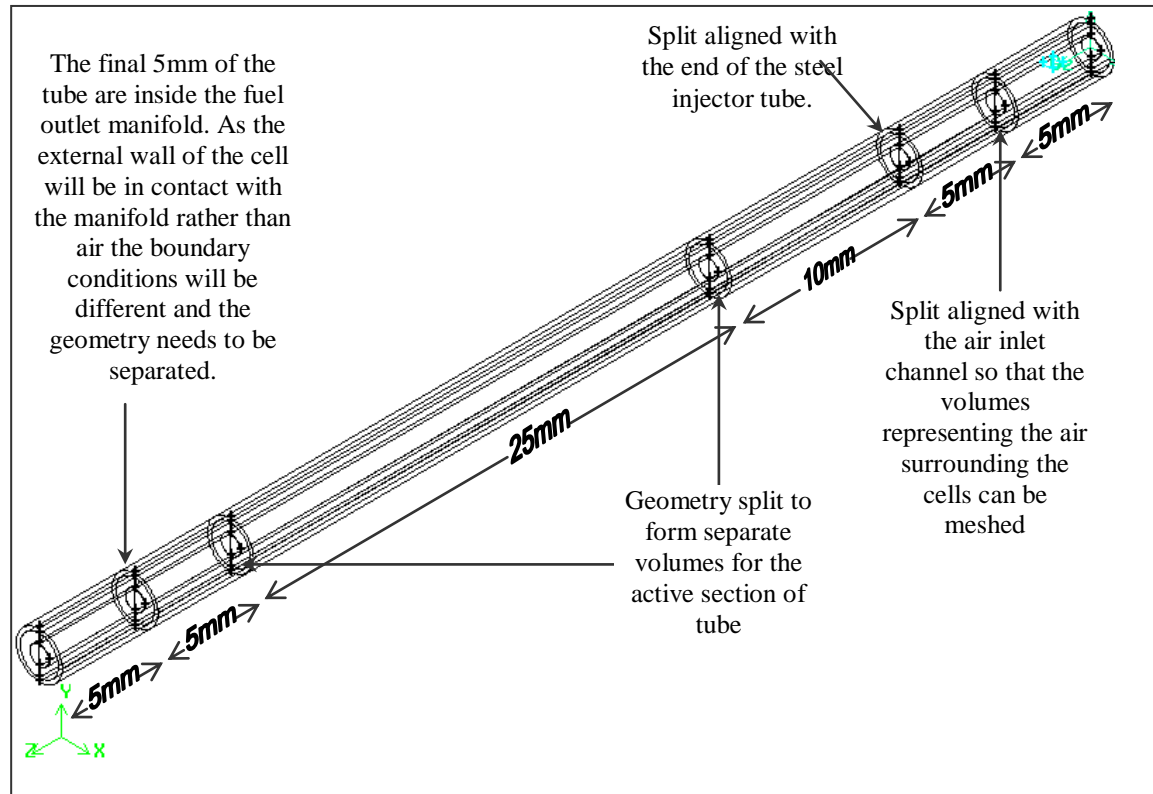


Fig. 4.5 Diagram to show decomposition of the volume presenting the fuel cell to enable meshing and specification of boundary conditions

4.6.2 The air chamber

Once the scheme for decomposing the fuel cell geometries had been determined, the next stage was to construct the geometry representing the surrounding air chamber. Again, the air chamber was decomposed into smaller volumes to permit greater control of the mesh generation. The air chamber was split into 21 sections across its width, corresponding to the divisions relating to the axis of each of the fuel cells. Fig. 4.6 shows the cross section of the geometry representing the air chamber in blue with the 31 different sections.

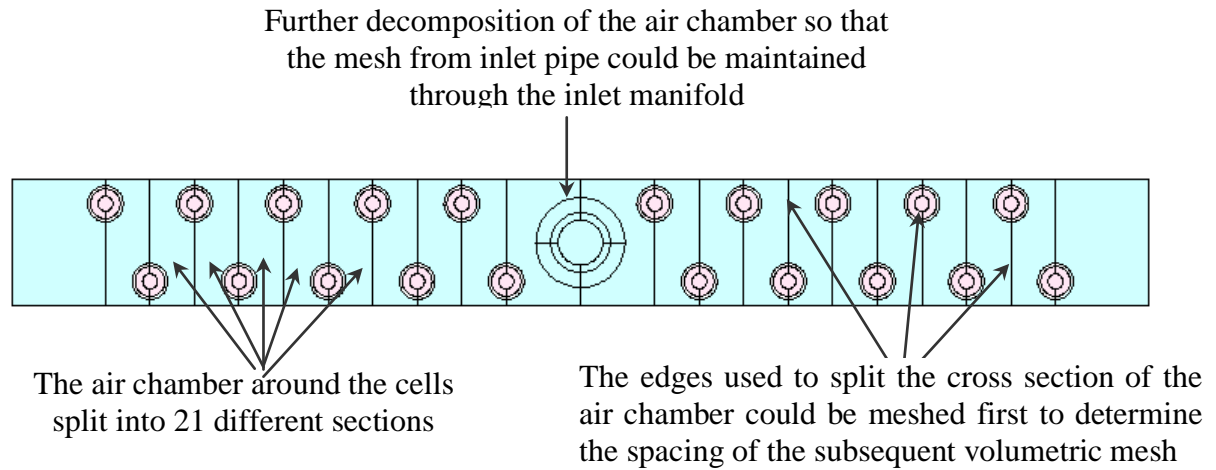


Fig. 4.6 Diagram showing decomposition of volume representing the air chamber around the cells

Once the faces for the cross section had been created, as in Fig 4.6, a number of extrusions were performed on the faces to form a series of volumes that would make up the air chamber around the cells. The extrusions were split into 5 phases as shown in Fig 4.7, rather than by a single extrusion so that the chamber would actually consist of 105 smaller volumes to facilitate greater control over the mesh density.

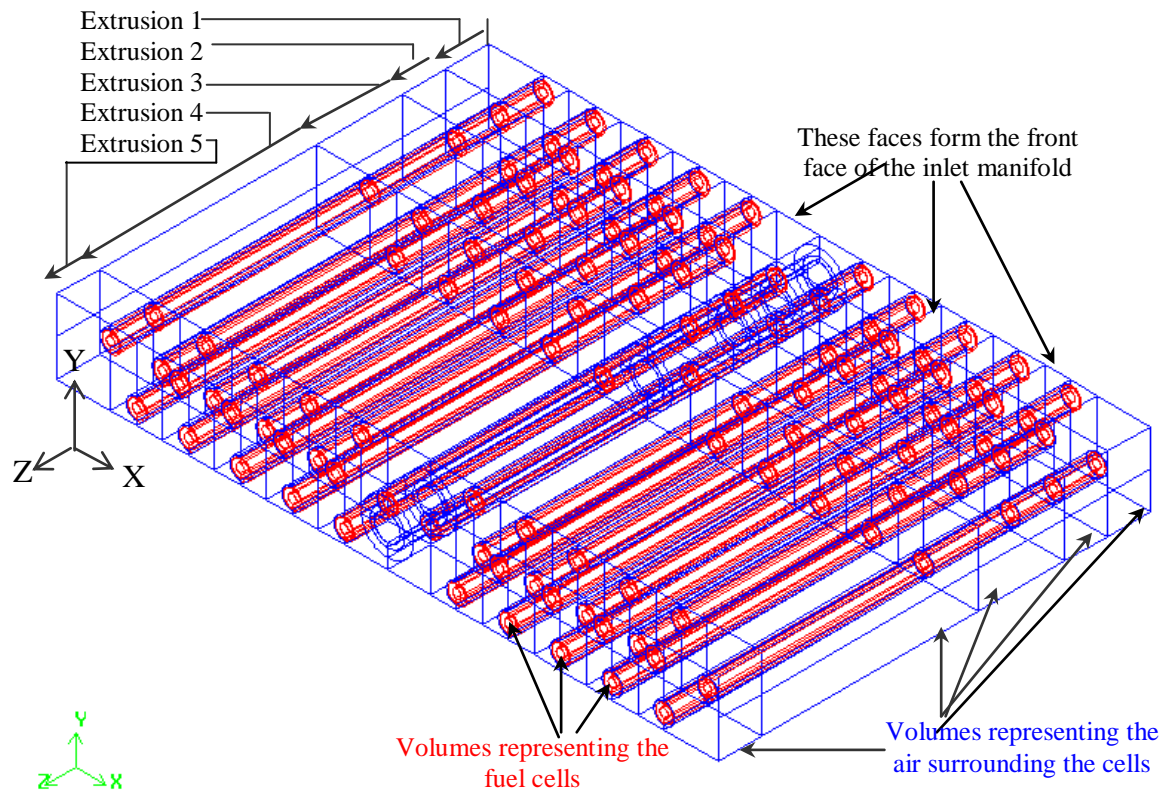


Fig. 4.7 The air chamber decomposed into smaller and more regular volumes

4.6.3 The fuel inlet manifold

As the steel inlet manifold is fabricated from steel and separates the hot air entering the chamber around the cells from cold fuel, it was anticipated that the heat transfer through the inlet manifold would have a significant effect on the temperature profile throughout the stack. With this in mind the geometry of the inlet manifold was modelled as closely as possible to the experimental system.

The manifold was constructed by extruding the faces shown in Fig. 4.7 by 1.25 mm in the -Z direction to create the front wall then a further 12 mm to create the interior volume of the manifold, with a further 1.25 mm extrusion forming the back wall. Vertices were

positioned above the extruded volumes and joined to create edges, which in turn were joined to make faces, then eventually the volumes that formed the top and bottom walls of the manifold. Finally the ends of the manifold were added using the same method as the top walls.

4.6.4 The fuel outlet manifold

The fuel outlet manifold was simplified in order to make meshing easier. The manifold used in the experiment was fabricated from a block of Macor with a square cross section of 15×15 mm with a 8 mm diameter circular channel drilled through the block to create a chamber to collect the fuel from the outlet of the cells. It would be difficult to form a mesh that complied with the mesh used for the fuel cells and surrounding air, so this channel was simplified to a channel of rectangular cross section 10.5×5 mm as shown in Fig. 4.8.

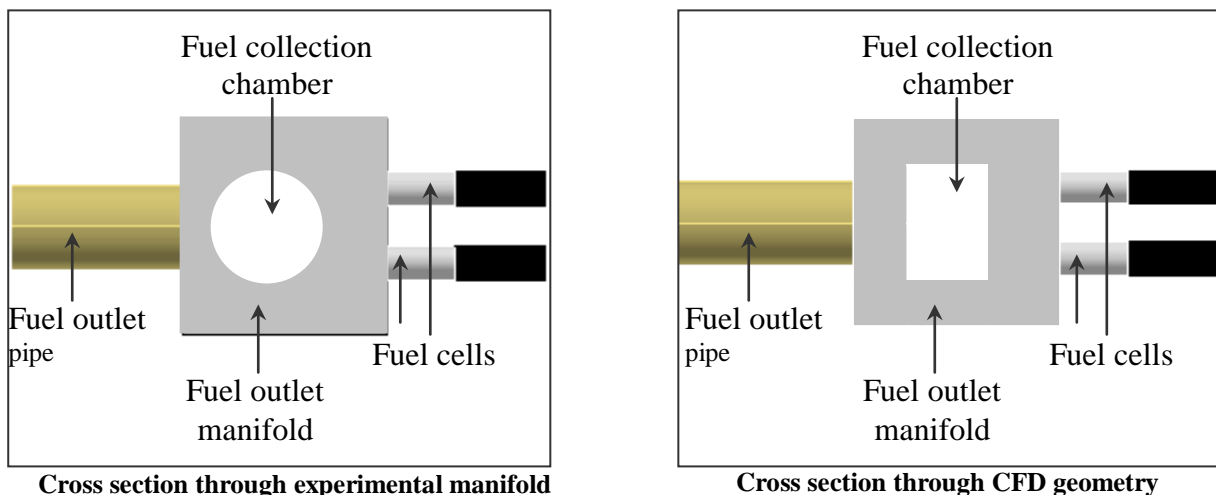


Fig. 4.8 Diagram showing simplification of the fuel outlet manifold for modelling

This simplification only resulted in a 4 % increase in the volume available for flow in the CFD model than compared with the experiment. As there will be less difference in

temperature between the fuel and the air at the end of the stack it is not expected that this simplification will affect the predicted temperature profile throughout the stack significantly.

4.6.5 Outlet and inlet pipes and support rods

Once the geometries representing the fuel manifolds had been completed, the inlet and outlet pipes were added by extruding the appropriate faces on the outside of the inlet and outlet manifolds. The support rods between the two manifolds were also included as it was thought they would have a significant effect on the temperature distribution. Fig. 4.9 shows a photograph of the experimental system and a rendering of the CFD geometry to show the match between the two. Volumes representing the insulation were then constructed to surround the CFD cell stack in the same way as the insulation used in the experimental system.

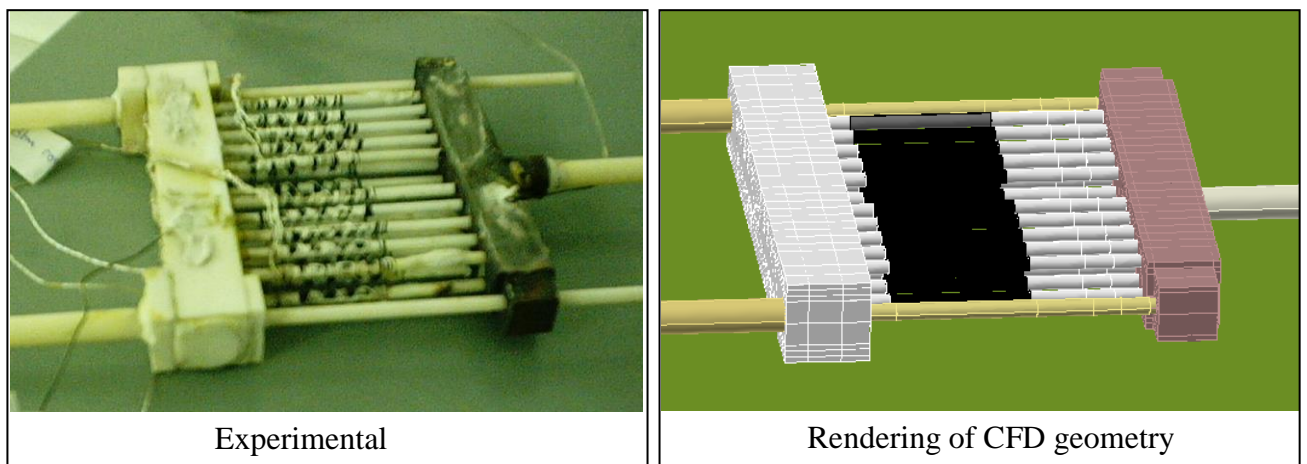


Fig. 4.9 Comparison of stack used in experiments to the CFD geometry

4.7 The Mesh

Once all of the different domains representing the various components of the stack had been constructed the computational mesh was generated. The size of the volumetric mesh elements was controlled by specifying the node spacing along the edges. Then specific face meshes were generated where desired, before using the meshing tools in GAMBIT to complete the volume mesh. The steps taken to generate the volumetric mesh for the cells and the air chamber are shown in Fig. 4.10.

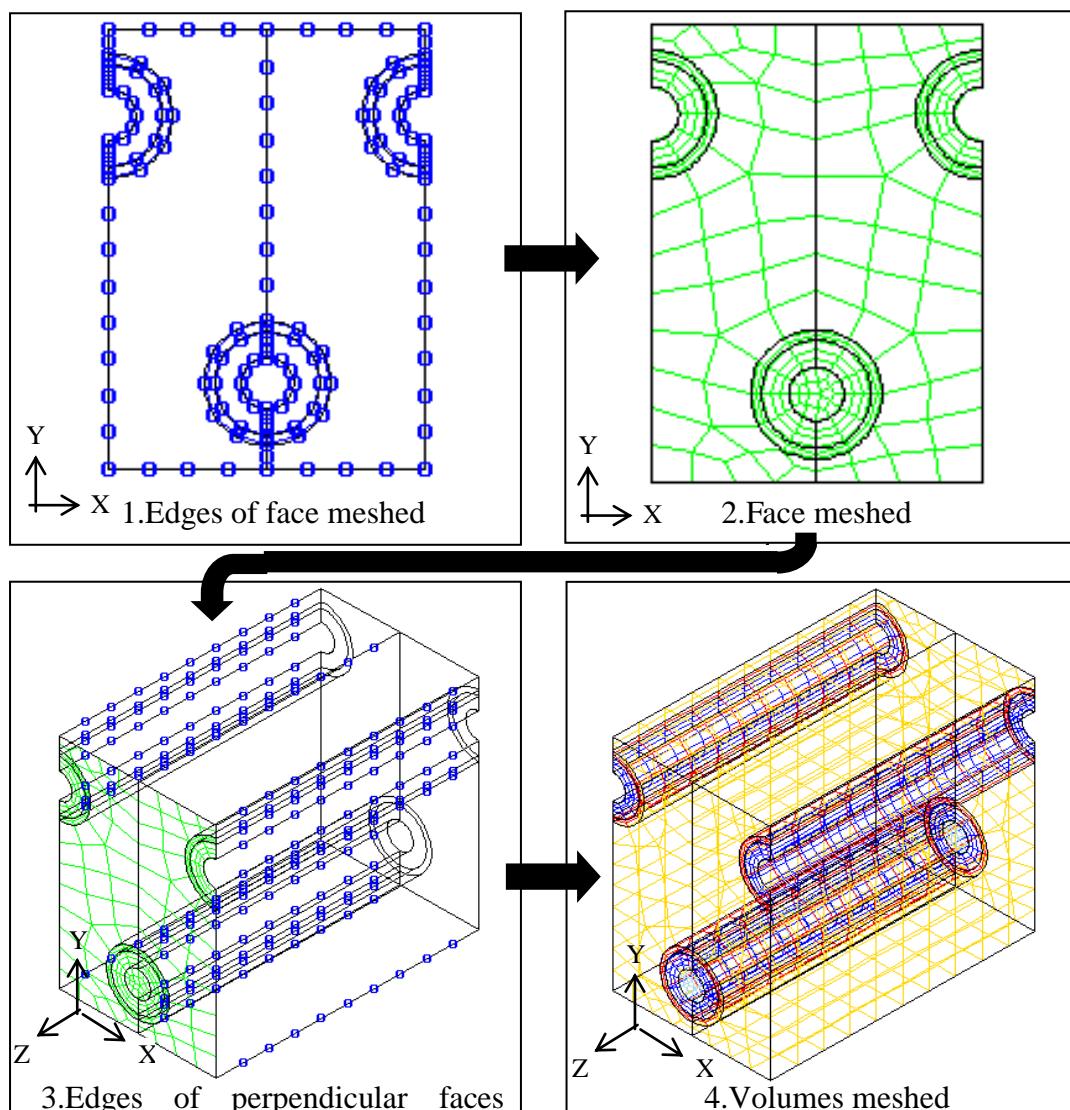


Fig. 4.10 Diagrams to showing meshing procedure

1. Edges of faces meshed

First the spacing of the nodes around the circumference of the fuel cell tubes and on the edges in the X-Y plane of the air chamber was specified. The mesh spacing on each of the different edges on the faces between the outlet manifold and the air and fuel cells is shown in Fig. 4.11. This figure shows the cross section through the air chamber in the X-Y plane. A close node spacing was specified in regions where the largest temperature and velocity gradients were envisaged such as at the boundary between the fuel and the inside wall of the fuel cell tube.

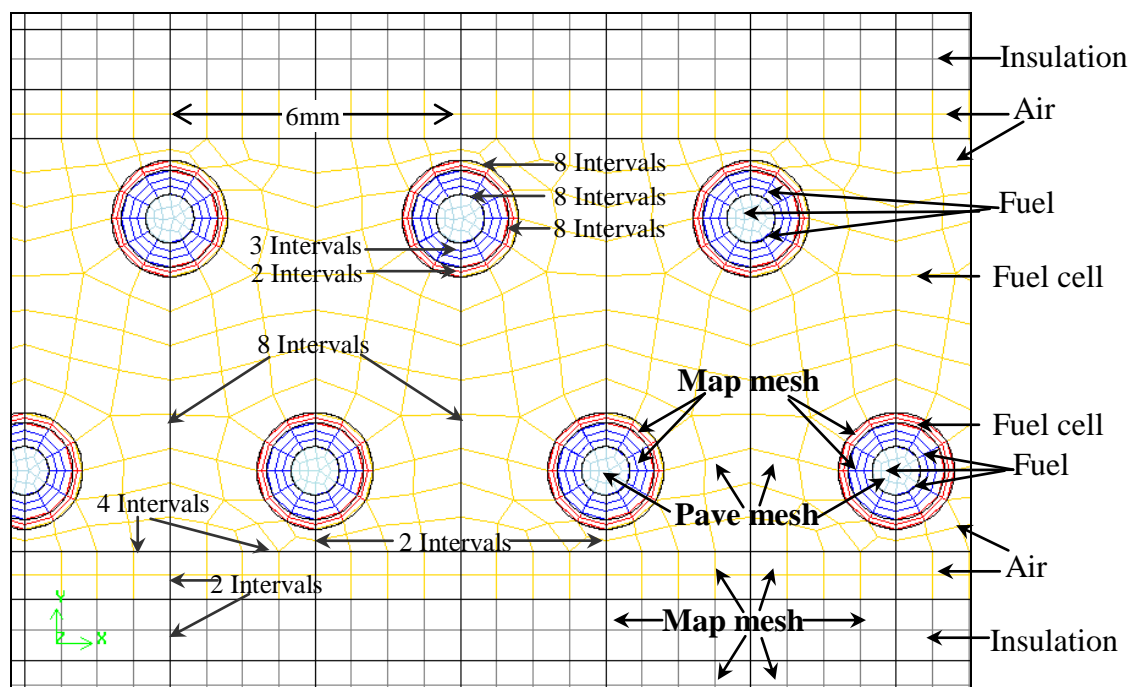


Fig. 4.11 Diagram showing interval sizes on cross section of the mesh

2. Faces meshed

The next stage was to mesh the faces in the X-Y plane. There are a number of different meshing schemes available in Gambit in which the user can specify the options for the ‘element’ parameter, which defines the shape of the mesh elements, and the ‘type’ parameter which defines the pattern of mesh elements on the face^[140]. The scheme used to

mesh the faces largely determined the shape of the elements in the volumetric mesh so time was taken to find the most appropriate formats. The ‘map’ and ‘quad’ option were specified for the ‘type’ and ‘element’ where possible to generate a structured mesh of quadrilateral elements but this option could only be used where the face being meshed represented a logical rectangle. This was the reason for splitting the fuel volume into small components through its cross section, as splitting the face into two regions and using a map mesh for the boundary layer facilitated greater control of the mesh density. An example of this is Fig.4.12 and Fig 4.13.

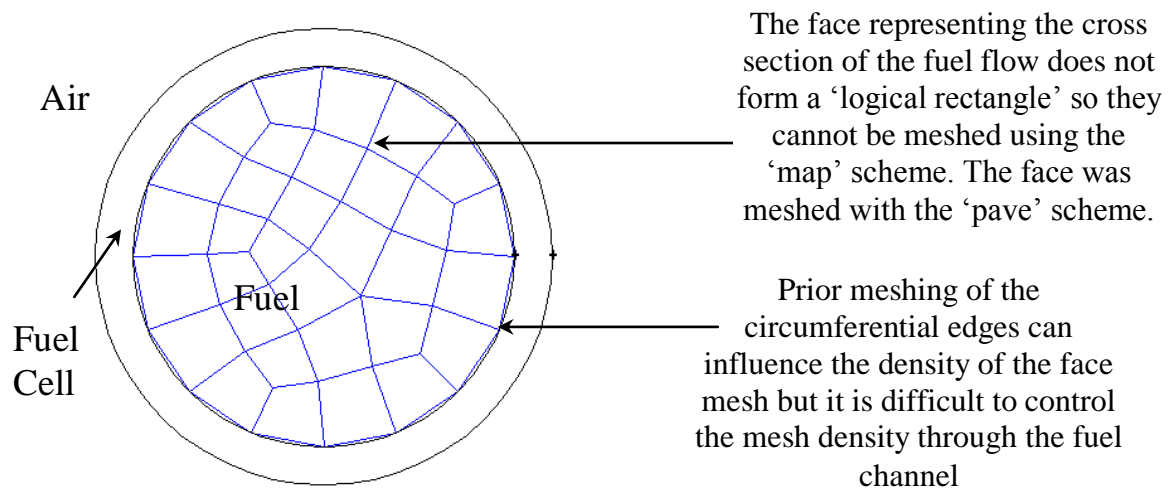


Fig. 4.12 Cross section of fuel channel meshed with *pave* scheme

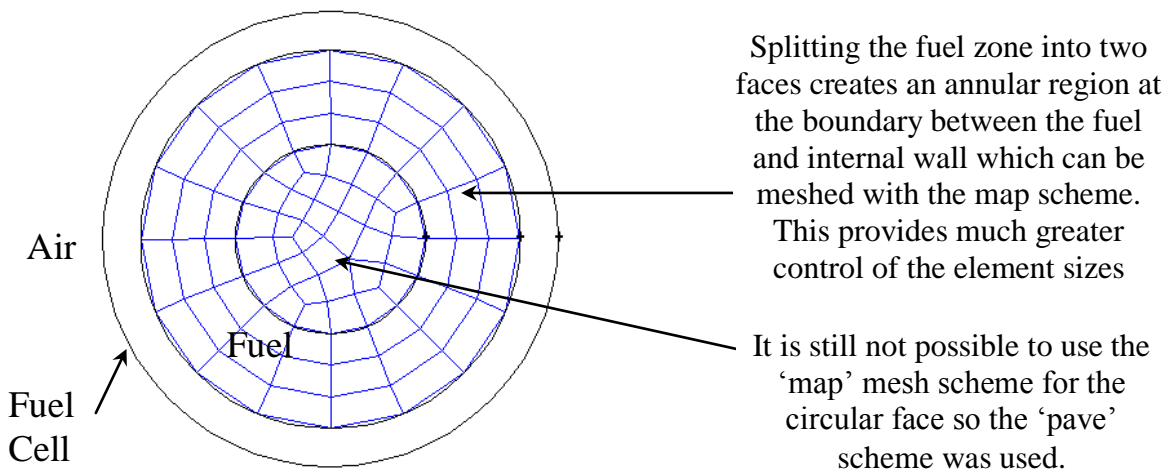


Fig. 4.13 Cross section of fuel channel split into two faces and meshed with *map* and *pave* schemes

3. Edges of perpendicular faces meshed

Having established a reasonable mesh for the faces in an X-Y plane through the centre of the stack, the next stage was to determine the mesh spacing in the Z direction by meshing the edges. The nodes were spaced at 1 mm intervals along the length of the cells and surrounding air chamber but only 3 mm were used along the outlet and inlet pipes to try to reduce the computational effort requirement.

4. Volumes meshed

The volumes were meshed systematically in order that the meshes on faces common to more than one volume were suitable for meshing all of the volumes involved. Again the ‘map’ mesh scheme was used where possible.

The centre of the fuel channel of each of the cells was meshed first using the ‘Cooper’ meshing scheme as the map scheme was not available since the circular faces of the volumes could not be mapped. With the ‘Cooper’ scheme the circular faces were specified as ‘source’ faces. Gambit then created a map mesh on the non-source faces using the spacing determined by the edge meshes. The face mesh on the source face was then projected through the volume onto the opposite source to complete the meshing of the volume.

The outer part of the fuel channel, the fuel cell and the surrounding air channel were then meshed in sequence. The ‘Cooper’ scheme was also employed to mesh the volumes representing the air. Once the volumes representing the fuel cells and surrounding fuel had been meshed, the manifolds and fuel pipes were meshed in the same way.

The final stage was to mesh the insulation surrounding the stack. The mesh density for the insulation was largely determined by the surface mesh on the faces of the insulation in contact with the manifolds or the air chamber around the cells. Despite this restriction, the node spacing in the centre of the thermal insulation walls was increased as much as possible, as a very accurate representation of the temperature profile was less important here than around the cells. The mesh density used for the insulation is show in Fig. 4.14. A double-sided mesh growth ratio of 1.2 was used. This meant the size of each mesh interval was increased by 20% from the previous interval to make the mesh denser at the boundaries of the insulation.

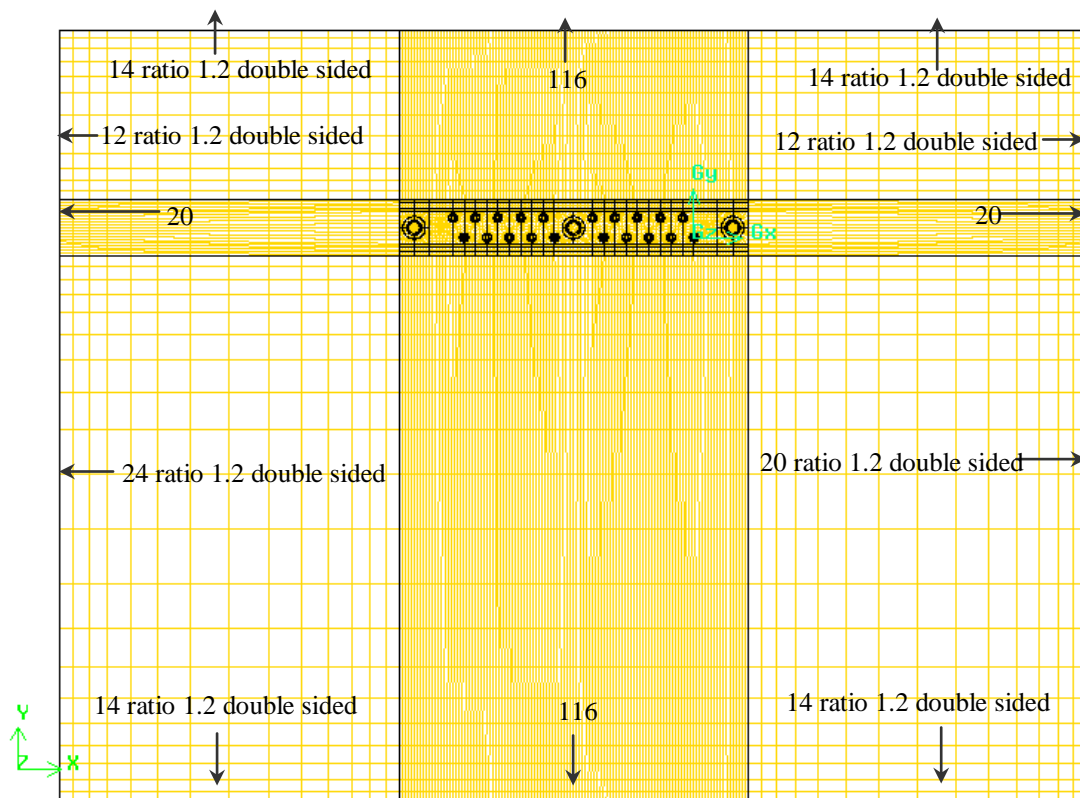


Fig. 4.14 Diagram to show mesh density through the insulation

4.8 Material Properties

Once the mesh file had been exported from GAMBIT to FLUENT, the mesh was scaled and checked. The next stage was to specify the material properties and the boundary conditions.

Material	Density	Heat capacity	Thermal Conductivity	Viscosity
	(kg m ⁻³)	(J kg ⁻¹ K ⁻¹)	(W m ⁻¹ K ⁻¹)	(kg m ⁻¹ s ⁻¹)
Air	1.225 (Default)	1006.43 (Default)	0.0242 (Default)	1.7894e-05 (Default)
Helium	0.1625 (Default)	5193 (Default)	0.512 (Default)	1.998-05 (Default)
Steel	8030 (Default)	502.48 (Default)	16.27 (Default)	NA
Macor	2520	790	1.5	NA
Zirconia	6000	400	2	NA
Micropore	400	1000	0.03	NA

Table 4.1 Table showing material properties used in the CFD model

Table 4.1 gives the material physical properties used in the CFD model. The default properties from the materials library in FLUENT were used for the fluids and steel. Initially, constant gas densities were assumed which were later modified to ideal gas behaviour once the solver had obtained a stable solution.

4.9 Boundary conditions

The first step was to define the material properties though each of the domains; this is required by FLUENT for the specification of boundary conditions. Many of the default

boundary conditions remained unchanged but details of the other boundary conditions are given below.

4.9.1 Inflows and outflows

The inflow and outflow were defined using the mass flow rate inlet condition and the pressure outlet condition. The mass flow rate at the air inlet was $1.97 \times 10^{-4} \text{ kg s}^{-1}$ corresponding to 10 l min^{-1} at standard temperature and pressure. The air inlet temperature was set to 1073 K. The fuel inlet flow was $8.72 \times 10^{-7} \text{ kg s}^{-1}$ corresponding to $0.320 \text{ std. l min}^{-1}$ of Helium. Helium was specified as the anode gas initially for comparison with data from validation experiments. The inlet pressure for the air and fuel was set to 101355 Pa gauge pressure and the outlet pressures were set to atmospheric pressure.

4.9.2 External walls

In keeping with the goal of accurate modelling of heat losses to the atmosphere the mixed heat transfer condition was used at the external wall of the insulation so that radiation and convective heat transfer from the external walls would be coupled to the conductive heat transfer through the insulation. The emissivity was set to 0.8 and the convective heat transfer coefficient was estimated as $7 \text{ W m}^{-2} \text{ K}^{-1}$ on all the external walls. The ambient temperature was set to 298 K.

4.9.3 The air inlet channel

In the experimental system the air was heated from ambient temperature at the inlet to 1073 K at the junction of the inlet channel and the chamber around the cells. The heating was achieved using electrical elements in the channel with the heat load controlled on the

basis of the deviation from the set point temperature. It would be demanding to model this process, so the simulation was simplified by specifying the air inlet temperature at 1073 K and setting the heat flux across the walls of the air inlet channel to zero so that the air entering the chamber around the cells was still at 1073 K as shown in Fig. 4.15.

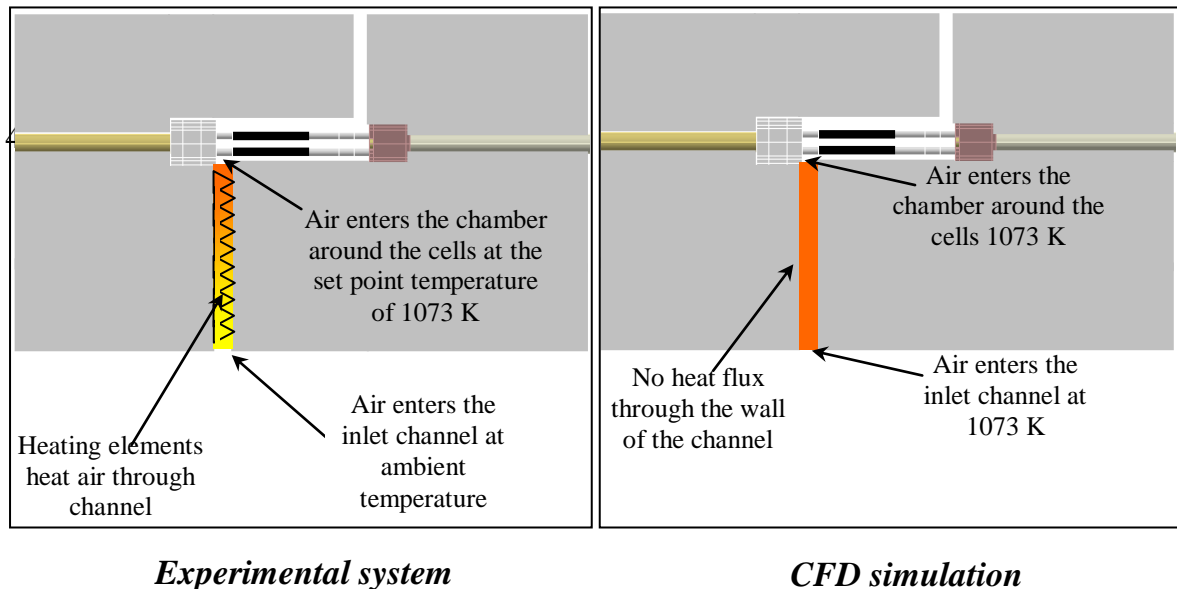


Fig. 4.15 Diagrams to show simplification of the air channel in the CFD simulation

The simplification means there will be no heat transfer from the inlet channel to the insulation which will mean the temperature through the insulation below the fuel cells will be quite different in the experimental system compared to CFD simulation. Some simplification was necessary, however, to prevent the computational effort required to solve the problem from becoming impractical.

The other internal boundaries between the different domains in the stack used the default coupled boundary conditions where the heat transfer across the boundaries was detected by the conditions on either side of the boundary.

4.10 Running the solver

4.10.1 No energy balance

Once the boundary conditions had been set, the solver was run with the energy balance equations switched off so that a stable velocity profile could be obtained before the solver attempted to balance the equations derived from the conservation of energy. Fig. 4.16 shows the scaled residuals from the solver plotted against the number of iterations performed. The residuals are scaled against the initial residual of the momentum and continuity balances. The plot of the residuals indicates that the solution approaches convergence after about 575 iterations.

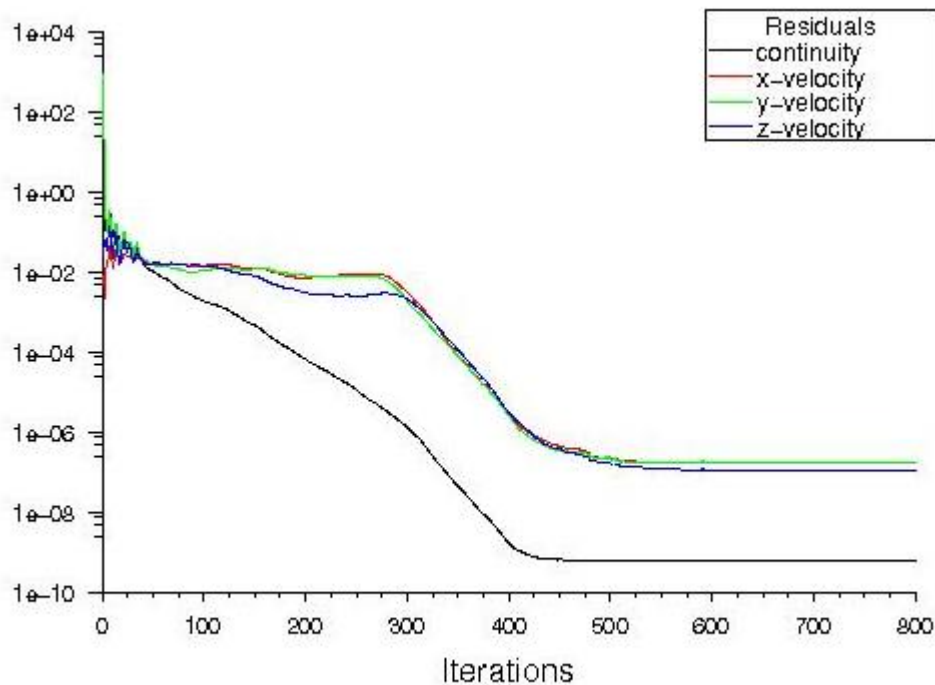


Fig. 4.16 Plot from Fluent showing convergence of the scaled residuals for the model with ideal gas behaviour

In addition to checking the plot of the residuals produced by the solver, the mass balance around the system was checked by summing the mass fluxes at the inlets and outlets. Obviously, at steady state, there should be no accumulation of mass, so a mass balance around the system can be a further method of checking the simulation has converged to a rational solution. Table 4.2 shows the mass balance around the system using the inlet and outlet fluxes calculated by the solver.

Iteration	Air inlet kg s ⁻¹	Air outlet kg s ⁻¹	Fuel inlet kg s ⁻¹	Fuel outlet L kg s ⁻¹	Fuel outlet R kg s ⁻¹	Accumulation kg s ⁻¹
100	1.98×10 ⁻⁰⁴	5.34×10 ⁻⁰⁵	8.73×10 ⁻⁰⁷	-1.74×10 ⁻⁰⁵	1.35×10 ⁻⁰⁵	2.48×10 ⁻⁰⁴
150	1.98×10 ⁻⁰⁴	-1.39×10 ⁻⁰⁴	8.73×10 ⁻⁰⁷	-1.57×10 ⁻⁰⁶	1.13×10 ⁻⁰⁶	5.93×10 ⁻⁰⁵
200	1.98×10 ⁻⁰⁴	-1.83×10 ⁻⁰⁴	8.73×10 ⁻⁰⁷	-5.04×10 ⁻⁰⁷	-3.36×10 ⁻⁰⁷	1.47×10 ⁻⁰⁵
250	1.98×10 ⁻⁰⁴	-1.97×10 ⁻⁰⁴	8.73×10 ⁻⁰⁷	-4.42×10 ⁻⁰⁷	-4.32×10 ⁻⁰⁷	4.43×10 ⁻⁰⁷
300	1.98×10 ⁻⁰⁴	-1.98×10 ⁻⁰⁴	8.73×10 ⁻⁰⁷	-4.37×10 ⁻⁰⁷	-4.36×10 ⁻⁰⁷	2.93×10 ⁻⁰⁸
350	1.98×10 ⁻⁰⁴	-1.98×10 ⁻⁰⁴	8.73×10 ⁻⁰⁷	-4.36×10 ⁻⁰⁷	-4.36×10 ⁻⁰⁷	-6.87×10 ⁻⁰⁸
400	1.98×10 ⁻⁰⁴	-1.98×10 ⁻⁰⁴	8.73×10 ⁻⁰⁷	-4.36×10 ⁻⁰⁷	-4.36×10 ⁻⁰⁷	-5.30×10 ⁻⁰⁹
450	1.98×10 ⁻⁰⁴	-1.98×10 ⁻⁰⁴	8.73×10 ⁻⁰⁷	-4.36×10 ⁻⁰⁷	-4.36×10 ⁻⁰⁷	1.19×10 ⁻⁰⁹
500	1.98×10 ⁻⁰⁴	-1.98×10 ⁻⁰⁴	8.73×10 ⁻⁰⁷	-4.36×10 ⁻⁰⁷	-4.36×10 ⁻⁰⁷	8.72×10 ⁻¹⁰
550	1.98×10 ⁻⁰⁴	-1.98×10 ⁻⁰⁴	8.73×10 ⁻⁰⁷	-4.36×10 ⁻⁰⁷	-4.36×10 ⁻⁰⁷	8.72×10 ⁻¹⁰
600	1.98×10 ⁻⁰⁴	-1.98×10 ⁻⁰⁴	8.73×10 ⁻⁰⁷	-4.36×10 ⁻⁰⁷	-4.36×10 ⁻⁰⁷	8.71×10 ⁻¹⁰
650	1.98×10 ⁻⁰⁴	-1.98×10 ⁻⁰⁴	8.73×10 ⁻⁰⁷	-4.36×10 ⁻⁰⁷	-4.36×10 ⁻⁰⁷	8.71×10 ⁻¹⁰
700	1.98×10 ⁻⁰⁴	-1.98×10 ⁻⁰⁴	8.73×10 ⁻⁰⁷	-4.36×10 ⁻⁰⁷	-4.36×10 ⁻⁰⁷	8.71×10 ⁻¹⁰
750	1.98×10 ⁻⁰⁴	-1.98×10 ⁻⁰⁴	8.73×10 ⁻⁰⁷	-4.36×10 ⁻⁰⁷	-4.36×10 ⁻⁰⁷	8.71×10 ⁻¹⁰
800	1.98×10 ⁻⁰⁴	-1.98×10 ⁻⁰⁴	8.73×10 ⁻⁰⁷	-4.36×10 ⁻⁰⁷	-4.36×10 ⁻⁰⁷	8.71×10 ⁻¹⁰

Table 4.2 Table showing mass fluxes across the boundaries calculated by the solver with constant gas densities

The accuracy of the mass balance improved with each iteration until around 550 iterations had been performed. Further iterations yielded only incremental improvement until 800 iterations when the solution remained constant with an error in the mass balance of $8.719 \times 10^{-10} \text{ kg s}^{-1}$, which represents an error of 0.00044 % as percentage of the total inflow. This was adjudged to be an acceptable error.

As a final step to check the feasibility of the simulation results, the velocity profile across each of the fuel cells were plotted to check they were rational and if the flow was evenly distributed between the cells.

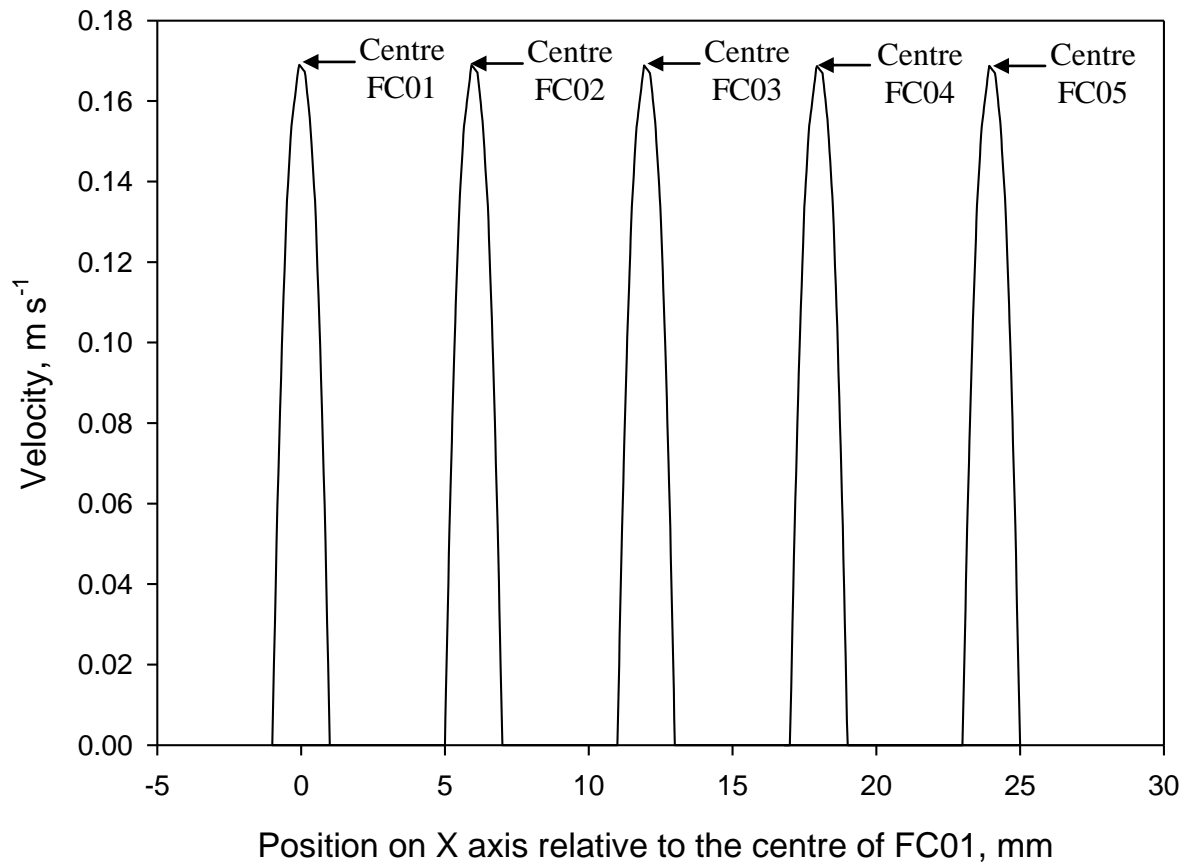


Fig. 4.17 Velocity profile across cells 1 to 5

Assuming the 0.320 l min^{-1} of Helium fed to the anode side of the cells was split evenly between the 20 cells, the mean axial velocity in the cells would be 0.085 m s^{-1} . The velocities plotted in Fig 4.17 appear to be consistent with this and show only a slight variation between the maximum velocities reached in each of the fuel cells, providing further evidence that the simulation results were plausible.

4.10.2 With energy balance

Once a stable solution had been obtained the equations for the conservation of energy were then activated using the default constant density fluid properties for the air and Helium. The effect of activating the energy balance is shown in Fig. 4.18. After less than a further 50 iterations the residuals had re-converged, but the time taken to complete each iteration was increased significant from around 6 seconds to around 56 seconds.

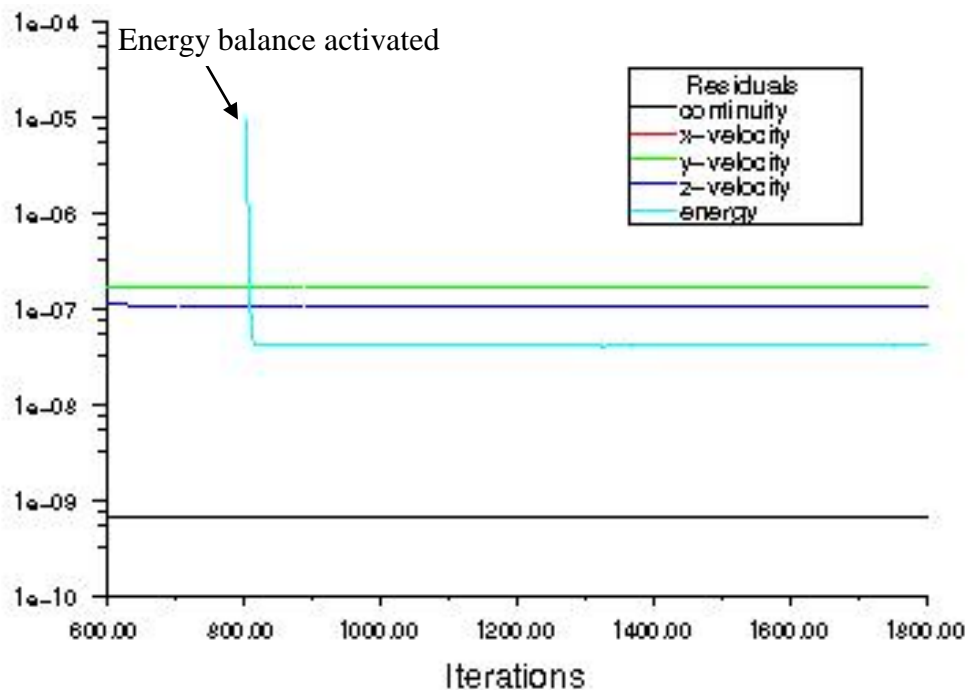


Fig. 4.18 Plot of scaled residual against number of iterations performed

In addition to monitoring the sum of the weighted residual to check for convergence, the mass and energy fluxes across the fluid inlet and outlet and heat flux across the external walls were recorded. At steady state there should obviously be no accumulation of energy and the net heat flux from the simulation was 0.004725 W, which was considered negligible as was the accumulated mass flux of $8.7 \times 10^{-10} \text{ kg s}^{-1}$. The sum of the mass balance remained virtually constant. The net heat energy balance approached convergence after less than 50 iterations but when the simulation was run for further iterations the net

heat transfer rose slightly with every iteration. To check whether this trend was going to be significant, the simulation was run for a total of 2000 iterations. The result of the simulation was shown to be stable as the net heat transfer increased by only 0.0008 W from 400 iterations to 2000 iterations.

For a further check of convergence, the temperature profile through the stack after 1000 and 2000 iterations was plotted along a line through the stack, by plotting temperature versus position in the z direction along a line above the 4th cell on the bottom row. The greatest difference in temperature between the profile after 1000 iterations compared with after 2000 iterations at 100 points through the stack was 0.01 K so the simulation result was adjudged to have converged by 1000 iterations.

In order to get a more comprehensive look at the predicted temperature profile, the temperature contours on a plane through the centre of the stack were plotted to see if they were feasible.

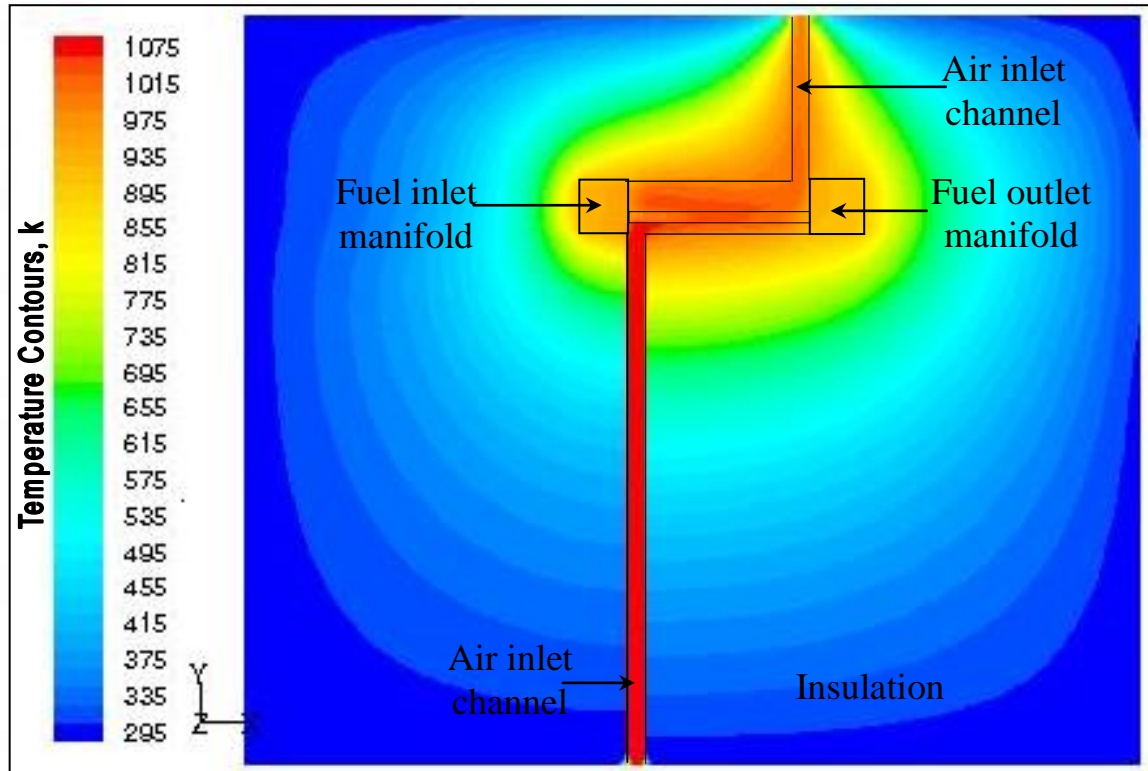


Fig. 4.19 Plot of temperature contours on vertical plane through the cell 04

The temperature contours shown in Fig. 4.19 look feasible apart from the sharp temperature difference at the boundary between the air inlet channel and the surrounding insulation. This abnormality was expected from the assumption of no heat flux across the wall of the air inlet channel. We can see the fuel entering the stack is cooler than the surrounding air until it is about 10 mm into the cell.

4.10.3 With ideal gas behaviour

Satisfied that the solution obtained at this stage was stable and feasible, the complexity of the model was increased by exchanging ideal gas behaviour for the constant density assumption.

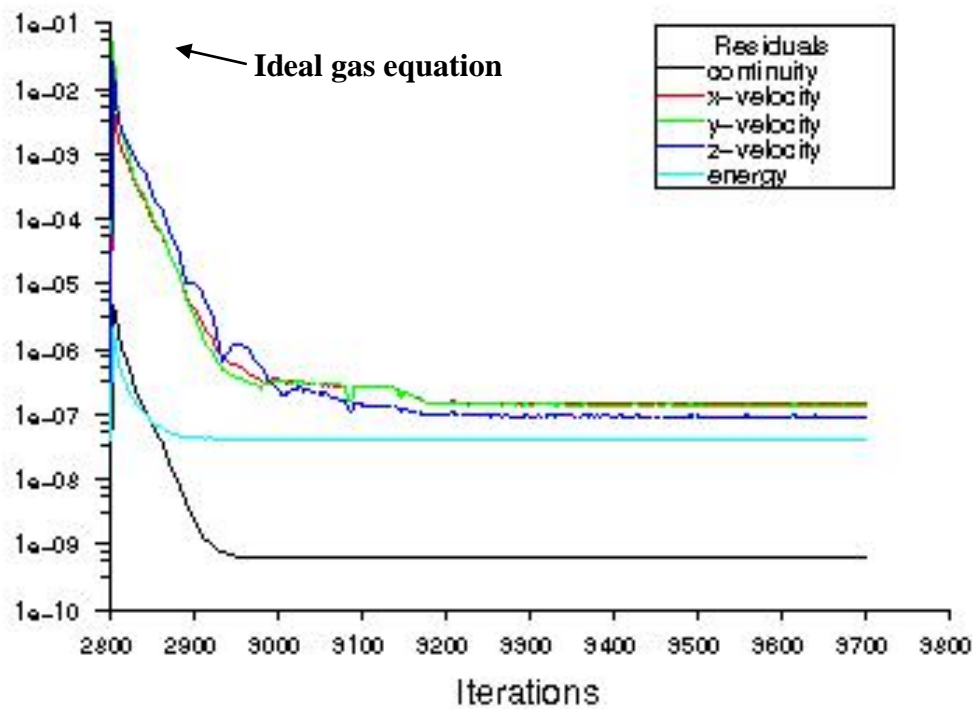


Fig. 4.20 Scaled residuals for ideal gas simulation

The solution re-converged within 400 further iterations and the time required for each iteration did not increase significantly as shown in Fig. 4.20. A mass and energy balance was carried out to check the accuracy of the solution, by summing the mass fluxes across the external balances. The accumulated mass flow was $8 \times 10^{-10} \text{ kg s}^{-1}$, which was considered negligible, and close to the discrepancy produced with the constant density assumption. The accumulated heat was 0.007 W so there was a small deterioration of 0.003 W compared to the constant density model.

4.11 Effect of mesh size

The next stage was to investigate if the chosen mesh size was suitable by testing if changes to the mesh density affected the simulation results.

4.11.1 Effect of mesh size through the insulation

The first step in the investigation into the effect of mesh size was to increase the mesh density for the domain representing the insulation. This was achieved by adding 2 mesh nodes to the vertical and horizontal edges as shown Fig. 4.21 and Table.4.3.

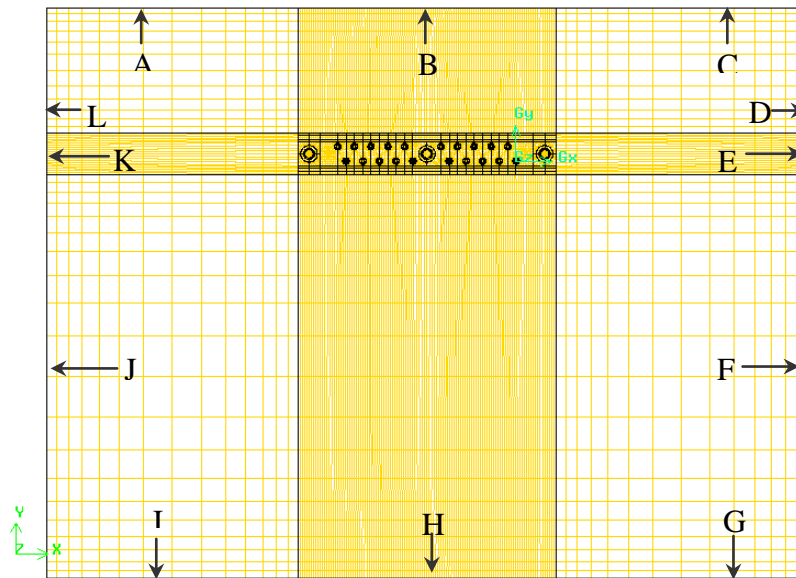


Fig. 4.21 Diagram to labelling of edges as referred to in Table 4.3

Mesh	Number of intervals per edge												Net mass flux kg s^{-1}	Net heat flux W	Mean fuel outlet temp. K	Mean air outlet temp. K
	A	B	C	D	E	F	G	H	I	J	K	L				
M_0	14	116	14	12	20	20	14	116	14	20	20	12	8.0×10^{-10}	0.007	946.8	330.83
M_1	16	116	16	14	20	22	16	116	16	22	20	14	7.9×10^{-10}	0.009	946.2	332.32
M_2	18	116	18	16	20	24	18	116	18	24	20	16	7.1×10^{-10}	0.009	945.2	330.65

Table 4.3 Refinement of mesh representing the insulation and the effect on the simulation results

Fig. 4.23 shows that the net heat transfer was slightly closer to zero with increased mesh resolution but the improvement of $9.0 \times 10^{-11} \text{ kg s}^{-1}$ was not considered significant. There

was a slight increase to the heat lost with the fuel exiting the system, This represented a 1.5 K increase in the average exit temperature when the simulation was run with using mesh, M_1 but this increase was reversed when mesh, M_2 was employed.

The temperature profile through the stack was plotted for the modified meshes, M_1 and M_2 and compared with the profile predicting using the original mesh. The greatest temperature difference was found to be between the simulation results for the original mesh and M_1 and this was only 2 K at the edges of the insulation. When the mesh density was increased further by forming mesh M_2 the maximum difference in temperature was less than 1 K.

The evidence from the investigation into the density of the mesh through the insulation volume suggested that the mesh was sufficiently dense such that further refinement would not change the simulation results.

4.11.2 Effect of the mesh size around the cell perimeter

Changing the mesh density around the cells was more cumbersome than changing the mesh through the insulation. The central location of the cells within the geometry meant that any changes to the mesh density through the cells required almost all of the surrounding volumes to be re-meshed. However, it was acknowledged that appropriate mesh size through the volumes representing the cell and surrounding air was crucial to the simulation results so the mesh was refined once and the simulation solved using the new mesh. The mesh was refined by increasing the number of intervals around the perimeter of each of the cells from 12 to 16 as shown in Fig.4.24 and Table 4.4.

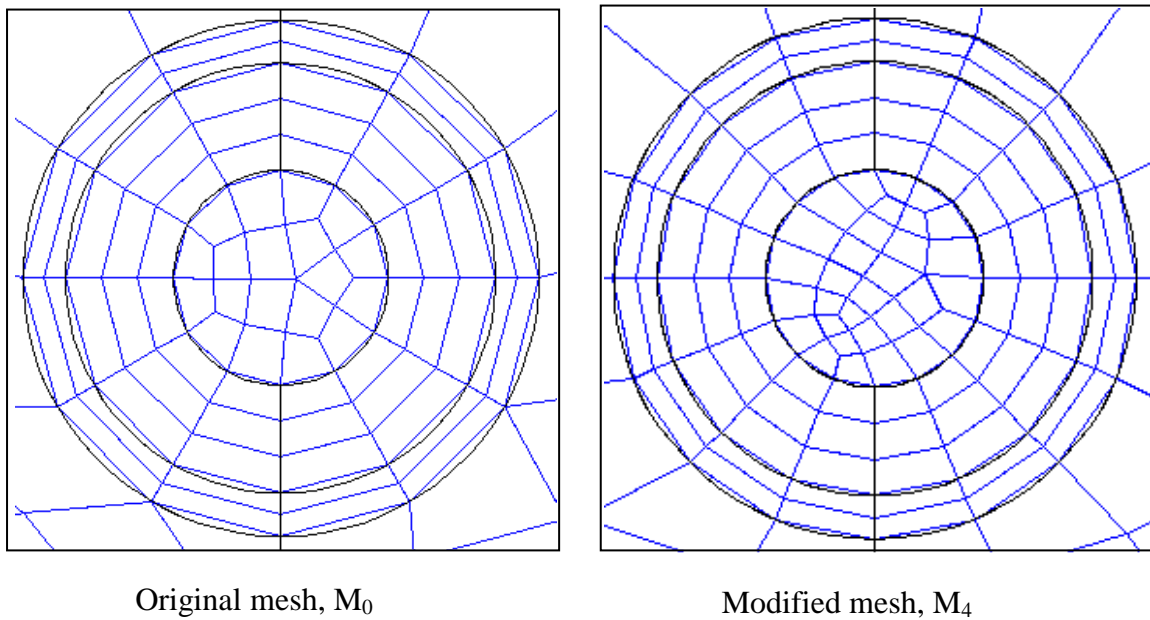


Fig. 4.22 Diagram showing refinement of the mesh around the fuel cells

	Net mass flux	Net heat flux	Mean air outlet temp.	Mean fuel outlet temp.
	Kg sec ⁻¹	W	K	K
M ₀	8.0x10 ⁻¹⁰	0.007	946.82	330.83
M ₄	4.1 x10 ⁻¹⁰	0.002	945.51	332.09

Table 4.4 Effect of increased mesh density around the cells on the simulation solution

Table 4.4 shows that refining the mesh around the fuel cells had little effect on the simulation results. When the temperature profile along a line through the stack was plotted the maximum temperature difference, between the profile produced using the original mesh and mesh, M₄, was only around 1 K so the original mesh was deemed sufficiently dense.

4.12 Conclusions

In this Chapter the development of a CFD model of a 20-cell micro-tubular SOFC system was presented. The model represents the first published model of a micro-tubular SOFC system and several criteria were identified to ensure that the model was relevant for predicting performance of the thermal design of small micro-tubular systems. These included accurate modelling of the air channel around the cells and the heat losses through the surrounding insulation.

The cell geometry and the physical and electro-chemical process involved with its operation were simplified for the purposes of the model. The cells were represented merely by a single-layer tube split into 3 regions along their length in which volumetric heat source terms could be specified to represent the heat produced by electrochemical reactions. With the advent of increasing computing power this model could serve as a basis for future work that incorporates more of the electrochemistry.

The suitability of the mesh used in the model was evaluated by looking at the sensitivity of the results to changes in the mesh size. No significant changes to the predicted temperature profile were observed when the mesh size was increased which indicated that the refinement of the mesh was sufficient. The validation of the model developed in this Chapter is described in Chapter 5.

5. Validation experiments and simulations

5.1 Introduction

This Chapter describes the validation of the CFD simulation of the 20-cell SOFC stack discussed in Chapters 4. The objective of the work reported in this Chapter was to investigate if a simplified computational model could be used to provide a reasonable estimate of the temperature profile through a micro-tubular stack. Successful validation of the model would pave the way for the same approach to be used to model larger stacks and to analyse the viability of different stack designs and operating conditions.

Validation is an important part of the modelling process^[133] but can prove difficult and has been excluded in many published works on the modelling of SOFC systems^[83-87,99,100,107,124]. Whilst some of the works concerned with the modelling of SOFC have only been validated against other modelling studies^[74,124] it was considered essential in this work to check the model performance against some experimental data.

Experiments were carried out with an inert gas passing through the anodes on the inside of the cells. This meant the effect of heat generated by electrochemical reactions was eliminated from the validation exercise. It was thought that if the temperature profile predicted by simulation, without electrochemical reaction, matched the experimental results then the model would have a good basis for future development.

5.2 Experimental procedure

The experimental equipment was operated as described in Chapter 3. The Helium was delivered to the anode side of the cells at a rate of 5.33×10^{-6} std. $\text{m}^3 \text{s}^{-1}$. With the cells only fed with inert gas, there was no need to monitor the electrochemical performance so no electrical load was placed across the cells. The air inlet temperature was 1073 K and the cathode side flow rate was 1.977×10^{-4} std. $\text{m}^3 \text{s}^{-1}$. The temperature was monitored through the stack until the temperature remained constant. The temperatures recorded through the stack appeared to have stabilised after 7 hours operation, but the experiment was left to run for 24 hours to ensure that the final temperatures that were recorded were steady state values. The experiment was repeated three times to check the reproducibility of the results and agreement was found between the results. The temperatures recorded at all of the thermocouple positions were within ± 2 K of the value recorded in the original tests.

5.3 CFD simulation and prediction of temperature

5.3.1 Boundary conditions

The boundary conditions were set to match the experimental conditions with Helium through the anode side of the cells. The convective heat transfer coefficient, h , at the external walls was specified as $7 \text{ W m}^{-2} \text{ K}^{-1}$ and the emissivity, ϵ was specified as 0.8 ^[141] with the external temperature at 300 K. The pressure at the air outlet was specified as atmospheric pressure and 101355 Pa gauge pressure at the air inlet. The inlet temperature to the air inlet channel was specified as 1073 K.

5.3.2 Running the solver

The solver was run according to the procedure outlined in Chapter 4 with 0.32 std. l min⁻¹ on the anode side of the cells and 10 std. l min⁻¹ of air preheated to 1073 K on the cathode side of the cells.

5.3.3 Post processing of the CFD simulations

In order to view the temperature and velocity profiles in the air and fuel regions of the stack additional surfaces and lines had to be constructed for post processor. Vertical planes were created to view the temperature and velocity contours, but for a more accurate comparison between different simulations and experimental results, a line was mapped out which could be used to retrieve the temperatures predicted at intervals along its length.

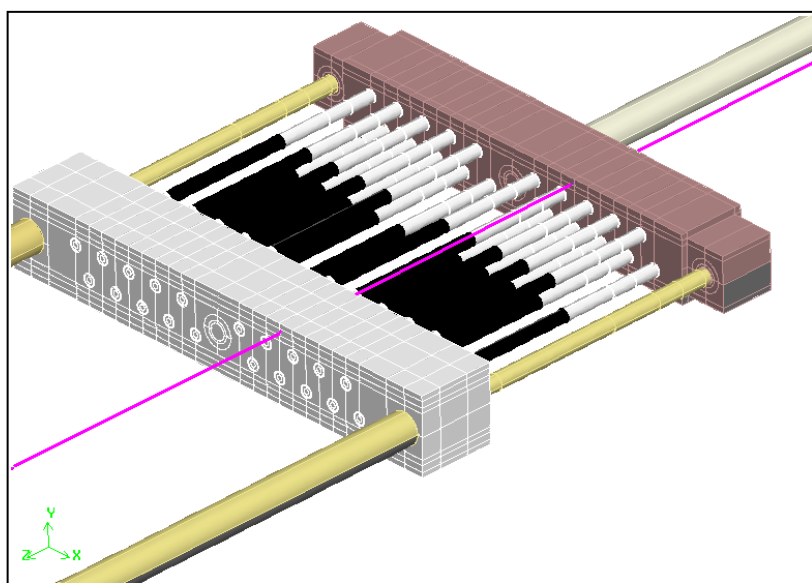


Fig. 5.1 Diagram showing the line used to provide temperature data for comparison with experimental readings

The pink line in Fig 5.1 shows the line used to extract the predicted temperatures across the air chamber at a position 7.4 mm above the axis of cell FC04. The tips of five

thermocouples were positioned along this line in the experiment, as discussed in Chapter 3. The location of the post processing line in relation to the cells is also shown in Fig. 5.2 for clarity.

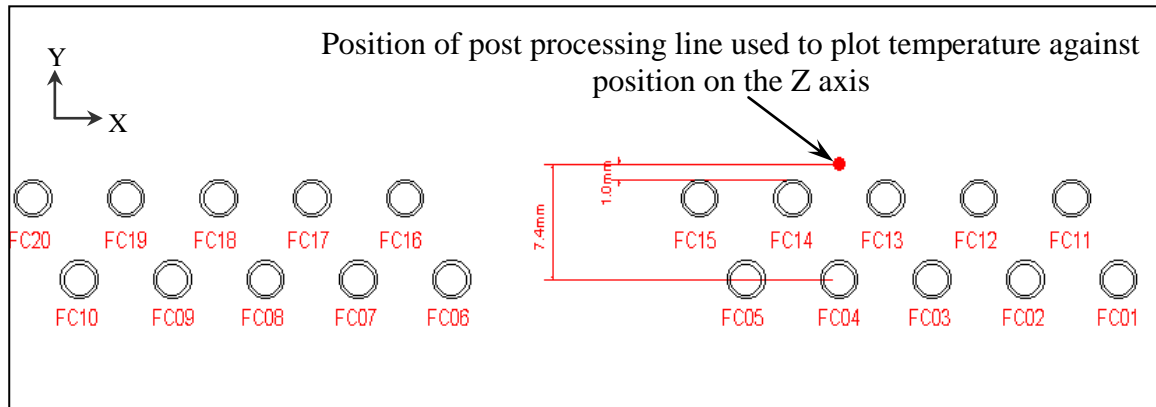


Fig. 5.2 Diagram showing the cross section through the SOFC stack to show the position of the post processing line in relation to the cells

This position was chosen to compare the temperatures predicted by simulation and experiment because along this line the temperature field is influenced by many factors including the heat transfer between the air, many cells and the walls, so should provide a good test of the accuracy of the model.

5.3.4 Results

The plots shown in Fig 5.3 show the comparison of the temperature predicted by CFD simulation along the processing line shown in section 5.3.3 and the temperatures recorded by thermocouples at 5 locations along the line in the experimental study.

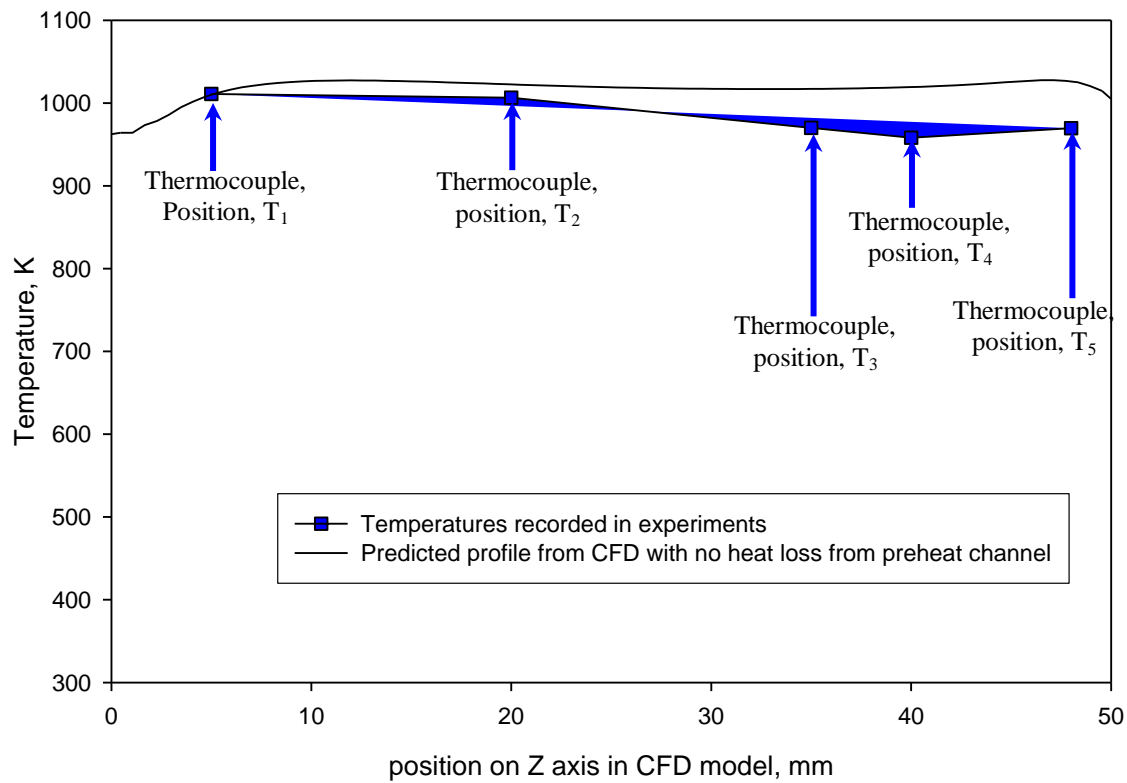


Fig. 5.3 Comparison between temperatures predicted by the CFD model and the experimental results

There is excellent agreement between the CFD simulation and the experimental recording at the first two thermocouple positions to within 10 K. The general trend in both the experimental and CFD results is one of decreasing temperature along the length of the fuel cell, followed by an increase in temperature close to the end of the cells and the air exit.

The explanation for the temperature rise can be observed more clearly by looking at the temperature contours and velocity vectors from the CFD model which have been plotted on a vertical plane through FC04 as shown in Fig 5.4 and 5.5. The plots show the hottest

region follows the path of the bulk air flow through the cell chamber with heat lost to the walls as the fluid progresses through the chamber.

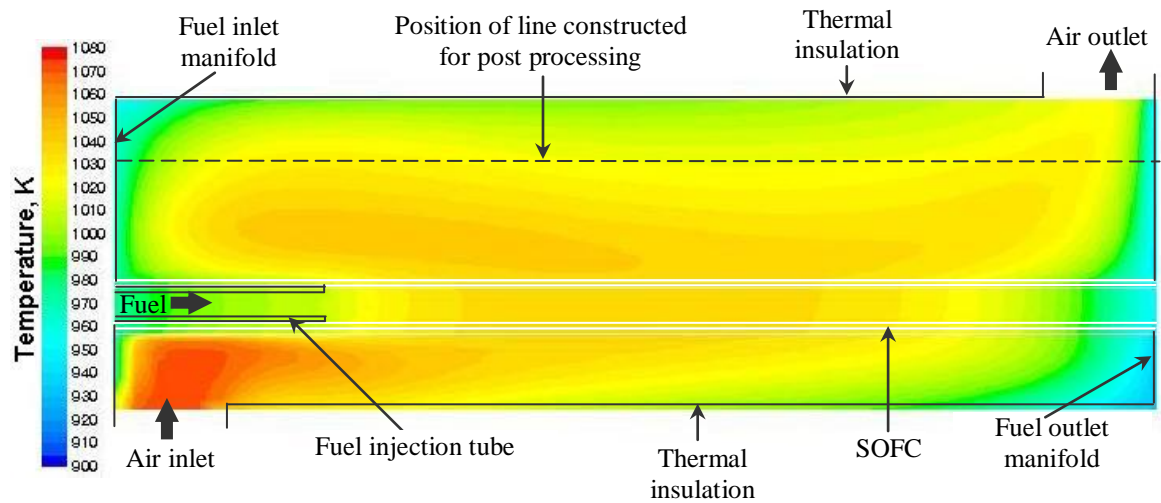


Fig. 5.4 Contours showing temperature on a vertical plane through FC04

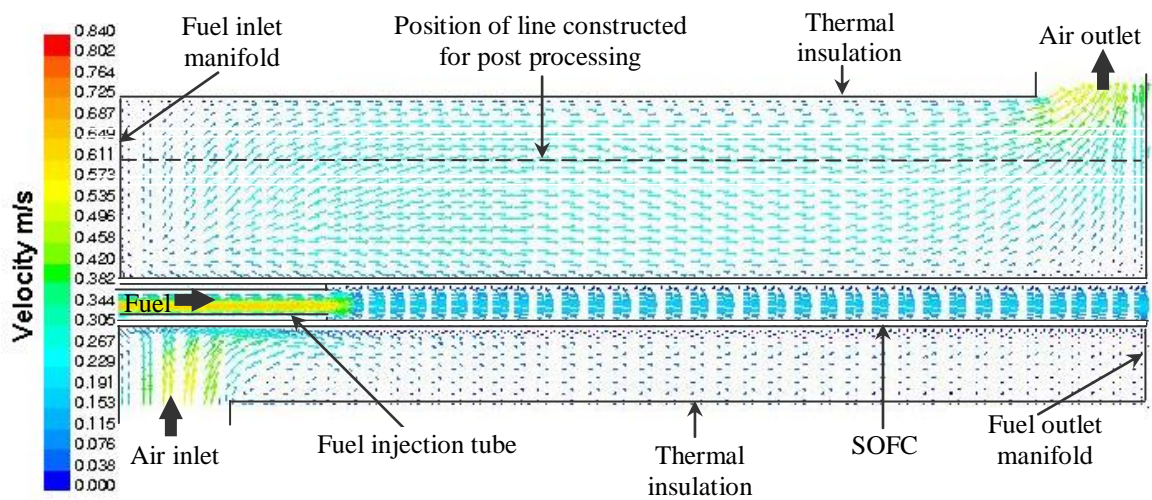


Fig. 5.5 Showing velocity vectors on a vertical plane through FC04

Whilst the first two experimental points are very close to the temperature predicted by the simulation the final two temperatures recorded by experiment are up to 40 K lower than the temperature predicted at the equivalent position in the CFD simulation. Various

possible explanations for the deviations towards the outlet end of the cell were proposed and these are discussed in the following sections.

5.4 Consistency across the stack

To check that the same trend and agreement between simulation and practical results was produced across the stack the thermocouples were relocated to new positions and the experiments re-run under the same conditions. Further post processing lines were constructed in the CFD model to obtain the temperatures predicted by simulation at positions equivalent to the locations of the thermocouples.

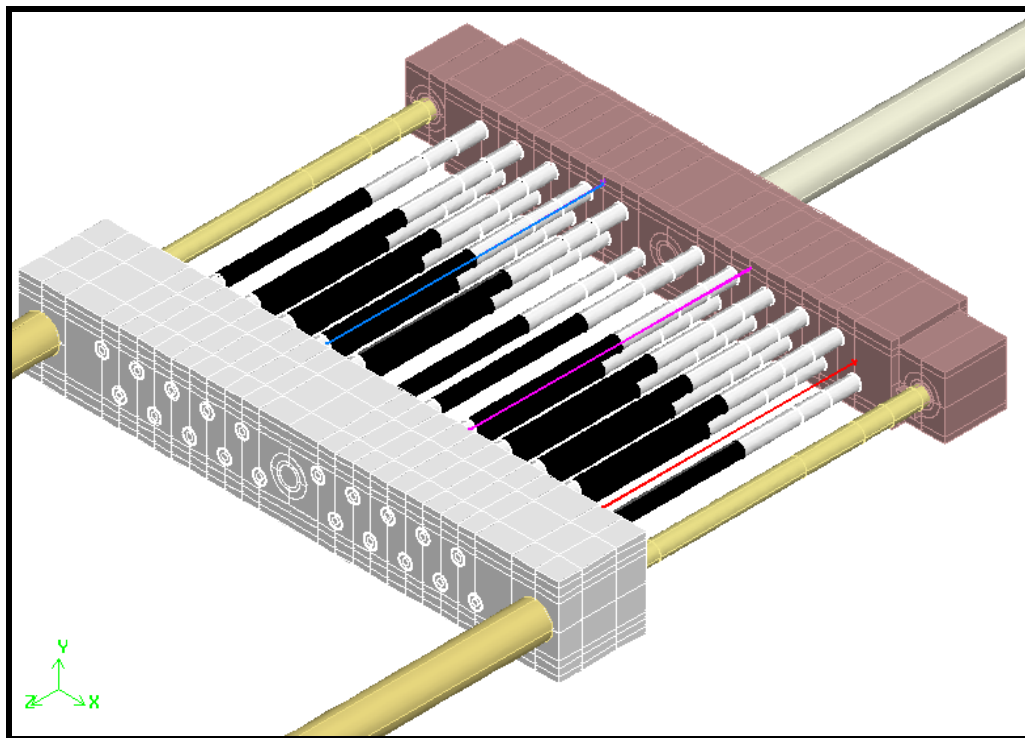


Fig. 5.6 Diagram showing new post processing lines to for comparison of the predicted and experimental temperature profile

The thermocouples were relocated to positions above FC01 along the red line shown in Fig 5.6. This was to test the accuracy of the model because at the edge of the stack the

temperature would be more strongly influenced by heat losses to the wall. This experiment was followed by another with the thermocouples repositioned along the length of FC07, 7.4 mm above its axis, as indicated by the blue line in Fig. 5.6.

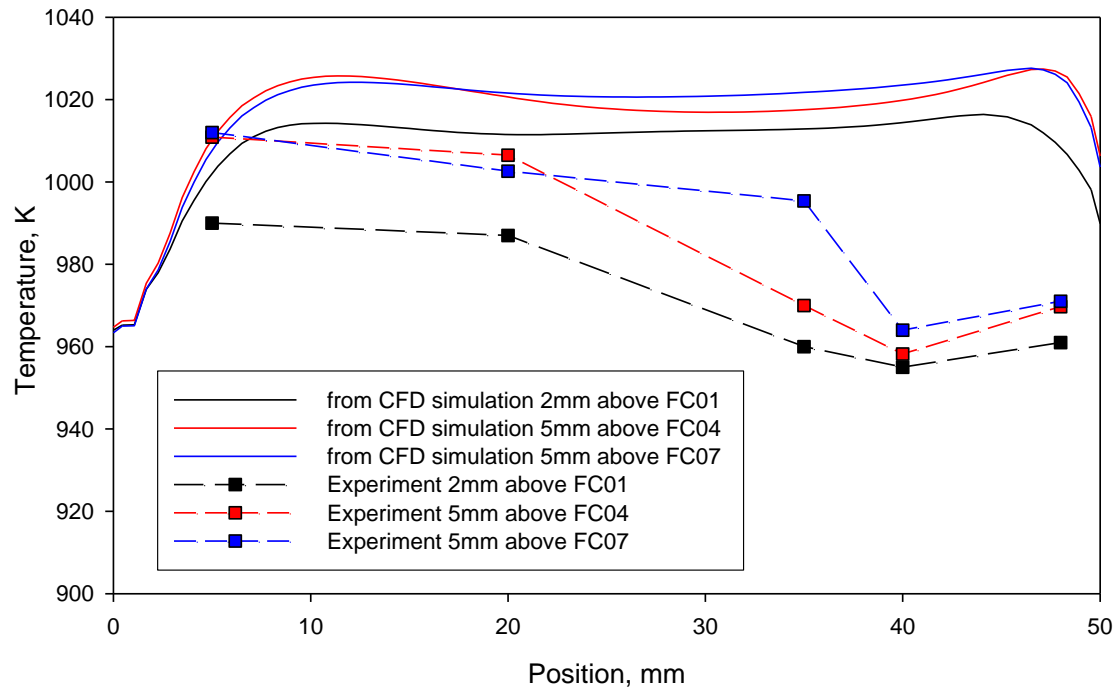


Fig. 5.7 Plot showing comparison of experimental and simulated temperature profile above different cells in the SOFC stack

The shape of the temperature profile above FC01 and FC07 was similar to that above FC04, with a gradual decrease in temperature across the stack, rising again towards the outlet end of the stack (Fig. 5.7). The profiles generated by CFD followed the general shape of those from the experimental results and in all three plots the temperature predicted close to the inlet was within 10 K of the experimental findings. However, in each plot the temperature decrease across the stack, found by experiment, was more pronounced than that in the CFD predictions, and the measured temperature at the outlet end of the stack was up to 40 K lower than in the CFD predictions.

5.5 Effect of Current collectors on the temperature distribution

Whilst the current collection wires have been omitted from the CFD model it was thought that their location close to the thermocouples T4 and T5 could be one reason for the impaired match between the experiment and simulation results at these thermocouple positions.

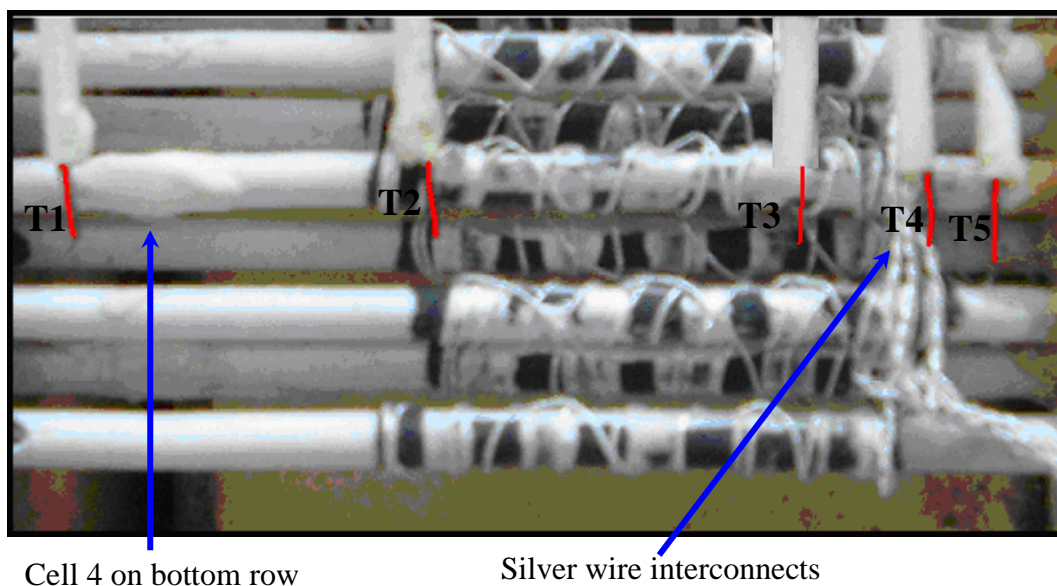


Fig. 5.8 Photograph of thermocouple positions

Fig 5.8 shows the location of the thermocouples, which have been coloured red for clarity, in relation to interconnects. It was proposed that these interconnect wires would alter the gas flow around them which could result in the temperatures recorded by T4 and T5 being lower than predicted by the simulations. To investigate this theory the wires were cut away from the fuel cell stack and the experiment was repeated. The temperature profile measured was essentially identical to that produced with the interconnects in place so the influence of the interconnects was ruled out and the decision to neglect them from the CFD model appeared valid.

5.6 Improved modelling of the air pre-heating

The next line of investigation to try to improve the accuracy of the CFD model was to look at the effect of the simplified modelling of the air pre-heating. In the experimental stack the air enters the stack at the bottom of air inlet channel and is preheated using electrical heating elements so that the temperature of the air at the top of the inlet channel meets the set point temperature. In the initial CFD model, air enters the bottom of the inlet channel at the set point temperature and adiabatic boundary conditions at the wall of the channels ensure that this temperature is maintained to the top of this channel. This assumption means that energy is not transferred from the inlet channel to the surrounding insulation, which in turn means the temperature predicted for the insulation below the SOFC stack is likely to be lower than in the test system as illustrated by Fig. 5.9.

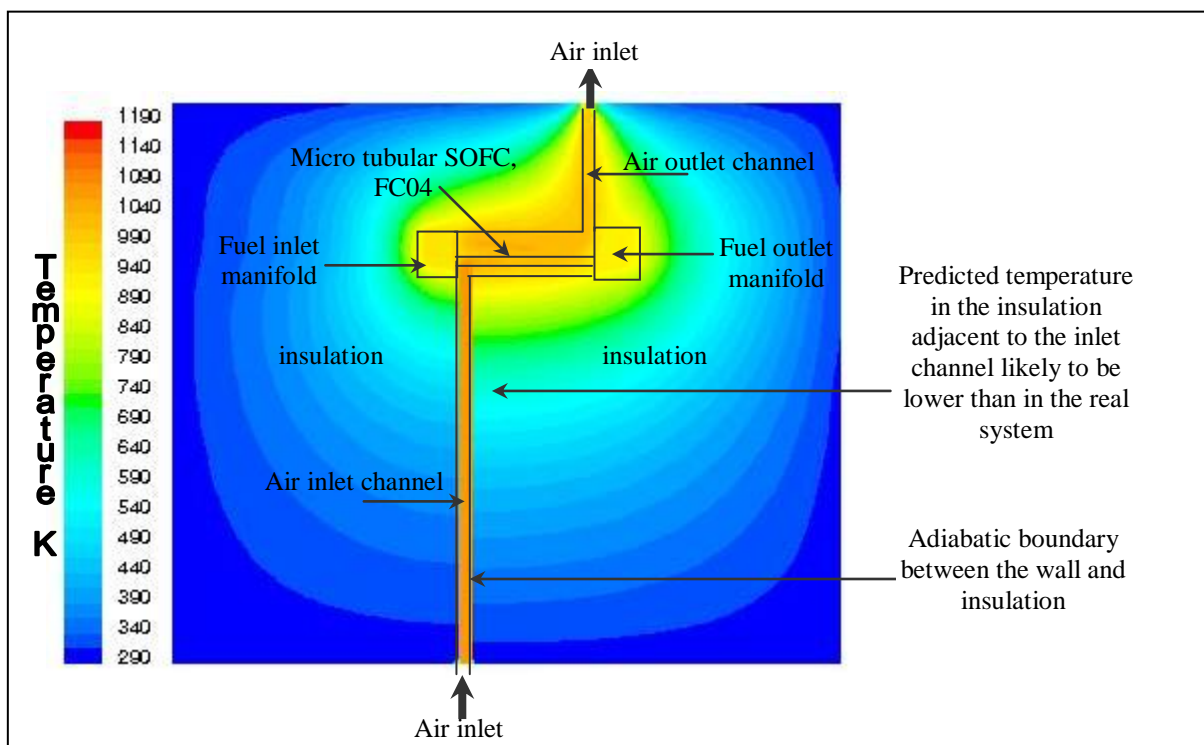


Fig. 5.9 Predicted temperature profile on a vertical plane through FC04 with adiabatic wall to the air inlet channel

With no heat transfer from the air inlet channel to the thermal insulation, the temperature through the insulation close to the inlet channel would be lower than expected. This could

in turn affect the rate of heat transfer between the hot air passing through the stack and the wall of the chamber.

The first attempt to improve the model of the air pre-heater was to simply specify a uniform heat source across the whole volume of the air inlet channel. An initial estimate for the energy source term of 147 W, corresponding to the adiabatic energy change to raise the air temperature from 300 K to 1073 K was specified. The simulation was then run with the new conditions until the solution re-converged. The mean temperature across the top of the air inlet channel was calculated and the energy source term for the pre-heater was then adjusted accordingly before the solver was run again. This procedure was repeated until the mean temperature across the top of the air inlet channel was 1073 K. The magnitude of heat source term required to achieve this condition was found to be $2.4216 \times 10^6 \text{ W m}^{-3}$, corresponding to 162.4 W over the total volume of the air inlet channel, 147 W being used to raise the enthalpy of the air from room temperature to 1073 K, whilst the remainder was 'lost' through the insulation surrounding the channel. Fig.5.10 shows the contours through the stack plotted on the vertical plane through the cell FCO4 with the energy source term to preheat the air feed to the stack distributed across the whole of the inlet channel.

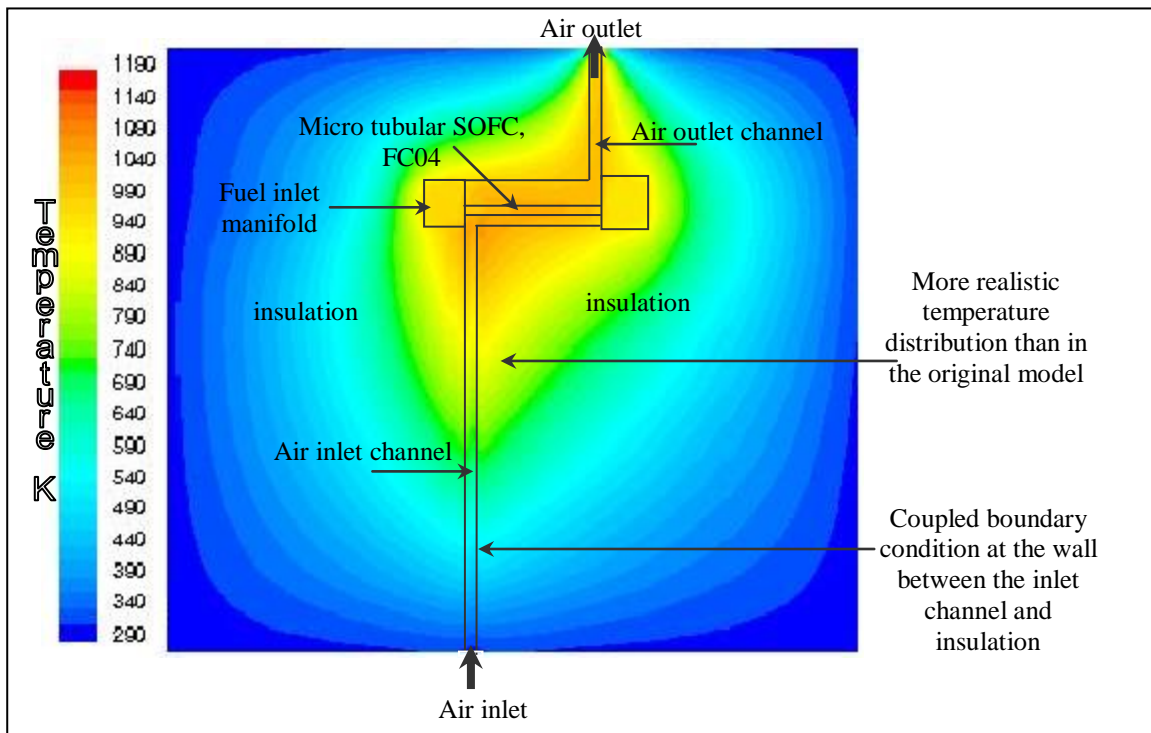


Fig. 5.10 Contours on a plane through Fco4 with the heat source across the whole channel

The plots of the temperature contours through the stack show that the temperature is higher at the walls of the channel than in the adjacent air. This is because with the energy source applied right up to the walls of the channel lots of energy was dispersed into the insulation. This was analogous to installing the heating elements with them touching the thermal insulation which would result in an unnecessarily large loss of heat through the insulation to the atmosphere. It was decided that this was an undesirable and unrealistic situation so the geometry was modified to create a boundary layer between a heated section of the inlet channel and the walls of the channel. No heat source was specified in the boundary layer so that the bulk of the air flowing through the channel would be heated without excess energy heating the walls of the channel. The channel was split into different volumes such that a heat source could be specified for the central section of the channel, with a 0.5 mm region at the edge of the channel where there was no volumetric

heat source. A section was also created at the inlet of the channel so that the energy source could be excluded from the first 30 mm of the channel, as shown in Fig. 5.11, as this was a closer representation of the experimental system.

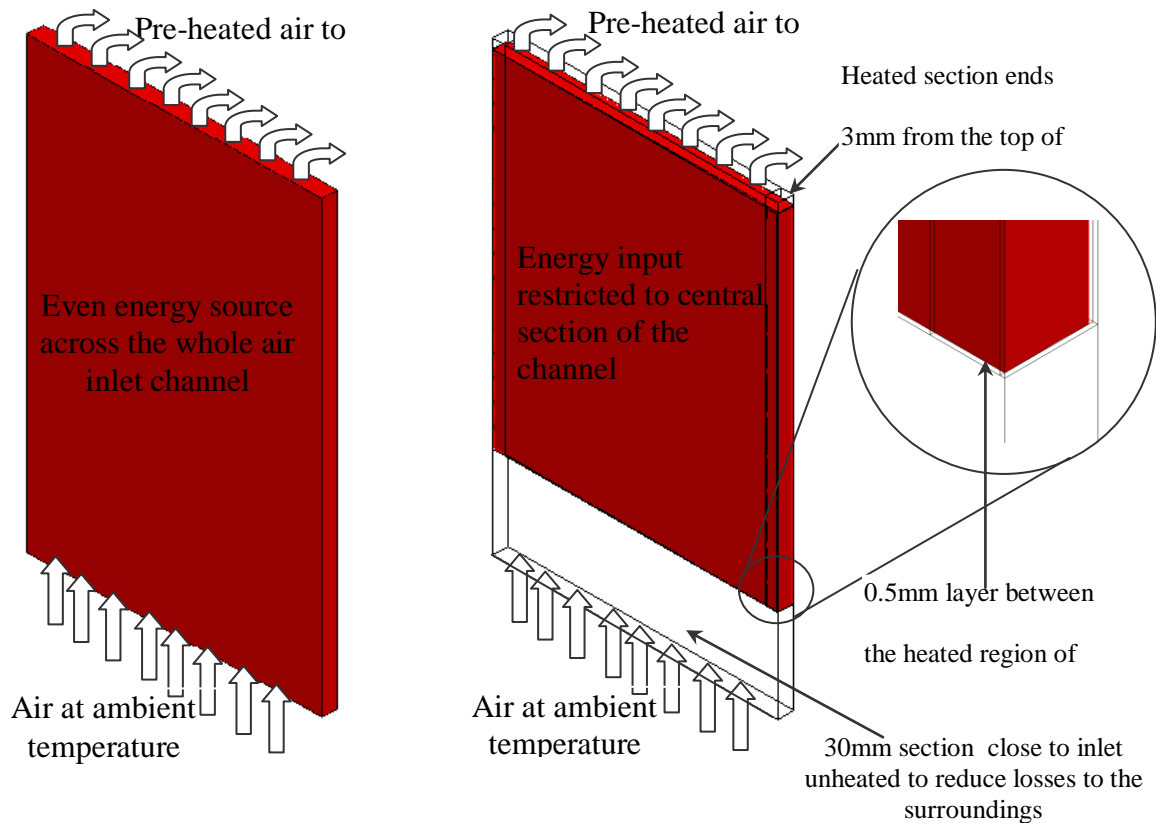


Fig. 5.11 Diagram showing differences in modelling of air preheating

The energy and momentum balances were then resolved using FLUENT for the modified geometry and the magnitude of energy source was adjusted until the mean temperature across the boundary where the air leaves the inlet channel had reached 1073 K. This was found to be $3.46 \times 10^6 \text{ W m}^{-2}$, corresponding to 160.45 W over the heated section of the channel. This meant 2.51 W less energy was lost to the insulation than with the heat source distributed across the whole inlet channel. The temperature profile that resulted from this is shown on a vertical plane through FC04 in Fig. 5.12. When compared to

Fig.5.10, one can see that the effect of leaving a gap between walls of the air channel and the heated section of the channel reduces the temperature in the inlet manifold and the surrounding insulation.

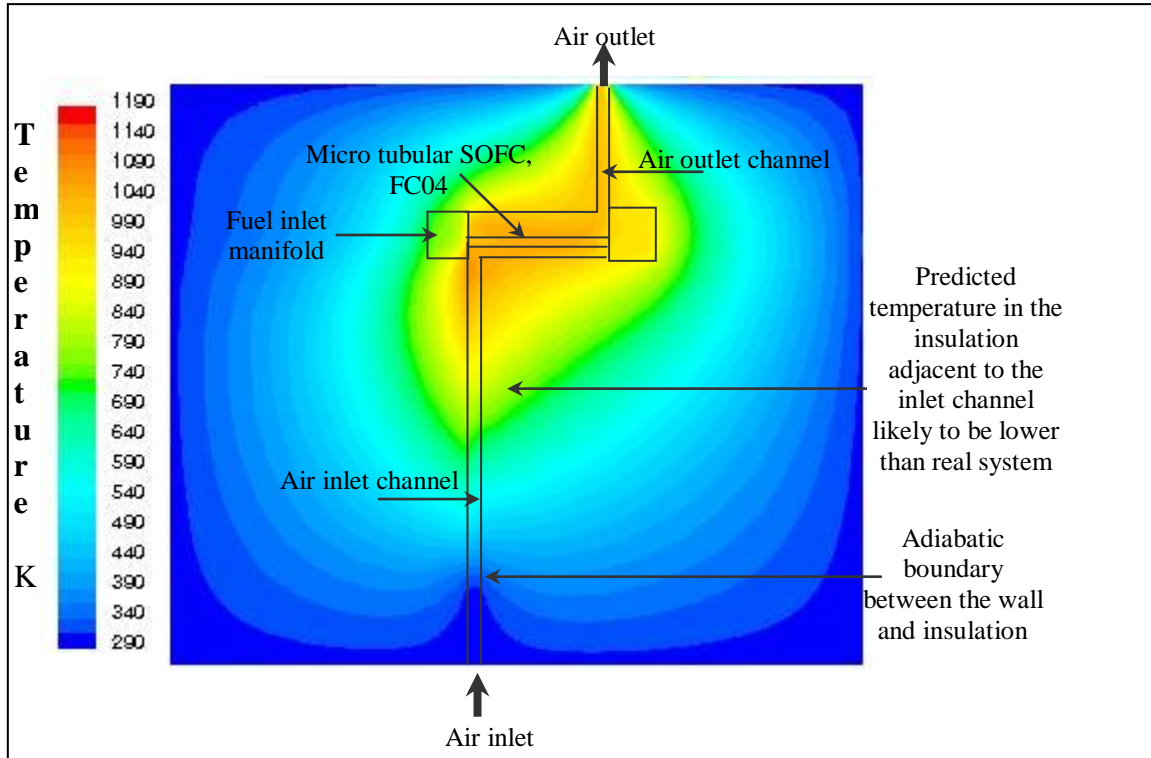


Fig. 5.12 Contours on a plane through FC04 for third heater.

It was anticipated that the changes to the temperature through the insulation would influence the temperature of the SOFC stack. To study this effect, the temperature of the air along the length of cell FCO4 was plotted for the three different cases of the adiabatic wall of; the inlet channel; the heat source uniformly distributed across the whole channel and the modified inlet channel with just a heated central section.

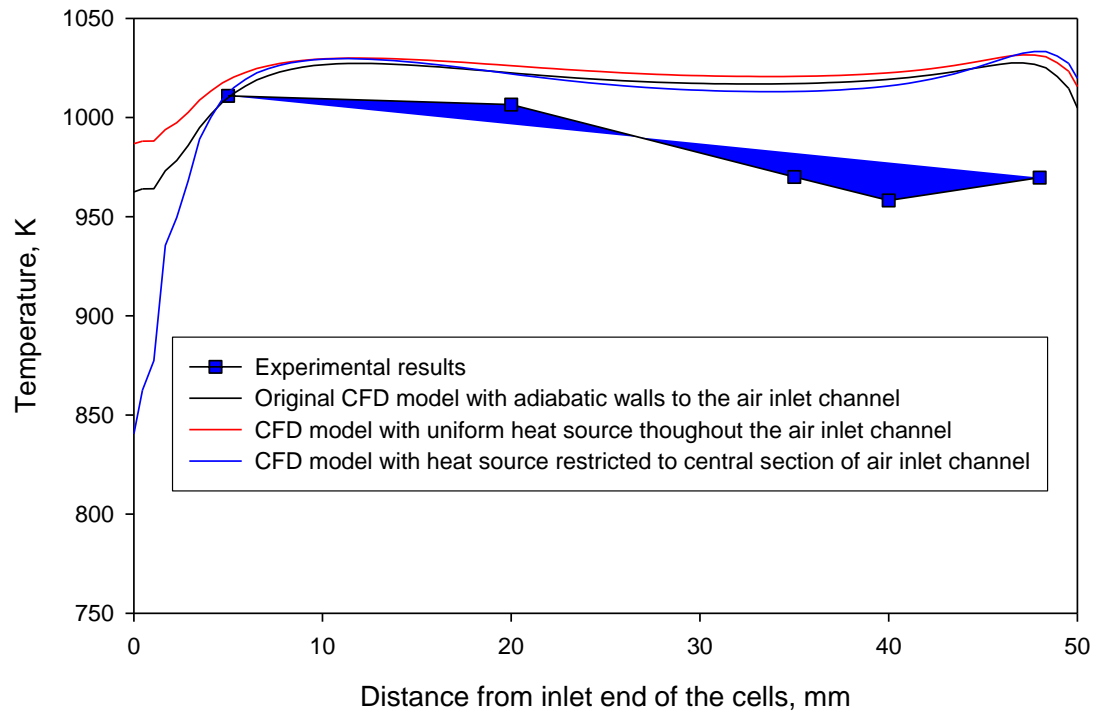


Fig. 5.13 Graph showing comparison of experimental and CFD results with 10 std. l min⁻¹ of Air and 0.32 std. l min⁻¹ of Helium

Fig 5.13 shows that changing the way in which the preheating of the air was modelled did not make a significant difference to the temperature profile through the central section of the cell chamber but had a more distinct effect close to the inlet and outlet.

Although this may seem relatively unimportant to predicting the temperature distribution across the cells, the improved modelling of the air preheating makes a substantial difference to the temperatures predicted through the thermal insulation. This could be important to the placing of peripheral stack components within the system so that they are at the appropriate temperature.

5.7 Radiation modelling

Radiation modelling has only been included at the external walls of the insulation and the external surfaces of the fuel inlet and outlet pipes. Although it has been commonplace in the literature to neglect radiation modelling^[83,85,123,124,142] with the temperatures in the region around the cell in the range of 900 K to 1073 K radiation would obviously play a role in the heat transfer around the stack. The importance of radiation in modelling SOFC has been highlighted recently by various authors^[74,108,143]. There are various radiation models available in FLUENT but these could not be initiated for the internal surfaces of the micro-tubular stack, as there are so many radiating surfaces in close proximity. It was thought that preclusion of radiation modelling could be the major reason for the predicted temperatures at the outlet end of the cell being further from the experimental values.

Fig. 5.14 shows where radiation model has been included and neglected from the model and why this is likely to have a more affect on the accuracy of the model towards the outlet end of the cell. Whereas throughout the stack the temperature difference between opposing surfaces is typically 900 to 1073 K, at the outlet end of the cell difference between he radiating and absorbing surface will be around 1000 K to around 300 K. This arises due to the opening in the insulation for the air exit channel which creates a clear path for heat to radiate from the surfaces of the cells and walls of the chamber to external objects and the surrounding atmosphere.

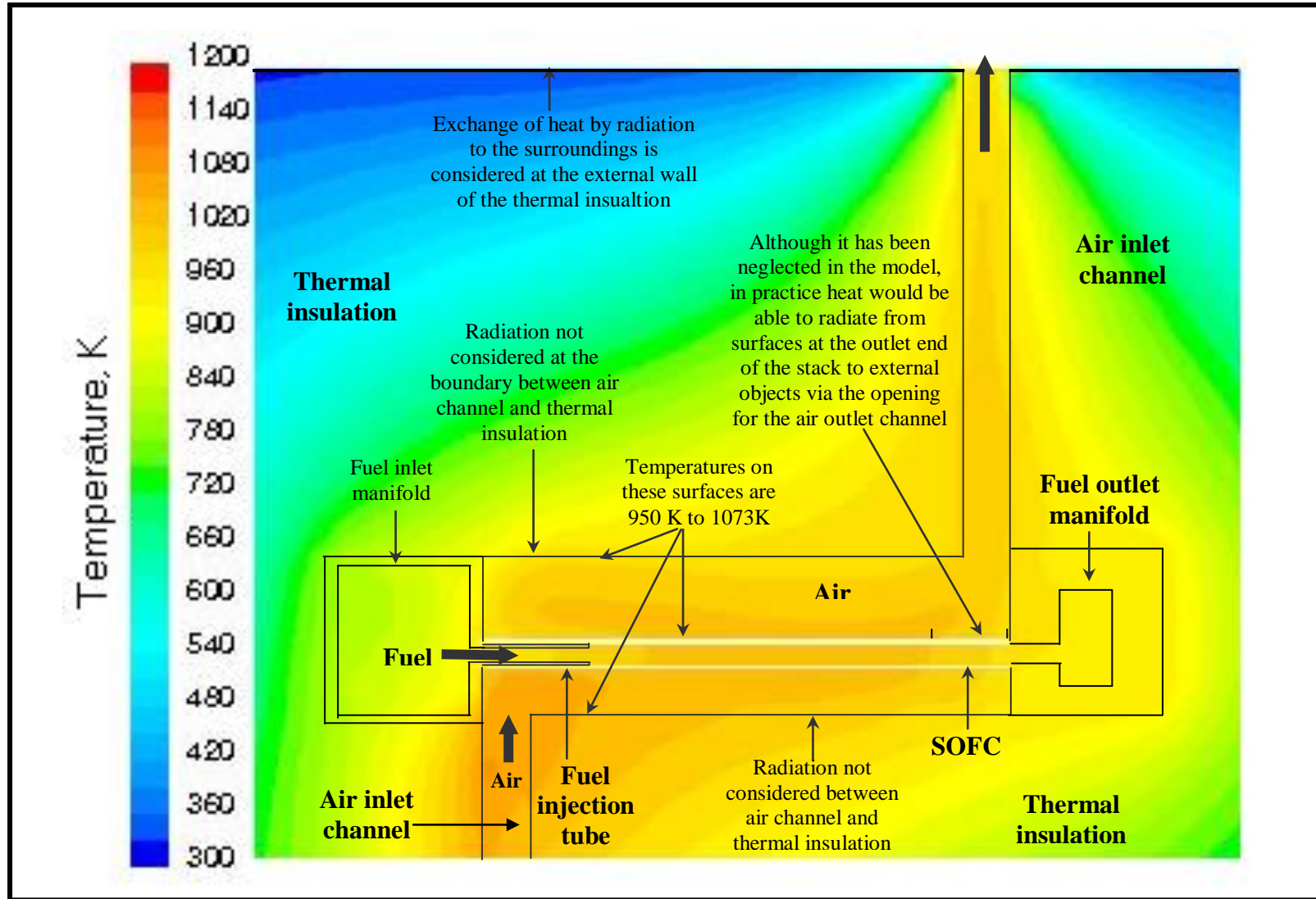


Fig. 5.14 Temperature contours plotted on a vertical plane through FC04 used to show the effect of radiation modelling

A calculation was carried out to assess the influence of the radiation at the inlet end and central section of the stack compared to the region directly below the air outlet. The emissive power, E , can be calculated as:

$$E = \varepsilon\sigma(T_1^4 - T_2^4) \quad \text{Eq. 5.1}$$

where ε is the emissivity, σ is the Stefan-Boltzmann constant and T_1 and T_2 are the temperatures of the emitting and absorbing surfaces, respectively.

For the surfaces in the middle of the chamber and towards the inlet end of the cells the biggest temperature difference is from about 1073K to 940 K hence

$$E = 0.8 \times 5.67 \times 10^{-8} (1073^4 - 940^4) = 2.47 \times 10^4 \text{ W m}^{-2}$$

Whereas the biggest temperature difference at the end of the cell opposite the air outlet channel is around 1000 K to room temperature:

$$E = 0.8 \times 5.67 \times 10^{-8} (1000^4 - 300^4) = 4.4993 \times 10^4 \text{ W m}^{-2}$$

This crude calculation shows that the emissive power is over 80% higher in the region below the air outlet channel compared with the rest of the stack. Thus the neglect of radiant heat transfer could go some way to explaining why the agreement between the CFD model and the experimental results is weakest towards the outlet end of the cell, with the heat lost to the environment being underestimated by the adopted CFD model.

Whilst it is acknowledged that there will be inaccuracies in the temperature profiles predicted from the SOFC stack without inclusion of radiation models, the present model appears to provide sufficient accuracy to be a useful design tool. It was therefore decided that the omission of radiation modelling would not prohibit the use of the model but that

results should be treated with some caution. With advances in software and computing hardware in the coming years it is likely to be possible to add on radiation modelling more readily in future work.

5.8 Variation of air flow rate

In order to check that the model was valid for different air flow rates this parameter was varied in both the experimental study and the CFD simulation. It was expected that the simulation would be less accurate with lower air flow rates, as convective heat transfer would become less important relative to radiation which was neglected from the model. First of all the air flow rate was halved to 5 std. l min⁻¹ and the stack was run for 24 hours to be sure that steady state conditions had been established. This test was followed by another with the air flow increased to 15 std. l min⁻¹. The temperature profiles obtained from these experiments are shown in Fig. 5.15 alongside those predicted by the model for the same conditions.

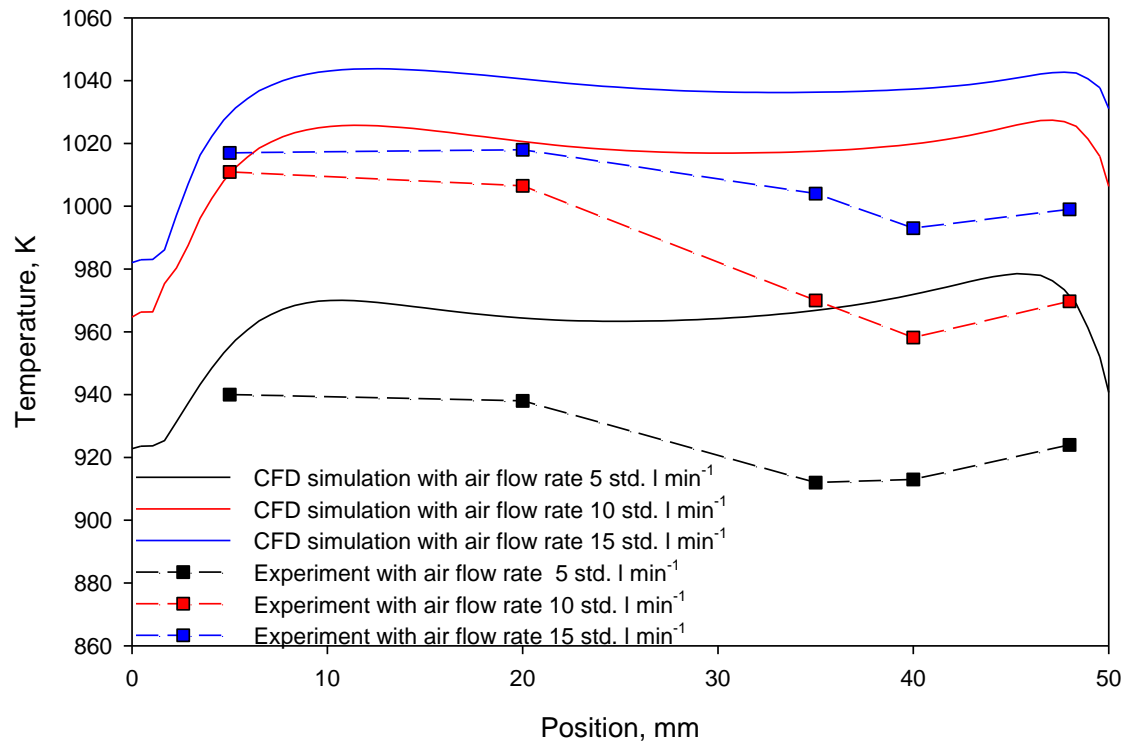


Fig. 5.15 CFD and experimental results for different flow rates

The agreement between CFD and the experimental results is similar at the different flow rates. In all cases the CFD predictions match the experimental results to within 10 K at the inlet end of the stack. At all of the flow rates the CFD simulations predict a similar shaped temperature profile to the experimental findings but seem to underestimate the heat lost from the stack such that the predicted temperature is around 40 K higher than the experimental readings at the outlet end of the stack. The air flow rate seems to make little difference to the deviation between experimental and predicted temperature profiles. The work to vary the flow rates does reveal that 5 std. l min⁻¹ air preheated to 1073 K is insufficient to maintain the temperature across the stack at a temperature at which the SOFC would operate without heat generated by electrochemical processes.

5.9 Effect of additional heat lost from the stack

Another effect that is difficult to quantify but could produce the discrepancy between experimental and CFD results is that the simulation assumes that the SOFC stack is perfectly sealed inside the thermal insulation, apart from the air inlet and outlet. In practice this is not the case in as shown in Fig.5.16.

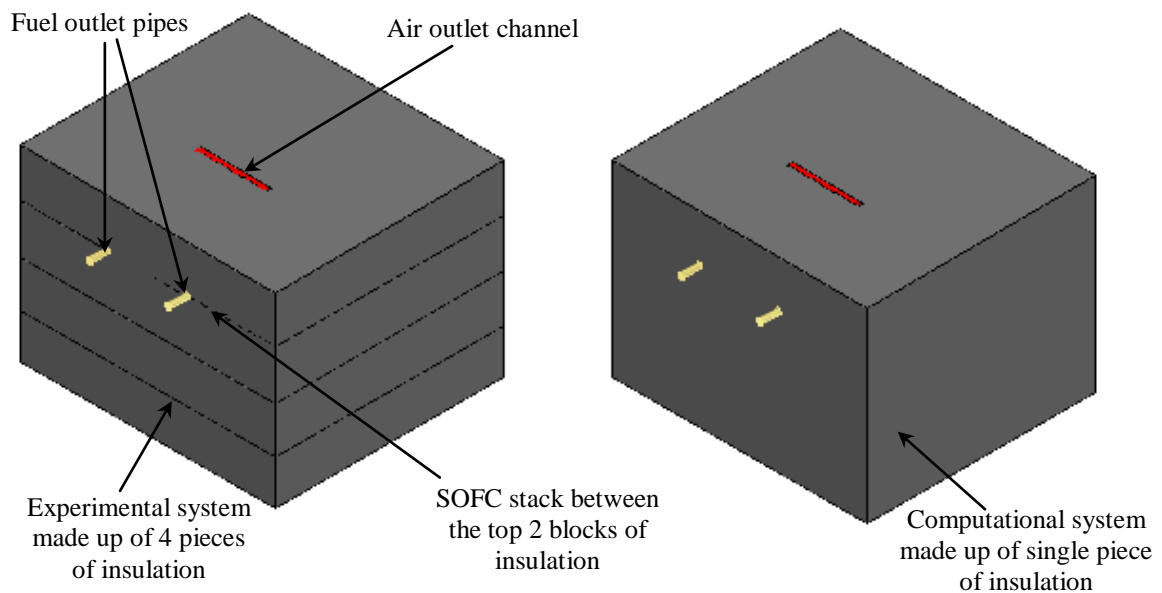


Fig. 5.16 Schematics to highlight difference between experimental insulation and idealised insulation in the CFD model

To facilitate assembly, the thermal insulation was constructed from 4 blocks, rather than a single section. The SOFC stack was housed between the top 2 pieces of insulation with the lower pieces housing the air pre-heater. Clamps were used to press the layers of insulation together but was thought likely that the heat lost from the stack to the environment would be higher than predicted due to relatively high rates of heat loss at the junction of the separate blocks of insulation.

To try to evaluate if there was an increased rate of heat loss along the joints between the blocks of insulation, thermocouples were put in contact with the outer wall of the thermal insulation. The stack had previously been run for 24 hours to ensure that steady state conditions had been established with $0.320 \text{ std. l min}^{-1}$ Helium through the cell and $10 \text{ std. l min}^{-1}$ of air preheated to 1073 K . The temperature was measured at 21 different positions on each face with some of the reading taken halfway up each block and the others at the joints between 2 blocks. The thermocouple readings are shown in Fig. 5.17

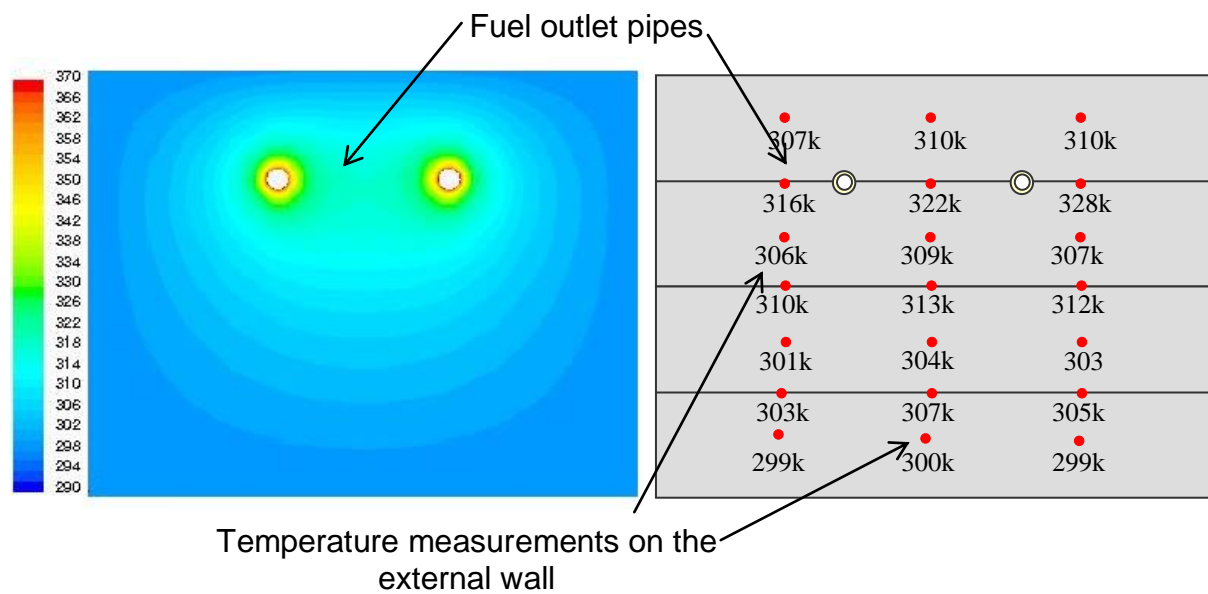


Fig. 5.17 Recorded temperature on an external wall of the stack insulation compared with temperature contours predicted by CFD for the same wall

As mentioned previously it is difficult to quantify how much the losses would affect the rate of heat loss from the stack. The simulation geometry could have been constructed with the layer of insulation separated by a thin layer of air but the gap is so small between the layers that it would be difficult to predict its thickness and the flow conditions for the air in the gap. Alternatively once a SOFC stack design had been firmly established,

thermal insulation could be custom made with a step joint between the adjacent blocks to reduce the heat loss between joints. This would have been an expensive option for a single unit though because of the time required to set up the cutting machinery used by the insulation manufacturers to produce such items.

5.10 Conclusion

In this Chapter the results of a validation exercise for a steady-state CFD model of a micro-tubular SOFC stack were presented. The validation focussed on the capacity of the CFD model to predict the temperature distribution through a SOFC stack with the required accuracy. The influence of electrochemical processes was eliminated from the test by using inert gas as the fluid circulated through the anode side of the cells.

Within the validation exercise the simplification of geometry by neglecting silver current collection wires was upheld as a valid representation, as it was found to have no significant effect on the temperature distribution. The effect of simplifying the air inlet channel to an unheated channel with adiabatic walls was found not to significantly affect the temperature distribution around the SOFC cells, but affected the predicted temperature in the inlet manifold and surrounding insulation.

The SOFC simulations were found to provide accurate predictions of temperature towards the inlet end of the stack and the trend in the shape of the predicted temperature across the stack mirrored the profile found by experimental analysis. This agreement was upheld at different positions across the stack and for different air flow rates.

It was found that although the computer simulations accurately predicted the trend in the shape of the temperature profile, the predicted temperatures towards the outlet end of the end of the cells were higher than found in experiments. The largest discrepancy was about 40 K. The reason for the difference appears to be that the CFD model slightly underestimates the heat lost to the atmosphere from the air flowing across the stack. This was thought to arise from the fact that the experimental system is not perfectly sealed, as in the model, so the rate of heat loss will be higher along the joints between the blocks of insulation.

It was acknowledged that the absence of radiation modelling was a key limitation of the model and could contribute to the weaknesses in predicting the temperature directly beneath the air outlet channel where radiation is likely to be more influential in determining the local temperature. Even conceding this limitation the results of the validation exercise were encouraging. It was thought that provided predicted results were treated with a degree of caution, the model could serve as a useful tool to analyse potential stack designs and provide a good estimate of the temperature profile under different operating scenarios. Therefore the model was further used to study different operating conditions for the 20-cell stack, as described in Chapter 6.

6. Study of a 20-cell SOFC stack fuelled with Hydrogen

6.1 Introduction

In Chapter 5 it has been shown that the CFD model provides a reasonable estimate of temperature profile through a 20-SOFC stack without the influence of electrochemical reactions. In this Chapter Hydrogen replaced Helium as the fluid passed through the tubular SOFCs; this was in order that the effect of heat generated by the electrochemical processes on the stack temperature could be investigated. The CFD model was then used to predict the temperature profile that would develop through the stack under different operating scenarios. These predictions were later used to identify the operating conditions that would lead to stack temperatures suitable for functional operation of the stack. The target was to find the operating conditions that would maintain the minimum temperature in the stack above 973 K whilst not exceeding a maximum temperature of 1173 K, beyond which the stack could be damaged.

Simulations were initially run without heat generation in the SOFCs to simulate the stack at open circuit. These were used to predict the operating conditions that would raise the stack temperature such that it was ready to produce electrical power. The next development to the model was introducing energy sources to represent the thermal energy that would be produced as a result of irreversible processes, in conversion of fuel to electrical energy. Taking the result of these simulations into account, an experimental test was then carried out on the 20-cell stack.

6.2 Simulation to investigate the effect of the air inlet temperature on the stack temperature under open circuit conditions

6.2.1 Objectives

The first investigation carried out using the steady-state CFD simulation was set up with the purpose of predicting the air inlet temperature and flow required for the SOFC stack to be maintained at an operating temperature suitable for power generation whilst no power was being drawn from the cells. This simulates the practical situation where an SOFC stack is held on 'stand-by', with the cells at open circuit but ready to produce electrical power almost instantaneously. In addition to providing a guide to the conditions required whilst the stack was on stand-by, the results of this investigation would also provide an indication of the conditions required for the start-up of the stack from ambient temperature.

6.2.2 Boundary conditions and procedure

In the validation experiments and simulations it was shown that introducing air at a flow rate of 10 std. l min⁻¹ (1.94×10^{-4} kg s⁻¹) produced a reasonable temperature distribution across the stack. The temperatures measured in the experiment ranged from 1020 K to 960 K. So 10 std. l min⁻¹ seemed to be a sensible initial air flow rate to begin running the simulations with Hydrogen as the anode gas. The flow rate of Hydrogen was 0.5 std. l min⁻¹ (6.8×10^{-7} kg s⁻¹), as this corresponded to 0.025 std. l min⁻¹ per cell, which had been shown to be a suitable flow rate based on single cell tests. The simulation was run to convergence with an air inlet temperature of 1073 K, taking around 800 iterations to converge and around 50 seconds per iteration. The temperature variation across the stack chamber ranged from a maximum of 1072.7 K to a low of 809.0 K.

To study the effect of the air inlet temperature on the temperature distribution produced through the stack the boundary conditions for the air inlet were changed at 10 K intervals from 1023 K to 1173 K. Separate files were saved for each of these different boundary conditions and the solver was run for each case until a stable solution had been achieved for every condition.

6.2.3 Results

The suitability of the temperature profile produced by each of the different inlet temperatures was assessed by using the 'surface integral' facility in FLUENT to find the maximum, minimum and mean temperature in the region around the tubular SOFCs. Since the temperature in and around the section of the cells coated with electrodes would be of prime importance, the post processing features in FLUENT were also used to find the maximum, minimum and mean temperature in these specific parts of the stack.

Fig 6.1 shows the results of the simulations of the stack at open circuit. A line has been plotted on the graph at a temperature of 1173 K. This is to show the upper limit for the temperature anywhere in the stack if damage through melting the silver interconnects is to be avoided. A second line has been plotted at a temperature of 973 K. In single cells tests it was found that if the temperature was reduced below 973 K the power output of the micro-tubular SOFCs fell to below 25% of their output at 1133 K. Based on these tests it was decided that this should be the target for the minimum temperature in the electroded section of the cells.

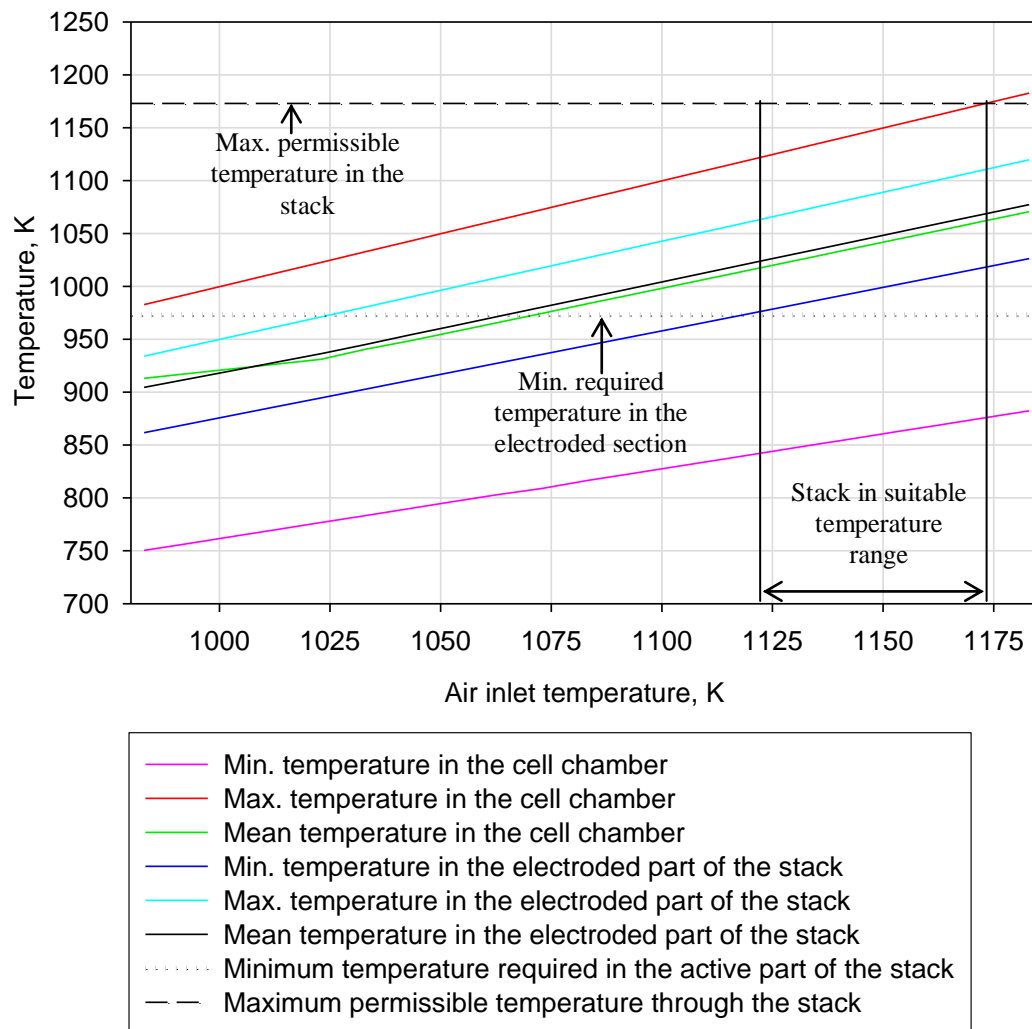


Fig. 6.1 Graph to show results of simulations with the stack under open circuit conditions and air flow rate of 10 std. l min⁻¹

The simulation results indicate that in order to keep the whole of the electroded section of the cell above 973 K the inlet temperature must be 1123 K or higher. As one would expect once the air inlet temperature is increased beyond 1173 K parts of the stack will be close to exceeding temperatures that would damage the silver wire interconnects as their melting point is around 1190 K and their mechanical strength diminishes as this temperature is approached.

These simulation results provide a guide to the inlet temperatures to be used if the stack were held at open circuit ready for power generation. They also provide a guide to the air inlet temperature required during start-up.

6.3 Effect of air flow rate on the stack temperature at open circuit

6.3.1 Objectives

The next stage in the investigation was to test how increasing or decreasing the air flow rate affected the predicted temperature profile across the stack. The air flow rate was first halved to 5 std. l min⁻¹. The other conditions were unchanged, whilst the procedure of running the simulation with different air inlet temperatures was performed as described in section 6.2. This procedure was then repeated for 15 std. l min⁻¹. In each case it took around 160 iterations for the solutions to re-converge. The results were plotted as done previously in section 6.2 to identify the air inlet temperatures that lead to acceptable stack temperatures.

6.3.2 Results

6.3.2.1 Air flow rate of 5 std. l min⁻¹

The minimum, maximum and mean stack temperatures predicted for air inlet temperatures from 983 K to 1073 K are plotted in Fig. 6.2.

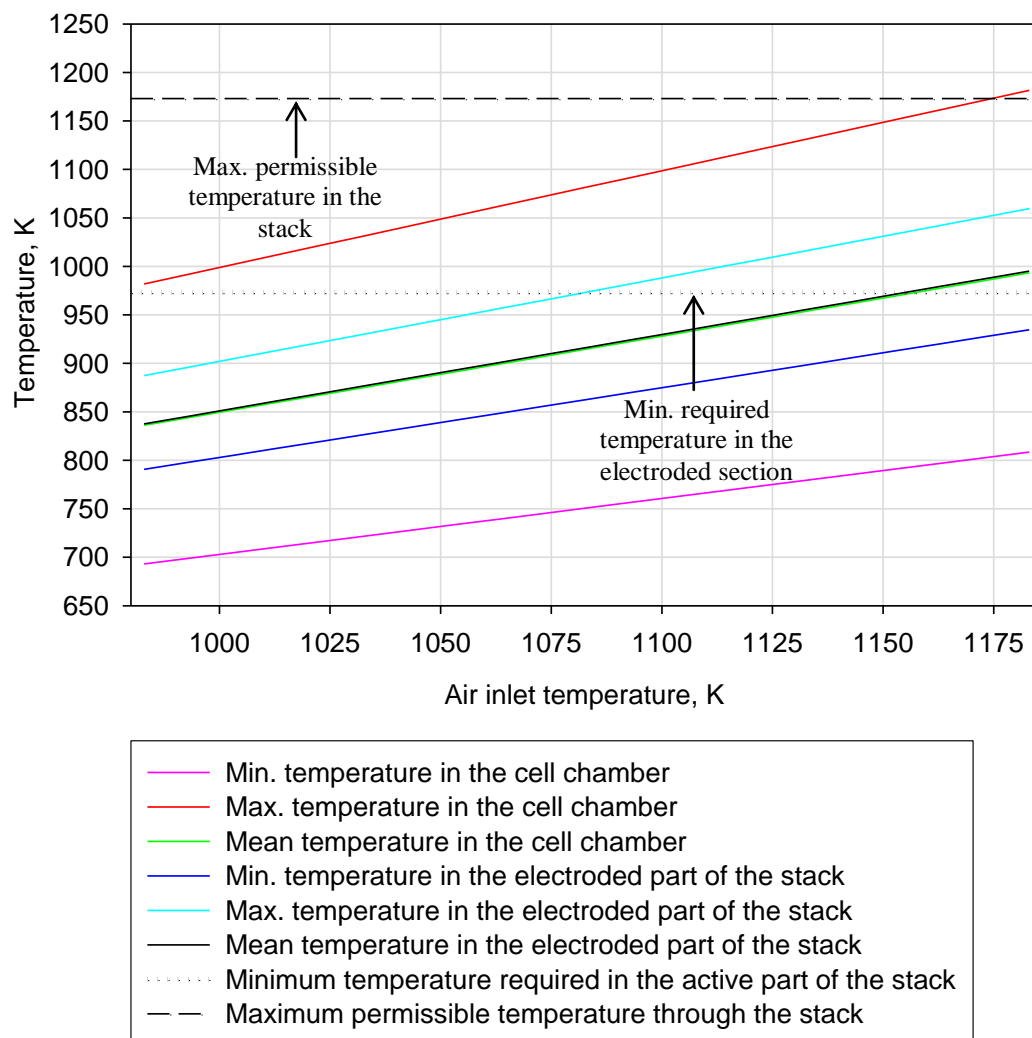


Fig. 6.2 Graph to show results of stack simulations with Hydrogen through the cells at open circuit with 5 std. $l\ min^{-1}$ of Air

With the air flow rate reduced to 5 std. $l\ min^{-1}$, even when heated to 1173 K, the minimum temperature in the active part of the stack does not exceed the desired 973 K. If the air inlet temperature is further increased the maximum temperature reached in the stack would lead to damage to the silver interconnects at the hot spots. Therefore the simulations indicate that 5 std. $l\ min^{-1}$ of air is not really sufficient to obtain stack temperatures suitable for instantaneous achievement of maximum electrical power output. However, the maximum temperature in the active part of the stack would be sufficient to

support some electrochemical reaction. The heat generated by this process could raise the temperature of the stack in turn increasing the electrical power output and heat generated by the cells. So if the urgency for maximum power, from when the stack was switched from open circuit, was not of top priority, the stack might be maintained close to operating temperature using 5 std. l min⁻¹ of air heated to 1173 K which would require around half the energy required to preheat the air with 10 std. l min⁻¹ of air.

6.3.2.2 Air flow rate of 15 std. l min⁻¹

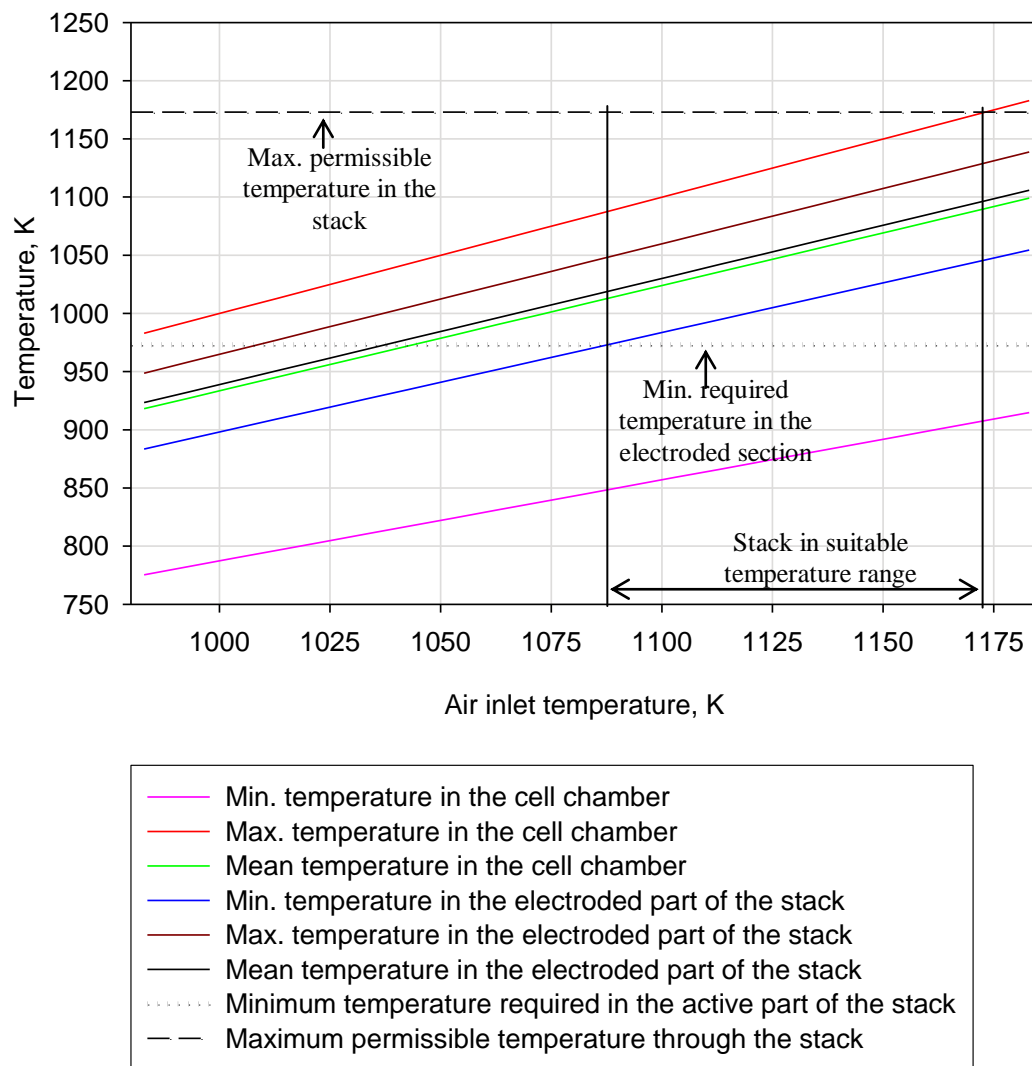


Fig. 6.3 Graph to show results of stack simulations with Hydrogen through the cells at open circuit and 15 std. l min⁻¹ of Air

When the air inlet flow was increased to 15 std. l min⁻¹ the temperature gradient across the stack became much more even. Fig 6.3 shows the range of inlet temperatures that would produce suitable temperatures throughout the stack. This range was increased from 1123 K to 1073 K, predicted with 10 std. l min⁻¹, to 1083 K to 1173 K. This would demand less rigorous control of the air inlet temperature. For example: if the set point was set to 1128 K the inlet temperature could fluctuate by ± 45 K and the stack would be maintained at a suitable temperature.

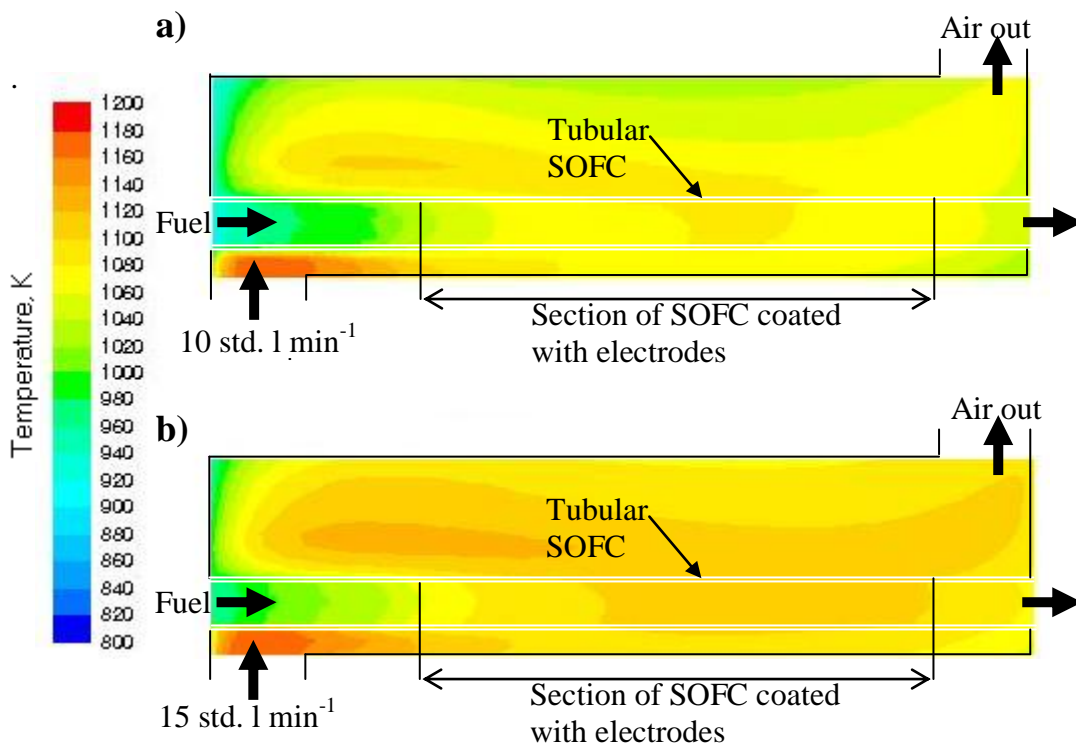


Fig. 6.4 Predicted temperature contours for a plane through FCO4 for

a) 10 std. l min⁻¹ of air introduced preheated to 1173 K

b) 15 std. l min⁻¹ of air introduced preheated to 1173 K

It is also predicted that using 15 std. l min⁻¹ of air would produce a significant improvement to the mean temperature across the active part of the stack that could be

achieved without exceeding 1173 K at any position. This increased from 1068.5 K with 10 std. l min⁻¹ of air to 1096.7 K with 15 std. l min⁻¹. Fig. 6.4 shows the temperature contours with 10 and 15 std. l min⁻¹ of air preheated to 1173 K on a vertical plane through cell FC04. The plot shows the coldest position to be at the inlet end of the stack above the cell. The hottest section occurs where the hot air first enters the chamber around the stack. As one would expect, this hot air is cooled by heat exchange with the fuel on the inside of the cell and the walls of the chamber as it moves across the cell.

With 15 std. l min⁻¹ of air, the plot shows that a large portion of the 'active' part of the fuel cell is between 1100 to 1120 K which is close to the ideal temperatures for power generation from the cell. The potential increase in power output that would arise from increasing cell temperature would have to be balanced against the significant increase in the energy required to preheat the larger flow of air. The energy required for preheating the air to 1173 K would increase from 166 W to 249 W if the flow rate was increased from 10 std. l min⁻¹ to 15 std. l min⁻¹.

6.4 Simulation of the effect of heat from electrochemical reactions

6.4.1 Objectives

The next stage in the investigation was to predict the change in the temperature profile across the stack with a given air inlet temperature when heat is generated by electrochemical reactions in the fuel cells. The effect of heat generated by the electrochemical reactions was simulated by specifying a constant heat source through the volume of the fuel cell tube corresponding to the section coated with electrodes. Obviously in practice the electrical output from the cell, and in turn the by-product heat would vary with temperature, the fuel and air flow rate, and the properties of the

individual cell. However, the assumption of a constant energy source was seen as a way of obtaining estimates of the stack temperature whilst current was being drawn from the cells. In due course it was thought this assumption would be replaced by an algorithm linking the heat production to the physical properties of the cell and local conditions.

Once again the simulation results were used to give a guide to the air temperatures and flow rates that could be used to achieve acceptable stack temperatures.

6.4.2 Boundary conditions and procedure

The boundary conditions were unchanged from the previous simulations apart from the addition of the energy source in the volumes corresponding to the section of the cell coated with electrodes. The magnitude of this energy source was estimated based on the performance of micro-tubular cells and a series of assumptions.

It was found from single cell testing, that operating to provide maximum electrical power output, with 0.025 std. l min⁻¹ of fuel at 1123 K, a micro-tubular cell would readily produce 0.5 W_e. It was assumed that when operating to provide the maximum possible electrical power, the cells would only operate with around 50% electrical efficiency. It was then further assumed that the energy 'lost' due to these polarisation losses would all be transformed to heat. Therefore it was postured that the heat generated in the cell whilst current was being drawn through the external circuit would roughly match the 0.5 W electrical output. The magnitude of this energy source was required by FLUENT in terms of Watts per unit volume and so was specified as 1.447 W m⁻³ for each of the cells.

The model was solved again for a range of air inlet temperatures from 983 K to 1183 K, with the energy source added in the central part of the cells. The addition of the constant energy source made no difference to the time taken to perform each iteration and the solutions re-converged within 50 iterations.

6.4.3 Results

6.4.3.1 Air flow rate of 5 std. l min⁻¹

Air inlet Temp.	Temperature through the SOFC stack chamber		Temperature around the only electroded section of the cells						Energy to pre-heat air
	Min	Max	Min	Change from Temp. at OC	Max	Change from Temp. at OC	Mean	Change from Temp. at OC	
(K)	(K)	(K)	(K)	(K)	(K)	(K)	(K)		(W)
983.0	693.8	1005.2	795.8	+5.0	1004.2	+116.8	913.2	+75.6	67.1
993.0	699.5	1013.2	803.0	+5.1	1012.2	+116.2	921.0	+77.0	68.1
1003.0	705.3	1021.3	810.2	+5.1	1020.2	+115.6	928.9	+75.6	69.1
1013.0	711.1	1029.3	817.4	+5.1	1028.2	+115.0	936.8	+75.5	71.1
1023.0	716.8	1037.3	824.6	+5.1	1036.2	+114.4	944.6	+75.5	72.1
1033.0	722.6	1045.3	831.8	+5.2	1044.2	+113.8	952.5	+75.5	73.1
1043.0	728.4	1053.3	839.1	+5.2	1052.2	+113.2	960.3	+75.5	74.1
1053.0	734.1	1061.3	846.3	+5.2	1060.2	+112.6	968.2	+75.5	75.1
1063.0	739.9	1069.3	853.5	+5.2	1068.2	+112.0	976.0	+75.4	76.1
1073.0	745.7	1077.4	860.7	+5.3	1076.2	+111.4	983.9	+75.4	77.1
1083.0	751.4	1085.4	867.9	+5.3	1084.2	+110.8	991.7	+75.4	78.1
1093.0	757.2	1093.4	875.2	+5.3	1092.4	+110.3	999.6	+75.4	79.1
1103.0	763.0	1101.6	882.4	+5.3	1100.4	+109.8	1007.5	+75.4	80.1
1113.0	768.8	1111.6	889.6	+5.3	1108.4	+109.2	1015.3	+75.3	81.1
1123.0	774.5	1121.6	896.8	+5.3	1116.5	+108.6	1023.2	+75.3	82.1
1133.0	780.3	1131.6	903.9	+5.3	1124.5	+108.1	1031.0	+75.3	83.1
1143.0	786.1	1141.6	911.1	+5.3	1132.6	+107.5	1038.9	+75.3	84.0
1153.0	791.8	1151.6	918.3	+5.3	1140.6	+107.0	1046.7	+75.3	85.0
1163.0	797.6	1161.5	925.5	+5.3	1148.6	+106.4	1054.6	+75.2	86.0
1173.0	803.4	1171.5	932.7	+5.3	1156.7	+105.8	1062.4	+75.2	87.0
1183.0	809.1	1181.5	939.9	+5.3	1164.7	+105.3	1070.3	+75.2	88.0

Table 6.1 Table showing results of simulations for 20 cell stack with 5 std. l min⁻¹ air and 0.5W of heat produced by each cell

The solutions were post processed in a similar way to the simulations of the stack at open circuit. The change in the temperature around the active part of the stack from what was predicted at open circuit was also noted. The results with an air flow rate of 5 std. l min⁻¹ are shown in Table 6.1 for various temperatures.

The simulations of the stack with the cells producing heat as a by-product of the electrochemical reactions predicted an increase in the maximum temperature in the active part of the stack of over 100 K compared with those predicted for the same conditions but with no heat generation from the cells. The increase in the minimum temperature in the active part of the stack was much lower at just over 5 K. This large temperature gradient meant that 5 std. l min⁻¹ would be an insufficient air flow to maintain the whole of the 'active part' of the cells above 973 K, even with 0.5 W of heat generated in each of the cells. The only option would be to increase the air flow rate as it would not be possible to increase the inlet temperature further without reaching damagingly high temperatures in the hottest parts of the stack. In fact in practice, without significant improvements in cell technology, the current generated in the cells under these conditions would be sufficient to produce the 0.5 W of by-product heat that has been assumed in the model. Even if the power could be generated at lower temperatures the temperature difference of over 300 K would put the stack at high risk of damage through diverging rates of thermal expansion.

6.4.3.2 Air flow rate of 10 std. l min⁻¹

The results from the simulations run with 10 std. l min⁻¹ of air have been reported in Table 6.2. The results corresponding to the inlet air conditions that lead to acceptable temperatures throughout the stack have been shaded.

Air inlet Temp.	Temperature through the SOFC stack chamber		Temperature around the only electroded section of the cells						Energy to pre-heat air
	Min	Max	Min	change from Temp. at OCV	Max	change from Temp at OCV	Mean	change from Temp at OCV	
(K)	(K)	(K)	(K)	(K)	(K)	(K)	(K)		(W)
1073.0	810.1	1113.9	946.0	10.3	1113.2	95.6	1037.0	56.6	154.2
1083.0	816.7	1122.7	954.3	10.4	1122.1	95.2	1045.8	56.6	156.2
1093.0	823.3	1131.6	962.6	10.5	1131.0	94.8	1054.6	56.6	158.2
1103.0	829.8	1140.5	970.9	10.5	1139.8	94.4	1063.4	56.6	160.1
1113.0	836.4	1149.4	979.3	10.6	1148.7	94.0	1072.2	56.5	162.1
1123.0	843.0	1158.3	987.6	10.7	1157.6	93.6	1081.0	56.5	164.1
1133.0	849.6	1167.2	995.9	10.9	1166.5	93.2	1089.8	56.5	166.2
1143.0	856.2	1176.1	1004.3	11.0	1175.4	92.8	1098.6	56.5	168.1
1153.0	862.8	1185.0	1012.6	11.1	1184.3	92.4	1107.4	56.5	170.1
1163.0	869.4	1193.9	1020.9	11.2	1193.2	92.0	1116.2	56.5	172.1
1173.0	876.1	1202.8	1029.3	11.3	1202.1	91.6	1125.0	56.5	174.1

Table 6.2 Table showing results of simulations for 20 cell stack with 10 std. l min⁻¹ air and 0.5W of heat produced by each cell

When the air flow rate is increased to 10 std. l min⁻¹ it is predicted that the stack could be maintained at suitable temperatures provided the air was preheated to between 1113 K and 1133 K. In section 6.2.2 it has been shown that with the stack at open circuit the incoming air could be heated to 1123 K to 1173 K. Unless the set point for the incoming air was to be turned down when the cells were loaded, it would need to be fixed to between 1123 K and 1133 K to prevent the stack over heating when current was drawn from the cells. As the range of air inlet temperature with which acceptable stack temperatures could be achieved is smaller when heat is produced in the cells it would also demand more rigorous control of the air inlet temperature.

The model predicts that when the cells generate heat it will be possible to maintain a higher average temperature through the electroded parts of the cells. It is predicted that a temperature of 1089 K could be sustained which is 56 K higher than predicted for when the cells are at open circuit and would improve the performance of the stack. The

predicted temperature contours through cell FC04 with the stack fed with 10 std. l min⁻¹ air preheated to 1033 K are shown below for the stack at open circuit and when 0.5 W of heat is generated in each cell.

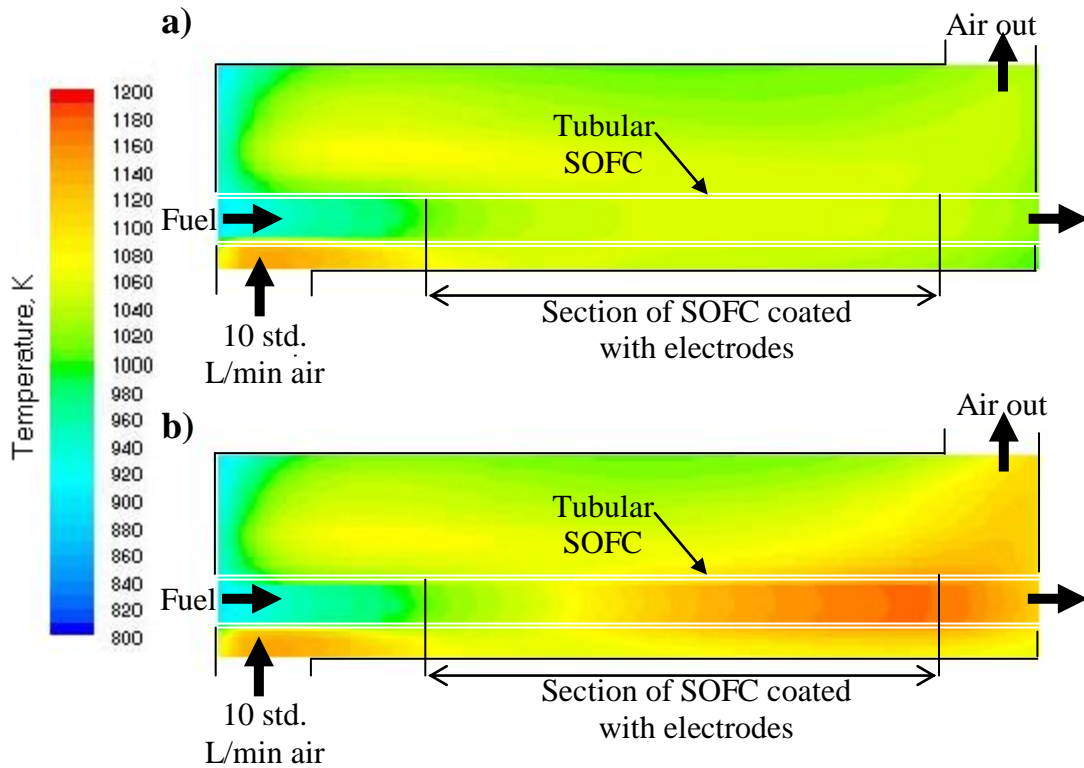


Fig. 6.5 Contours for the stack with 10 l min⁻¹ preheated to 1133 K

a) at open circuit

b) 0.5W of heat generated in each cell

The contours show that whilst the electroded section of the cell is at between 1000 K and 1060 K under open circuit conditions, once the cell is producing 0.5 W of heat the temperature across most of the active part of the cell is above 1100 K. Under these conditions the assumption that the cells would produce 0.5 W of heat is likely to be reasonable as we know from single cells tests that electrical output in the region of 0.5W is viable and from the literature 50% efficiency is probably a sensible estimate.

6.4.3.3 Air flow rate of 15 std. l min⁻¹

The results for the 20 cell stack simulation with 15 std. l min⁻¹ are shown in Table 6.3.

Air inlet Temp.	Temperature through the SOFC stack chamber		Temperature around the only electroded section of the cells						Energy to pre-heat air
	Min	Max	Min	change from Temp. at OCV	Max	change from Temp at OCV	Mean	change from Temp at OCV	
(K)	(K)	(K)	(K)	(K)	(K)	(K)	(K)		(W)
1053.0	824.4	1106.1	961.8	18.5	1106.0	90.8	1036.7	49.5	225.3
1063.0	831.4	1115.3	970.7	18.7	1115.1	90.4	1045.8	49.5	228.3
1073.0	838.4	1124.5	979.5	19.0	1124.3	90.1	1054.9	49.5	231.3
1083.0	845.3	1133.7	988.3	19.3	1133.5	89.8	1064.1	49.5	234.3
1093.0	852.3	1142.9	997.1	19.5	1142.7	89.5	1073.2	49.5	237.2
1103.0	859.3	1152.0	1005.9	19.8	1151.8	89.1	1082.3	49.5	240.2
1113.0	866.2	1161.2	1014.7	20.1	1161.0	88.8	1091.4	49.5	243.2
1123.0	873.2	1170.4	1023.5	20.3	1170.2	88.5	1100.6	49.5	246.2
1133.0	880.2	1179.6	1032.3	20.6	1179.4	88.2	1109.7	49.5	249.2
1143.0	887.2	1188.8	1041.1	20.8	1188.5	87.8	1118.8	49.5	252.2
1153.0	894.1	1198.0	1049.9	21.1	1197.7	87.5	1128.0	49.5	255.2
1163.0	901.1	1207.2	1058.7	21.4	1206.9	87.2	1137.1	49.5	258.2
1173.0	908.1	1216.4	1067.5	21.6	1216.1	86.9	1146.2	49.5	261.1

Table 6.3 Table showing results of simulations for 20 cell stack with 15 std. l min⁻¹ air and 0.5W of heat produced by each cell

The results shown of the simulations with 15 std l min⁻¹ of air indicate that the range of air inlet temperatures that will produce acceptable stack temperatures was 1073 K to 1123 K (shaded results), when 0.5 W of heat was produced in each cell. This is a smaller range than when the cells were under open-circuit conditions and so it is clear that more precise temperature control would be required when current is drawn from the SOFC stack.

Table.6.3 also shows that with 15 std. l min⁻¹ of air the model predicts that a mean temperature of 1100 K could be achieved across the active part of the stack without breaching the 1173 K limit anywhere in the stack. This mean stack temperature is 10 K higher than the best that could be achieved with 10 std. l min⁻¹ of air.

6.5 Summary of CFD simulations of the 20 cell stack

The CFD model of the 20 cell stack clearly predicts that 5 std. l min⁻¹ would be an insufficient air flow to produce suitable temperature across the stack if the air is introduced at one side of the stack. This was because the temperature of the air drops as it crosses the air chamber. The fall in temperature arises due to heat losses through the inlet and outlet manifolds and the insulation surrounding the chamber, and heat transfer with the fuel on the inside of the cell. Even if we suppose 0.5 W of heat were generated in each SOFC, the temperature of the air will still fall too low around the cell for the SOFC to be capable of producing power with 5 std. l min⁻¹ of air.

It was found that the temperature losses through the walls are relatively constant. Thus it was predicted that if the flow rate of air is increased to 10 std. l min⁻¹ or 15 std. l min⁻¹, the temperature decrease across the stack will be sufficiently small that the stack could maintain a temperature such that it would be ready to produce maximum power almost instantaneously. Under these conditions it is predicted that if current were drawn from the stack, the magnitude of heat likely to be produced by polarisation effect would be sufficient for the temperature of the fuel and surrounding air to actually rise as it passed along the length of the fuel cells.

Certain values were identified for the temperature of the air introduced to the stack that would produce temperatures across the stack suitable for maximisation of the electrical power output of the cells whilst preventing damage to the silver wire interconnects. It is predicted that if 10 std. l min⁻¹ of air was preheated to 1123 K and 1133 K, and the stack was at open circuit, the temperature across the stack would be such that it would be ready to produce close to maximum power instantaneously when demanded. It is also envisaged

that under these conditions current could be drawn from the stack without changing the air inlet temperature. The same effect could be achieved with 15 std. l min⁻¹ of air if the air was preheated to between 1093 and 1123 K. Using the higher flow rate of air could yield a mean temperature across the active part of the stack 10 K higher than with 10 std. l min⁻¹. This increase in temperature would be likely to yield higher electrical output from the cells but would be at the expense of an increased energy requirement for the preheating of the air. Further increases in the flow rate of the air would be likely to yield more even temperature distributions across the stack and subsequently provide higher mean operating temperatures. However, for a 20 cell stack producing around 10 W of electrical power and 10 W of heat, the energy requirement to preheat the air would be in the order of 16 to 25 times the electrical power output. With sound engineering some of the energy required for preheating could be recovered from the exit streams but it was thought impractical to increase the air flow rate beyond 15 std. l min⁻¹

6.6 Experimental system operating under Hydrogen

6.6.1 Objectives

The construction of the 20 cell experimental system has been described previously in Chapter 3 and its operation with Helium passed through the cells has been reported in Chapter 5. The next stage in the experimental study was to feed Hydrogen to cells and investigate if the temperature profiles across the stack matched those predicted by the CFD model.

6.6.2 Start-up

The equipment was configured as discussed in section 3.3. The anode was supplied with Helium at a flow rate of 0.3 std. l min⁻¹. The air flow rate was set to 10 std. l min⁻¹. When the air flow rate had been set, the air pre-heater was switched on with the air inlet

temperature set to 1073 K. This was 50 K lower than the inlet temperature that the predictions from the CFD model indicated would be required to maintain the temperature in the electroded section of the cells above 973 K. It was considered sensible to take this cautious approach rather than risk damaging the stack. Once the temperature in the chamber around the cells had reached 700K the flow of Hydrogen into the inlet manifold was gradually increased, and the Helium flow reduced, using mass flow controllers until, after 2 minutes, the Hydrogen flow was $0.5 \text{ std l min}^{-1}$ and the Helium was switched off. This start-up procedure was employed to prevent a build up of Hydrogen before the temperature had risen above the auto ignition temperature of Hydrogen, as the sudden combustion of Hydrogen could have damaged the cells.

6.6.3 Electrochemical performance

The cells were initially at open circuit whilst the stack warmed up. After 100 minutes the stack temperature had reached around 1100 K, around 200 K higher than predicted by the CFD model. At this time open circuit voltage had settled at 2.31V and 2.36V for the top and bottom rows of cells respectively. This was expected given that the typical open circuit voltage for a single cell operating under these conditions is 1.1-1.2 V, and that each row comprised of a series connection between two bundles of 5 cells wired in parallel. Once the open circuit voltage had been recorded an electrical load was applied to each row of cells using the potentiostat. Each row was loaded to 1.1V. i.e. 50% of the system open circuit voltage. The electrical performance is shown Table 6.4.

	Voltage	Current	Power
	V	mA	W_e
Top Row	1.1	111	0.122
Bottom Row	1.1	727	0.800

Table 6.4 Result of electrochemical test

Electrochemical output of between $2 W_e$ and $5 W_e$ was expected for each row of 10 cells so these results represent very disappointing performance. The stack was returned to open circuit conditions and then loaded again periodically until the test had to be terminated but there was no improvement in performance. Analysis of the temperature profile across the stack revealed some likely causes of the poor performance.

6.6.4 Temperature profile

Fig.6.6 shows the temperature profile recorded through the stack with a flow of $0.5 \text{ std. l min}^{-1}$ of Hydrogen.

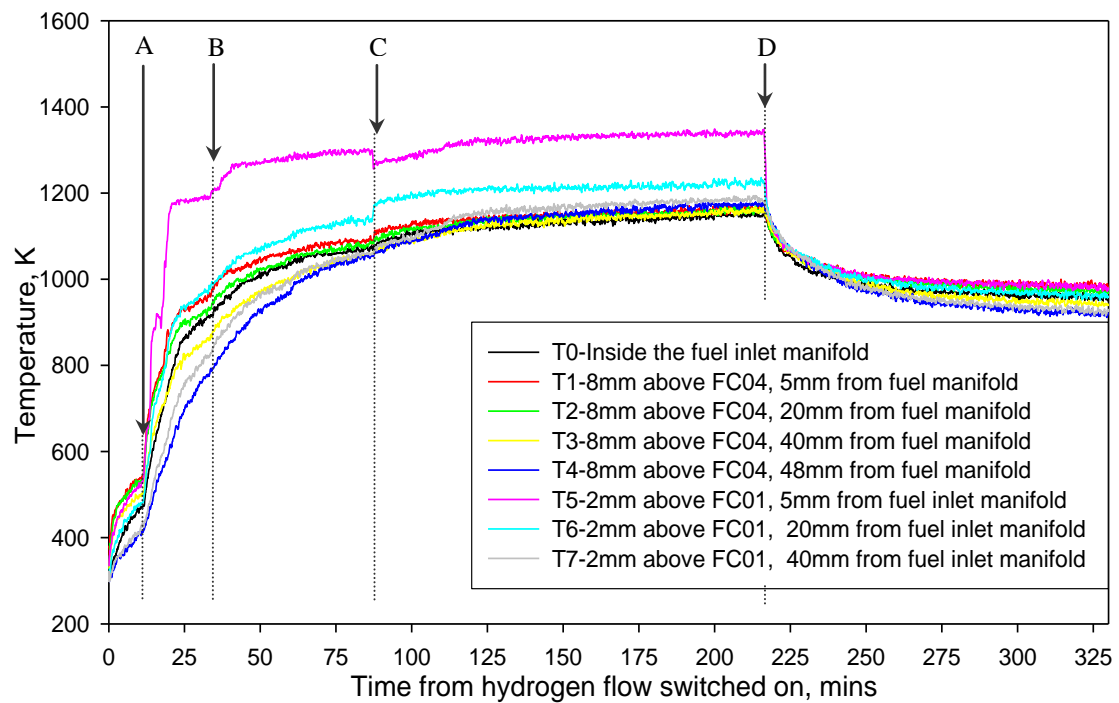


Fig. 6.6 Plot of temperatures recorded from 20cell SOFC stack test with $0.5 \text{ std. l min}^{-1}$ of Hydrogen

From the temperature profile shown in Fig.6.6 it is clear that 4 events occurred during the stack operation that altered the temperature profile. These are discussed below as events A, B, C and D indicated by arrows in Fig. 6.6.

6.6.4.1 Event A-Increase in the rate of the temperature arise across the stack

The temperature rises fairly uniformly for the first 10 minutes but then there is a sharp rise in temperature. The temperature rise is most dramatic at thermocouple position T5 that was above cell FC01 and 5 mm from the inlet manifold. It was thought that temperature rise was likely to have been caused by combustion at the site of a leak of Hydrogen caused by a small crack in one of the cells.

6.6.4.2 Event B-Sharp increase close to the inlet manifold

After a further 25 minutes of operation there was a further rise at thermocouple position 5. This was thought to have been caused by further damage to the cell at the site of the original leak, leading to an increase in the volume of Hydrogen and hence the heat generated by combustion.

6.6.4.3 Event C-Slight Decrease in temperature close to the inlet manifold

After 87 minutes of operation the temperature rise across the stack was beginning to plateau but there was a slight decrease in the temperature at T5 and a sharp rise at T1 and T6. This could be explained by a further leak occurring in another cell resulting in combustion causing the increased temperature around T6. The fuel leaking from the second leak could have reduced the loss of fuel at the original leak and explained the reduction in temperature at T5.

6.6.4.4 Event D-Hydrogen was switched off and Helium supplied to the cells

After 2 hr 15 min the temperature across the stack was still rising and the temperature around the active section of the cells approached 1150 K. It was feared that continued operation would lead to the silver interconnects melting so the test was terminated. Prior to shutting the stack down completely, the Hydrogen flow was switched off and Helium was delivered to the cells whilst the air inlet temperature was maintained at 1073 K. This was in order to assess if the temperature rises across the stack had been caused by combustion of leaking Hydrogen, and to what extent this had altered the temperature profile. Once the Hydrogen was turned off the temperature profile became much more uniform indicating that the higher temperatures recorded by thermocouples, T5 and T6 had been due to combustion of local leaks of Hydrogen. The temperatures across the stack under Helium were over 200K lower than with Hydrogen. An attempt to quantify the level of leaking Hydrogen was made by assuming the leaks had caused an adiabatic temperature rise of 200 K to the airflow through the stack.

Calculation of the estimated volume of leaking fuel:

$$\text{Molar Flow of air, } \dot{n} = \frac{p\dot{V}}{RT} = \frac{101355 \times \left(\frac{10}{60 \times 1000} \right)}{8.314 \times 298} = 0.006818 \text{ mol.s}^{-1} \quad \text{Eq.6.1}$$

$$\text{Energy required to raise air temperature from 900K to 1100K, } \dot{Q} = \dot{n} \int_{900}^{1100} c_p dT \quad \text{Eq.6.2}$$

$$\text{For air } c_p = 28.09 + 0.1965 \times 10^{-2} T + 0.4799 \times 10^{-5} T^2 - 1.965 \times 10^{-9} T^3 \quad \text{Eq.6.3}$$

$$\dot{Q} = 44.8W$$

The heat of combustion for Hydrogen at 298K is 241.838 kJ mol⁻¹.



To find the heat of reaction at 900 K, the energy required to change the temperature of the reactants from 900 K to 298 K, and the energy required to change to the temperature of the reaction products from 298 K to 900 K is added to the enthalpy change for the reaction at 298 K. Based on this calculation the enthalpy of combustion for Hydrogen at 900 K is 239.50 kJ mol⁻¹.

$$\text{Flow of leaking hydrogen, } \dot{n}_{\text{leak}} = \frac{44.84}{239500} = 1.872 \times 10^{-4} \text{ mol s}^{-1}$$

$$\text{Flow of leaking hydrogen, } \dot{n}_{\text{leak}} = \frac{\dot{Q}}{\Delta H_{\text{Combustion}}^{900\text{K}}} \quad \text{Eq.6.5}$$

$$\text{Volumetric flow of leaking fuel, } \dot{v}_{\text{leak}} = \frac{\dot{n}_{\text{leak}} RT}{P} \quad \text{Eq.6.6}$$

$$\dot{v}_{\text{leak}} = \frac{1.872 \times 10^{-4} \times 83.314 \times 298}{101355} = 4.576 \times 10^{-6} \text{ std. m}^3 \text{ s}^{-1}$$

$$\dot{v}_{\text{leak}} = 0.275 \text{ std.l min}^{-1}$$

The estimated flow rate of 0.275 std. l min⁻¹ of leaking fuel represents over half of the total fuel flow. This was a crude estimate as it assumes uniform heating of the air across the channel, neglects additional heat losses to the atmosphere, and that additional energy would be required to increase the temperature of the fuel as well as the air. Fuel leakage of this magnitude would explain the poor electrochemical performance as well as the temperature profile. The electrical output is strongly dependent on flow rate so reducing the flow of fuel to the cells by well over 50% could induce the poor performance observed.

After cool down the stack was examined. A large crack was found in cell FC11. It is thought that Hydrogen leaking at small initial cracks in the cells caused more catastrophic

cracking due to thermal stress produced at the hot spot created by the leaking Hydrogen. These cracks were sealed with Zirconia paste and the experiment was repeated several times but in each time after a short period of operation under Hydrogen the seal was damaged or new cracks in other cells appeared. It is believed that one of the reasons for the cracking of the cells was due to the cell not being perfectly straight. This meant rather than being able to move freely with thermal expansion the would have been stressed by contact between the cell and steel fuel injectors, as shown in Fig.6.7. This problem may be reduced with improved production techniques that would evolve from large-scale production of the micro-tubular cells but at the current scale of manufacture were difficult to avoid.

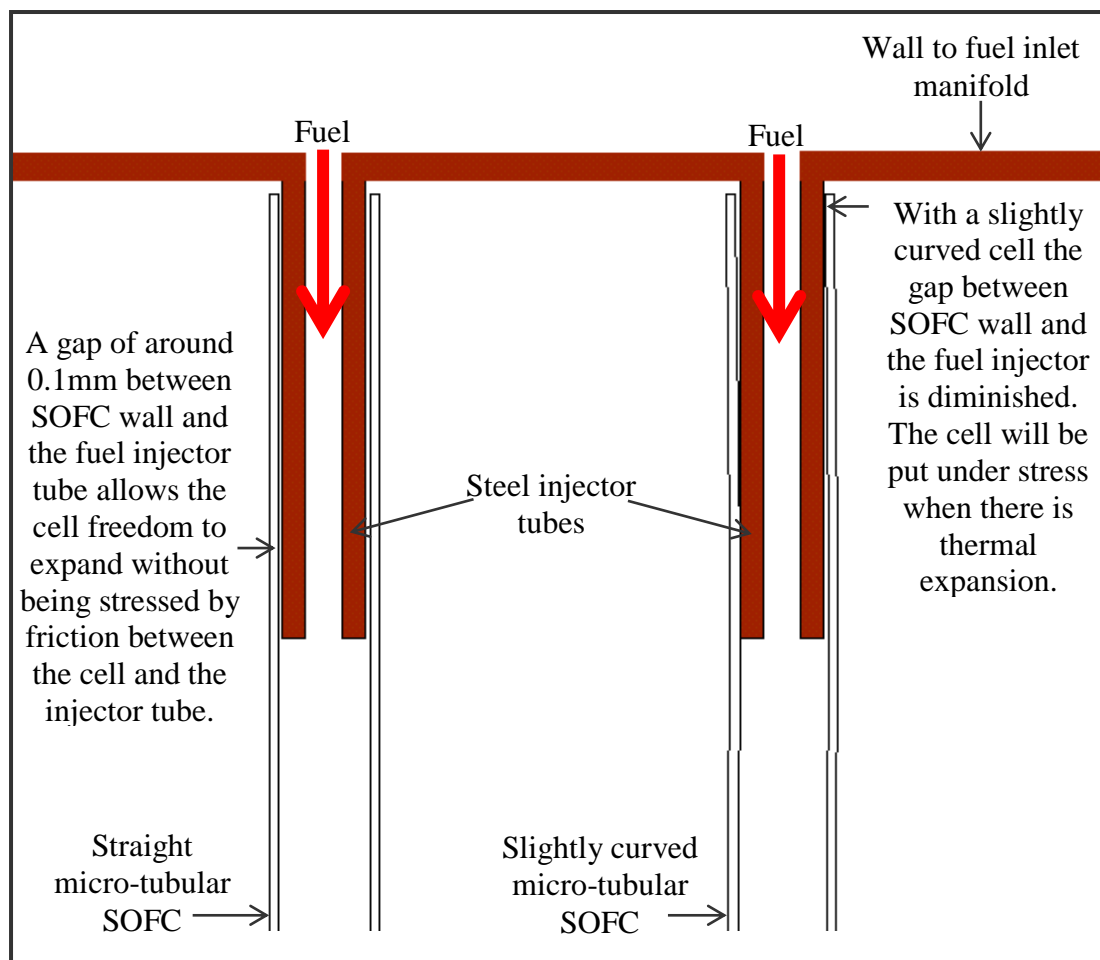


Fig. 6.7 Diagram to show problems caused by slightly bent cells

6.7 Conclusion

A CFD model of a 20-cell SOFC micro-tubular stack design has been used to predict temperature profiles with the stack under open circuit conditions and when electrical power is produced. This was used to investigate the possibility of using preheated air to keep the SOFC stack at the desired operating temperature.

The air inlet temperature and flow rate were varied in the simulations to predict which operating conditions would give rise to a suitable temperature across the SOFC stack. The findings from these simulations were that 5 std. l min⁻¹ air flow was insufficient to obtain the desired stack temperature and that a higher air/fuel ratio would be required. Air inlet temperatures were identified for flows of 10 and 15 std. l min⁻¹ that could be used to maintain the stack at a suitable temperature. Increasing the air flow increased the uniformity of the temperature profile but this would need to be offset against the increased component cost and energy consumption.

This is one of few works on stack modelling to have included attempts to validate findings with experimental data. The 20-cell SOFC stack was tested on Hydrogen in order to validate the CFD predictions, but they had to be terminated due to a failure to prevent damage to the silver interconnects. The temperatures recorded in the stack were over 200 K higher than predicted in the CFD model. It was clear that these differences had arisen from the combustion of leaking fuel and that this was one of the major issues to be addressed in the scale up of micro-tubular stacks.

Whilst the method used to manifold the cells had been used successfully for 4-cell demonstration stacks it appeared that it might not be suitable for larger stacks. There are a

number of possible reasons why the system was less successful when the number of cells was increased from 4 to 20. With 20 cells rather than 4, there is an increased chance that one of the cells will suffer a crack. Whilst some of the 4 cell stacks ran for a long time, others did suffer failure due to cell fracture. Increasing the number of cells would clearly increase the chance of this happening. Once one cell had broken the local temperature rise produced by combustion of the leaking fuel would increase the stress on neighbouring cells caused by differing rates of thermal expansion. Therefore there would be an increased chance of a second breakage. This is what appeared to have happened during the reported test.

Using preheated air to warm the stack, rather than electrical heating elements mounted around the cells, was seemingly a less robust method of temperature control. The electrical heating system in the 4-cell stack produced a very even temperature distribution along the length of the cell compared with introducing hot air at one end of the stack. Also the electrical heating is likely to be able to cope with leaking fuel more readily. If more heat was generated inside the cell chamber, through combustion of leaking fuel, the control system would simply reduce the heat dissipated by the heating elements. The overall conclusion of the stack testing was that some development work was needed to turn the 20-cell system into a viable design.

Whilst the thermal management of the stack was unsuccessful in the testing of the stack on Hydrogen, heating the stack by preheating the air supply is attractive, as the energy for preheating the air could be supplied through heat exchange with gases from the combustion of fuel from the same source as used to fuel the SOFC. The CFD simulations predict that preheating the air could be a successful method of temperature control if there

were no leaks. The question arose of what levels of leakage, if any, could be tolerated whilst maintaining a temperature profile that could sustain the operation of the fuel cells. In order to address this question it was decided to attempt to develop the CFD model so that it included simulation of the effect of fuel leakage. This would then be used to determine if it is viable to pursue a stack with 'leaky seals' heated by hot air or if efforts need to be focused on perfecting a method of sealing the cells to the inlet and outlet manifolds. This investigation is reported in Chapter 7.

7. Simulation of leaks in a 20-cell micro-tubular SOFC stack

7.1 Introduction

In Chapter 6 predictions from CFD simulations were used to identify air flow rates and inlet temperatures that would produce suitable operating temperatures in a 20-cell SOFC stack. During the evaluation of these predictions with experimental tests, it became clear that the combustion of leaking fuel, ignored in the original models, had a strong influence on the temperature distribution. The effect of heat generated by leakage was found to be so dominant that the experiments had to be terminated to prevent the stack from overheating. The work brought into question whether it was viable to deploy the simple manifolding system that had been successful with 4-cell stacks, in larger SOFC systems, or if a more advanced solution, which prevented any leakage of fuel, was needed. Therefore, the objective of this Chapter was to further investigate the effect of fuel leakage on stack temperature.

Since it was difficult to control the flow of leaking fuel in an experimental system, the CFD model was used to simulate and analyse the effect of fuel leakage. Whilst the reduction to the flow of fuel to the SOFC anodes and subsequent reduction in electrical output was obviously a major consequence of fuel leakage, a more critical issue was the local temperature rise caused by the combustion of the fuel. This prevented the stack temperature from being controlled at appropriate levels for the electrochemical reactions to take place during the experiments described in Chapter 6. Therefore, the modelling of leaks in the CFD model focused on the simulation of the heat generated by the combustion of the leaking fuel. The result of these simulations would reveal some guidelines for the design of future micro-tubular stacks. In previous works^[101] the effect of leakage on cell performance due to changes to the composition of the fuel and air streams

has been taken into account, but none have reported the effect of the heat generated by the combustion of the fuel.

7.2 Simulation of uniform leakage of fuel at the cell inlet

7.2.1 Objectives

In order to assess if it was viable to have a stack manifold system that naturally allowed some fuel leakage from the inlet of cells, the CFD model was used to simulate the effect of heat generated by the combustion of varying amounts of fuel leaking from the inlet end of the SOFCs. The first situation to be simulated was that of an even flow rate of fuel leaking from each cell at the inlet.

7.2.2 Method and boundary conditions

As discussed previously in the introduction to this Chapter, the focus of the modelling of the fuel leakage was the heat created by its combustion. At this stage, not enough detail was known about the flow and pressure conditions within the SOFC tubes for it to be possible to model the flow of fuel from the tube through the gap between the fuel injection tube and the wall of the SOFC tube. Even if details of these conditions were known, the detailed modelling of the flow in the gap between the SOFC and fuel injector would be at a smaller length scale to the model of the complete stack and thermal insulation. Inclusion of such details would vastly increase the computational requirements to resolve the velocity and temperature distributions. In order to simplify the situation, the mass transfer of the fuel to the outside of the cell was disregarded, and the combustion of leaking fuel was merely represented by addition of a constant energy source. This energy source was specified in the volume representing the 10 mm length of the SOFC tube closest to the fuel inlet manifold. The magnitude of this energy source was calculated

based on a given flow rate of fuel undergoing complete combustion in this region of the cell. A diagram has been shown in Fig. 7.1 to explain this situation.

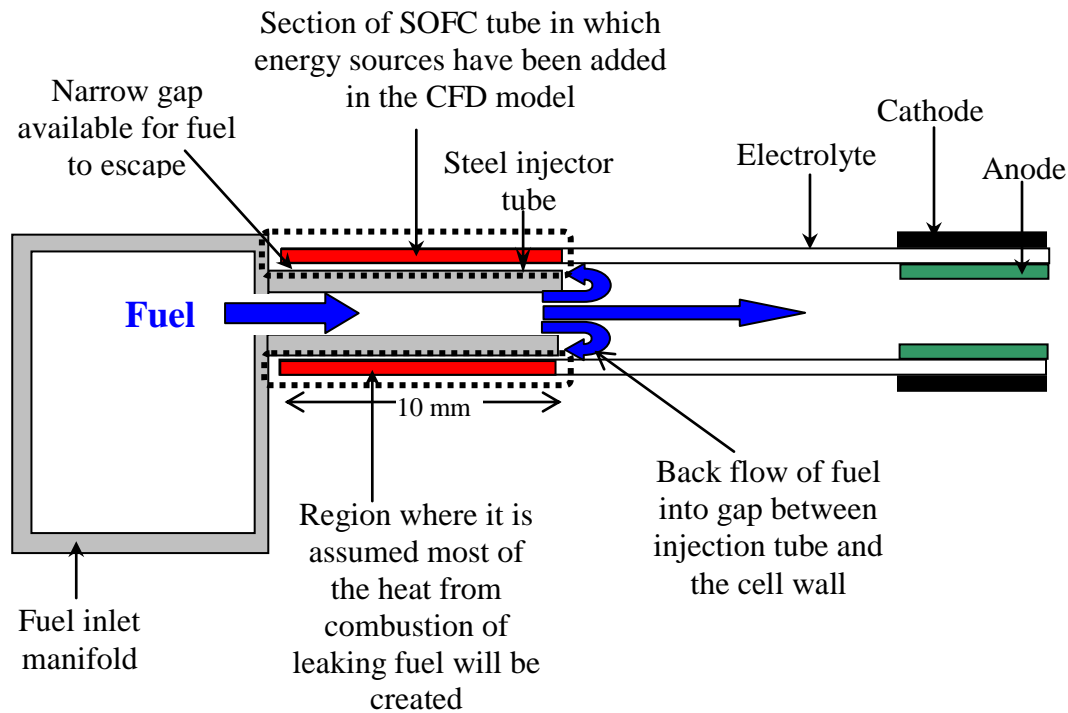


Fig. 7.1 Schematic to explain modelling of fuel leakage

The region enclosed by dotted lines in Fig. 7.1 represents the area where it is assumed that most of the heat is generated by the leaking fuel. This is where the fuel, which has entered the annulus between the fuel injection tube and wall of the SOFC, is most likely to come into contact with Oxygen from the air flowing around the cell. In practice, whether this occurs on the inside or outside of the tube will depend on the pressure inside the SOFC and the surrounding air. To approximate this in the model, the energy that would be released by the combustion has been introduced as a source term in the section of the SOFC corresponding to that shown in red in Fig. 7.1.

7.2.3 Simulation of even fuel leakage with the SOFC stack at open circuit

Initially it was assumed that the stack was at open circuit such that the only heat generated inside the stack would be that produced by combustion of the leaking fuel. To

begin with it was assumed that just 0.001 std. l min⁻¹ (1.36×10^{-9} kg s⁻¹) of Hydrogen leaked from each cell. The calculation of the heat generated by a leak of this size is shown below.

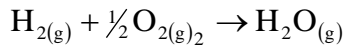
Calculation of Heat production at leaking seals:

Volumetric flow of leaking Hydrogen, $\dot{v} = 0.001$ std.l min⁻¹

$$\text{Volumetric flow of leaking Hydrogen, } \dot{v} = \frac{0.001}{60 \times 1000000} = 1.667 \times 10^{-8} \text{ m}^3 \text{ s}^{-1}$$

$$\text{Molar flow of leaking Hydrogen} = \dot{n} = \frac{P\dot{v}}{R_m T} = \frac{101355 \times (1.667 \times 10^{-8})}{8.314 \times 293}$$

$$\dot{n} = 6.935 \times 10^{-7} \text{ mol s}^{-1}$$



$$\Delta H_{\text{Combustion}}^{900\text{K}} = 239.50 \text{ kJ mol}^{-1}$$

$$\text{Rate of heat production per cell, } \dot{Q}_{\text{FC}} = \dot{n}_{\text{FC}} \cdot \Delta H_{\text{Combustion}}^{900\text{K}} = 6.935 \times 10^{-7} \times 239500$$

$$\text{Rate of heat production per cell, } \dot{Q}_{\text{FC}} = 0.166 \text{ W}$$

This value was then introduced to the FLUENT model as a constant value energy source in the solid domain representing the 10 mm of each fuel cell tube closest to the fuel inlet. The simulation was run until the solution had re-converged and the maximum, minimum and average temperatures around the cell were calculated. The magnitude of the energy source representing combustion of Hydrogen was then recalculated based on increasing volumes of gas leaking at the seals from 0.001 std. l min⁻¹ to 0.010 std. l min⁻¹. FLUENT case and data files were created for the different rates of fuel leakage, and a converged solution was obtained for each.

The post processing features in FLUENT were then used to find the maximum, minimum and mean temperature, across the whole stack, and also in just the section corresponding to where the cells are coated with electrodes. The results obtained for 10 std. l min⁻¹ of air preheated to 1073 K have been plotted in Fig. 7.2.

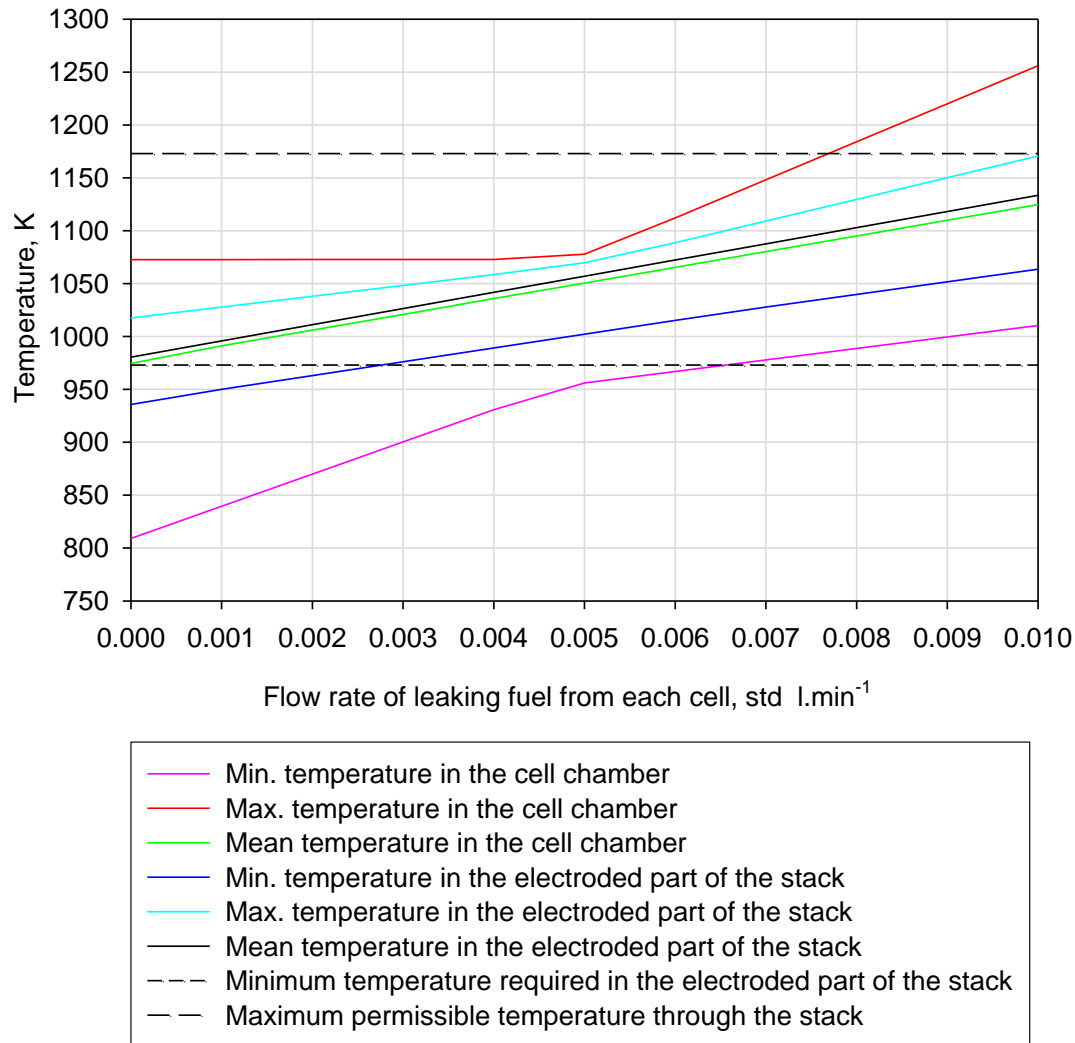


Fig. 7.2 Graph to show the effect of increasing flow rates of leaking fuel for the 20 cell stack at open circuit with 10 std. l min⁻¹ air preheated to 1073 K

Fig. 7.2 shows that the predicted minimum temperature in the electroded part of the stack is below the desired 973 K if less than 0.003 std. l min⁻¹ leaks from the cells. However, if the flow of fuel leaking from each cell increased to 0.005 std. l min⁻¹ it is predicted that

the maximum temperature in the stack would start to rise sharply with any further increases in the leakage. This change in the rate of maximum temperature rise with increasing fuel leakage arises because the part of the stack that is hottest shifts from the region immediately adjacent to the air inlet, to the zone around the source of the leaks. Once the region around the leaks has become the hottest section of the stack the maximum temperature is more strongly influenced by the affect of further leakage. This is illustrated by the temperature contours plotted in Fig. 7.3

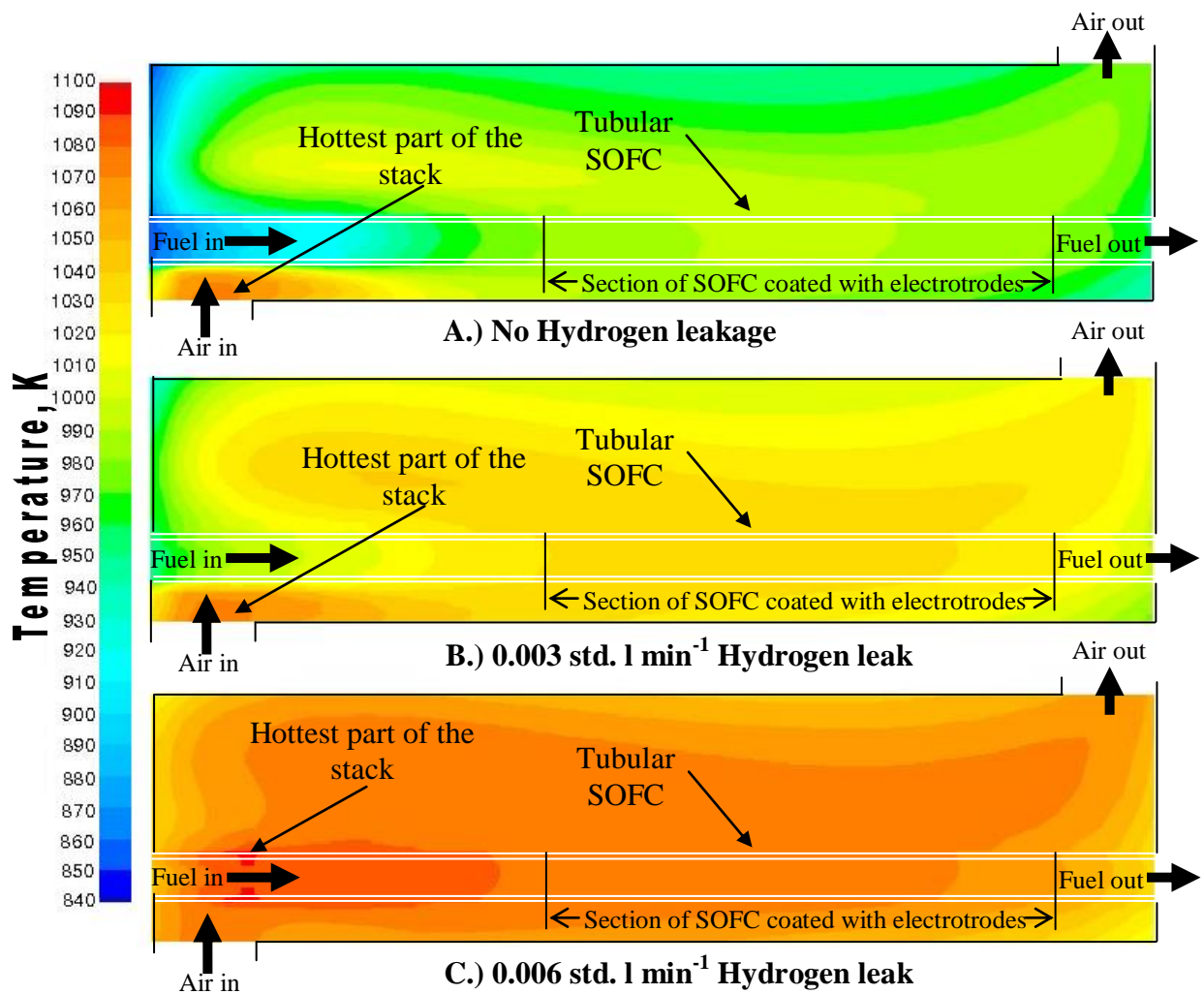


Fig. 7.3 Predicted temperature contours on a vertical plane through FC04 with 10 std. l min⁻¹ air preheated to 1073 K and the 20 cell stack at open circuit

Plot A. shows that with no fuel leakage, the hottest region of the stack is the area adjacent to where the preheated air is introduced. When heat is generated by only $0.003 \text{ std. l min}^{-1}$ of Hydrogen leaking from the inlet of each cell, the model predicts that the temperature profile across the stack will be more uniform but the hottest region is still where the preheated air enters the chamber housing the SOFC stack. However, the plot shown in Fig. 7.3 C. shows that if the rate of fuel leakage is increased to just $0.006 \text{ std. l min}^{-1}$ the hottest part of the stack is now at and around the walls of the tubular SOFC, where the combustion of leaking fuel is assumed to take place.

Whilst it is predicted that a small amount of fuel leakage actually reduces the temperature gradient across the 20 cell stack at open circuit, it was found that a leak of more than $0.008 \text{ std. l min}^{-1}$ of fuel will cause the maximum temperature to raise above 1173 K, which would mean that damage to the silver interconnects would be likely to occur. One option to prevent the stack from over heating would be to decrease the temperature of the preheated air. To study the impact of changes to the air inlet temperature, this variable was changed to progressively lower temperatures in the model, and solutions generated for the different rates of fuel leakage. The results for various different air preheat temperatures with $0.008 \text{ std. l min}^{-1}$ of Hydrogen leakage per cell are shown in Fig 7.4.

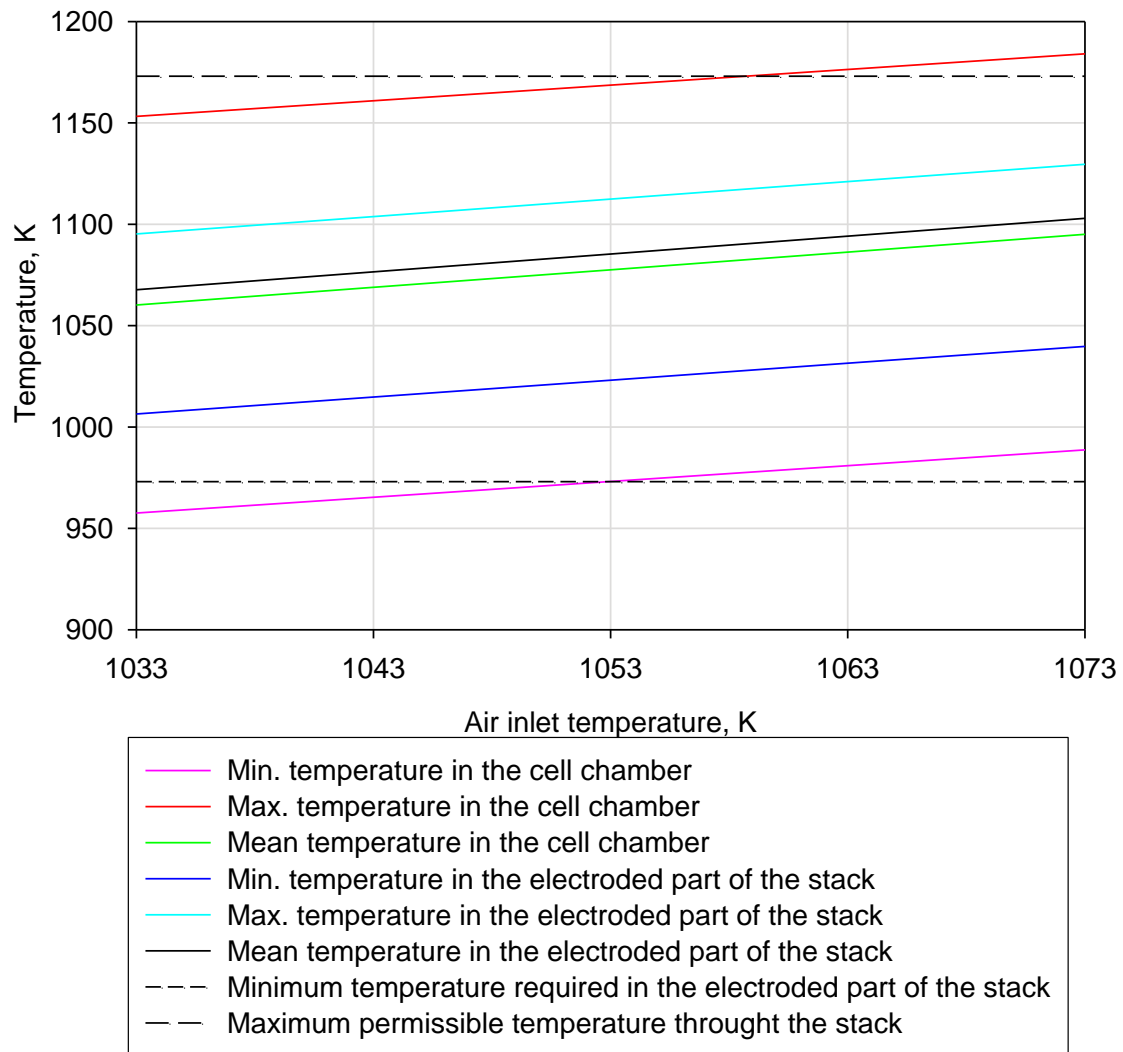


Fig. 7.4 Graph to show affect of reducing the air inlet temperature on the stack temperature if $0.008 \text{ std. l min}^{-1}$ of Hydrogen was leaking from each cell

From the simulation results shown in Fig 7.4 it is predicted that with $0.008 \text{ std. l min}^{-1}$ of Hydrogen leaking from each SOFC, the inlet temperature would need to be reduced to at least 1053 K to prevent the stack from over-heating.

Post processing of simulations run at several inlet temperatures and rates of fuel leakage, was used to determine both the maximum air inlet temperatures required to keep the stack temperature below 1173 K, and the minimum air inlet temperature that would cause the temperature around the active part of the cell to be above 973 K. The results of this analysis are plotted in Fig. 7.5.

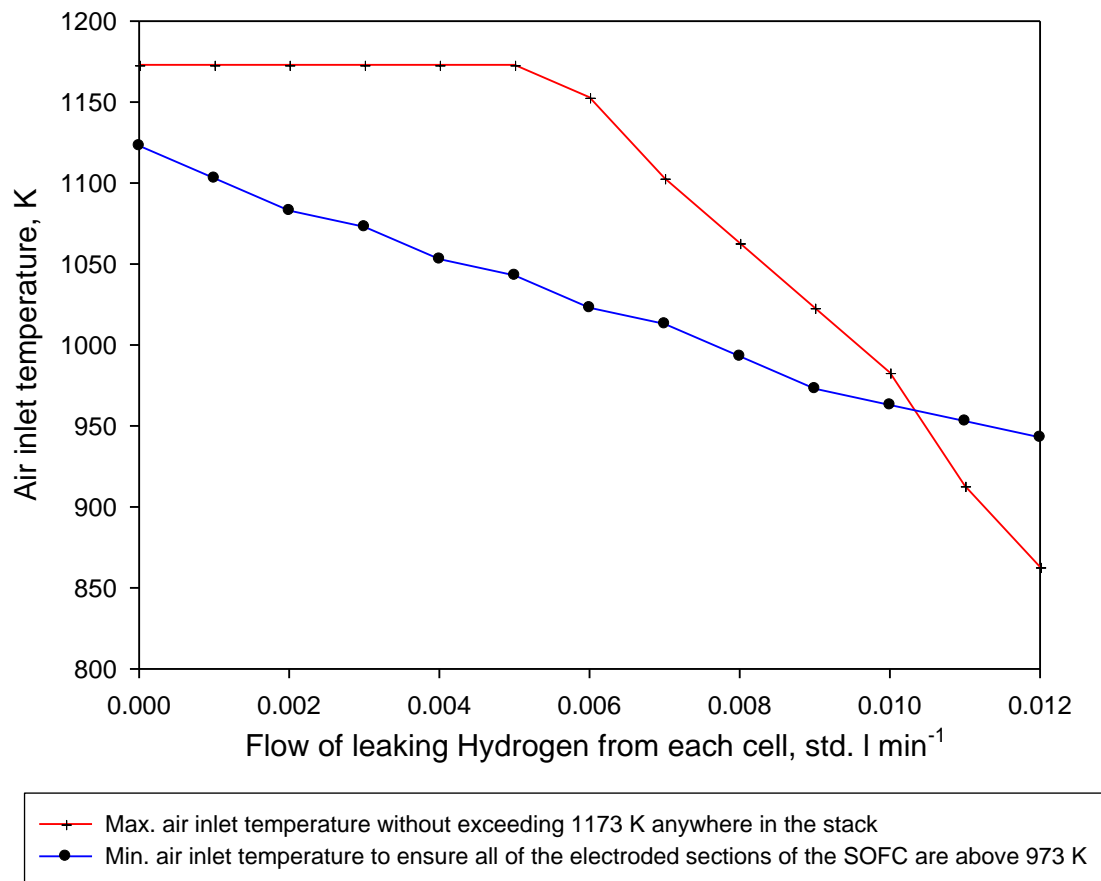
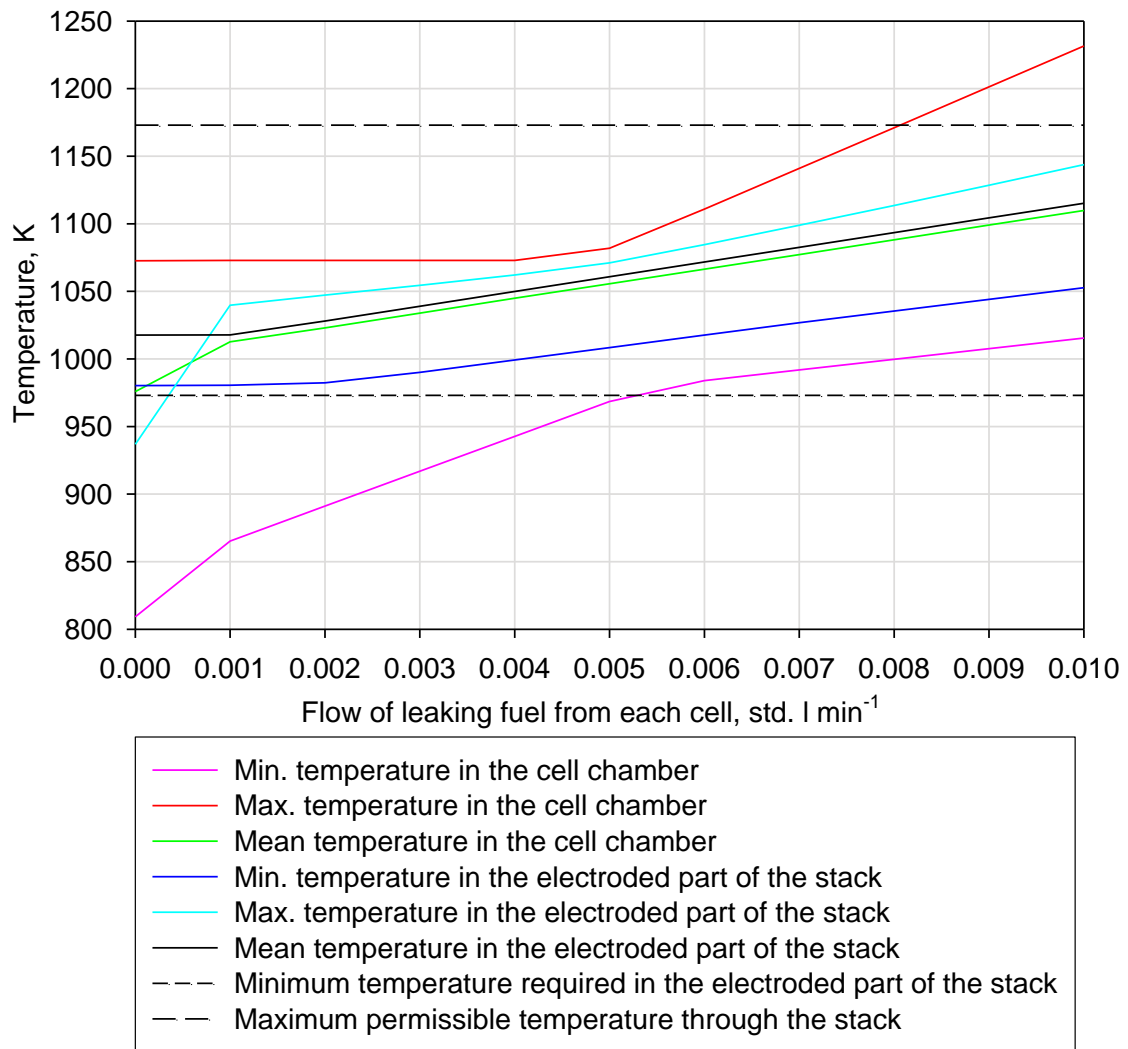


Fig. 7.5 Graph showing air inlet temperature required to keep the stack between 973 K and 1173 K with 10 std. l min⁻¹ air

The red line in Fig 7.5 illustrates the maximum permitted air inlet temperature that will prevent the hottest parts of the stack exceeding the limit of 1173 K. The line shown in blue shows the minimum air inlet temperature required to maintain the whole of the

active part of the stack above 973 K. It was found that it should be possible to keep a 20 cell stack at a viable operating temperature by reducing the air inlet temperature, even if up to 0.010 std. l min⁻¹ of Hydrogen leaked from all of the cells. With 0.010 std. l min⁻¹ leaking from the cells the air inlet temperature would need to be reduced to below 973 K. With this level of fuel leakage, the air inlet temperature would need to be precisely controlled between 963 K and 973 K. If the level of fuel leakage increased further it is predicted that it would become impossible to maintain the stack temperature within the operating window of 973 to 1173 K.

In the control of the stack temperature, when there is fuel leakage, an alternative to reducing the air inlet temperature would be to increase the air flow rate. The effect of increasing the air flow rate to 15 std. l min⁻¹ was studied using the CFD model. This was achieved by simply increasing the mass flow rate specified as a boundary condition at the air inlet. The temperatures predicted in the stack for 15 std. l min⁻¹ of air heated to 1073 K are plotted in Fig. 7.6.



+

Fig. 7.6 Chart to show predicted temperatures with fuel leakage and 15 l min⁻¹ of air heated to 1073 K

It is shown that if 0.008 std. l min⁻¹ leaked from each of the cells the maximum stack temperature would rise above the threshold set to avoid damage to the silver interconnects. Thus, when the air flow rate was increased to 15 std. l min⁻¹ the maximum tolerable level of fuel leakage was only fractionally more than with 10 std. l min⁻¹. The following calculation shows that 15 std. l min⁻¹ of air with 0.5 std. l min⁻¹ of Hydrogen corresponded to a relative air/fuel ratio of 12.6 : 1.

$$\text{Relative air/fuel ratio, } \lambda = \frac{(\dot{v}_{\text{fuel}}/\dot{v}_{\text{air}})_{\text{stoichiometric}}}{(\dot{v}_{\text{fuel}}/\dot{v}_{\text{air}})_{\text{actual}}} = \frac{(0.5/1.19)}{(0.5/15)} = 12.605 \quad \text{Eq. 7.1}$$

This amount of excess air is significantly higher than values used for other types of SOFC technology. Such a large excess of air would increase the energy consumption of the compressor and these increased parasitic losses would reduce the system efficiency. Therefore, it was not thought sensible to increase the air flow further. Consequently it appears from the results of the simulation, that reduction of the inlet temperature is a more sensible method of controlling the stack temperature when leaks are present.

7.2.4 Simulation of leaks and heat generated by electrochemical reactions

Whilst the simulations described in 7.2.3 indicated that it would be possible to prevent the stack from over-heating due to fuel leakage when the cells are at open circuit, it was thought that this would prove more difficult when the cells were fully loaded. Under these conditions the temperature may rise across the length of the cell due to the heat generated by electrochemical reactions in addition to any heat generated by combustion of burning fuel. Therefore, to check that it would still be possible to keep a 20 cell SOFC stack at its operating temperature under these conditions, simulations were run to model simultaneous generation of heat from electrochemical reaction and from combustion of leaking fuel. The heat generated by electrochemical reactions was modelled in the same way as described in Chapter 6. It was assumed that 0.5 W of heat would be generated in the electroded section of each of the SOFCs. The predicted temperatures in the stack for increasing fuel leakage and the SOFCs producing 0.5 W of heat are shown in Fig. 7.7 with 10 std. l min⁻¹ of air heated to 1073 K.

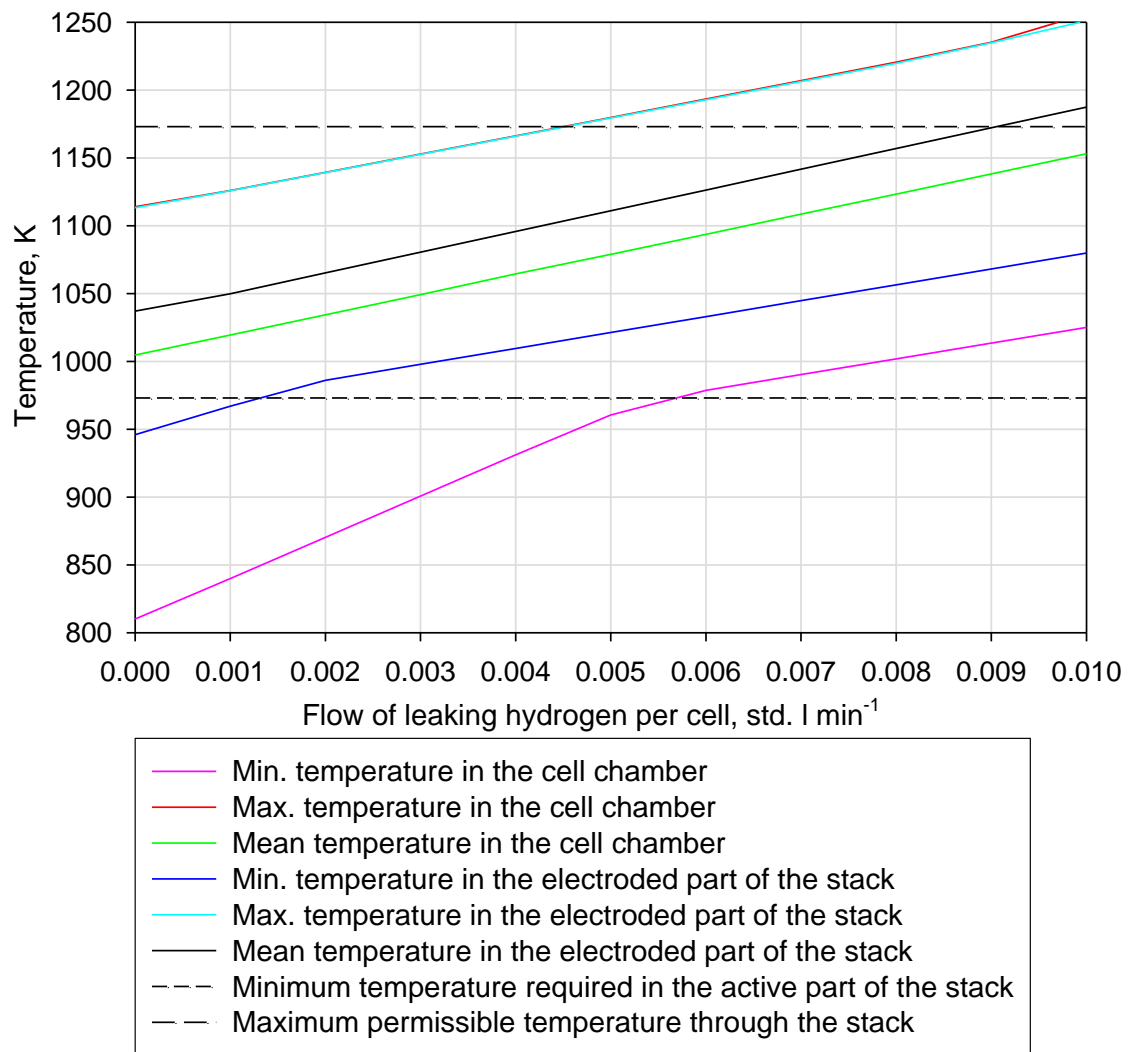


Fig. 7.7 Graph showing the effect of combustion of leaking Hydrogen on the stack temperature with the cells producing 0.5 W of heat with 10 l min⁻¹ air preheated to 1073 K

Although the model predicted that, with the cells producing 0.5 W of heat, the stack would not get up to the ideal temperature without the influence of leaks, Fig. 7.8 shows that the model predicted that the combustion of 0.004 std. l min⁻¹ of leaking fuel from each cell would generate enough heat to create hot spots where the stack could be damaged.

From the simulations described in Chapter 6, it was predicted that with the SOFCs producing 0.5 W of heat, the air could be preheated to 1123 K to achieve the highest possible stack temperatures whilst keeping the maximum temperature below 1173 K. The results shown in Fig. 7.8 show that under these conditions if just 0.001 std. l min⁻¹ leaked from each of the cells, the stack would be at risk of damage due to over heating.

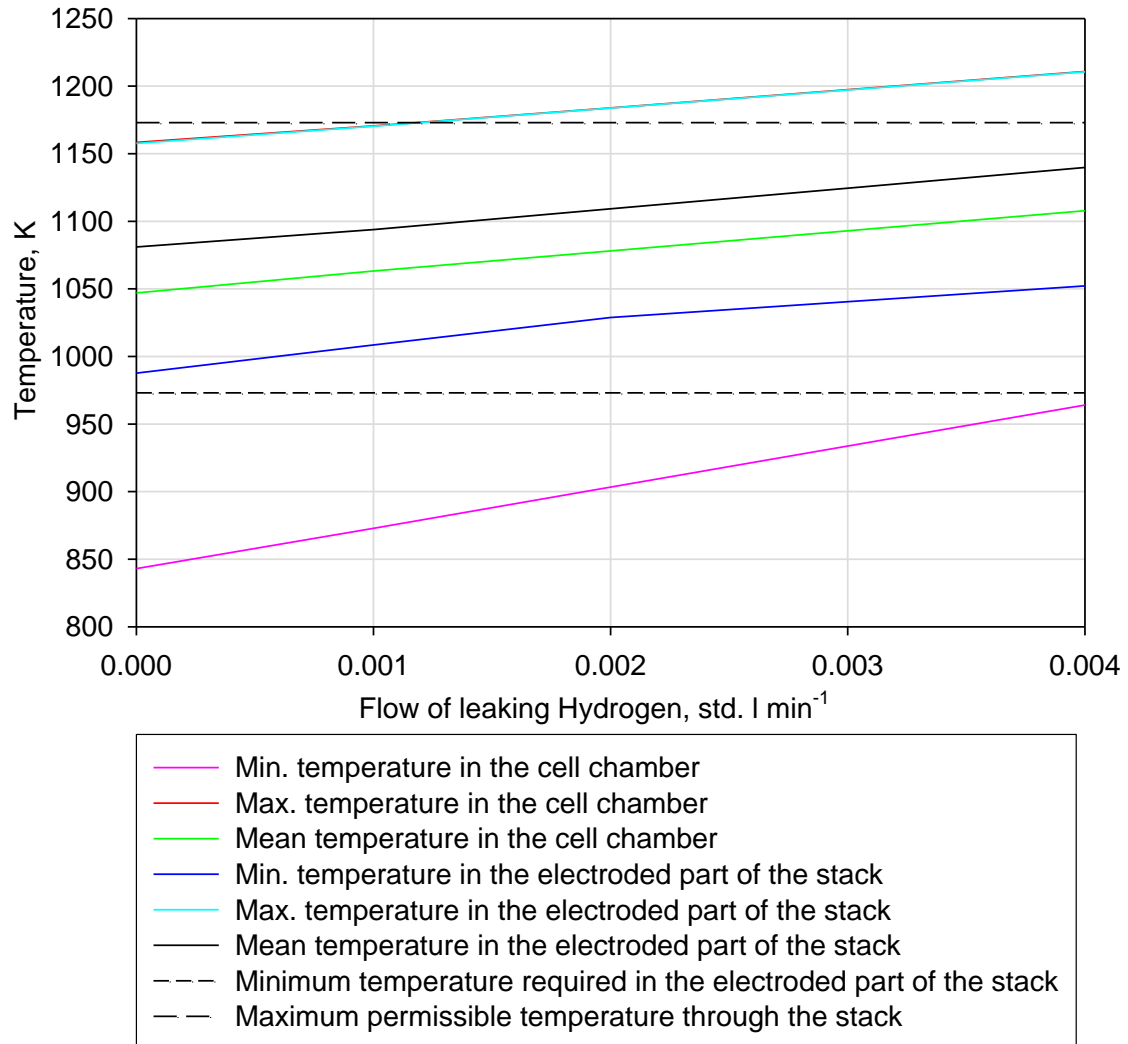


Fig. 7.8 Effect of leaking fuel on the stack temperature with 10 l m⁻¹ of air preheated to 1123 K and the cells producing 0.5 W of heat

The temperature contours plotted in Fig. 7.9 show how even a small leak ($0.002 \text{ std l. min}^{-1}$) of fuel at the inlet end of the cell could affect the stack temperature and create a hot spot at the opposite end of the cell.

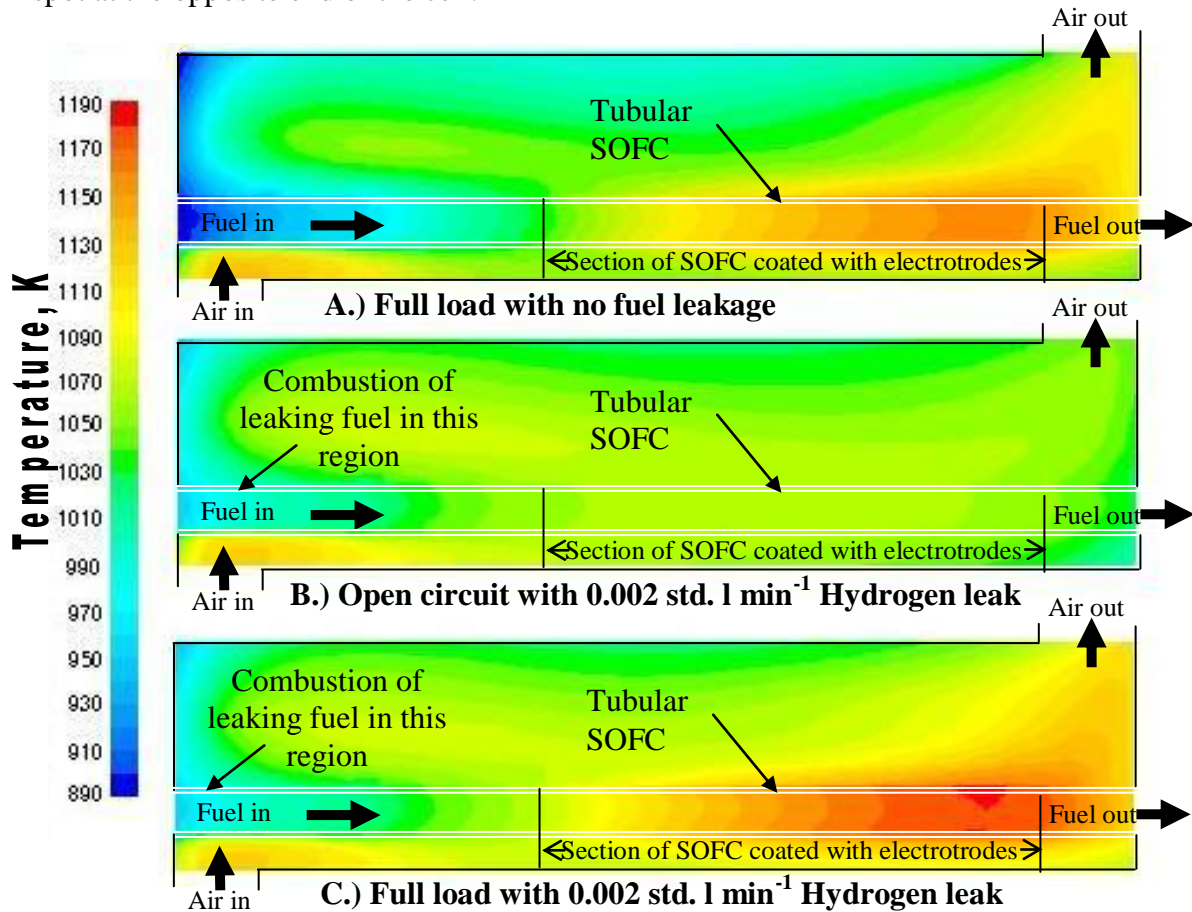


Fig. 7.9 Temperature contours through FC04 at open circuit with preheated to 1123K and $0.002 \text{ std. l min}^{-1}$ Hydrogen leaking from each cell

Plot A in Fig. 7.9 shows the temperature through FC04 when there is no fuel leakage and the cell is fully loaded and generating 0.5 W of heat in each SOFC. Under these conditions the temperature rises towards the fuel exit cell due to the heat generated by the electrochemical reactions but the temperature does not exceed 1170 K . Plot B in Fig. 7.9 shows the temperature through FC04 when there is 0.002 l min^{-1} of Hydrogen leaks from each cell whilst the SOFC stack is at open circuit. Under these conditions the temperature is higher around the inlet end of the cell than when there is no fuel but this would not

impact on the operation of the stack as the maximum temperature is still well below 1173 K. Plot C shows the results of the simulation when the stack is fully loaded and 0.002 l min^{-1} of Hydrogen leaks from each cell. With this situation it is predicted that the temperature in the location of the leak, at the inlet end of the cell, would only be around 1000 K which would not be a problem. However, heat generated by combustion of the leaking fuel causes the fuel inside the cell, and the surrounding air, to enter the active part of the cell at a temperature 10 to 20 K higher than when there is no fuel leakage. This small increase in temperature combined with the heat released as a by-product of the electrochemical reaction is enough to create a hot spot towards the exit end of the SOFC where the temperature reaches 1181 K. At this temperature the silver interconnects on the cathode side of the cell would be vulnerable to damage. An interesting result to come from analysis of these simulations is that if a cell had been damaged running under the conditions described in plot C, the damage to the cell would be sustained at the opposite end of the cell to the source of the fuel leakage. Therefore a SOFC stack could sustain damage to the silver interconnects caused by a heat generated by leaking fuel and yet there may be no signs of fuel leakage close to the damaged area.

Post processing of the predicted temperature distributions from simulations performed with different levels of fuel leakage and various inlet temperatures was used to identify the maximum and minimum suitable air inlet temperature for a given rate of fuel leakage. This information is displayed in Fig. 7.10.

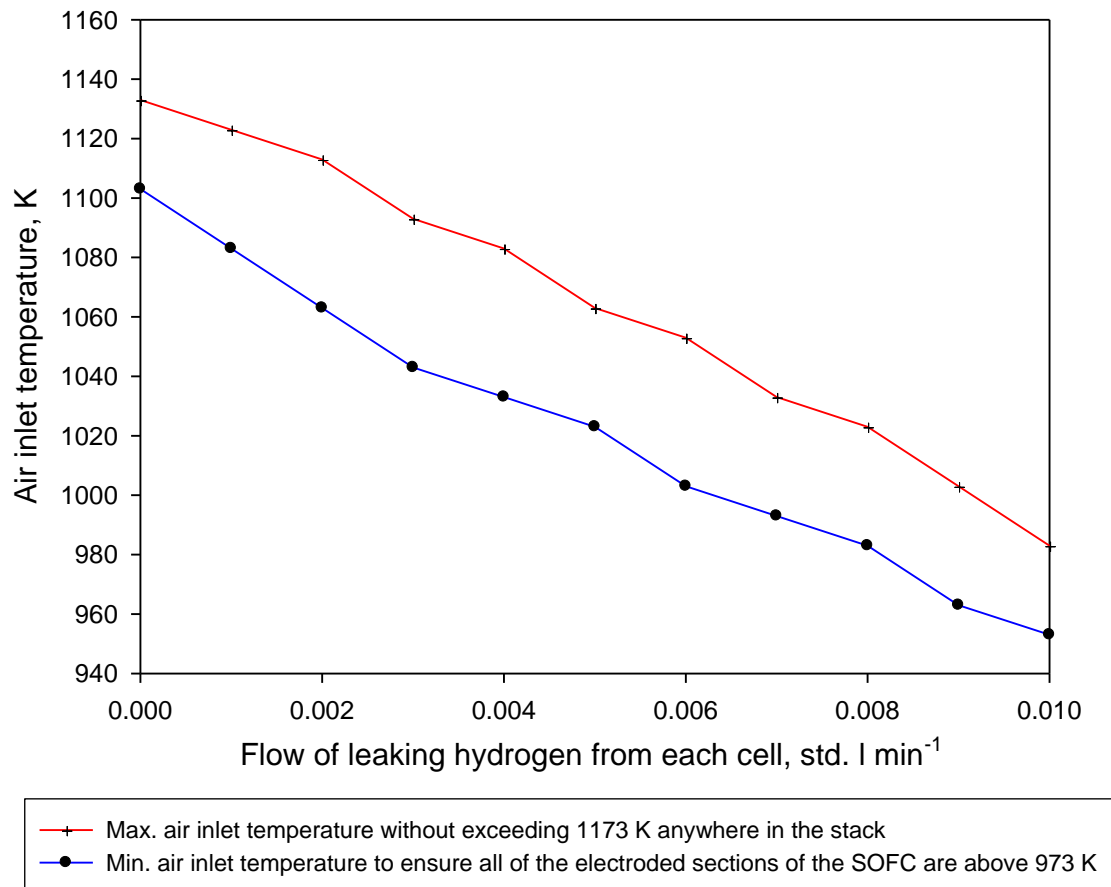


Fig. 7.10 Graph to show inlet temperatures that will produce stack temperatures between 973 K and 1173 K with different amount of leaking fuel

The redline in Fig. 7.10 shows by reducing the air inlet temperature, the SOFC stack could be maintained at a suitable temperature when heat is generated in the stack by electrochemical reaction and combustion of up to 0.01 std. l min⁻¹ leaking Hydrogen from each cell.

7.3 Simulation of leakage of fuel from one damaged cell

7.3.1 Objectives

In section 7.2 it was shown that a small amount of fuel leakage could be tolerated from each SOFC in a stack. Based on this a SOFC stack could be 'designed to leak', provided

the leakage was less than $0.008 \text{ std. l min}^{-1}$ per cell. Even if this controlled leakage at the inlet was eliminated altogether, the operation of the stack could still be threatened by uncontrolled leaks caused by damage to one or more of the cells. It was thought that heat generated by combustion of a broken cell led to the forced termination of the experiments reported in Chapter 6, so this is clearly a key issue. Therefore, the next stage in the investigation was to investigate how uncontrolled leaks, caused by damage to one or more of the SOFCs, would affect the temperature profile in a micro-tubular stack. A key question to be addressed was whether a crack in one of the cells would force the stack to shut down or if the stack could continue to operate with one broken cell.

7.3.2 Methods and Boundary conditions

As with the simulations performed in section 7.2 the combustion of leaking fuel was represented by a constant energy source specified in the wall of one of the SOFCs with the magnitude based on a certain flow rate of fuel undergoing complete combustion. Based on practical experience the most common place for a cell to break was at the inlet end where the steel injector tube entered the cell, so the combustion of leaking fuel was assumed to occur in the first 10 mm of the SOFC. The magnitude of the energy source was increased to represent the combustion of 0.005 to $0.05 \text{ std. l min}^{-1}$ of Hydrogen. Although the nominal gas flow to each cell was only $0.025 \text{ std. l min}^{-1}$ under normal operation, if a cell was to break it was anticipated that the portion of the fuel directed to this cell could increase significantly.

7.3.3 Simulation of leakage from a single cell with the SOFC stack at open circuit

The first case of leakage from a single cell to be simulated was with the rest of the stack at open circuit, such that the heat generated by combustion of the leaking fuel was the

only heat source inside the fuel cell chamber. In these simulations the air flow was specified as 10 std. l min⁻¹ preheated to 1073 K. The simulations were run to simulate the heat generation by increasing flows of fuel from FC02, then from FC14. The predicted stack temperature with increasing flows of leaking fuel from FC02 and then FC14 are shown in Fig. 7.11 and Fig. 7.12 respectively.

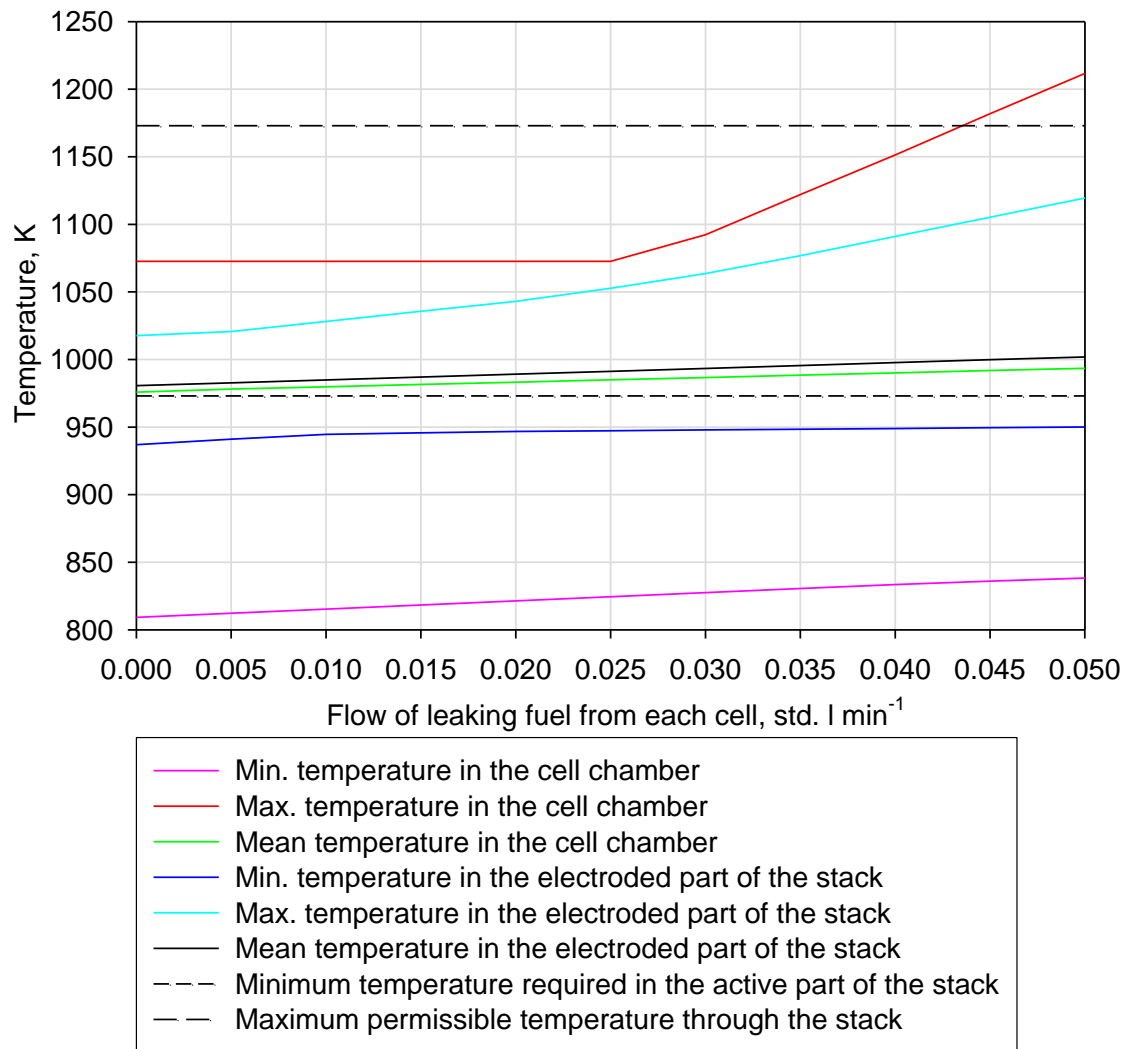


Fig. 7.11 Graph showing effect of increasing fuel leakage from FC02 on stack temperature

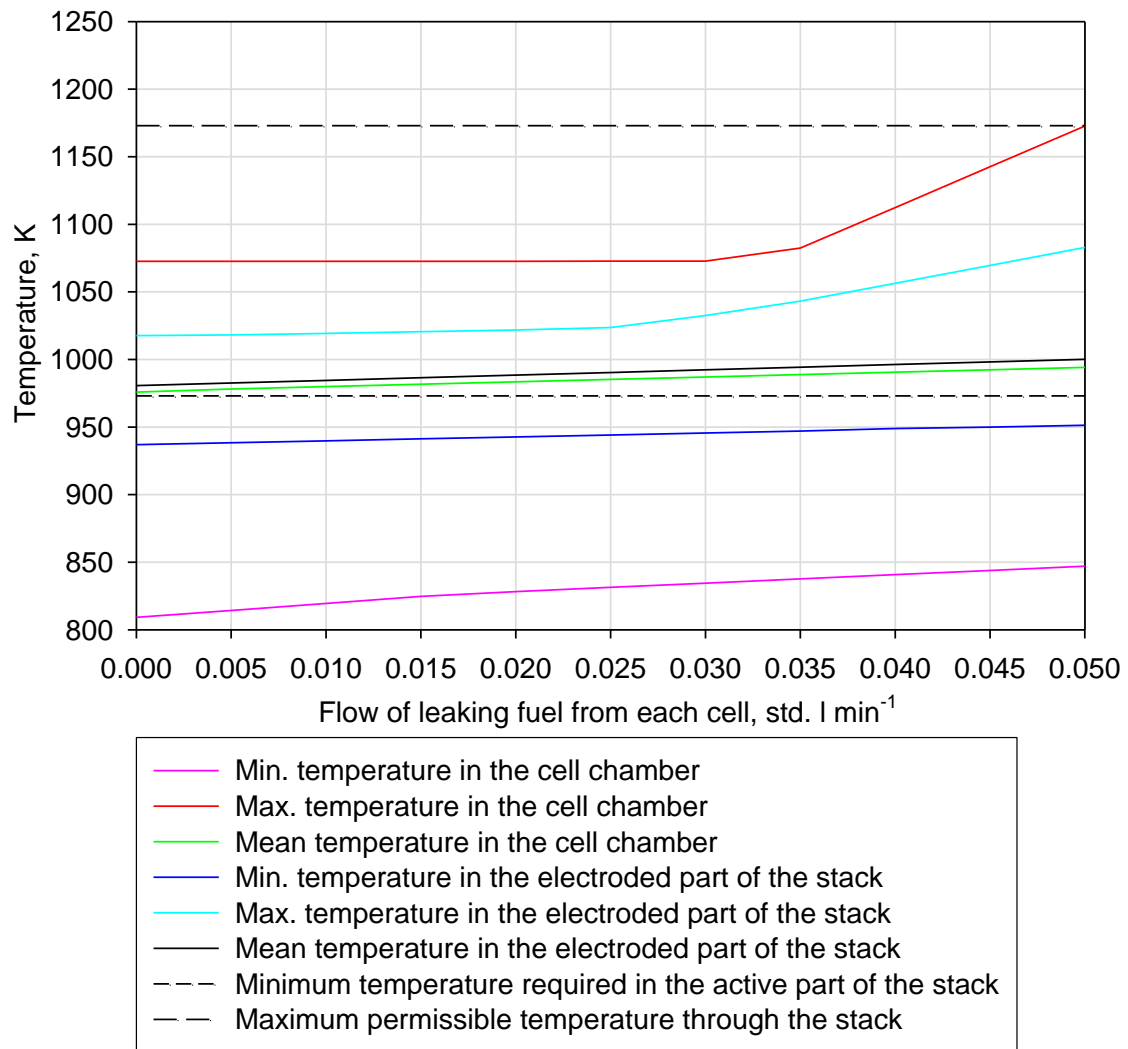


Fig. 7.12 Graph showing effect of increasing fuel leakage from FC14 on stack temperature

It can be seen that the temperature rise for a given flow of leaking fuel was higher when the leak occurred in FC02 rather than FC14. This difference arises because FC02 is positioned in the bottom row of cells where the temperature of the air flowing over the cells is highest so the addition of heat from combustion of a leak here causes the maximum temperature to be slightly higher than if there is a leak from one of the cells in the top row. However, the maximum temperature rise in the stack varied by a maximum

of 50 K depending upon the SOFC where the leak occurred and was between 1170 K and 1220 K if 0.050 std. l min⁻¹ leaked from any one of the cells. The results shown in Fig. 7.11 and 7.12 also indicate that whilst the fuel leaking from a single cell causes the maximum temperature to rise sharply, the mean temperature rise is more modest, increasing by only 20 K if the Hydrogen leak increases from none to 0.05 std. l min⁻¹. This arises because the increase in temperature is mainly restricted to the region where the leak is assumed to occur and along the length of the affected cell. The temperature contours plots shown in Fig. 7.13 illustrate the local nature of the increase in temperature.

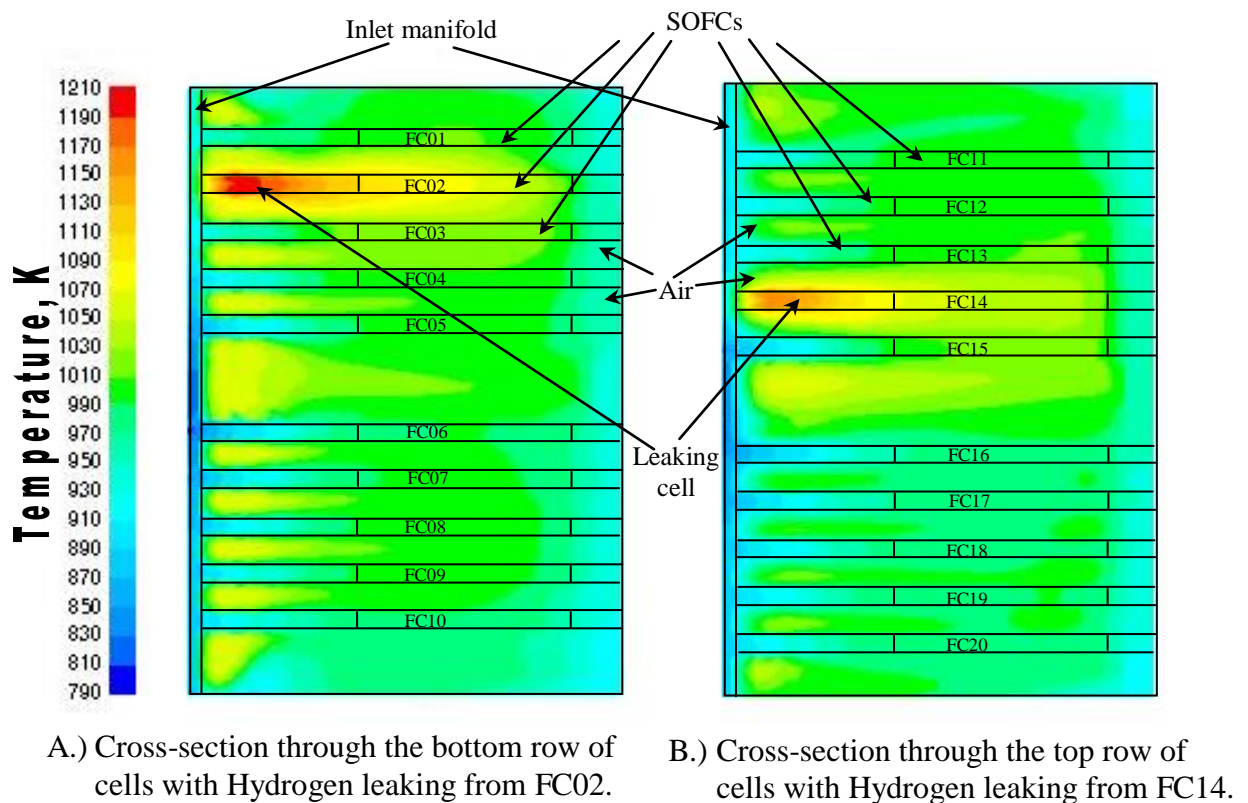


Fig. 7.13 Plots showing temperature contours with 0.050 std. l min⁻¹ from individual cells with 10 std. l min⁻¹ of air preheated to 1073 K

Fig 7.13 A shows the temperatures predicted on a horizontal plane through the axis of the SOFCs on the bottom row of the 20 cell stack if 0.05 std. l min⁻¹ of Hydrogen leaks from

cell FC02. Fig 7.13 B shows the predicted temperature distribution on a horizontal plane through the top row of cells if the same flow of fuel leaked from FC14.

From these results it is predicted that the stack would survive provided that the flow of leaking Hydrogen was less than $0.04 \text{ std. l min}^{-1}$. This shows another advantage of micro-tubular stacks over planar cells. A crack in one of the micro-tubular cells would require the stack to be shut down, but the damaged cell could be replaced with relatively little expense, whereas the thermal stress caused by a small leak would be likely to cause more extensive damage to a planar stack.

7.3.4 Simulation of leakage from a single cell with the rest of the SOFCs loaded

The next situation to be simulated was fuel leaking from a single cell whilst the other cells were producing electrical power and heat. It was assumed that the leaking cell would not produce electrical power but all of the other cells produced power and heat as normally. The results for increasing rates of fuel leakage from FC02, with the other SOFCs each producing 0.5 W of heat are shown in Fig. 7.14

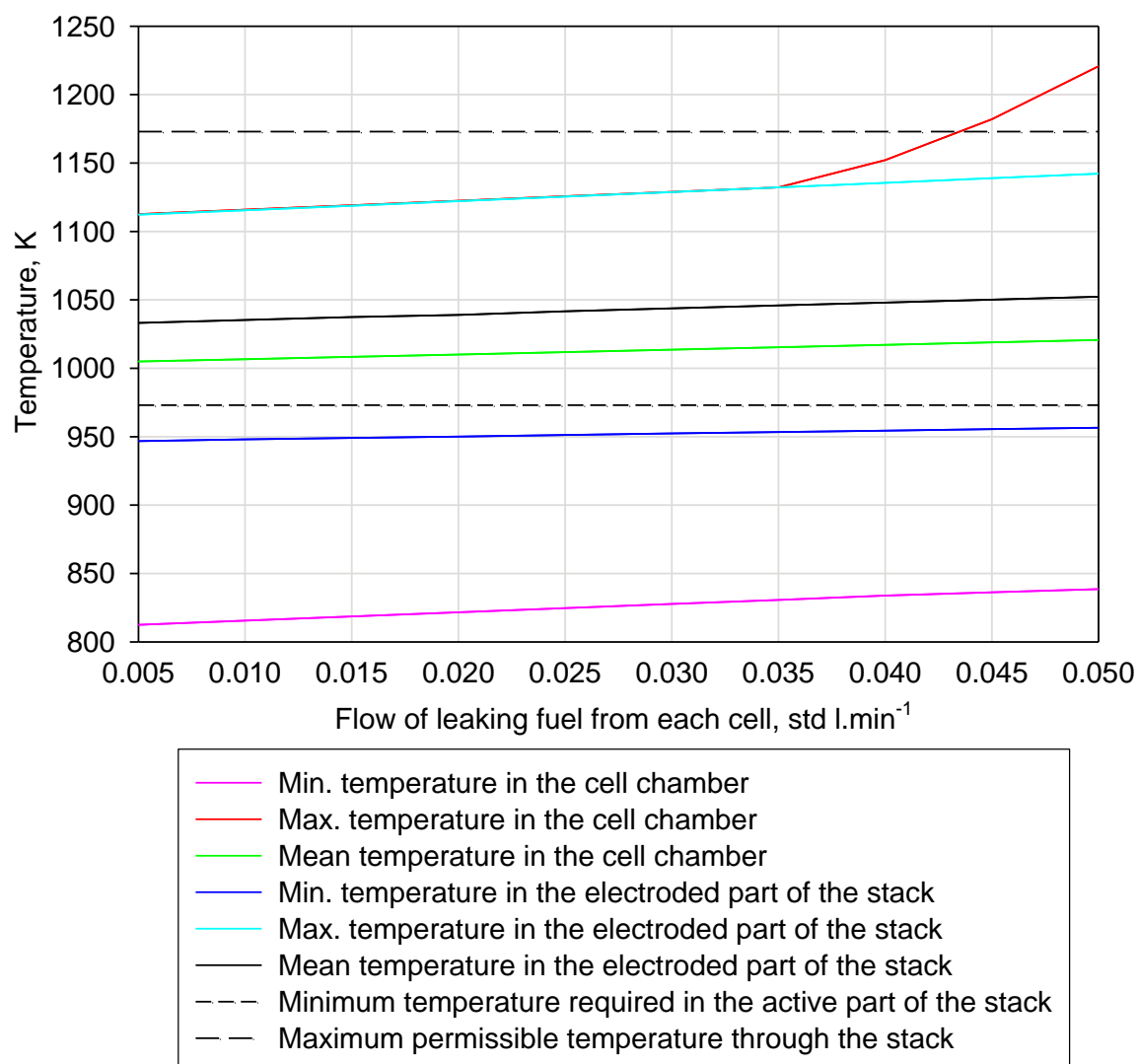


Fig. 7.14 Graph showing effect of increasing fuel leakage from FC02 on stack temperature with the rest of the stack fully loaded

From the results plotted in Fig. 7.14 it can be seen that with less than 0.035 std. l min⁻¹ of Hydrogen leaking from FC02 the hottest part of the stack is in the electroded section of the cells. This is apparent from the fact that the maximum temperature in the stack as whole, and the maximum temperature in the active part of the stack only, are the same. Once the rate of combustion of leaking fuel increases to beyond 0.035 std. l min⁻¹ the temperature at the inlet end of the cell rises more sharply. Therefore it was concluded that

the SOFC stack may be able to continue to operate with one cell that was cracked, provided that crack did not cause the flow of Hydrogen to that cell to increase significantly beyond the nominal operating flow of 0.025 std. l min⁻¹.

7.4 Conclusion

In this Chapter the effect of leaks on the temperature profile through a micro-tubular stack were investigated using a CFD model. This is the first time that work has been published on the issue of leaks in micro-tubular stacks.

The model was first used to simulate the effects of an even rate of fuel leakage from all of the cells. It was shown that if the stack was supplied with 10 std. l min⁻¹ of air heated to 1073 K, just 0.008 std. l min⁻¹ of Hydrogen leaking from each cell would generate temperature exceeding the 1173 K limit applied of the silver interconnects.

Strategies for dealing with the effects of fuel leakage were investigated using the CFD model. It was found that reducing the energy supplied to preheat the air was a more feasible method of temperature control than increasing the air flow. However, if the stack was at open circuit and supplied with 10 std. l min⁻¹ of air, suitable stack temperatures could not be maintained if the rate of Hydrogen leakage exceeded 0.01 std. l min⁻¹.

The techniques used in this Chapter to model the 20 cell stack were then applied to the simulation of a 100-cell micro-tubular SOFC stack, which is reported in Chapter 8.

8. Simulation of leaks in a 100-cell micro-tubular SOFC stack

8.1 Introduction

Whilst the 20 cell system studied in the previous Chapters was useful to analyse some of the issues associated with stack design and the development of a modelling approach, the applications for an SOFC stack producing only 10 W of power are limited. Therefore, in this Chapter the issue of scale up is investigated. This is an issue that has been given little attention in previous work on micro-tubular stacks, and yet it poses serious questions about the stack design; such as, how can an even temperature distribution be maintained through the increased volume of the stack?

To examine this issue the 20 cell design was scaled up to include 100 cells and was simulated using the same modelling approach as described in Chapters 4-6 to predict the temperature distribution.

8.2 Geometry

The first stage was to create the geometry for the model. Attempts were made to follow the design of the 20 cell system as closely as possible so that the effect of scale up could be studied without the influence of other major geometric changes.

8.2.1 Stack configuration

The same cell spacing was used as in the 20-cell system with the SOFCs aligned in rows of ten with 6 mm between the axis of neighbouring cells. However, rather than constructing the geometry and mesh for a complete 100 cell stack, the system was split into two symmetric halves. Symmetry boundary conditions were imposed on all of the faces that were created on the vertical plane that was used to split the stack in two. The cross section through the geometry is shown in Fig. 8.1 to show the cell spacing.

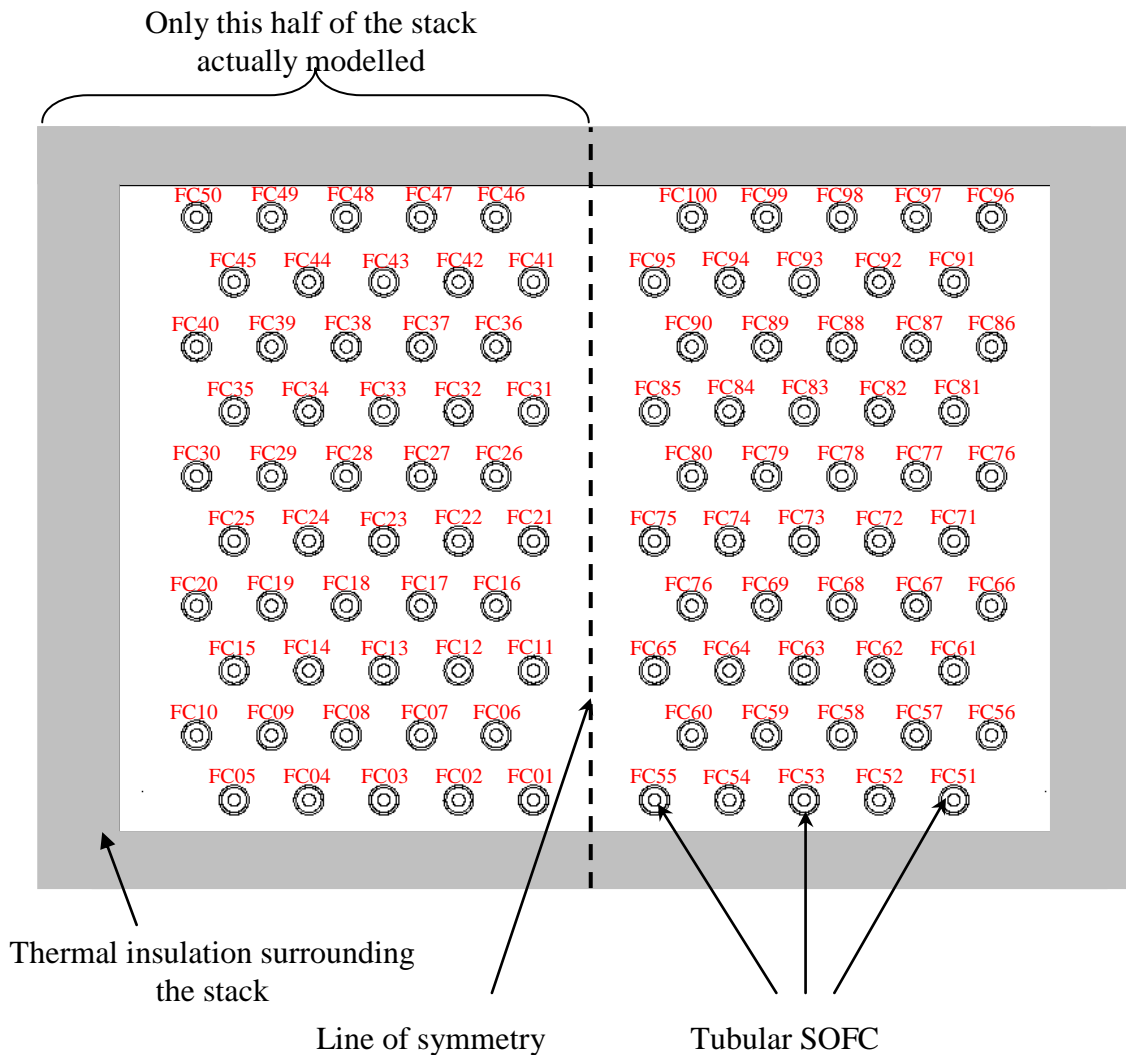


Fig. 8.1 Diagram showing cell spacing

Although the geometry was only created for cells FC01 to FC50, they were modelled as though they were part of a 100-cell stack, with the conditions in the right hand half of the stack mirroring those in the left hand side. For example, using the symmetry boundary condition it was assumed that the temperature and flow through FC51 is identical to through FC05.

A novel aspect of the modelling in this thesis is that the details of the manifold supplying the cells with fuel were included in the simulation. This is because it was believed that the heat transfer through them would significantly affect the temperature profile for a small

SOFC system. The features of the steel fuel inlet manifold and ceramic outlet manifold were retained from the 20-cell model but enlarged to accommodate the extra cells. A diagram of the half of the stack created in the FLUENT pre-processing software, Gambit, is shown in Fig. 8.2.

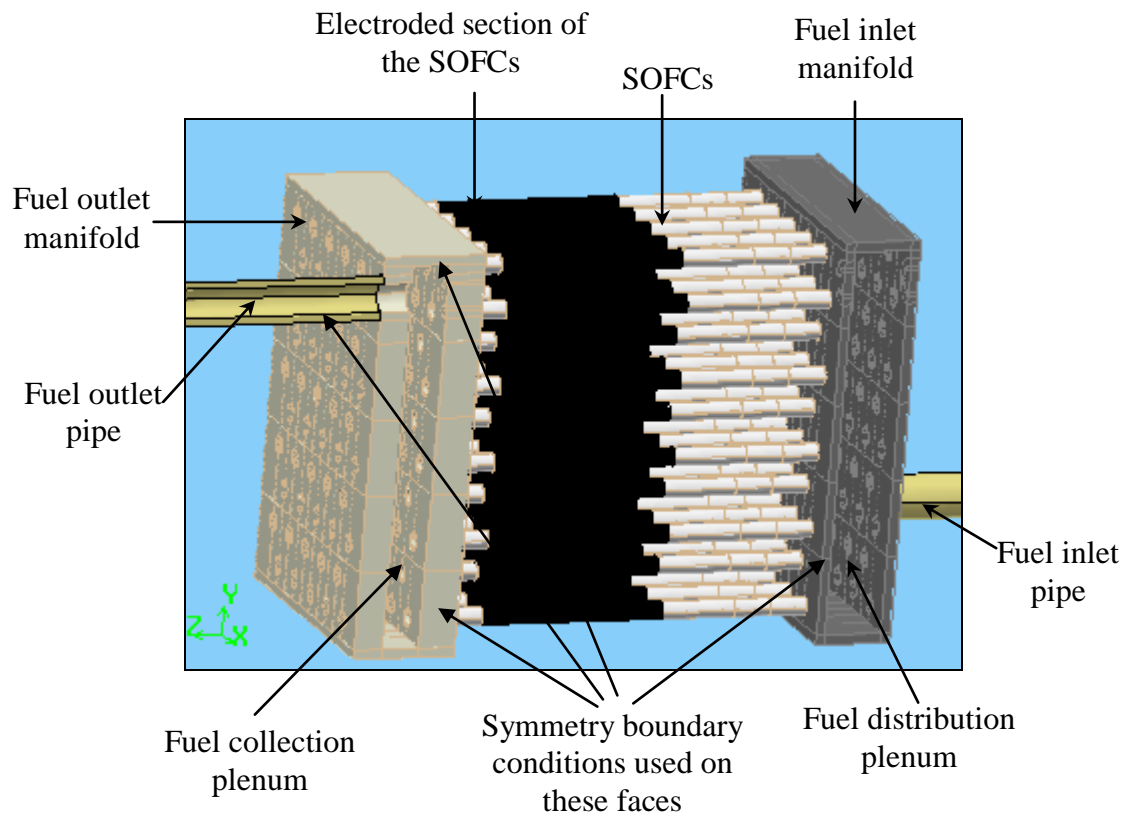


Fig. 8.2 Diagram showing the half of the stack to be simulated

Fuel was introduced through a pipe in the bottom corner of the stack to a plenum in the fuel inlet manifold, so the system was modelled with two fuel inlet pipes with one in each half of the stack. The system of steel injector tubes was again deployed to deliver fuel from the plenum to each of the cells. At the outlet end of the cells the fuel was collected in a Macor ceramic manifold and left the system through a single ceramic pipe. This pipe was bisected by the line of symmetry so only half of the pipe was constructed with symmetry boundary condition imposed on the vertical faces. All of this was then surrounded by 50 mm of thermal insulation.

8.2.2 Air Flow configuration

Air was introduced to the stack through a 5 mm wide channel spanning the width of the stack, cutting through the thermal insulation. Two air flow configurations were tested. The first case to be simulated was with the air introduced at the bottom of the stack, close to the fuel inlet manifold, and leaving through a channel at the top of the stack next to the fuel outlet manifold. This configuration was similar to that used in both the 20 cell simulation and experiments and has been represented by a schematic in Fig. 8.3. This was as close to a co-current flow arrangement as could be achieved without increasing the complexity of the system by constructing an air distributor and collector in front of the fuel inlet and outlet manifolds.

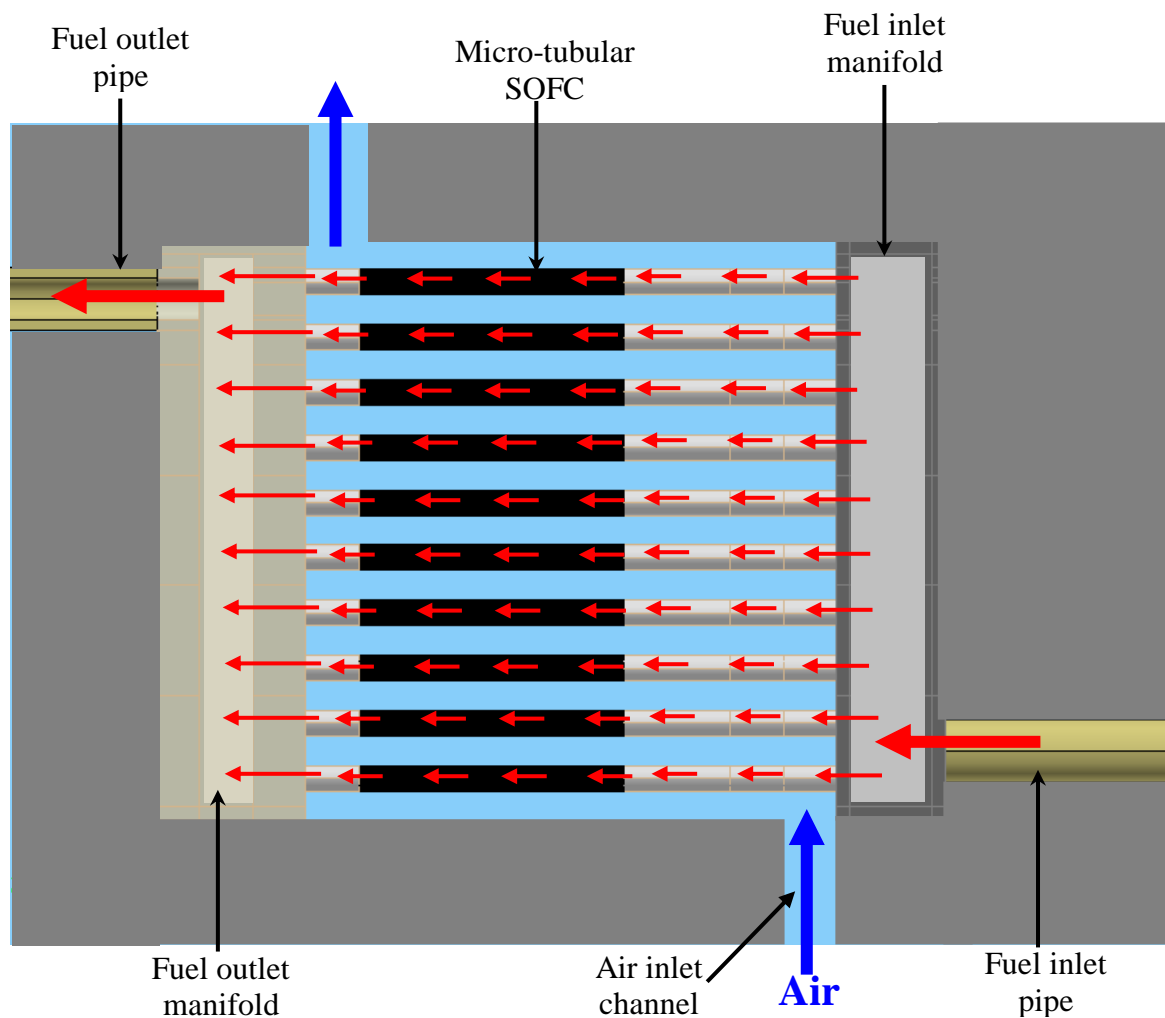


Fig. 8.3 Schematic to show 'co-current' air flow configuration

In the second configuration the air was again introduced at the bottom of the stack but this time at the outlet end of the SOFCs. The air outlet was in turn moved towards the fuel inlet manifold so that the air flow direction was counter-current to the fuel flow. This system has been depicted in Fig. 8.4.

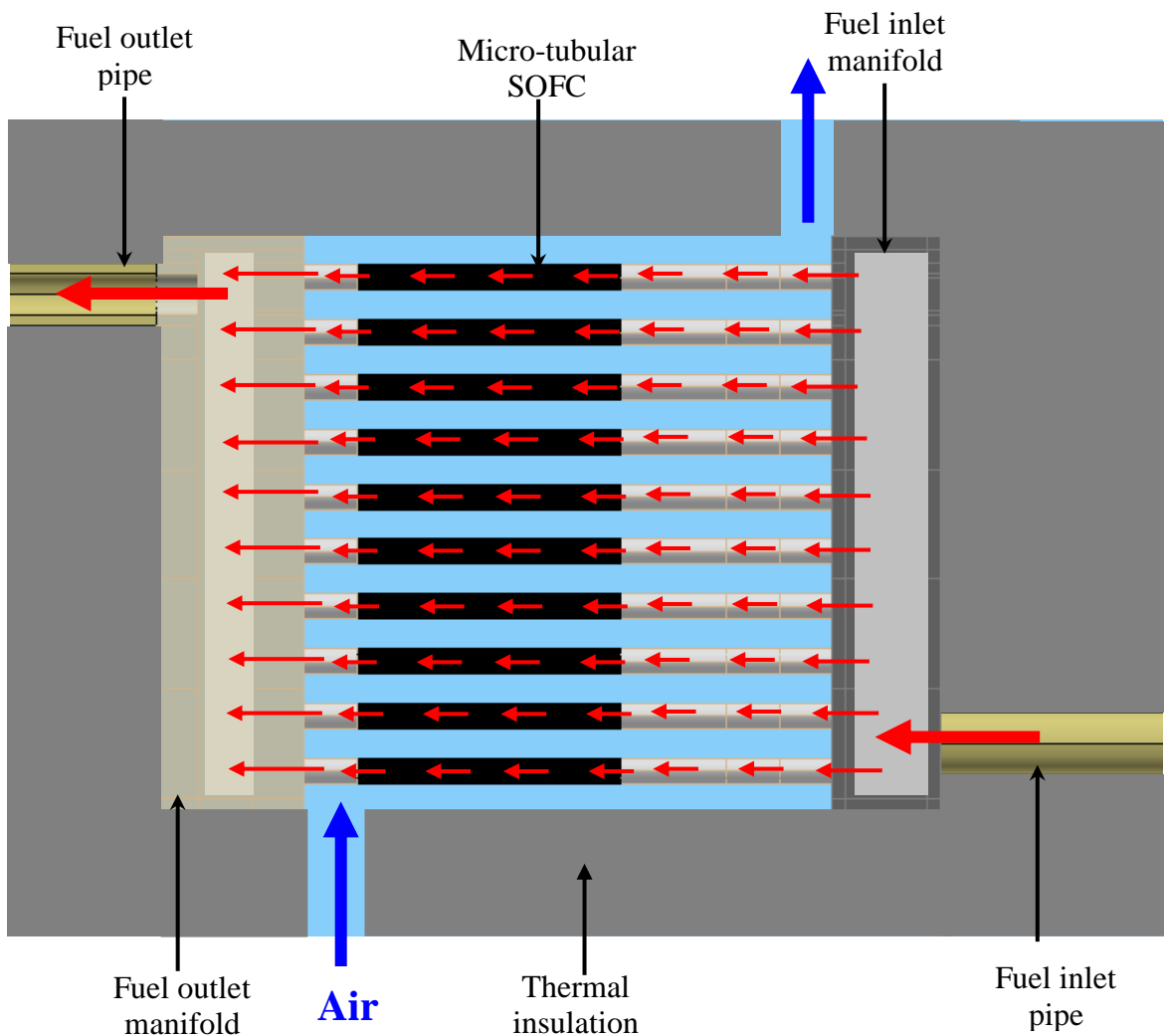


Fig. 8.4 Schematic to show the 'counter-current' air flow configuration

8.3 The mesh

The domains representing the fuel cells and air chamber were subdivided in the same way as for the 20-cell model to enable a structured hexahedral mesh to be constructed. Where

possible the mesh spacing was also kept the same as in the 20 cell model which meant the mesh comprised of a total of 2782494 elements.

8.4 Boundary conditions

Apart from the introduction of symmetry conditions through the centre of the stack material properties and boundary conditions were unchanged from the 20 cell model and have been described in detail in Chapter 4. Hydrogen was specified as the fuel at a flow of 0.025 std. l min⁻¹ per cell, corresponding to a total mass flow rate of 1.7×10^{-6} kg s⁻¹ to the modelled half of the stack. Ideal gas behaviour was assumed.

The generation of heat due to resistance losses in the fuel cells was again specified as 0.5 W per cell and this was dissipated evenly through the section of the tubular cells to which the electrodes are applied. The inlet temperature of the air was specified at the entrance of the air inlet channel, and the walls of the inlet channel were set as adiabatic so that the air entered the chamber housing the stack at the specified temperature.

8.5 Running of the simulations

The simulation was initially run with the energy balance switched off so that the simulation could converge on a stable velocity distribution without the influence of the energy balance. Convergence was achieved within 800 iterations, taking approximately 10 seconds per iteration. The energy equation was then switched on, which increased the time taken to perform each iteration to over 2 minutes, but only a further 50 iterations were required for the solution to re-converge. Once the stable solution had been obtained the maximum temperature through the stack was observed to check that it did not exceed the limit of 1173 K. The air inlet temperature was then adjusted and the simulation run again until the maximum air inlet temperature that did not cause the stack temperature to exceed 1173 K was found.

8.6 Effect of air flow and the stack temperature

8.6.1 Co-current flow with 20 std. l min⁻¹ of air

The first case to be simulated was with the co-current flow arrangement and with a total air flow to the stack of 20 std. l min⁻¹ pre-heated to 1123 K. Under these conditions the model predicted that the maximum temperature would reach 1338 K around the bottom row of cells. This would be unacceptable as it would lead to damage of the silver interconnects. It was found that the air temperature would need to be reduced to 936 K before the maximum temperature in the stack would fall below 1173 K. The predicted temperature contours through cell FC06 are shown in Fig. 8.5 for these conditions.

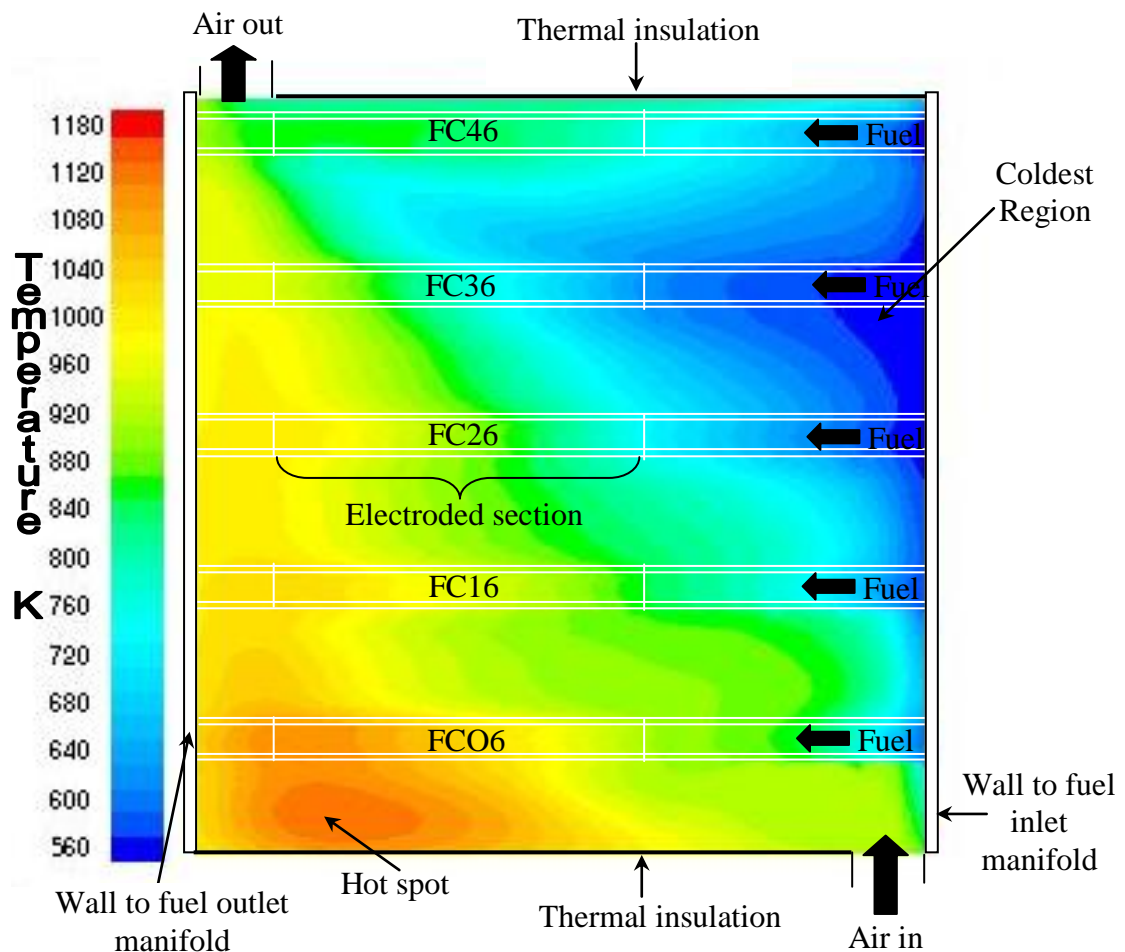


Fig. 8.5 Temperature contours on a vertical plane through FC06 with 20 std. l min⁻¹ of air preheated to 936 K

The temperature ranged from 563 K to 1173 K within the hot spot, which restricted the inlet temperature, created towards the outlet end of the cells on the bottom row of the stack. In this region there is only a weak flow of air to absorb the heat produced in the active part of the cells, as shown in the plot of the velocity vector in Fig. 8.6. The problem is compounded by the fact that the temperature of fuel flowing into the active part of the cell will already have been greatly increased by heat exchange with the hot air close to where it is introduced to the stack.

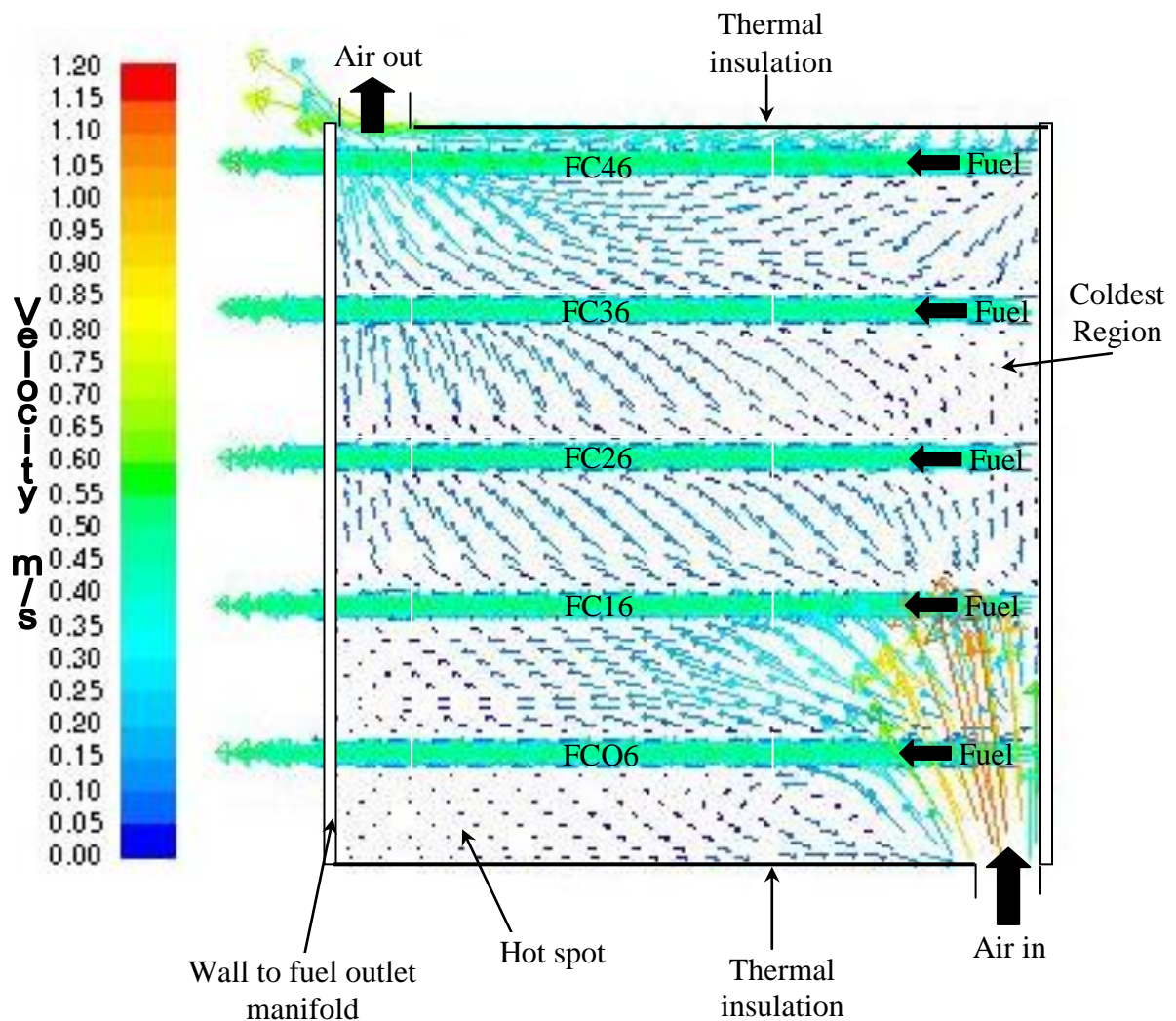


Fig. 8.6 Velocity vectors on a vertical plane through FC06 with 20 std. l min⁻¹ of air

From the simulations it was predicted that the coldest region would occur around the inlet end of the cells in the top half of the stack where the fuel enters without having been

preheated and the flow of air for heat exchange is low. This problem is heightened by the fact the air which does flow through this region has already been cooled by passing over the colder parts of the cells in the lower half of the stack.

For the cells to produce a significant amount of power, the temperature in the active part of each cell is required to at least be in excess of 1023 K. All of the cells in the top half of the stack were well below that temperature. Therefore the simulation results indicate that these operating conditions are not acceptable.

8.6.2 Co-current flow with 100 std. l min⁻¹ of air

To investigate if a more even temperature distribution could be achieved by increasing the air flow rate, the simulation was run again with the mass flow rate specified at the air inlet boundary increased to $9.9 \times 10^{-4} \text{ kg s}^{-1}$ corresponding to 50 std. l min⁻¹. This would represent a flow of 100 std. l min⁻¹ for the complete 100 cell stack and a somewhat high relative air/fuel ratio of 16.8 : 1. The maximum inlet temperature that could be used with this configuration was found to be 1008 K. The temperature contours predicted through cell FC06 under these conditions are shown in Fig.8.7.

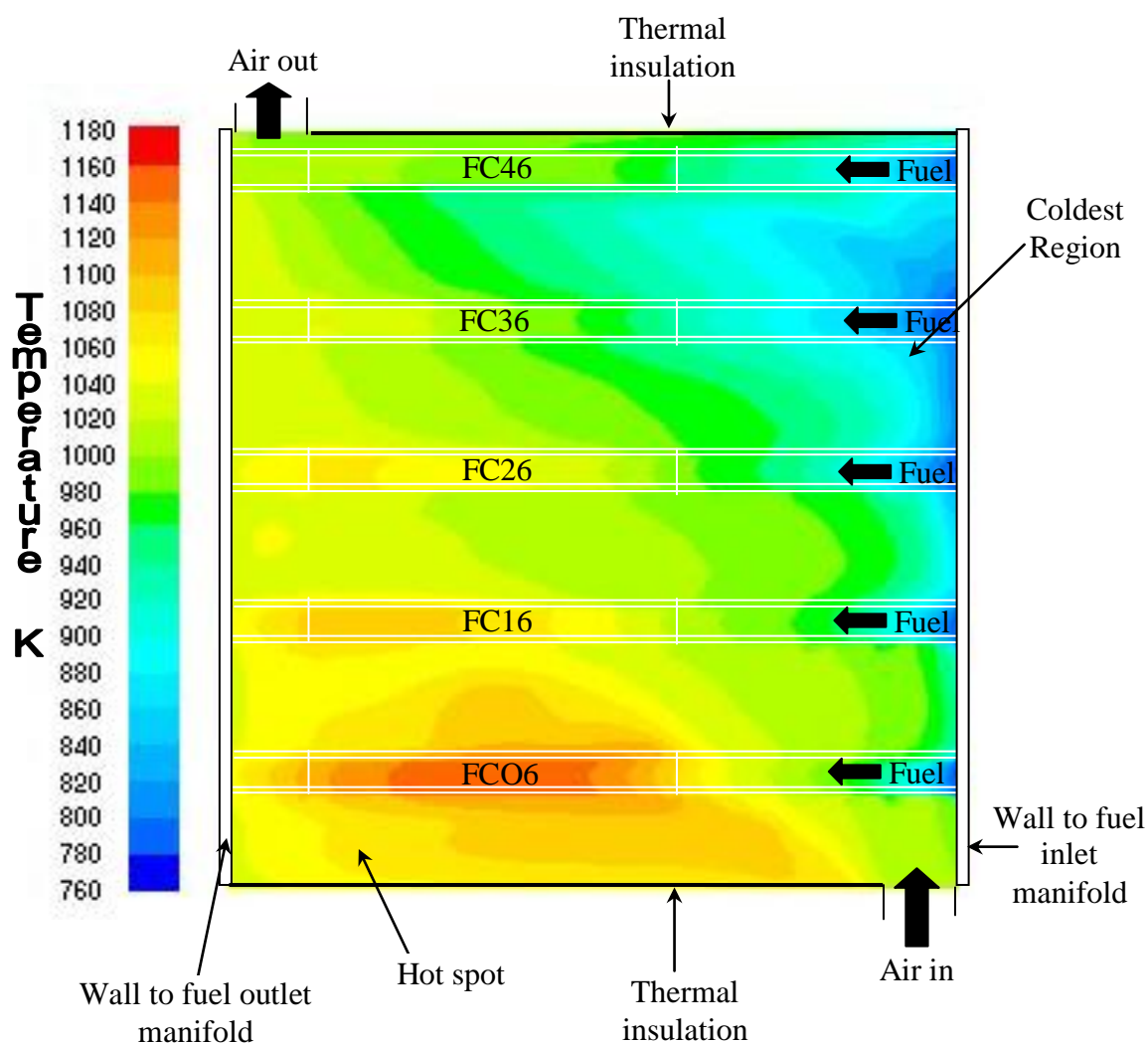


Fig. 8.7 Predicted temperature contours on a vertical plane through FC06 with 100 std. l min⁻¹ of air introduced at 1008 K

The temperature range between the coldest and hottest parts of the stack was predicted to be 771 to 1173 K, a difference of 402 K compared to 610 K when the air flow was only 20 std. l min⁻¹ of air. The increased flow of air meant the heat released by the electrochemical reactions caused a less significant temperature increase which meant a higher air inlet temperature could be used, which in turn helped to increase the minimum temperature in the stack.

The velocity contours plotted in Fig. 8.8 also show the increased flow caused increased recirculation in the bottom part of the stack which would have also contributed to a more even temperature distribution in the lower part of the stack.

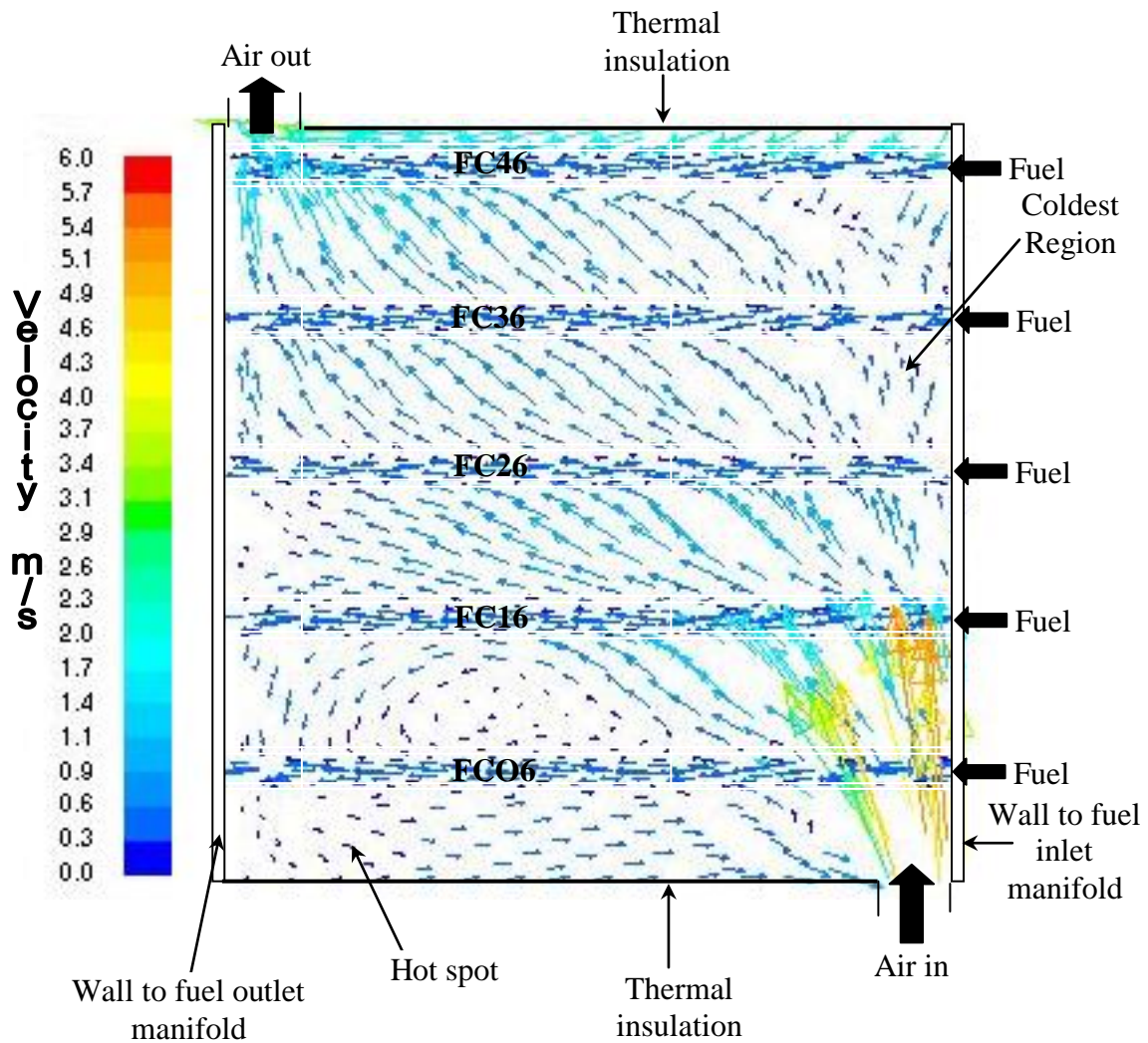


Fig. 8.8 Velocity vectors on a vertical plane through FC06 with 100 std. l min⁻¹ of air

Despite these improvements brought about by the increased air flow the predicted temperature is only just above the desired 1023 K through the electroded section of FC36 and is below that temperature on the top row of cells.

8.6.3 Counter-current flow with 20 std. l min⁻¹ of air

With the inlet and outlet moved so that the air flow was in the opposite direction to the fuel flow there was a clear change in the temperature distribution. The hottest part of the stack shifted from the bottom of the stack to the top as shown in Fig. 8.9.

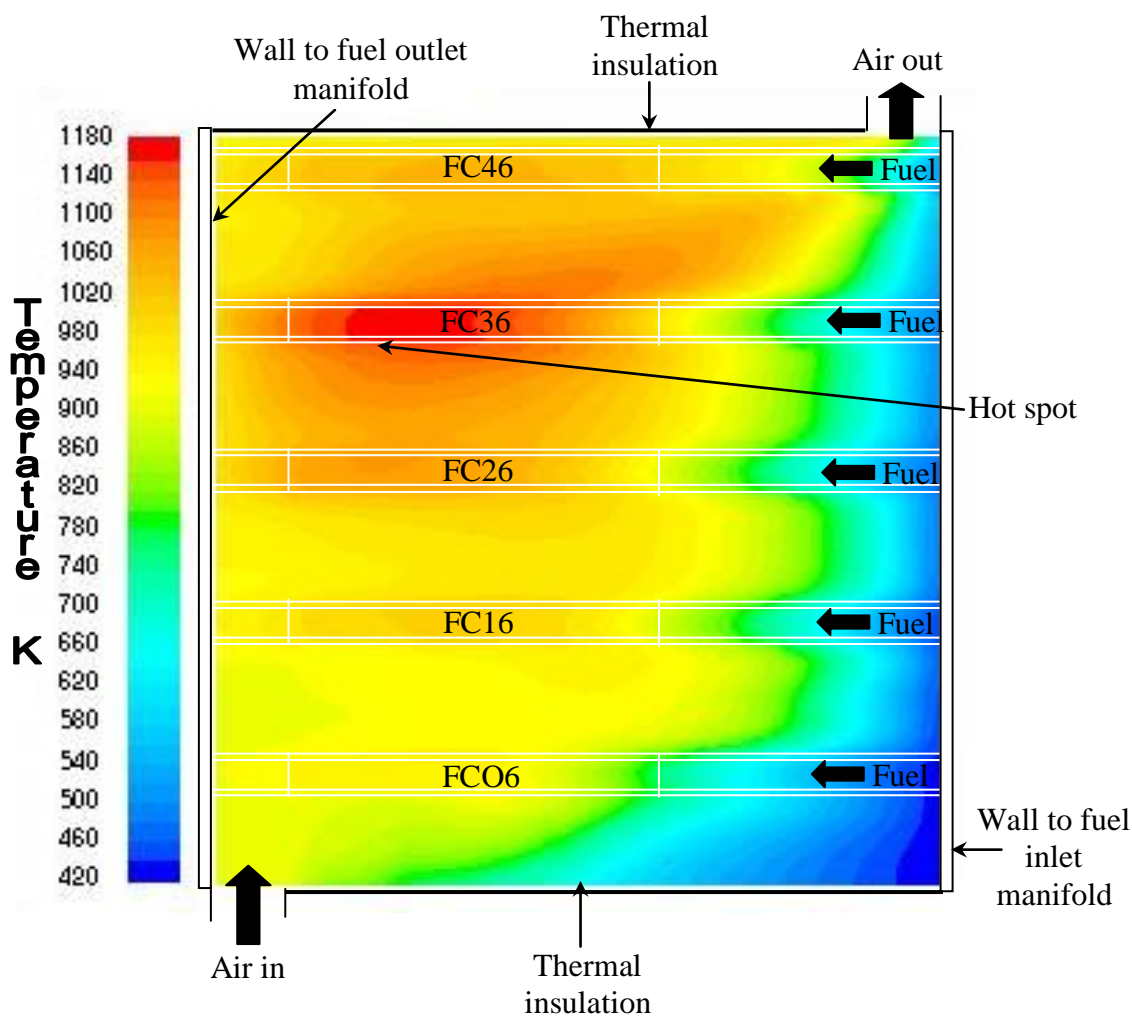


Fig. 8.9 Temperature contours on a vertical plane through FC06 with 20 std. l min⁻¹ of air preheated to 913 K

The temperature range in the stack, from 426 K to 1173 K, was the largest produced by the four sets of conditions to be tested. This was because the air inlet temperature had to be lowered to 913 K to prevent the temperature at the hot spot exceeding 1173 K.

However, the active parts of the cells were above 900 K, an improvement on the temperature distribution produced with the same air flow rate in the co-flow configuration.

The hot spot in the plane shown in Fig. 8.9 occurs towards the end of the active section of FC36. There are two reasons for this: firstly fuel entering the active part of the stack is warmer than in the cells lower down the stack due to heat exchange with the strong flow of air toward the inlet end of the cell; secondly the air flow around the hot spot is weak, as shown by Fig. 8.10 so there is less air to absorb the heat produced by the electrochemical processes.

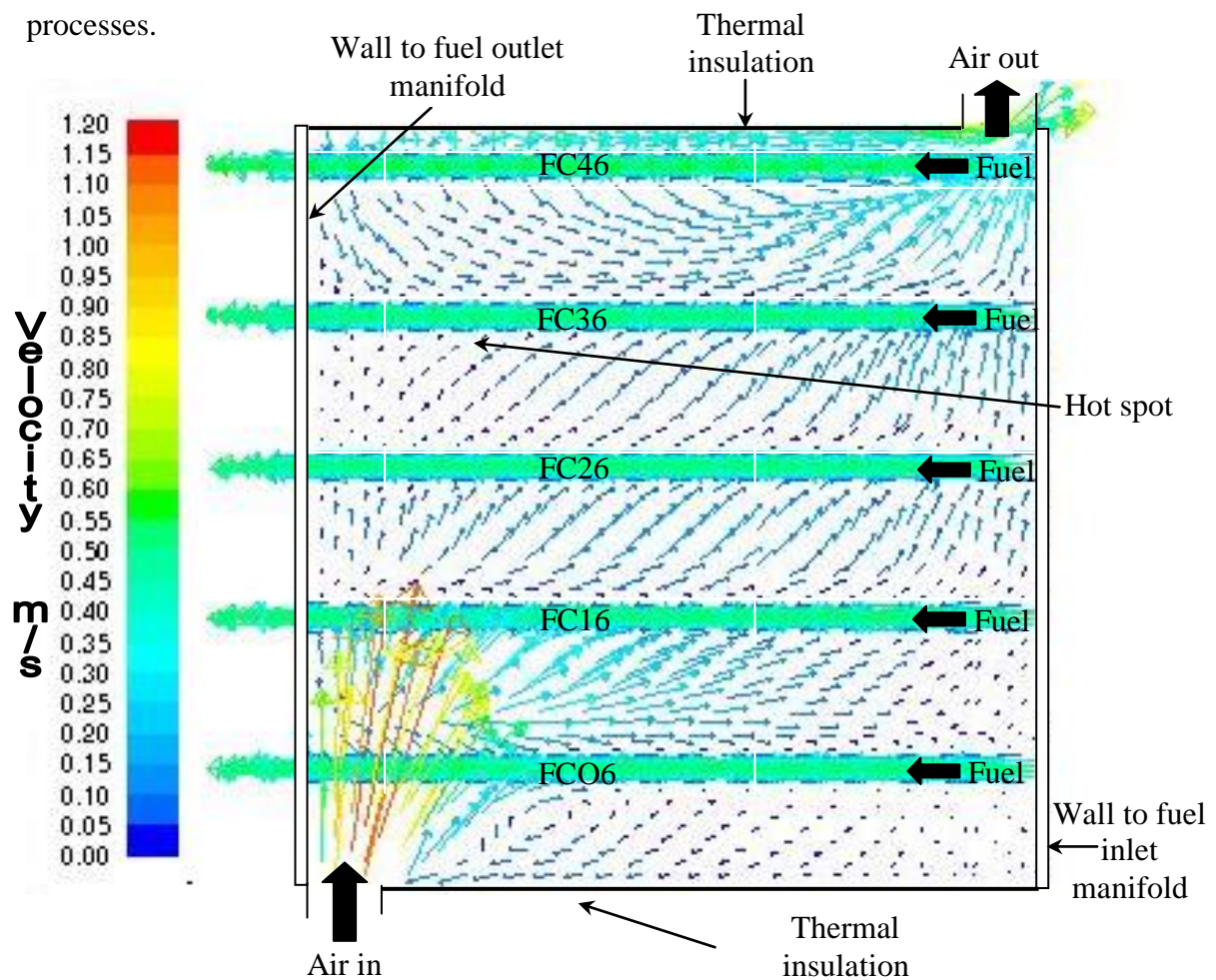


Fig. 8.10 Velocity vectors on a vertical plane through FC06 with 20 std. l min⁻¹ of air

8.6.4 Counter-current flow with 100 std. l min⁻¹ of air

As a final comparison the counter current configuration was also simulated with a flow rate of 100 std. l min⁻¹ of air. The predicted temperature contours through FC06 are shown in Fig. 8.11.

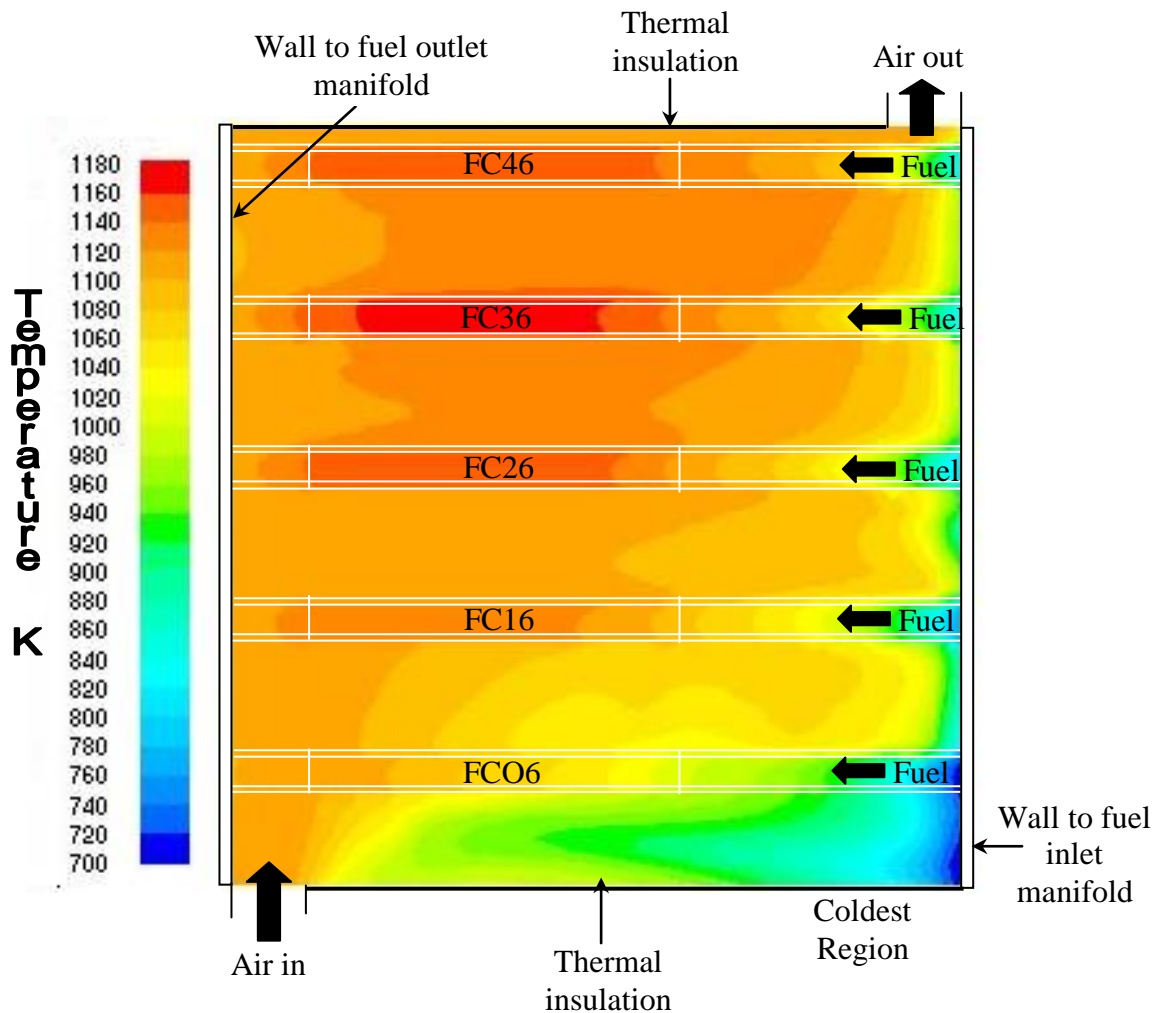


Fig. 8.11 Temperature contours on a vertical plane through FC06 with 100 std.l min⁻¹ of air preheated to 1108K

The temperature distribution is much more even than predicted for the co-flow configuration with the same flow rate of air. On the 4th, 6th, 8th, and 10th rows of cells the predicted temperature through the active part of the each of the cells is between 1100 K

and 1173 K which would be optimal for the maximum power output from the micro-tubular SOFCs. The only drawback to these operating conditions is the increased energy requirement to pump the high flow rate of air and raise its temperature to 1108 K.

Only the bottom two rows of cells experienced temperature below the ideal for maximum power output. Therefore it might be possible to improve the temperature distribution if the pre-heat channel ran horizontally rather than vertically and was separated from the stack chamber by a thin layer of insulation as shown in Fig. 8.12:

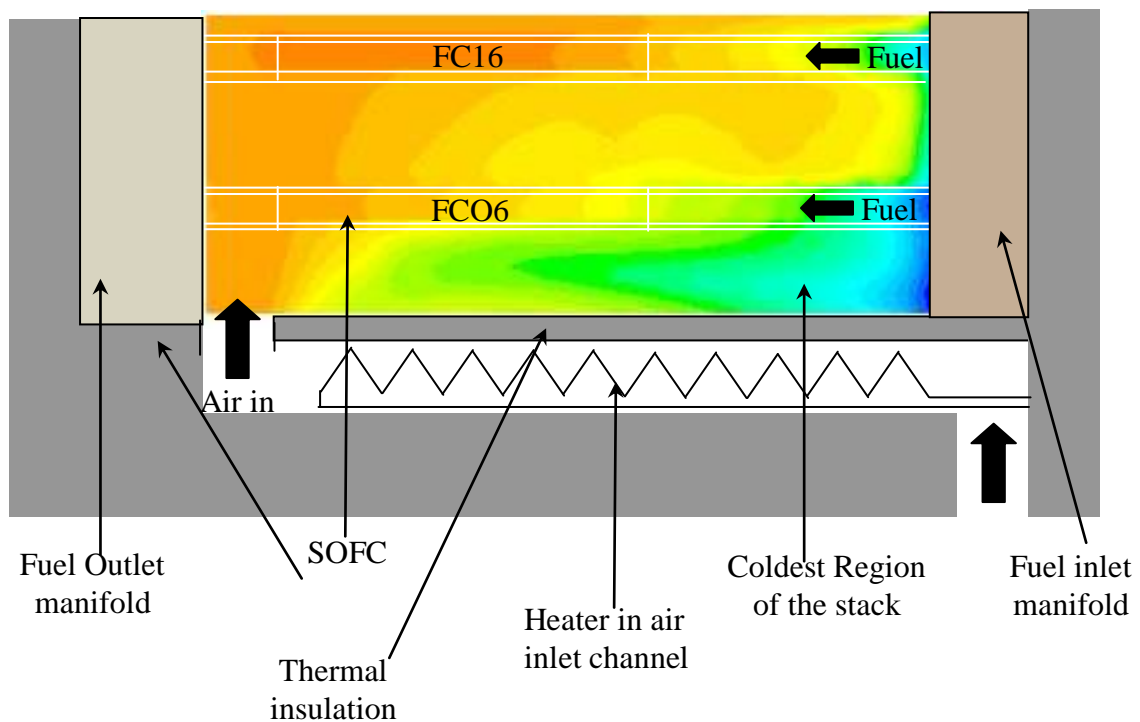


Fig. 8.12 Potential re-design to reduce temperature gradient

8.6.5 Summary of effects of air flow rate

Although $20 \text{ std. l min}^{-1}$ represents a relative air/fuel ratio of 3.36, which is higher than values normally quoted for SOFC operation of around 2^[131], the temperature gradients produced with this air flow rate in both the co- and counter-current configurations would prevent the stack from achieving maximum power.

$$\text{Relative air/fuel ratio, } \lambda = \frac{(\dot{v}_{\text{fuel}}/\dot{v}_{\text{air}})_{\text{stoichiometric}}}{(\dot{v}_{\text{fuel}}/\dot{v}_{\text{air}})_{\text{actual}}} = \frac{(2.5/5.95)}{(2.5/20)} = 3.36$$

If a lower flow of air is to be used with a stack of this size the flow of air through the stack needs to be more carefully orchestrated either by the addition of carefully positioned baffles or the use of an air distributor and/or collector. The model could be used to assist with the design and placement of these items.

Even when the air flow rate was increased to 100 std. l min⁻¹ the predicted temperature gradients with the co flow configuration were not acceptable as the hot spot prevented the temperature of the air entering the stack from being increased whilst areas of the stack were at temperatures well below those suitable for maximum power output.

Of the operating conditions simulated, the counter-current configuration with 100 std. l min⁻¹ of air produced by far the most satisfactory stack temperatures. Even at low flow rates the counter-current flow configuration still produced more suitable stack temperatures than at the same flow rate in co flow.

There are a number of assumptions made that could affect these findings. Variations in the magnitude of the cell heat outputs due to polarisation losses could cause alterations to the temperature distribution but with a large excess of both fuel and air and a temperature profile that is fairly even, large variations would not be expected. A more significant assumption is the use of Hydrogen as fuel, if this were replaced by a hydrocarbon and the influence of endothermic reforming reactions were introduced the results could change significantly. The other significant omission from the simulation is the influence of heat

generation due to leaks which in Chapter 7 has already been shown to have the potential to alter the temperature distribution in a micro-tubular SOFC stack.

8.7 Variation in temperature with proximity to the wall

A unique aspect of this study has been the detailed modelling of heat losses to the environment through the thermal insulation surrounding the SOFC stack, rather than assumption of adiabatic walls. A test of the importance of this assumption is the variation in the temperature of the cells as their proximity to the wall changes. This was investigated using the predicted temperature profiles from the 100 cell stack simulations. Fig. 8.13 shows the temperature profile through the cross section of the stack 45 mm from the inlet end of the cells with the counter-current configuration.

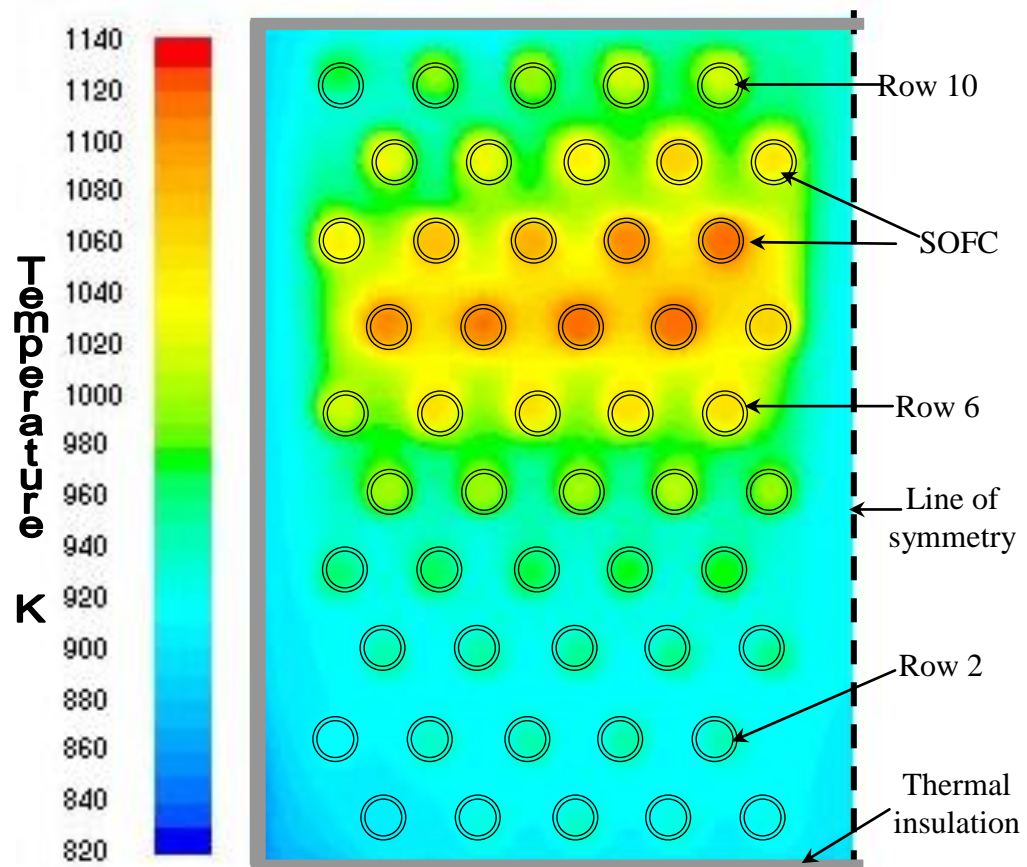


Fig. 8.13 Temperature contours through a cross section of the stack 45 mm

from the inlet of the cells with 20 std. std. $l\ min^{-1}$ of air introduced at 913 K

From the contours plotted in Fig. 8.13 we can see that the predicted temperature varies considerably across the stack, tending to be lower around the cells closest to the wall. To observe this trend more clearly the temperature along a line through the centre of rows 2, 6 and 10, at a position 5 mm from the end of the cells has been plotted in Fig. 8.14.

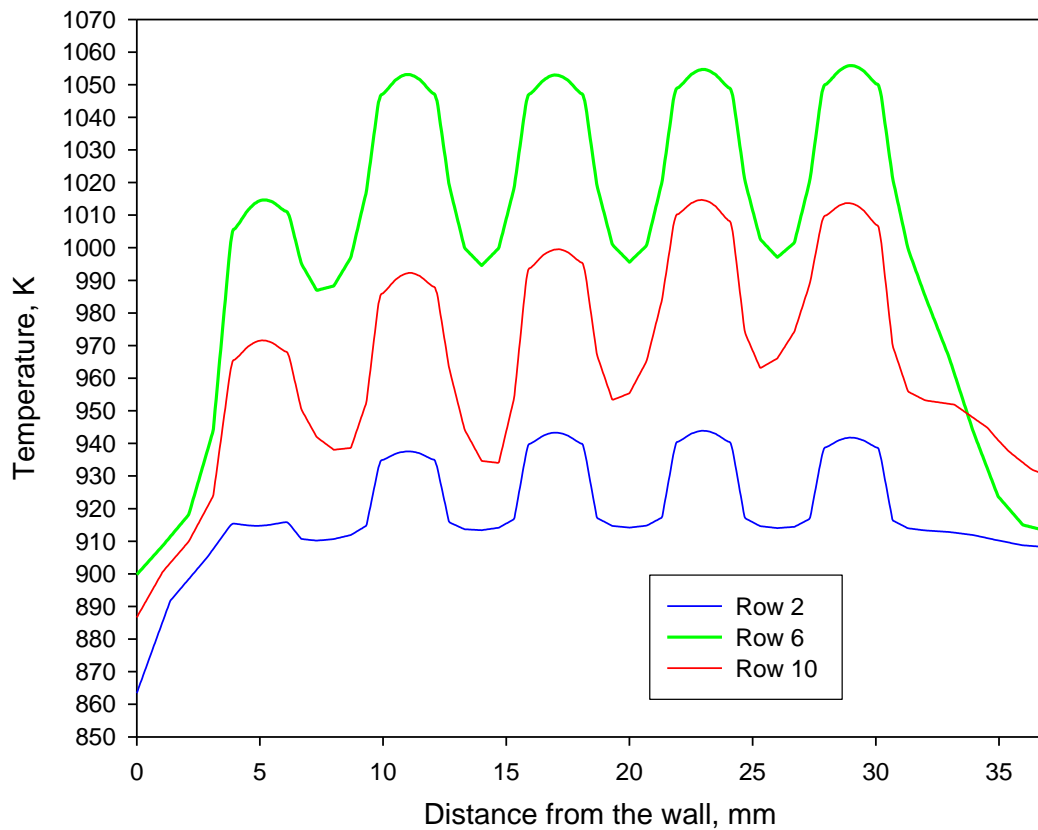


Fig. 8.14 Graph to show predicted temperature v's positions across the stack at a distance 5 mm from the outlet of the fuel cells with 20 l min^{-1} of air heated to 913 K in the counter- current flow configuration

The peaks in temperature on each plot in Fig. 8.14 correspond to the centre of each of the fuel cells. The temperature is coolest through the cells closest to the wall on all of the rows of cells, with the temperature through the cell at the centre of the stack and the one at the edge varying by up to 50 K. This level of temperature difference would impact on the stack performance as the electrical output from the cells at the edge of the cells would be substantially lower than those at the centre. This result shows how the CFD model could be a useful tool in diagnosis of differences in performance between cells in a stack.

The variation of temperature with position across the stack was also plotted for the simulation results with 100 std. l min⁻¹ as shown in Fig. 8.15.

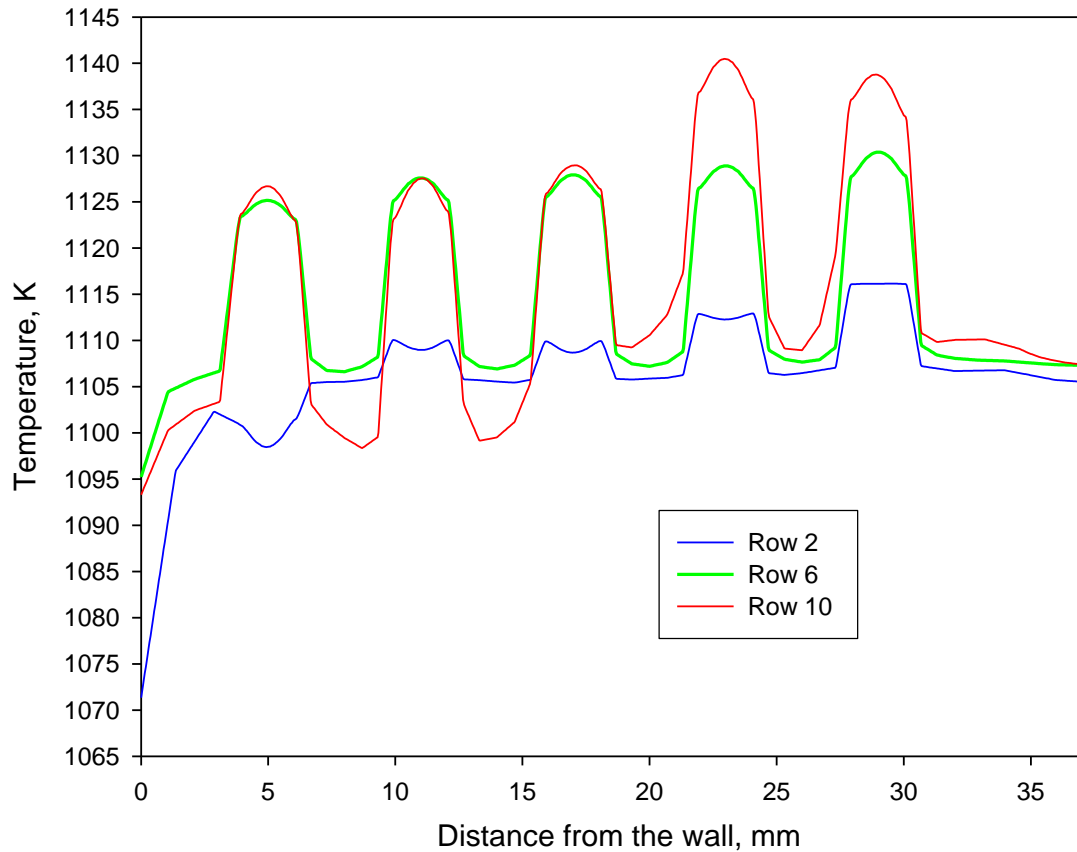


Fig. 8.15 Graph to show predicted temperature v's positions across the stack at a distance 5 mm from the outlet of the fuel cells with 100 l min⁻¹ of air heated to 913 K in the counter- current flow configuration

The temperature difference across the stack becomes less significant when the air flow rate is increased with a maximum range of around 15 K between the cells at the centre of the stack and those near the wall. Therefore, if the behaviour of a micro-tubular stack was to be modelled in the future with a high air flow rate, and knowledge of the energy balance and precise temperature distribution was not the prime motivation for the model,

adiabatic or constant heat flux boundary conditions might be considered at the walls to reduce the computation requirements.

8.8 Energy balance

The FLUENT post processing features were used to find the enthalpy of the streams entering and leaving the stack and the energy lost through the external walls of the insulation so that the energy balance around the system for different operating conditions could be studied, as shown in Table 8.1. The appropriate values have been doubled so that they represent the values for the whole stack rather than one just half.

	Inlet					Outlet				
Flow	Air flow rate	Air temp.	Total Air enthalpy	Fuel Inlet temp.	Total fuel enthalpy	Air temp	Total Air enthalpy	Fuel temp	Total fuel enthalpy	H _{in} -H _{out}
	l min ⁻¹	K	W	K	W	W	W	K	W	W
Co	20.00	936.00	252.93	300.00	0.17	835.34	216.31	919.36	61.82	25.03
Counter	20.00	913.00	243.81	300.00	0.16	870.03	213.26	903.03	60.40	29.69
Co	100.00	1008.00	1428.83	300.00	0.16	979.92	1381.72	967.15	66.67	19.39
Counter	100.00	1108.00	1630.11	300.00	0.17	1079.57	1574.51	1030.61	73.18	17.41

Table 8.1 Table to show the enthalpy of the streams into and out of the stack

The enthalpy of the streams at the outlet are based on the temperature of the gases as they exit the thermal insulation. The predicted temperature of the air as it left the air chamber housing the stack was higher than when it left the thermal insulation but the temperature would then drop due to heat losses through the thermal insulation.

Since no composition changes have been modelled and the heat generated inside the stack was assumed to be constant at 0.5 W per cell, the differences in the increase to the

enthalpy of the fluid stream leaving the stack depends on the heat loss through the insulation. The heat flux on each of the external faces of the insulation was also obtained from the FLUENT simulations and the total for all of the walls is reported in Table 8.2.

Flow	Flow rate	Inlet temp	$H_{out}-H_{in}$	Energy losses through the thermal insulation	Heat Generated by polarisation losses
	$l\ min^{-1}$	K	W	W	W
Co-current	20	936	-25.03	-24.97	50
Counter-current	20	913	-29.69	-20.31	50
Co-current	100	1008	-19.39	-30.60	50
Counter-current	100	1108	-17.41	-32.58	50

Table 8.2 Showing the energy balance around the 100 cell SOFC stack

The heat loss through the insulation varies by up to 12.2 W depending upon the operating conditions. The lowest heat losses through the insulation occur with 20 std. $l\ min^{-1}$ of air in the counter current arrangement. This may be due to the fact that under these conditions the temperature is relatively low along the wall of chamber next to the steel fuel inlet manifolds which is a good conductor of heat compared to the material of the other internal walls.

It is significant that the total energy assumed to be produced by the cells for the 100 cell stack exceeds the heat losses to the atmosphere. Although a lot of energy is required to preheat the air in order to produce suitable stack temperatures, this energy could potentially be recovered from the outlet streams. Therefore with a stack of this size there would not be a net consumption of energy to maintain the stack temperature other than the use of the 'waste' heat from the electrochemical processes. Heat could be exchanged from the outlet air and fuel streams to the incoming air stream, or more efficient scenario would be if air hot streams could be used in down stream process such as for space or water heating.

8.9 Conclusion

In this Chapter the first reported model of a 100-cell micro-tubular stack has been presented. The model was used to look at the problem of maintaining an even temperature distribution when the number of cells in the stack is increased.

Different flow configurations were considered, one a mix between cross-flow and co-flow and the other a mix between cross-flow and countercurrent flow. The counter-current configuration produced a more suitable temperature distribution at both moderate and high air flow rates. It was also found that high air flow rates were needed to produce an even temperature distribution within the stack.

Accurate modelling of the heat losses to the atmosphere showed that the heat produced inside a 100 cell micro-tubular stack would exceed the heat loss through the thermal insulation. The modelling approach also enabled the study of variations in the temperature of SOFCs at the edge of the stack compared to those at the centre, showing that variations in temperature of up to 50 K could be expected across a row of just 6 cells.

9. Conclusions and further work

9.1 Conclusions

The aim of this thesis was to start address some of the many unanswered questions regarding the design of micro-tubular SOFC stacks, particularly those concerning the thermal management and control of temperature. To investigate these issues a 20-cell stack was developed which was the first of this size using short cells sealed inside the hot part of the stack. In order to investigate the possibility of using computer simulations to assist with analysis and development of stack designs a CFD model of this 20-cell stack was created. This model was used to predict the temperature profile through the stack with Helium flowing through the cells and various flow of pre-heated air flowing over the cells. The simulation findings were compared to temperatures measured in the experimental stack under the same conditions. Good agreement was found between the simulation and experimental results. Therefore, the model was used to predict the stack temperature when operating with Hydrogen fed to the cells under the conditions of both open circuit and full load. Attempts to operate the experimental system under the same conditions were blighted by problems caused by leaking fuel. As this issue had a strong influence on the operation of the stack it was the object of a further investigation using the CFD model. Finally, the issue of scale up was investigated using the same modelling approach to simulate the operation of 100-cell stack of the same design as the 20 cell stack. Significantly, it was found that the heat generated inside the 100-cell stack would exceed that lost to the surroundings through the thermal insulation. During the work a number of other key observations came to the fore:

- The slow approach to establishing steady-state heat losses from the stack on start up, due to accumulation of heat in the thermal insulation;
- Importance of the effect of heat generated by combustion of leaking fuel;

- The strong influence of the air flow rate and direction on the temperature profile through the stack;

There are areas of experimental work and modelling that require further development or investigation but the CFD model should be a useful design tool for further development and analysis of micro-tubular stacks.

9.2 Further Experimental work

9.2.1 Cell development and characterisation of performance

More detailed modelling of micro-tubular SOFC stacks will require further experimental work to investigate the response of the electrical output and efficiency of the cells, to changes in temperature, flow rate, pressure, and external load. This work would benefit from more consistent cell performance, which may require work to develop alternative methods of current collection at the anode and increased mechanisation of the production process.

9.2.2 Investigation of leakage and alternative sealing methods

The experimental and CFD investigations showed that fuel leakage can be a problem and needs to be minimised. Further investigations are required to see if this can be achieved using the manifolding system employed in this study, or if more alternative sealing methods need to be pursued. One possible option might be the use of a brazing technique to seal the cell to the manifold.

Some of the problems were caused by the SOFCs cracking. This was attributed to the cells lacking straightness, which meant rather than being free to slide freely over the steel injector tube, part of the cell was pressed against the tube. Work is needed to investigate

if the straightness of the tubes can be improved by some adjustments to the manufacturing process.

9.2.3 Stack testing

Once these first two sections of work are completed, then it would be desirable to move towards the testing a larger stack. Since the CFD simulations showed that the heat produced by a 100-cell SOFC stack would be sufficient to exceed the heat loss through the 50 mm thick thermal insulation, the logical progression would be to build a stack to test this theory.

9.3 Further Modelling work

There are some additional investigations that could be carried out with the existing model without major changes, and there are also some more substantial improvements to be pursued.

9.3.1 Investigation of the effect of changing the insulation properties and thickness

The current model could readily be used to investigate the effect of the thickness and type of thermal insulation used to surround the stack by modifying the geometry or changing the material properties specified in the model. This would be much faster and cheaper than an experimental investigation into the effect of the same parameters.

9.3.2 Constant energy term due to polarisation losses

One of the major simplifications to the fuel cell model was the assumption of constant heat generation in the fuel cells. Work is needed to investigate the impact of this simplification on the predicted temperature profiles. This could begin with modification

of the magnitude of the constant energy source for every cell in the stack or selected cells. Ultimately it would be desirable to develop the model so that the heat generation in the cells varied with the local temperature and other conditions.

9.3.3 Modelling of leaks

The effect of leaks in a larger stack could readily be studied using the 100-cell stack model combined with the same approach as described in Chapter.7. If a manifold system allowing some fuel leakage continues to be used, then more accurate modelling of the leakage may be beneficial. In this study the heat generated by combustion of leaking fuel was assumed to be dispersed in the 10 mm closest to the fuel inlet. In reality, depending on the rate of fuel leakage, a flame may move away from the surface of the cell which may alter the effect of the leak on the stack temperature distribution. Work to accurately model the flow of fuel that would leak from the cells under different conditions would be a useful development.

9.3.4 Time dependent modelling

The experimental study showed that special attention would need to be devoted to optimisation of the start-up phase of the stack operation, especially if the stack is to be capable of producing power within minutes from a cold start. Work began on modelling the heat up phase for the 20-cell stack (see appendix 2) but the computation time to model the first 20 minutes of the stacks operation was around 1 month. Work is needed to reduce this to a more practical duration, which maybe achieved by further simplification of the model or improved computing facilities.

9.3.5 Investigation of changing to a hydrocarbon fuel

Future work should include the modelling of more complex fuels than Hydrogen, starting with Methane. Endothermic reforming reactions will have a significant effect on the temperature profile and how the stack should be configured to minimise gradients.

9.3.6 Inclusion of radiation modelling inside the stack

Radiation has so far been omitted in the modelling of heat transfer inside the stack. An objective for future work would be to take this into account. The first step might be to model only the radiation between the cells at the extremities of the stack and the thermal insulation.

References

- N. G. Minh, and T. Takahashi, 1995, Introduction, Science and technology of ceramic fuel cells, Chapter 1, 1-14, Elsevier.
- 2 J. Larminie and A. Dicks, 2003, Introduction, Fuel cell systems explained, 2nd Edition, 1-24, Wiley
- 3 UK government white paper, 2003, Our energy future-creating a low carbon economy, 19.
- 4 Mark C. Williams, Joseph P. Strakey and Wayne A. Surdoval, 2003, The US department of energy, office of fossil energy stationary fuel cell program, Journal of Power Sources, 143, 191-196.
- 5 Mamdouh G. Salameh, 2003, Can renewable and unconventional energy sources bridge the global energy gap in the 21st century?, Applied Energy, 75, 33-42. .
- 6 Mamdouh G. Salameh, 2000, Global oil outlook: return to the absence of surplus and its implications, Applied Energy, 65, 239-250.
- 7 Jens Leifeld and Jürg Fuhrer, 2005, Greenhouse gas emissions from Swiss agriculture since 1990: implications for environmental policies to mitigate global warming, Environmental Science & Policy, 8, 410-417.
- 8 Kozo Nagase, 2005, "Carbon–Money Exchange" to contain global warming and deforestation, Energy Policy, 33, 1233-1238.
- 9 Olav Kaarstad, 1995, Fossil fuels and responses to global warming, Energy Conversion and Management, 36, 869-872.
- 10 Ambuj D. Sagar, 1995, Automobiles and global warming: Alternative fuels and other options for carbon dioxide emissions reduction, Environmental Impact Assessment Review, 15, 241-274.
- 1 Michael P. Walsh, 1990, The importance of fuel cells to address the global warming problem, Journal of Power Sources, 29, 13-28.
- 2 Franz Hackl and Gerald J. Pruckner, 2003, How global is the solution to global warming? Economic Modelling, 20, 93-117.
- 3 Peter Lazare, 2001, It's Time to Tax Global Warming, The Electricity Journal, 14, 62-68.
- 4 J. OM. Bockris, 2002, The origin of ideas on a Hydrogen Economy and its solution to the decay of the environment, International Journal of Hydrogen Energy, 27, 731-740.

References

- 5 S.S. Penner, 2006(online 2005), Steps toward the Hydrogen Economy, *Energy*, 31, 33-43.
- 6 Phillip Tseng, John Lee and Paul Friley, 2005, A Hydrogen economy: opportunities and challenges, *Energy*, 30, 2703-2720.
- 7 Carl-Jochen Winter, 2005, Into the Hydrogen energy economy—milestones, *International Journal of Hydrogen Energy*, 30, 681-685.
- 8 B.C.R. Ewan and R.W.K. Allen, 2005, A Fig. of merit assessment of the routes to Hydrogen, *International Journal of Hydrogen Energy*, 30, 809-819.
- 9 Brenda Johnston, Michael C. Mayo and Anshuman Khare, 2005, Hydrogen: the energy source for the 21st Century, *Technovation*, 25, 569-585.
- 20 S.A. Sherif, Frano Barbir and T.N. Veziroglu, 2005, Towards a Hydrogen Economy, *The Electricity Journal*, 18, 62-76.
- 2 Woodrow W. Clark, Jeremy Rifkin, Todd O'Connor, Joel Swisher, Tim Lipman, Glen Rambach et al., 2005, Hydrogen energy stations: along the roadside to the Hydrogen economy , *Utilities Policy*, 13, 41-50.
- 22 L Barreto, A Makihiro and K Riahi, 2003, The Hydrogen economy in the 21st century: a sustainable development scenario, *International Journal of Hydrogen Energy*, 28, 267-284.
- 23 S.A. Sherif, F. Barbir and T.N. Veziroglu, 2005, Wind energy and the Hydrogen economy—review of the technology, *Solar Energy*, 78, 647-660.
- 24 Rajesh K. Ahluwalia and X. Wang, 2005, Direct Hydrogen fuel cell systems for hybrid vehicles, *Journal of Power Sources*, 139, 152-164.
- 25 Arun K. Sehra and Woodrow Whitlow, Jr, 2004, Propulsion and power for 21st century aviation, *Progress in Aerospace Sciences*, 40, 199-235.
- 26 Reuel Shinnar, 2003, The Hydrogen economy, fuel cells, and electric cars, *Technology in Society*, 25, 455-476.
- 27 Ayoub Kazim, 2003, Introduction of PEM fuel-cell vehicles in the transportation sector of the United Arab Emirates, *Applied Energy*, 74, 125-133.
- 28 S. C. Singhal, 2002, Solid oxide fuel cells for stationary, mobile, and military applications, *Solid State Ionics*, 152-153, 405-410.
- 29 Michael Wang, 2002, Fuel choices for fuel-cell vehicles: well-to-wheels energy and emission impacts, *Journal of Power Sources*, 112, 307-321.
- 30 Steven G. Chalk, James F. Miller and Fred W. Wagner, 2000, Challenges for fuel cells in transport applications, *Journal of Power Sources*, 86, 40-51.

References

- 3 Wolfgang Drenckhahn, 1999, SOFC in Power Generation, Journal of the European Ceramic Society, 19, 861-863.
- 32 T. Ishihara, N. Sammes, O. Yamamoto, 2003, Electrolytes, High temperature solid oxide fuel cells fundamentals, design and applications, Eds. S. C. Singhal and K. Kendall, Chapter 4, 83-117, Elsevier.
- 33 J. Larminie and A. Dicks, 2003, Medium and high temperature fuel cells, Chapter 7, Fuel cell systems explained, 2nd Edition, 163-228, Wiley.
- 34 Osamu Yamamoto, 2000, Solid oxide fuel cells: fundamental aspects and prospects, Electrochimica Acta, 45, 2423-2435.
- 35 J. P. P. Huijsmans, F. P. F. van Berkel and G. M. Christie, 1998, Intermediate temperature SOFC – a promise for the 21st century, Journal of Power Sources, 71, 107-110.
- 36 S. Assabumrungrat, N. Laosiripojana, V. Pavarajarn, W. Sangtongkitcharoen, A. Tangjitmatee and P. Praserttham, 2005, Thermodynamic analysis of carbon formation in a solid oxide fuel cell with a direct internal reformer fuelled by methanol, Journal of Power Sources, 39, 55-60.
- 37 Dong Ju Moon and Jong Woo Ryu, 2003, Electrocatalytic reforming of carbon dioxide by methane in SOFC system, Catalysis Today, 87, 255-264.
- 38 K. Eguchi, H. Kojo, T. Takeguchi, R. Kikuchi and K. Sasaki, 2002, Fuel flexibility in power generation by solid oxide fuel cells, Solid State Ionics, 152-153, 411-416.
- 39 R. Peters, R. Dahl, U. Klüttgen, C. Palm and D. Stolten, 2002, Internal reforming of methane in solid oxide fuel cell systems, Journal of Power Sources, 106, 238-244.
- 40 Richard Fellows, 1998, A novel configuration for direct internal reforming stacks, Journal of Power Sources, 71, 281-287.
- 41 S. C. Singhal, 2000, Advances in solid oxide fuel cell technology, Solid State Ionics, 135, 305-313.
- 42 Wolfgang Winkler and Hagen Lorenz, 2002, The design of stationary and mobile solid oxide fuel cell–gas turbine systems, Journal of Power Sources, 105, 222-227.
- 43 F. J. Gardner, M. J. Day, N. P. Brandon, M. N. Pashley and M. Cassidy, 2000, SOFC technology development at Rolls-Royce, Journal of Power Sources, 86, 122-129.
- 44 K. Kendall, 1994, Solid oxide fuel cell structures, Patent Number: W09422178.
- 45 W. J. Dollard, 1992, Solid oxide fuel cell developments at Westinghouse, Journal of Power Sources, 37, 133-139.

References

- 46 N. G. Minh, and T. Takahashi, 1995, Stack design and fabrication, Science and technology of ceramic fuel cells, Chapter 9, 233-306, Elsevier.
- 47 H. Itoh, M. Mori, N. Mori and T Abe, 1994, Production cost estimation of solid oxide fuel cells, Journal of Power Sources, 49, 315-332.
- 48 R. George and N. F. Bessette, 1998, Reducing the manufacturing cost of tubular solid oxide fuel cell technology, Journal of Power Sources, 71, 131.
- 49 K. Kendall and S. C. Singhal, 2003, Introduction to SOFCs, High temperature solid oxide fuel cells fundamentals, design and applications, Eds. S. C. Singhal and K. Kendall, Chapter 1, 1-19, Elsevier.
- 50 K Kendall and G Sales, 1994, A rapid heating fuel cell, Proceedings of the 2nd international conference on 'Ceramics in Energy Applications', Institute of Energy, London, 55-63.
- 5 I. P. Kilbride, 1996, Preparation and properties of small diameter tubular SOFC for rapid start-up, Journal of Power Sources, 61, 167-717.
- 52 C. Hatchwell, N. Sammes, I.W.M. Brown and K. Kendall, 1999, Current collectors for a novel tubular design of SOFC, Journal of Power Sources, 77, 64-68.
- 53 R.J. Boersma, N.M. Sammes, and C.J. Fee, 2000, Losses resulting from in-plane electricity conduction in tubular solid oxide fuel cells, Solid State Ionics, 135, 493-502.
- 54 M. Prica, T. Alston and K Kendall, 1997, Mechanical and thermal properties of a 200 tube SOFC reactor, Electrochemical society Proceedings: Solid Oxide fuels cells V, 18, 619-625.
- 55 T Alston, K. Kendall, M. Palin, M. Prica, and P. Windibank, 1998, A 1000-cell SOFC reactor for domestic cogeneration, Journal of Power Sources, 71, 271-274.
- 56 Acumentrics Corp. (US), 2004, Integrated solid oxide fuel cell and reformer, Patent publication number: IL135330.
- 57 M. Brown and B. Fenton, 2004, Horizontal fuel cell tube systems and methods, Patent publication number: CN1539176, Acumentrics Corp(US).
- 58 R. England and G. A. Mook, 2003, Fuel cell stacking and sealing, Patent publication number: AU2003215318, Acumentrics Corp.
- 59 Fuel cell Bulletin News Item, May 2002, SECA rewards Acumentrics progress in tubular SOFCs, Fuel Cell Bulletin, 1.
- 60 Fuel cell Bulletin News Item, May 2002, Acumentrics ships first rapid-start SOFC UPS, Fuel Cells Bulletin, 4.

References

- 6 Fuel cell Bulletin News Item, March 2003, Fuel Cells Bulletin, Five more Acumentrics SOFCs for ChevronTexaco, 4.
- 62 Fuel cell Bulletin News Item, Jan 2005, Acumentrics ships SOFC for NREL biogas study, Fuel Cells Bulletin, 6.
- 63 M. Lockett, M.J.H. Simmons, and K. Kendall, 2004, CFD to predict temperature profile for scale up micro-tubular SOFC stacks, Journal of Power Sources, 131, 243-246.
- 64 C. Finnerty, N. J. Coe, R.H. Cunningham and R.M. Ormerod, 1998, Carbon formation on and deactivation of nickel-based/zirconia anodes in solid oxide fuel cells running on methane, Catalysis Today, 46, 137-145.
- 65 C. Finnerty and R. M. Ormerod, 2000, Internal reforming over nickel/zirconia anodes in SOFCs operating on methane: influence of anode formulation, pre-treatment and operating conditions, Journal of Power Sources, 86, 390-394.
- 66 K. Kendall, C.M. Finnerty, G. Saunders and J.T. Chung, 2002, Effects of dilution of methane entering an SOFC anode, Journal of Power Sources, 106, 323-327.
- 67 K. Kendall, C.M. Finnerty, G. A. Tompsett, P. Windibank and N. Coe, 2000, Rapid heating SOFC system for hybrid applications, Electrochemical Society of Japan, 68, 403-406.
- 68 J. Staniforth, and K. Kendall, 2000, Cannock landfill gas powering a small tubular solid oxide fuel cell- a case study, Journal of Power Sources, 86, 401-403.
- 69 J. Staniforth, K. Kendall, 1998, Biogas powering a small tubular solid oxide fuel cell, Journal of Power Sources, 71, 275-277.
- 70 C. Finnerty, T. Alston, R. M. Ormerod and K. Kendall, 1999, A solid oxide fuel cell demonstration kit operated on Butane/Propane, Proceedings of the international conference with exhibition portable fuel cells, 27-34, European Fuel Cell Forum, Switzerland.
- 7 K. Kendall and M. Palin, 1998, A small solid oxide fuel cell demonstrator for microelectronic applications, Journal of Power Sources, 71, 268-270.
- 72 G. A. Tompsett, C. Finnerty, K. Kendall, T. Alston, and N. Sammes, 2000, Novel Applications for micro-SOFCs, Journal of Power Sources, 86, 376-382.
- 73 M. A. Khaleel and J.R Selman, 2003, Cell, Stack and System modelling, High Temperature Solid Oxide fuel cells fundamentals design and applications, Ed. S. C. Singhal, K. Kendall, Chapter 11, 293-331, Elsevier.
- 74 A. Haynes, W. J. Wepfer, 2001, Characterizing heat transfer within a commercial-grade tubular solid oxide fuel cell for enhanced thermal management, International Journal of Hydrogen Energy, 26, 369-379.

References

- 75 S. Campanari, 2001, Thermodynamic model and parametric analysis of a tubular SOFC module, *Journal of Power Sources*, 92, 26-34.
- 76 A. Haynes, W. J. Wepfer, 2000, 'Design for power' of a commercial grade tubular solid oxide fuel cell, *Energy Conversion & Management*, 41, 1123-1139.
- 77 Pei-Wen Li, Minking. K. Chyu, 2003, Simulation of the chemical/electrochemical reactions and heat and mass transfer for a tubular SOFC in a stack, *Journal of Power Sources*, 124, 487-498.
- 78 M. L. Ferrari, A. Traverso, and L. Magistri, 2005, Influence of the anodic recirculation transient behaviour on the SOFC hybrid system performance, *Journal of Power Sources*, 149, 22-32.
- 79 R. J. Boersma, N.M. Sammes, C. Fee, 2000, Integrated fuel cell system with tubular solid oxide fuel cells, *Journal of Power Sources*, 86, 369-375.
- 80 S. Nagata, A. Momma, T. Kato, Y. Kasuga, 2001, Numerical analysis of output characteristics of tubular SOFC with internal reformer, *Journal of Power Sources*, 101, 60-71.
- 8 L. Petruzi, S. Cocchi, F. Fineschi, 2003, A global thermo-electrochemical model for SOFC systems designs and engineering, *Journal of Power Sources*, 118, 96-107.
- 82 P. Costamagna, 1997, The benefits of solid oxide fuel cells with integrated air pre-heater, *Journal of Power Sources*, 69, 1-9.
- 83 Y. Chen, and J. W. Evans, 1996, Cool-down time of solid oxide fuel cells intended for transportation application, *Journal of Power Sources*, 58, 87-91.
- 84 J. Yuan, M. Rokni, and B. Sunden, 2003, Three dimensional computational analysis of gas and heat transport phenomena in ducts relevant for anode-supported solid oxide fuel cells, *International Journal of Heat and Mass Transfer*, 46, 809-821.
- 85 K.P. Recknagle, R. E. Williford, L. A. Chick, D. R. Rector, and M. A. Khaleel, 2003, Three dimensional thermo-fluid electrochemical modelling of planar SOFC stacks, *Journal of Power Sources*, 113, 109-114.
- 86 M. Iwata, T. Hikosaka, M. Morita, T. Iwanari, K. Ito, K. Onda, Y. Esaki, Y. Sakaki, and S. Nagata, 2000, Performance analysis of planar-type unit SOFC considering current and temperature change, *Solid State Ionics*, 132, 297-308.
- 87 E. Achenbach, 1994, Three dimensional and time-dependent simulation of a planar solid oxide fuel cell stack, *Journal of Power Sources*, 49, 333-348.

References

- 88 S. Lin, J.W. Stevenson, M.A. Khaleel, 2003, The effect of interconnect rib size on the fuel cell concentration polarisation in planar SOFC, *Journal of Power Sources*, 117, 92-97.
- 89 D. Larrain, J. Van Herle, F. Marechal, D. Favrat, 2004, Generalized model of planar SOFC repeat element for design optimization, *Journal of Power Sources*, 131, 304-312.
- 90 H. Yakabe, M. Hishinuma, M. Uratani, Y. Matsuzaki, I. Yasuda, 2000, Evaluation and modeling of performance of anode supported solid oxide fuel cell, *Journal of Power Sources*, 86, 423-431.
- 91 P. Aguiar, C.S. Adjiman, N. P. Brandon, 2004, Anode-supported intermediate temperature direct internal reforming solid oxide fuel cell. I: model-based steady-state performance, *Journal of Power Sources*, 138, 120-136.
- 92 N. Bundschuh, M. Bader and G. Schiller, 2004, Modelling of the heat process of a planar SOFC stack, *Proceedings of the 6th European Fuel Cell Forum, Lucerne*, 2, 589-598.
- 93 W. Becker, J. Wenck, H. M. Wigger and A. Muller, 2004, On the mechanical demands of an SOFC under service, *Proceedings of the 6th European Fuel Cell Forum, Lucerne*, 2, 609-624.
- 94 Yau-Pin Chyou, Tsang-Dong Chung, Jong-Sheng Chen and Ri-Fong Shie, 2004, An efficient computational methodology for electrochemical and heat transfer analyses of a planar solid oxide fuel cell, *Proceedings of the 6th European Fuel Cell Forum, Lucerne*, 2, 646-655.
- 95 P. Iora, S. Campanari, 2004, Parametric analysis of a planar SOFC model with geometric optimisation, *Proceedings of the 6th European Fuel Cell Forum, Lucerne*, 2, 656-669.
- 96 V. Ruzhnikov, V Subbotin, A Gulevich and N. Khramucshin, 2004, Simulation and investigation of electrical performance and gas pressure distributions in a planar SOFC, *Proceedings of the 6th European Fuel Cell Forum, Lucerne*, 2, 698-699.
- 97 E. Achenbach, 1995, Response of a solid oxide cell to load change, *Journal of Power Sources*, 57, 105-109.
- 98 H. Yakabe, T. Ogiwara, M. Hishinua, and I.Yasuda, 2001, 3-D model calculation for planar SOFC, *Journal of Power Sources*, 102, 144-154.
- 99 S. G. Neophytides, 1999, The reversed flow operation of a cross flow SOFC monolith, *Chemical Engineering Science*, 54, 4603-4613.
- 00 J. Hwang, C.K. Chen, and D.Y. Lai, 2005, Detailed characteristic comparison between planar and MOLB-type SOFCs, *Journal of Power Sources*, 143, 75-83.

References

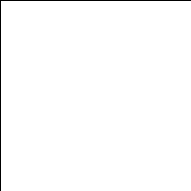
- 01 P. Costamagna, A. Selimovic, M. Del Borghi, and G. Agnew, 2004, Electrochemical model of the integrated planar solid oxide fuel cell (IP-SOFC), *Chemical Engineering Journal*, 102, 61-69.
- 02 B. Todd, and J. Young, 2004, Efficient modelling of an integrated planar SOFC, *Proceedings of the 6th European Fuel Cell Forum, Lucerne*, 2, 625-634.
- 03 P. Costamagna, T. Cerutti, R. Di Felice, R. Collins, R. Cunningham, M. Bozzolo, O. Tarnowski and G. Agnew, 2004, Integrated planar solid oxide fuel cell(IP-SOFC) coupled to a reforming reactor: Simulation analysis, *Proceedings of the 6th European Fuel Cell Forum, Lucerne*, 2, 635-645.
- 04 B. A. Haberman and J. B. Young, 2004, Three dimensional simulations of chemically reacting flows in the porous support structure of a IP-SOFC, *Proceedings of the 6th European Fuel Cell Forum, Lucerne*, 2, 689-698.
- 05 A Faghri, Z. Guo, 2004, Challenges and opportunities of thermal management issues related to fuel cell technology and modelling, *International Journal of Heat and Mass Transfer*, 48, 3891-3920.
- 06 B. Chachuat, A. Mitsos, P. I. Barton, 2005, Optimal design and steady-state operation of micro power generation employing fuel cells, *Chemical Engineering Science*, 60, 4535-4556.
- 07 T. Ota, M. Koyama, C. Wen, K. Yamada and H. Takahashi, 2003, Object based modeling of SOFC system: Dynamic behaviour of micro-tube SOFC, *Journal of Power Sources*, 118, 430-439.
- 08 S. Murthy, A. Fedorov, 2003, Radiation heat transfer analysis of the monolith type solid oxide fuel cell, *Journal of Power Sources*, 124, 453-458.
- 09 J. Van Herle, D. Larrain, N. Autissier, Z. Wulillemin, M. Molinelli, and D. Favrat, 2005, Modelling and experimental validation of solid oxide fuel cell materials and stacks, *Journal of the European Ceramic Society*, 25, 2627-2632.
- 10 M. A. Khaleel and J. R. Selman, 2004, Cell, stack and system modelling, *High temperature solid oxide fuel cells fundamentals, design and applications*, Chapter 11, 291-331.
- 11 E. Hernández-Pacheco, D. Singh, P. N. Hutton, N. Patel and M. D. Mann, 2004, A macro-level model for determining the performance characteristics of solid oxide fuel cells, *Journal of Power Sources*, 138, 174-186.
- 12 H. Zhu and R. J. Kee, 2003, A general mathematical model for analyzing the performance of fuel-cell membrane-electrode assemblies, *Journal of Power Sources*, 117, 61-74.
- 13 S. H. Chan, K. A. Khor and Z. T. Xia, 2001, A complete polarization model of a solid oxide fuel cell and its sensitivity to the change of cell component thickness, *Journal of Power Sources*, 93, 130-140.

References

- 14 R.T. Leah, N.P. Brandon and P. Aguiar, 2005, Modelling of cells, stacks and systems based around metal-supported planar IT-SOFC cells with CGO electrolytes operating at 500–600 °C, *Journal of Power Sources*, 145, 336-352.
- 15 J.J. Hwang, C.K. Chen and D.Y. Lai, 2005, Computational analysis of species transport and electrochemical characteristics of a MOLB-type SOFC, *Journal of Power Sources*, 140, 235-242.
- 16 S. Campanari and P. Iora, 2004, Definition and sensitivity analysis of a finite volume SOFC model for a tubular cell geometry, *Journal of Power Sources*, 132, 113-126.
- 17 M. A. Khaleel , Z. Lin , P. Singh, W. Surdoval and D. Collin, 2004, A finite element analysis modeling tool for solid oxide fuel cell development: coupled electrochemistry, thermal and flow analysis in MARC®, *Journal of Power Sources*, 130, 136-148.
- 18 A.C. Burt, I.B. Celik, R.S. Gemmen and A.V. Smirnov, 2004, A numerical study of cell-to-cell variations in a SOFC stack, *Journal of Power Sources*, 126, 76-87.
- 19 D. Larrain, J. Van herle, F. Maréchal and D. Favrat, 2003, Thermal modeling of a small anode supported solid oxide fuel cell, *Journal of Power Sources*, 118, 367-374.
- 20 N.G Minh, and T. Takahashi, 1995, Principles of operation, Science and technology of ceramic fuel cells, Chapter 2, 15-40, Elsevier.
- 21 K. Takano, S. Nagata, K. Nozaki, A. Monma, T. Kato, Y. Kaga, A. Negishi, Ken Kato, T. Inagaki, H. Yoshida et al., 2004, Numerical Simulation of a disk-type SOFC for impedance analysis under power generation, *Journal of Power Sources*, 132, 42-51.
- 22 R. Suwanwarangkul, E. Croiset, M.W. Fowler, P.L. Douglas, E. Entchev and M. A. Douglas, 2003, Performance comparison of Fick's, dusty-gas and Stefan–Maxwell models to predict the concentration over potential of a SOFC anode, *Journal of Power Sources*, 122, 9-18.
- 23 K. Sudaprasert, R.P. Travis, and R.F. Martinez-Botas, 2004, A computational fluid dynamics model of a solid oxide fuel cell, *Proc. Institute of Mechanical Engineers*, 219, 159-167.
- 24 J.R. Ferguson, J.M. Fiard, and R. Herbin, 1996, Three-dimensional numerical simulation for various geometries of solid oxide fuel cells, *Journal of Power Sources*, 58, 109-122.
- 25 G.J. Saunders, K. Kendall, 2002, Reactions of hydrocarbons in small tubular SOFCs, *Journal of Power Sources*, 106, 258-263.

References

- 26 C. Finnerty, G. Tompsett, K. Kendall, R.M. Ormerod, 2000, SOFC system with integrated catalytic fuel processing, *Journal of Power Sources*, 86, 459-463.
- 27 P. Bance, N.P. Brandon, B. Girvan, P. Holbeche, S. O'Dea, and B.C.H. Steele, 2004, Spinning-out a fuel cell company from a UK University—2 years of progress at Ceres Power, *Journal of Power Sources*, 131, 86-90.
- 28 E. Fontell, T. Kivisaari, N. Christiansen, J.-B. Hansen, and J. Palsson, 2004, Conceptual study of a 250 kW planar SOFC system for CHP application, *Journal of Power Sources*, 131, 49-56.
- 29 R.A. George, 2000, Status of tubular SOFC field unit demonstrations, *Journal of Power Sources*, 86, 134-139.
- 30 Microtherm Insulation, 2001, Product and performance Data, Microtherm international Ltd, Upton, Wirral, England.
- 31 W. Winkler, *Thermodynamics*, 2003, High temperature solid oxide fuel cells—Fundamentals, design and applications, Eds. S.C. Singhal and K. Kendall, Chapter 3, 53-82, Elsevier.
- 32 P. Costamagna, E. Arato, P.L. Antonucci, and V. Antonucci, 1996, Partial oxidation of CH₄ in solid oxide fuel cells: simulation model of the electrochemical reactor and experimental validation, *Chemical Engineering Science* 51, 3013-3018.
- 33 H.K. Versteeg and W. Malalasekera, 1995, *Introduction to computational fluid dynamics: the finite volume method*, Longman.
- 34 H.-M. Jung, W.-Y. Lee, J.-S. Park, and C.-S. Kim, 2004, Numerical analysis of a polymer electrolyte fuel cell, *International Journal of Hydrogen Energy* 29, 945-954.
- 35 S. Maharudrayya, S. Jayanti, and A. P. Deshpande, 2004, Pressure losses in laminar flow through serpentine channels in fuel cell stacks, *Journal of Power Sources*, 138, 212-220.
- 36 P. T. Nguyen, T. Berning, and N. Djilali, 2004, Computational model of a PEM fuel cell with serpentine gas flow channels, *Journal of Power Sources* 130, 149-157.
- 37 Y. M. Ferng, Y. C. Tzang, B. S. Pei, C. C. Sun, and A. Su, 2004, Analytical and experimental investigations of a proton exchange membrane fuel cell, *International Journal of Hydrogen Energy* 29, 381-391.
- 38 U. Krewer, Y. Song, K. Sundmacher, V. John, R. Lubke, G. Matthies, and L. Tobiska, 2004, Direct methanol fuel cell (DMFC): analysis of residence time behaviour of anodic flow bed, *Chemical Engineering Science*, 59, 119-130.



References

- 39 A. Kumar, and R.G. Reddy, 2003, Effect of channel dimensions and shape in the flow-field distributor on the performance of polymer electrolyte membrane fuel cells, *Journal of Power Sources*, 113, 11-18.
- 40 Fluent Inc, 2004, *Gambit 2.1 modelling guide*.
- 41 Personal communication: Mr John Roberts, 2002, *Microtherm Ltd*.
- 42 U. Pasaogullari, and C. Wang, 2003, *Computational Fluid Dynamics Modelling of Solid oxide Fuel Cells*, *Solid oxide fuel cells VIII*, The Electrochemical Society, 1403-1412.
- 43 P. Aguiar, D. Chadwick, and L. Kershenbaum, 2002, *Modelling of an indirect internal reforming solid oxide fuel cell*, *Chemical Engineering Science*, 57, 1665-1677.